

*David J. Wegner*

500.03  
PRJ-10.0  
W637 L 779  
18095

THE GEOCHEMISTRY OF SURFACE WATER AND GROUNDWATER  
INTERACTIONS FOR SELECTED BLACK MESA DRAINAGES,  
LITTLE COLORADO RIVER BASIN, ARIZONA

by

Matthew Wickham

**GCES OFFICE COPY  
DO NOT REMOVE!**

---

A Thesis Submitted to the Faculty of the  
DEPARTMENT OF HYDROLOGY AND WATER RESOURCES  
In Partial Fulfillment of the Requirements  
For the Degree of  
MASTER OF SCIENCE  
WITH A MAJOR IN HYDROLOGY  
In the Graduate College  
THE UNIVERSITY OF ARIZONA

1992

W10409

## STATEMENT BY THE AUTHOR

This thesis has been submitted in partial fulfillment of the requirements for an advanced degree at the University of Arizona and is deposited in the University Library to be made available to borrowers under rules of the library.

Brief quotations from this thesis are allowable without special permission, provided that accurate acknowledgement of the source is made. Requests for permission for extended quotation from or reproduction of this manuscript in whole or in part may be granted by the head of the major department of the Dean of the Graduate College when in his or her judgement the proposed use of the material is in the interests of scholarships. In all other instances, however, permission must be obtained from the author.

Signed: 

## APPROVAL BY THESIS DIRECTOR

This thesis has been approved on the date shown below:

  
R. L. Bassett  
Associate Professor of Hydrology  
and Water ResourcesDate 4/30/92

## ACKNOWLEDGEMENTS

This thesis research is based, in part, by work supported by the U.S. Bureau of Indian Affairs and the U.S. Department of Justice through contracts with Hydro Geo Chem, Inc. The opinions and interpretations presented in this thesis do not necessarily represent those of any of the organizations listed above.

I am indebted to Drs. Gary Walter, Randy Bassett, and Stanley Davis who served on my thesis committee and provided encouragement, insight and essential technical review during this investigation. This thesis also benefitted from countless discussions with Dr. Harold Bentley and other colleagues at Hydro Geo Chem, Inc. I also profited from discussions with Alan Dulaney, Dr. Songlin Cheng and Jim Eychaner. Susan Maida provided invaluable guidance and advise with the ion chromatography. Rich "The Filter King" Roberts deserves credit for his tremendous contributions to the success and enjoyment of the field work. Special thanks also go out to the Hopi people for their assistance and support during the field work, and to Steve Blodgett and Nat Natungla with the Hopi Tribe's Division of Natural Resources.

Lastly, I thank my family and friends for their encouragement and support. But most of all, I thank my wife and son, for patiently doing without for so long.

## TABLE OF CONTENTS

LIST OF ILLUSTRATIONS .....	7
LIST OF TABLES .....	10
ABSTRACT .....	11
CHAPTER 1. INTRODUCTION .....	12
1.1 Background .....	12
1.2 Purpose, objective and scope .....	17
1.3 Report organization .....	18
1.4 Previous investigations .....	19
CHAPTER 2. PHYSIOGRAPHY, CLIMATE AND VEGETATION .....	23
2.1 Regional overview .....	23
2.2 Moenkopi Wash .....	26
2.3 Dinnebito Wash .....	30
CHAPTER 3. REGIONAL HYDROGEOLOGY .....	32
3.1 N-aquifer .....	32
3.1.1 Hydrostratigraphy .....	32
3.1.2 Mineralogy .....	39
3.1.3 Groundwater flow .....	44
3.2 D-aquifer .....	47
CHAPTER 4. SURFACE WATER HYDROLOGY .....	52
4.1 General description .....	52
4.2 Distribution of baseflow .....	57
CHAPTER 5. DATA COLLECTION .....	66
5.1 Historical water quality data .....	66
5.2 Water sampling .....	67
5.3 Sample identification .....	70
5.4 Laboratory analysis .....	71

## TABLE OF CONTENTS (cont.)

CHAPTER 6. GROUNDWATER GEOCHEMISTRY .....	75
6.1 Introduction .....	75
6.2 Geochemistry of the N-aquifer .....	75
6.2.1 General description of water quality .....	76
6.2.2 Qualitative analysis .....	78
6.2.2.1 Conceptual model .....	79
6.2.2.2 Ion exchange reactions .....	82
6.2.2.3 Calcite and gypsum dissolution/precipitation reactions .....	90
6.2.2.4 Weathering of silicates .....	98
6.2.3 Isotopic indications .....	100
6.2.3.1 Deuterium and Oxygen-18 .....	100
6.2.3.2 Sulfur-34 .....	104
6.3 Water quality of the D-aquifer .....	106
6.3.1 General description of water quality .....	107
6.4 Summary .....	108
CHAPTER 7. SURFACE WATER GEOCHEMISTRY .....	110
7.1 Introduction .....	110
7.2 General description of water quality .....	111
7.3 Qualitative analysis .....	115
7.3.1 Ion exchange reactions .....	116
7.3.2 Calcite and gypsum dissolution/precipitation reactions .....	121
7.4 Isotopic indications .....	127
7.4.1 Deuterium and Oxygen-18 .....	128
7.4.2 Sulfur-34 .....	132
7.5 Surface water and groundwater interactions .....	135
7.6 Summary .....	143
CHAPTER 8. GEOCHEMICAL MODELING .....	144
8.1 Thermodynamic speciation calculations .....	144
8.1.1 N-aquifer .....	145
8.1.2 Moenkopi Wash and Dinnebito Wash .....	148

## TABLE OF CONTENTS (cont.)

## CHAPTER 8. GEOCHEMICAL MODELING (cont.)

8.2 Reaction path modeling .....	149
8.2.1 N-aquifer .....	155
8.2.2 Moenkopi Wash and Dinnebito Wash .....	160
8.3 Summary .....	163

## CHAPTER 9. SUMMARY AND CONCLUSIONS ..... 168

## APPENDICES ..... 173

Appendix A - Analysis of streamflow data for Moenkopi Wash ..... 173

Appendix B - Statistical streamflow summary for Moenkopi Wash .. 181

Appendix C - Areal distribution of selected chemical constituents,  
N-aquifer .....

184

Appendix D - Water quality data .....

201

Appendix E - Profiles for selected chemical constituents and  
isotopes, Moenkopi Wash .....

225

Appendix F - Profiles for selected chemical constituents and  
isotopes, Dinnebito Wash .....

232

Appendix G - Procedures for determining transpiration from  
phreatophytes and evaporation from bare alluvial soils .

239

## REFERENCES ..... 245

## PLATES

## LIST OF ILLUSTRATIONS

1-1	Study area and areal extent of the N-aquifer .....	13
2-1	Principal physiographic subdivisions .....	24
2-2	Moenkopi Wash tributaries and reach designations .....	27
3-1	Conceptualized geologic cross-section of the Black Mesa area .....	33
3-2	Nomenclature and water-bearing characteristics for the N-aquifer .....	35
3-3	Structure contour map, top of the N-aquifer formations where buried ..	38
3-4	Estimated saturated thickness of the N-aquifer .....	40
3-5	Estimated potentiometric surface of the N-aquifer .....	46
3-6	Location and estimated potentiometric surface of the D-aquifer, undifferentiated .....	48
3-7	Nomenclature and water-bearing characteristics for the D-aquifer .....	49
4-1	Watersheds for Moenkopi Wash and Dinnebito Wash .....	53
4-2	Map showing perennial streams during 1903-13 and 1950-60 .....	59
4-3	Surface geology along Dinnebito Wash .....	60
4-4	Streamflow profile along Moenkopi Wash, February-March, 1990 .....	62
5-1	Electrical conductivity as a function of total dissolved ions for HGC groundwater samples and wash samples .....	73
6-1	Trilinear diagram for N-aquifer groundwater samples .....	77
6-2	Log activity diagram for $\text{Na}^+$ as a function of $\text{Ca}^{2+}$ , N-aquifer .....	84
6-3	$\text{Na}^+$ as a function of $\text{Cl}^-$ , N-aquifer .....	85
6-4	Excess Na as a function of corrected $\text{Ca}^{2+}$ , N-aquifer .....	87

## LIST OF ILLUSTRATIONS (continued)

6-5	Log activity diagram for $Mg^{2+}$ as a function of $Ca^{2+}$ , N-aquifer . . . . .	89
6-6	Alkalinity as a function of uncorrected and corrected $Ca^{2+}$ , N-aquifer . .	93
6-7	$SO_4^-$ as a function of uncorrected and corrected $Ca^{2+}$ , N-aquifer . . . . .	96
6-8	$\delta D$ as a function of $\delta^{18}O$ for the N-aquifer . . . . .	101
6-9	Geochemical sulfur cycle . . . . .	105
7-1	Trilinear diagram for wash samples . . . . .	112
7-2	$Na^+$ as a function of $Cl^-$ for N-aquifer and wash samples . . . . .	117
7-3	Log-activity diagram for $Na^+$ as a function of $Ca^{2+}$ for N-aquifer and wash samples . . . . .	118
7-4	Excess Na as a function of corrected $Ca^{2+}$ for wash samples . . . . .	120
7-5	Log-activity diagram for $Mg^{2+}$ as a function of $Ca^{2+}$ for N-aquifer and wash samples . . . . .	122
7-6	Alkalinity as a function of uncorrected and corrected $Ca^{2+}$ , for wash samples . . . . .	123
7-7	$SO_4^-$ as a function of uncorrected and corrected $Ca^{2+}$ , for wash samples . . . . .	126
7-8	$\delta D$ as a function of $\delta^{18}O$ for N-aquifer and Moenkopi wash samples . .	129
7-9	$\delta D$ as a function of $\delta^{18}O$ for N-aquifer and Dinnebito wash samples . .	130
7-10	The inverse of $SO_4^-$ as a function of $\delta^{34}S$ for N-aquifer and wash samples . . . . .	134
7-11	Electrical conductivity as a function of distance along Moenkopi Wash	138
8-1	Calcite and gypsum saturation indices for samples from the N-aquifer, and Moenkopi Wash and Dinnebito Wash . . . . .	146
8-2	Simulated reaction path models for the N-aquifer . . . . .	156

## LIST OF ILLUSTRATIONS (continued)

Plate 1 Sampling locations for Moenkopi Wash

Plate 2 Sampling locations for Dinnebito Wash

Plate 3 Surface geology along Moenkopi Wash

## LIST OF TABLES

6-1. Average concentrations for selected constituents in the D-aquifer . . . .	108
7-1. Hypothetical mixing and evaporative enrichment along Moenkopi Wash . . . . .	140
8-1. Phases considered in reaction path modeling . . . . .	154
8-2. Results of mass transfer and pH modeling, N-aquifer . . . . .	159
8-3. Results of mass transfer modeling, N-aquifer, Moenkopi Wash and Dinnebito Wash . . . . .	165

## ABSTRACT

Surface water and groundwater interactions involve complex physical processes that are not easily measured in most natural systems. Many of these processes can be indirectly evaluated by examining the geochemistry of the hydrologic system. In this investigation, a geochemical approach to investigating surface water and groundwater interactions is applied to perennial reaches of selected Black Mesa drainages in northeastern Arizona. The drainages, Moenkopi Wash and Dinnebito Wash, receive groundwater discharging from the regional N-aquifer.

Groundwater within the confined portion of the N-aquifer is chemically and isotopically distinct from that in the unconfined portion. Water in the majority of the confined N-aquifer exhibits a depleted  $\delta D$  and  $\delta^{18}O$  composition, a consequence of recharge under an earlier paleo climate. The small changes observed in chemical composition of baseflow along the streamcourse can be explained by chemical interaction with channel alluvium or minor exchange with groundwater from the alluvium.

## CHAPTER 1

### INTRODUCTION

#### 1.1 Background

Surface water and groundwater interactions involve complex physical processes that are not easily observed nor quantified in most natural systems. Although a change in streamflow is measurable, the observed fluctuations may be due to storm runoff, bank storage, regional groundwater flow, evapotranspiration or other processes. Examining the geochemistry of the surface water and groundwater components, however, provides information that is useful to understanding the role of individual processes.

In this investigation, a geochemical approach to investigating surface water and groundwater interactions is applied to the perennial reaches of two washes that are sustained by discharges from a regional aquifer. The surface water systems are Moenkopi Wash and Dinnebito Wash within the reservations of the Hopi Tribe and Navajo Nation in northern Arizona. The aquifer is referred to as the "N-aquifer" and is in northern Arizona and southern Utah. The groundwater discharge to the washes is the largest concentrated outflow from the regional N-aquifer. The study area, the N-aquifer and washes are shown in Figure 1-1.

The N-aquifer is exploited by water wells, and numerous, developed springs and seeps. Perennial streamflows are also utilized. Streamflow from Moenkopi

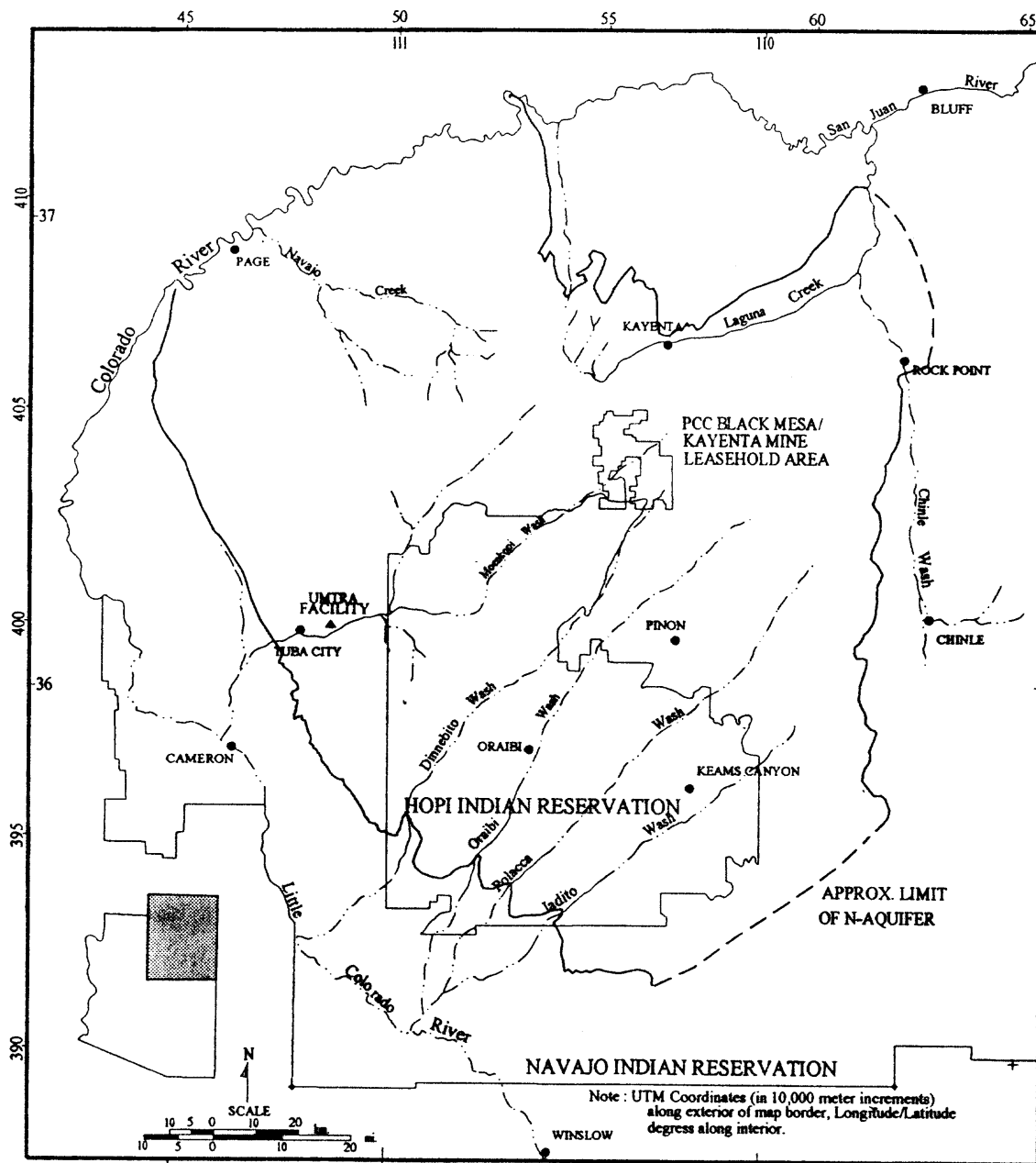


Figure 1-1. Study area and areal extent of the N-aquifer

Wash is diverted for irrigation near the villages of Upper Moenkopi and Lower Moenkopi along the floodplain through Kerley Valley (Plate 1). At the village of Sand Springs on Dinnebito Wash (Plate 2), streamflow is periodically dammed and the impounded water pumped to fields on the valley alluvium. Unlike the baseflow derived from aquifer discharges, storm runoff is not dependable and typically has sediment loads above acceptable concentrations for irrigation. In addition to irrigation and stock watering, the perennial streamflows are used for recreation and are essential to the development and maintenance of wildlife habitat.

N-aquifer discharge to springs and perennial washes is important to the Hopi Tribe, not only as a water resource, but as an integral part of their religious beliefs and heritage. Moenkopi means "place of the flowing stream" and is used in reference to the stream as well as the villages of Upper Moenkopi and Lower Moenkopi. The towns are built on and around sites occupied by migrating Hopi clans in the ancient past who used the perennial streamflows along Moenkopi Wash for stock watering and irrigation (James, 1988). Also referencing water, Dinnebito means "water of the people" and refers to the drainage system as well as a small Hopi Indian community centered about a trading post on Dinnebito Wash.

Inasmuch as the perennial reaches of these southwestern washes are sustained by groundwater discharge, withdrawals from the N-aquifer may affect these fragile systems. Peabody Coal Company (PCC) operates the largest coal strip-mine in the United States in the northern part of Black Mesa. The 100

square-mile leasehold area lies within the Navajo and Hopi Indian Reservation boundaries (Figure 1-1). From 1972 to 1986, PCC has pumped an average of 3820 acre-feet of water annually from the N-aquifer (Hill and Sottolare, 1987). The water is used to transport pulverized coal in a 270 mile-long pressurized pipeline to the Mohave Generating Station at Laughlin, Nevada. PCC also operates a system of more than 150 surface water impoundments within the Moenkopi and Dinnebito wash watersheds for sediment control (OSMRE, 1989). PCC has projected the operating life of the mine to the year 2031 with continued groundwater withdrawals from the N-aquifer.

Hart and Sottolare (1988) reported that municipal groundwater withdrawals from the N-aquifer have increased from an estimated 100 acre-feet per year in 1965 to about 2400 acre-feet in 1987. By the end of 1985, the combined municipal and mine-related groundwater withdrawals had resulted in water level declines of more than ten feet in most of the confined portion of the N-aquifer (Brown and Eychaner, 1988). Pumping centers in the towns of Tuba City and Moenkopi Village could also diminish baseflow along Moenkopi Wash through Kerley Valley.

The results of a regional groundwater modeling study provide some assessment of the potential impacts from groundwater withdrawals. Numerical simulations of groundwater flow in the N-aquifer suggest that for most projected groundwater pumping alternatives, some drawdown will extend to all confined areas (Brown and Eychaner, 1988). Projections for a 67 year period show that simulated

declines will exceed 100 feet over 310 square miles of the confined system, and water level declines of as much as 5 to 25 feet will occur at the margins of the area of confined conditions. At the start of perennial flows along Moenkopi Wash, for example, anticipated drawdowns were projected to reach 30 feet. The impact on the perennial reaches of the southwestern Black Mesa washes is largely unknown.

The Uranium Mill Tailings Remedial Action (UMTRA) project, overseen by the U.S. Department of Energy (1990) is at a site about six miles northwest of Tuba City and 1.5 miles north of Moenkopi Wash. A contaminant plume associated with the mill site has been identified in the N-aquifer with the principal direction of groundwater flow and contaminant movement to the south toward the wash. Aquifer restoration may require significant groundwater withdrawals that could effect flows and water quality along Moenkopi Wash.

Other processes and activities may also affect the perennial flows. Introduced in the 1940's, the phreatophyte tamarisk or salt cedar has invaded most of the major drainage systems with remarkable speed and density. Although it provides improved bank stabilization, it threatens to lower the alluvial water levels below the channel bottom. Also, variations in climate influence N-aquifer recharge, bank storage from storm runoff, and evapotranspiration rates. Overgrazing and the extensive land disturbance from strip mining and surface water impoundments may also influence the character of the rainfall-runoff relationships, natural channel aggradation and degradation processes, and nutrient balance along the streamcourse.

## 1.2 Purpose, objective and scope

The purpose of this study is to improve the understanding of the hydrologic and geochemical interactions between the groundwater and perennial streamflows for the southwestern Black Mesa washes. The objective of this study is three-fold:

- 1) to present the data collected and compiled during this investigation including measurements and observations made during the field activities, results of laboratory analysis of water samples for chemical constituents and selected isotopes, and tabulation of historical water quality data,
- 2) to interpret the chemical and isotopic composition of the N-aquifer to include water quality characterization, identification of the dominant reactions and reaction sequences, and supporting speciation and reaction path modeling, and
- 3) to interpret the chemical and isotopic composition of the sampled baseflow and spring discharges along Moenkopi and Dinnebito washes to include identification of dominant reactions along the streamcourse, and conclusions regarding the origin and distribution of aquifer discharges contributing to the observed baseflow.

The scope of the surface water investigation has been limited to Moenkopi Wash and Dinnebito Wash. These drainage systems are the dominant discharge mechanisms for the N-aquifer in the Little Colorado River Basin (LCRB). Discharge to Moenkopi Wash was estimated to be between 3170 and 5500 acre-feet per year (AF/Yr) from an estimated total discharge of between 13,560 to 19,400 AF/Yr for the groundwater system (Eychaner, 1981; Brown and Eychaner, 1988).

Although the scope of the groundwater investigation centers on the N-aquifer, evidence suggests that some hydraulic communication may exist between

the N-aquifer and the overlying D-aquifer. Previous studies have concluded that the effects of vertical communication on N-aquifer groundwater flow patterns and chemical composition are small (Eychaner, 1983; Dulaney, 1989). Therefore, a thorough description of the D-aquifer in this report is not deemed necessary nor practical. As will be discussed later, mixing between the two aquifers may be of local importance, therefore, brief descriptions of the hydrogeology and water quality for the D-aquifer are provided. A detailed study of the hydrogeology and aqueous geochemistry of the D-aquifer and its hydraulic communication with the N-aquifer is beyond the scope of this investigation.

This study was not intended to provide a definitive characterization or statistical analysis of the streamflows in Moenkopi and Dinnebito washes, nor was it intended to specifically address impacts from municipal and domestic groundwater pumping or PCC mining operations.

### 1.3 Report organization

This report is organized in much the same order that the investigation was conducted. The remainder of this chapter outlines relevant previous investigations. Chapter 2 provides a description of the location, physiography, climate and vegetation for the study area. Chapter 3 presents a description of the regional hydrogeology including hydrostratigraphic relationships, mineralogy, and patterns of groundwater flow. Chapter 3 concludes with a brief description of the

hydrogeology of the overlying D-aquifer. Chapter 4 provides a general overview of the surface water hydrology. Chapter 5 describes data collection for this investigation in terms of existing data and the water sampling program conducted during this investigation.

The geochemical analysis for groundwater and surface water systems is presented in chapters 6, 7 and 8. The qualitative analyses of the geochemistry of the N-aquifer and the surface water systems are described in chapters 6 and 7, respectively. Chapter 8 presents the methodologies and results of the quantitative analysis using geochemical modeling. The summary and conclusions are provided in chapter 9.

#### 1.4 Previous investigations

Numerous regional investigations in the study area have been conducted, most under the auspices of the U.S. Geological Survey. In the early 1940's, the USGS began an extensive hydrologic investigation within the Navajo and Hopi Indian Reservations in northern Arizona, Utah, New Mexico and Colorado during which information from wells, springs and seeps was collected, tabulated and published in a suite of documents (Cooley et al., 1964; Cooley, 1966; Cooley et al., 1969; Davis et al., 1963; Kister, 1963, McGavock, 1966). Other investigations include detailed stratigraphic studies and geologic mapping (Harshbarger et al., 1957), regional hydrogeology of the Navajo and Hopi Indian Reservations (Cooley

et al., 1969), and numerous localized water supply investigations and groundwater availability studies. The Black Mesa Monitoring Program began in 1971 to collect information necessary to assess long-term effects of PCC coal mining-related withdrawals on domestic and municipal supplies. It is jointly funded and operated by the U.S. Geological Survey and the Arizona Department of Water Resources. The program involves continuous and periodic measurement of groundwater levels, withdrawals and water quality, and discharge and chemical quality of selected springs and streams.

As part of the aforementioned monitoring program, the U.S. Geological Survey conducted modeling studies to simulate groundwater flow in the N-aquifer and project impacts from mine and municipal withdrawals on water supplies (Eychaner, 1983; Brown and Eychaner, 1988). Each of these studies addressed in general terms discharge to both Moenkopi and Dinnebito washes from the regional N-aquifer.

Peabody Coal Company's Black Mesa and Kayenta mines are within the study area and have been the focus of extensive data collection and analysis, not just for mineral resources, but to monitor various hydrologic processes impacted by mining. The mine plan was prepared by PCC in 1984 and provides volumes of data and analysis concentrated within the leasehold property. PCC operates a network of over 150 surface water impoundments largely within the Moenkopi Wash and Dinnebito Wash drainage systems. Data are collected regarding precipitation,

surface water quality and streamflows. Groundwater levels and water quality are monitored in the Wepo and Toreva formations where the coal ore is mined, and in the deeper N-aquifer from which PCC withdraws water for its coal-slurry pipeline.

Pursuant to the Surface Mining Control and Reclamation Act (SMCRA), a Cumulative Hydrologic Impact Assessment (CHIA) of the operations at the PCC Black Mesa/Kayenta mines was performed by the U.S. Office of Surface Mining and Reclamation and Enforcement (OSMRE). The investigation addressed, in part, baseflow along Moenkopi Wash in an attempt to determine what effects, if any, surface water impoundments and N-aquifer withdrawals were having on surface water resources at the town of Tuba City.

The study area has been the subject of several Master's theses, primarily investigations of the sedimentology and mineralogy (Luttrell, 1987; Sargent, 1984). Dulaney (1989) provided in his thesis the only published characterization of the geochemistry of the N-aquifer. A noteworthy contribution is the results of mineralogic analyses of cutting samples from the Navajo Sandstone and Wingate Sandstone. Dulaney also mapped various chemical constituents in groundwater and provided a description of the water quality of the N-aquifer. Several qualitative hypotheses regarding the geochemical evolution were also introduced. Many of the geochemical reactions proposed by Dulaney were reexamined in this investigation and are described in Chapter 6.

The most recent investigations, which include this study, are being undertaken in preparation for the pending general adjudications of all water rights and water use in the Little Colorado River system and source. Pertinent to this study is the work performed by Hydro Geo Chem, Inc. for the Bureau of Indian Affairs (BIA) and U.S. Department of Justice. The investigations include regional and site-specific geologic and hydrologic characterization of four major aquifer systems (including the N-aquifer), water sampling and analyses, regional and site specific groundwater flow modeling, and geochemical characterization. The interpretations and results of these investigations, however, are as yet unpublished and proprietary until settlement.

For a more detailed listing and description of related investigations, reports and publications, the reader is referred to Dulaney (1989), Eychaner (1983), and to the bibliography at the end of this report.

## CHAPTER 2

### PHYSIOGRAPHY, CLIMATE AND VEGETATION

Much of the information presented in this chapter on the physiography, climate and vegetation of the study area, in addition to personal observation, is after Cooley et al. (1969) who provided a comprehensive description of the physiography of the area with relationships of landforms to geologic structure and sedimentary rocks, and regional descriptions of climate and vegetation. The reader should consult this reference if additional information is desired.

In this report, the physiographic subdivisions used by Akers et al. (1958) were adopted for referencing general locations. These subdivisions include Black Mesa, Western Navajo Uplands, Eastern Navajo Uplands, Painted Desert, and Chinle Valley. These subdivisions are shown in Figure 2-1 and described below.

#### 2.1 Regional overview

The study area is in northern Arizona in an area referred to by Cooley et al. (1969) as the "navajo country" which is described as having "been subjected to vigorous cycles, which consist of periods of downcutting alternating with periods of planation and deposition. As a result, streams have carved a complex maze of plateaus, rock benches, and mesas." The most prominent of the many physiographic features is Black Mesa, a large highland that coincides with the Black Mesa

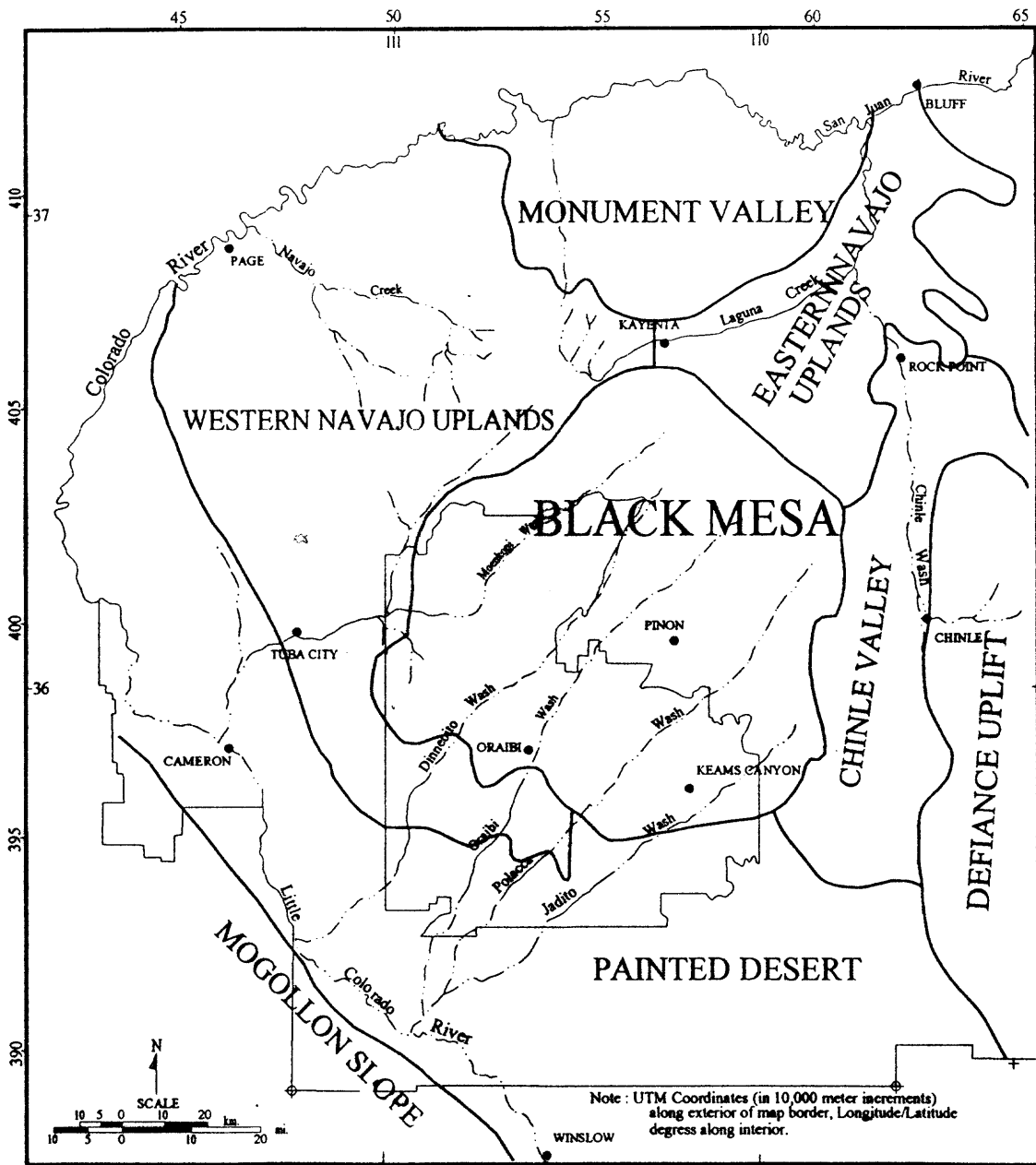


Figure 2-1. Principal physiographic subdivisions (after Akers et al., 1958)

hydrogeologic subdivision. It is delimited to the north by high outfacing sandstone cliffs and from the summit dips gently to the southwest. Elevations range from 4000 to 7500 feet above mean sea level (MSL). The major drainages within the Black Mesa subdivision include Moenkopi, Dinnebito, Oraibi, Polacca and Jadito washes. All of these watersheds drain to the west or southwest.

The Western Navajo Uplands is to the west and northwest of Black Mesa. The physiography of this subdivision is dominated by sand dunes and stripped plains with high mesas and buttes. To the north, the landscape is dominated by Navajo Mountain, the Navajo Creek drainage system and Glen Canyon (now partially inundated by Lake Powell). The southern arm of the Western Navajo Uplands roughly coincides with the outcrop of the Navajo Sandstone. The area is dissected by Moenkopi, Dinnebito, Oraibi and Polacca washes which drain across the arm to the southwest and incise the Navajo Sandstone. Elevations in the Western Navajo Uplands range from 10,300 feet (MSL) at the summit of Navajo Mountain to 3500 feet (MSL) at the Colorado River.

Climate in the study area varies widely but has a strong and fairly uniform relation to altitude and orographic effect. Along the lower reaches of the washes, climate may be classified as semiarid. Mean annual precipitation ranges from less than six inches per year in low lying areas to more than 18 inches at the highest elevations. Mean annual precipitation is reported to be 6.7 and 11.7 inches with a mean annual snowfall of 8.9 and 51.5 inches at Tuba City and Betatakin,

respectively. At higher elevations, typical annual snowfall exceeds 40 inches (Cooley et al., 1969). Precipitation is usually from either convectional summer monsoon storms, usually high intensity, short duration, and randomly distributed, or from winter precipitation as slow moving frontal systems, evenly distributed, and long duration.

Vegetation at the lower elevations is limited by climate and large areas of exposed bedrock. Native riparian vegetation in the alluvium along the lower reaches of the washes is also scarce and consists primarily of cottonwood and willow, with dense thickets of tamarisk. The alluvial valleys support only sparse grassland-shrub below about 5500 feet in elevation. Above 5500 feet, pinon-juniper forests are common along with fair to good rangelands and pine forests above 7500 feet.

## 2.2 Moenkopi Wash

The valley and channel geometry vary along Moenkopi Wash and allow for a distinction between different reaches. The tributaries along Moenkopi Wash and the different reaches described below are shown in Figure 2-2. The furthest-upstream reach terminates at the confluence of Black Mesa Wash and is referred to as the *headwaters* in this report. The headwaters is high in elevation, about 6000-7500 feet (MSL) and is largely forested. A large amount of tributary streamflow within the headwaters is diverted or impounded by an extensive system of dams and

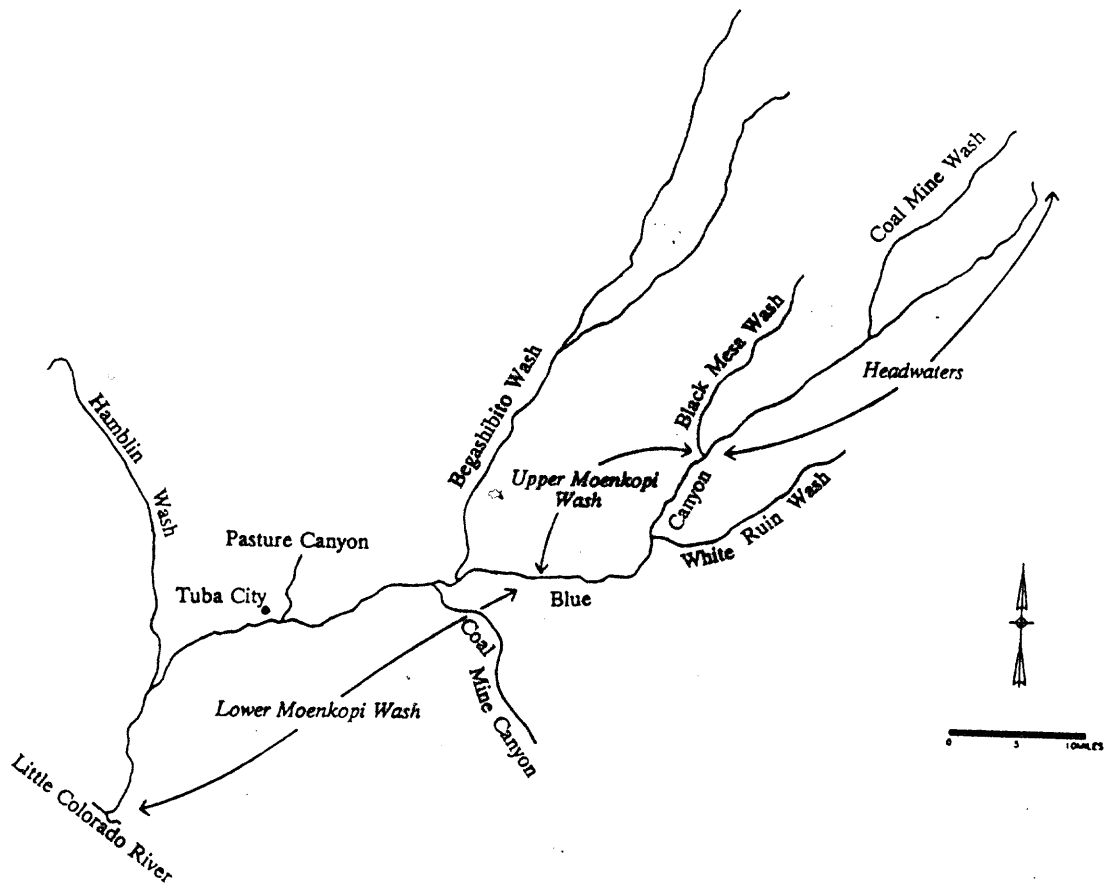


Figure 2-2. Moenkopi Wash drainage system and reach designations

impoundments established and maintained by PCC, primarily for sediment control and land reclamation. The impounded water does not directly re-enter the system as surface drainage but some amount may return to the stream alluvium as groundwater flow below the impoundments.

The next downstream reach, termed *upper Moenkopi Wash*, extends from Black Mesa Wash to the start of perennial flow through what is referred to as Blue Canyon by the Hopi's. The upper half of this reach has incised the Toreva Formation, Mancos Shale, and Dakota and Cow Springs sandstones. Tall escarpments line the canyon making access difficult along most of its extent. Riparian vegetation is scarce.

The canyon opens to a broader segment of upper Moenkopi Wash, several miles downstream of the confluence with White Ruin Wash. The alluvial valley is as much as one-quarter mile wide in places and the channel itself, as much as 150 feet wide. The banks are spotted with tamarisk thickets and occasional cottonwoods. Only minor intermittent surface flows were observed during the field investigation (January to March, 1990), most less than one-half cubic feet per second (cfs). Flow was continuous for only short distances, typically less than 100 feet. The source of the surface water was probably surfacing groundwater from the alluvium. This reach of Moenkopi Wash is dry for most of the year except during periods of storm runoff.

The next downstream reach is termed *lower Moenkopi Wash* and is the focus of this study. It begins at the *water caves* and extends downstream to the confluence with the Little Colorado River (Plate 1). The *water caves* (dubbed so during the field sampling because of its resemblance to the Navajo wind caves near Page, Arizona) is an extremely narrow, 50-75 feet deep, 200 yard-long gorge in the easternmost outcrop of the Navajo Sandstone. The ravine is in most places less than ten feet wide. During the field sampling, a minor amount of standing water was observed for 100 feet upstream of the caves. Flow into the water caves from this standing water was negligible. Discharge at the mouth of the water caves was visually estimated to be 0.75 to 1 cfs.

About one-quarter mile downstream of the water caves, the wash enters a sinuous, deep, narrow canyon walled by massive 100 to 200 feet escarpments of Navajo Sandstone, 75 to 300 feet apart, for a distance of approximately six miles. Beyond the confluence with Coal Mine Canyon, the canyon widens intermittently to  $\frac{1}{4}$  to  $\frac{1}{2}$  mile and a broad alluvial floodplain has developed. The wash follows deep vertical cuts into the alluvium, some as much as 60 feet deep. Some vegetation exists on occasional benches through the narrows and along the wash once the canyon widens. Approximately three miles upstream of the village of Moenkopi, small farmed plots may be found along the alluvial benches.

The canyon and channel again constrict near the Arizona State Highway 264 bridge where the Kayenta Formation is exposed (Plate 1). Downstream lies Kerley

Valley with the villages of Upper Moenkopi and Lower Moenkopi. The floodplain is occupied by irrigated fields and residences. The wash meanders through Kerley Valley, past the village of Lower Moenkopi, and on to the confluence with the Little Colorado River.

### 2.3 Dinnebito Wash

The segment of Dinnebito Wash considered by this investigation transects the Navajo Sandstone and underlying Kayenta Formation where they are exposed, and extends from Dinnebito Spring to approximately six miles downstream of the village of Sand Springs (Plate 2). The area may be described as broad alluvium gently sloping toward the wash. The valley alluvium is bounded by bedrock formations. In places, the alluvium is in excess of three miles across but is as little as one-half mile across where constricted between Garces and Howell mesas. Below Sand Springs, the valley alluvium narrows as the Navajo Sandstone has been removed by erosion and the more resistant Kayenta Formation is exposed. Land surface elevations range from 4900 to about 5500 feet (MSL).

Within the study area, Dinnebito Wash is eroded into the alluvium to depths of 75 feet. Alluvium occasionally slumps across the wash, temporarily damming surface flows. This was evident in aerial photographs as well as observed in the field during water sampling. Downstream of Sand Springs, the wash flows directly over the exposed Kayenta Formation. Very little vegetation exists along the wash

other than occasional tamarisk, due probably to the instability of the alluvium and to frequent flooding. In the alluvial valley, only occasional grasses and desert brush were observed.

## CHAPTER 3

### REGIONAL HYDROGEOLOGY

A basic understanding of the geology, stratigraphy, and direction and rates of groundwater movement is prerequisite to a description of the geochemical processes for the N-aquifer. Equally important is a knowledge of the mineralogic composition of the formations which provides constraints for conceptualizing and testing reaction pathways. The following sections describe the hydrostratigraphy, mineralogy and groundwater flow for the N-aquifer. A brief characterization of the overlying D-aquifer is appended to this chapter.

Time-stratigraphic diagrams and large-scale structure contour maps were prepared and are presented as figures in this chapter to assist the description of the various geologic units. A conceptual geologic cross-section under Black Mesa is presented as Figure 3-1. A detailed cross-section is available from Harshbarger et al. (1957).

#### 3.1 N-aquifer

##### 3.1.1 Hydrostratigraphy

The formations comprising the N-aquifer are part of the Glen Canyon Group of Jurassic and Triassic(?) age and include, in ascending order, the Wingate Sandstone, the Moenave Formation, the Kayenta Formation and the Navajo

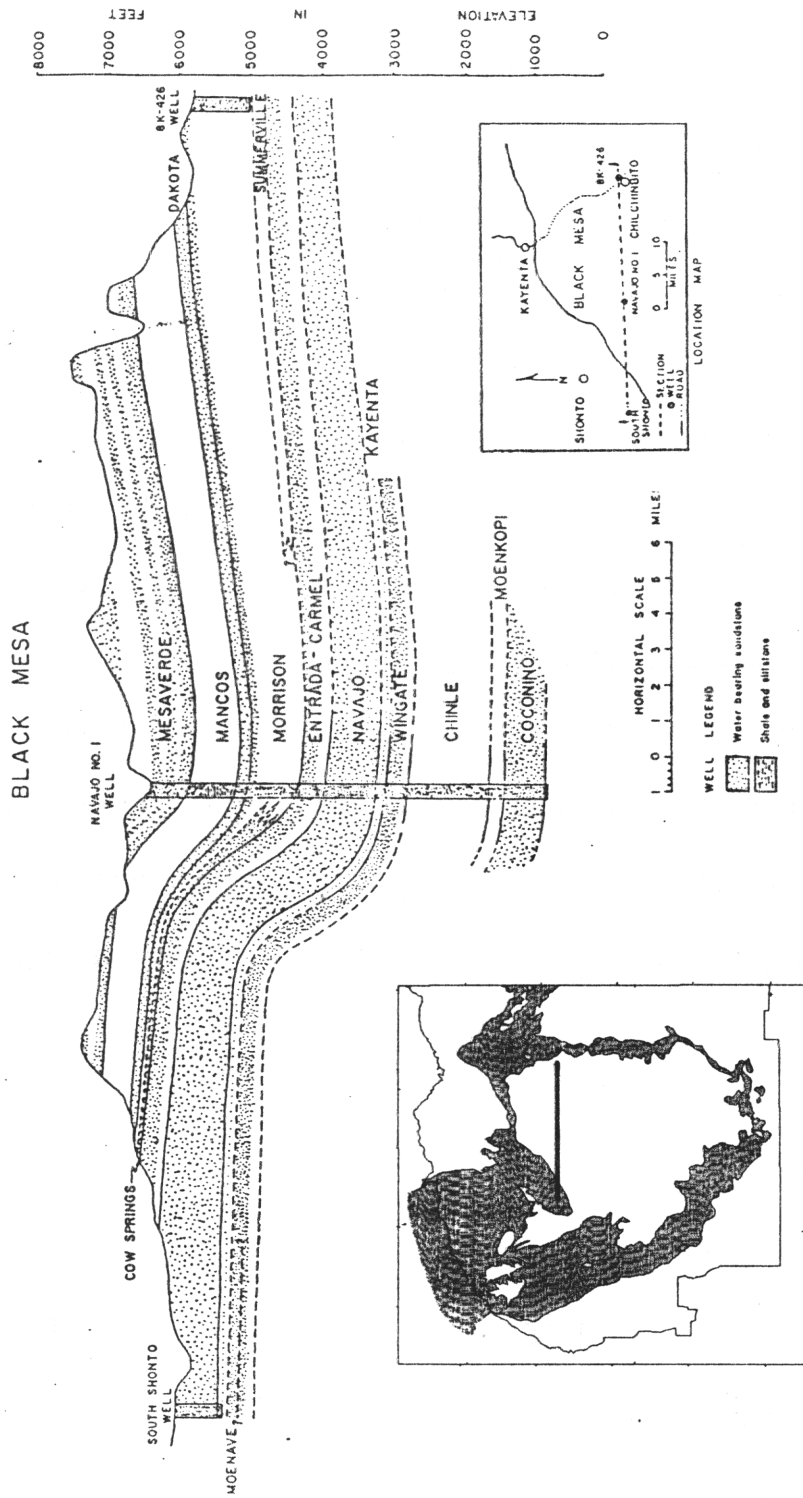


Figure 3-1. Conceptualized geologic cross-section of the Black Mesa area (from Stetson, 1966)

Sandstone. Of these, the major water-bearing formations include three distinct eolian sandstone units: the Navajo Sandstone, the sandy facies of the Kayenta Formation and the Lukachukai Member of the Wingate Sandstone. By contrast, the basal Rock Point Member of the Wingate Sandstone, the silty facies of the Kayenta Formation and the Moenave Formation are composed of siltstone and silty sandstone. They are believed to have been deposited by streams and are generally not considered water-bearing. The hydrostratigraphy of the N-aquifer is summarized in the time-rock stratigraphic diagram in Figure 3-2. Descriptions of the stratigraphy and water-bearing characteristics follow.

The Lukachukai Member of the Wingate Sandstone is the lowest water-bearing unit of the multiple N-aquifer system. It is a fine-grained quartz arenite of eolian origin. It is approximately 300 feet thick across much of the study area but thins to the west and south of Black Mesa (Harshbarger et al., 1957). The Lukachukai is believed to be hydraulically separated from the Navajo Sandstone where overlain by the fine-grained rocks of the Moenave Formation and the silty facies of the Kayenta Formation. The Wingate Sandstone is the main water-bearing unit in the N-aquifer under the Western Navajo Uplands.

The Moenave Formation of Triassic(?) age overlies the Wingate Sandstone throughout most of the western half of the study area. It is divided into the Dinosaur Canyon Sandstone and Springdale Sandstone members. The former consists of a sequence of lenticular units, predominantly of fluvial origin and firmly

NOMENCLATURE and WATER-BEARING CHARACTERISTICS for the N-AQUIFER <sup>1</sup>					
SYSTEM	STRATIGRAPHIC UNIT		LITHOLOGY	WATER-BEARING CHARACTERISTICS	
JURASSIC	SAN RAFAEL GROUP	CARMEL FORMATION		SANDSTONE AND SILTSTONE	UPPER CONFINING UNIT
		GLEN CANYON GROUP	NAVAJO SANDSTONE		SANDSTONE
	KAYENTA FORMATION		SILTY FACIES	SILTSTONE AND SANDSTONE	GENERALLY NOT WATER-BEARING
			SANDY FACIES	SANDSTONE AND SILTSTONE	MINOR WATER-BEARING FORMATION
	MOENAVE FORMATION		SILTY SANDSTONE AND SANDY SILTSTONE	GENERALLY NOT WATER-BEARING	
TRIASSIC	UPPER	WINGATE SANDSTONE	LUKACHUKAI MEMBER	SANDSTONE	SECOND MOST IMPORTANT WATER-BEARING UNIT IN THE N-AQUIFER
			ROCK POINT MEMBER	SILTSTONE AND SILTY SANDSTONE	GENERALLY NOT WATER-BEARING
		CHINLE FORMATION		ALTERNATING SHALY UNITS AND SANDSTONE BEDS	LOWER CONFINING UNIT

<sup>1</sup> AFTER HARSHBARGER AND OTHERS (1957); CRAIG AND OTHERS (1955); COOLEY AND OTHERS (1969)

Figure 3-2. Nomenclature and water-bearing characteristics for the N-aquifer

cemented with calcareous cement (Harshbarger et al., 1957). The Springdale Sandstone Member is a fine- to medium-grained sandstone, also with a firm calcareous cement. The Moenave Formation is generally not considered water-bearing although it yields water to wells from fractures.

The Kayenta Formation, of late Triassic and early Jurassic age, is a redbed assemblage consisting of course- to fine-grained siliciclastics (Luttrell, 1987). It has not been formally divided into members, however, at least two distinct lithofacies have been identified within the study area. Harshbarger et al. (1957) identified a sandy facies and a silty facies of which only the former is considered water-bearing. Sargent (1984) differentiated nine facies of the Kayenta Formation based on lithology and sedimentary structure. There is considerable intertonguing with the overlying Navajo Sandstone, the Moenave Formation, and between the facies. The thickness of the sandy facies averages about 150 feet where present (Harshbarger et al., 1957). The undifferentiated Kayenta Formation increases in thickness to the southwest and grades into the silty facies which has been characterized as a series of intercalated siltstones, mudstones, and sandstones. This silty facies has typically not been considered part of the N-aquifer, rather, it is considered an aquitard that separates the overlying Navajo Sandstone from the water-bearing members of the Wingate.

The uppermost formation of the N-aquifer is the Navajo Sandstone of Jurassic and Triassic(?) age. It is the principal water-bearing unit of the multiple

aquifer system. The Navajo Sandstone consists of a medium- to fine-grained quartz arenite, weakly cemented with calcium carbonate. The lithology is consistent throughout its extent (Harshbarger et al., 1957). The Navajo Sandstone is exposed at land surface throughout much of the study area and typically displays large-scale crossbeds. The Navajo Sandstone is deepest and thickest under Black Mesa; as much as 2300 feet below land surface and as much as 1100 feet thick. The formation pinches out along the western and southern margins of Black Mesa. It is unconformably overlain by the confining Carmel Formation, and intertongues with the underlying Kayenta Formation in the northwestern portion of the study area. A structure contour map of the top of the Navajo Sandstone where buried is shown in Figure 3-3.

The N-aquifer is separated from other major aquifers in the region by the Triassic Chinle Formation below, and by the Late-Jurassic Carmel Formation above. The undifferentiated Chinle Formation is 300-1500 feet thick across most of the study area. The uppermost unit of the Chinle is the Owl Rock Member, composed of limestone and calcareous siltstone (Akers et al., 1958). Below this unit lies the Sonela Sandstone Bed and the Petrified Forest members, a thick sequence of siltstones and mudstones. The Carmel Formation is the upper confining bed of the N-aquifer and unconformably overlies the Navajo Sandstone across much of Black Mesa. Although the Carmel has been divided into the fossiliferous limestone facies and red silty facies, only the latter occurs within the

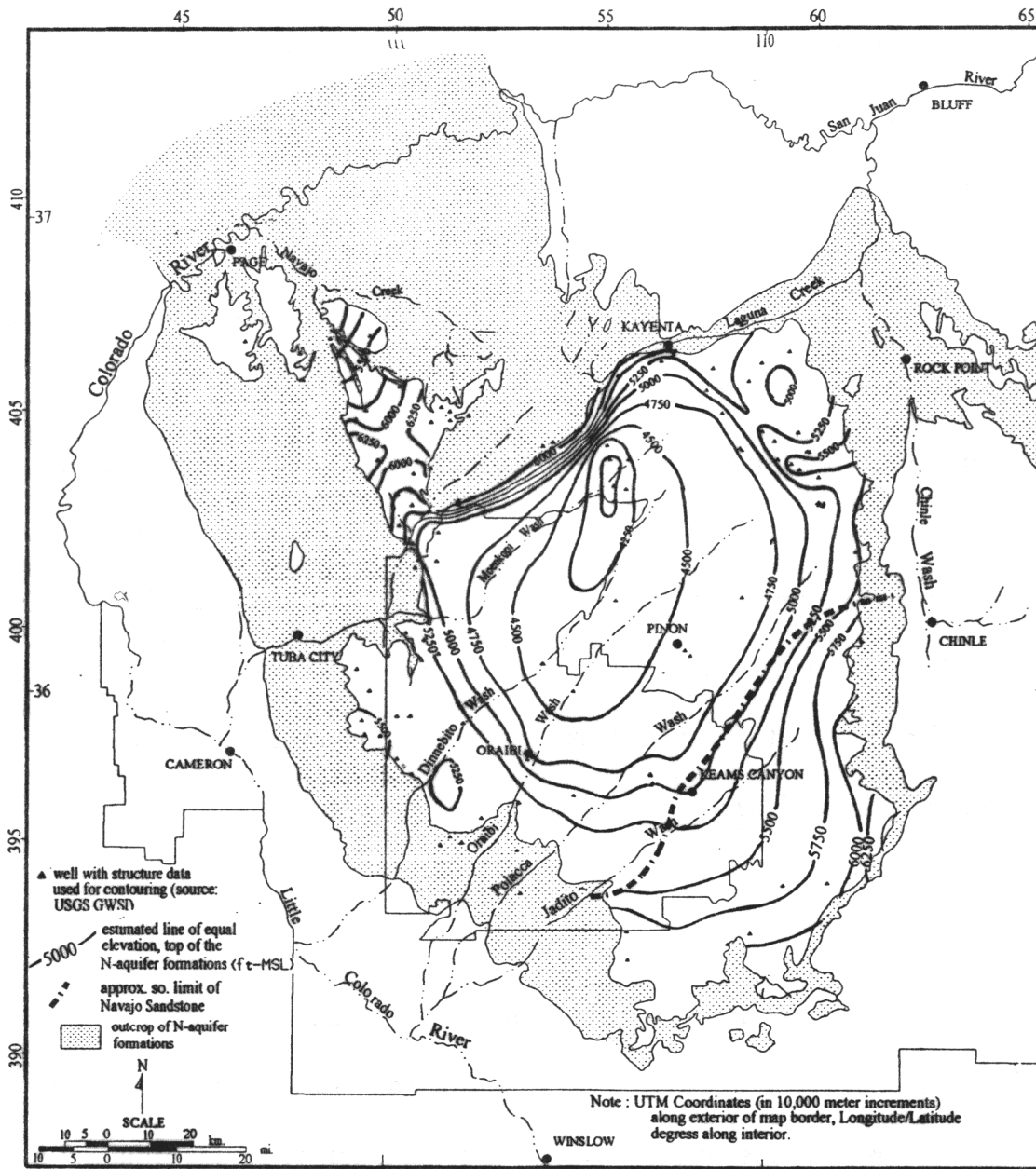


Figure 3-3. Structure contour map, top of the N-aquifer formations where buried, in feet-MSL

study area. It consists of resistant, ledge-forming sandstone beds separated by siltstone strata. In some areas, most notably along the extreme southwestern edge of Black Mesa near Coal Mine Canyon, the Carmel Formation exhibits a more sandy lithology and may not effectively retard the vertical movement of groundwater.

The N-aquifer is thickest in the northern portion Black Mesa where the Navajo Sandstone, the sandy facies of the Kayenta Formation, and the Lukachukai Member of the Wingate Sandstone are all hydraulically connected. To the south, the Moenave Formation and the silty facies of the Kayenta Formation separate the two main water-bearing units; the Navajo Sandstone and the Lukachukai Member of the Wingate Sandstone. Figure 3-4 shows the saturated thickness of the N-aquifer. The contours are approximate because the hydraulic connection between the various water-bearing formations is not well-defined.

### 3.1.2 Mineralogy

Knowledge of the mineralogy of the geologic formations that comprise the N-aquifer is useful to infer plausible sets of water-rock reactions that control the geochemistry. This chapter presents a compilation of results from mineralogic analyses in the available literature. The majority of the analyses were collected from three sources: 1) published reports presenting results of investigations into the economically recoverable mineral resources for reservations of the Navajo Nation

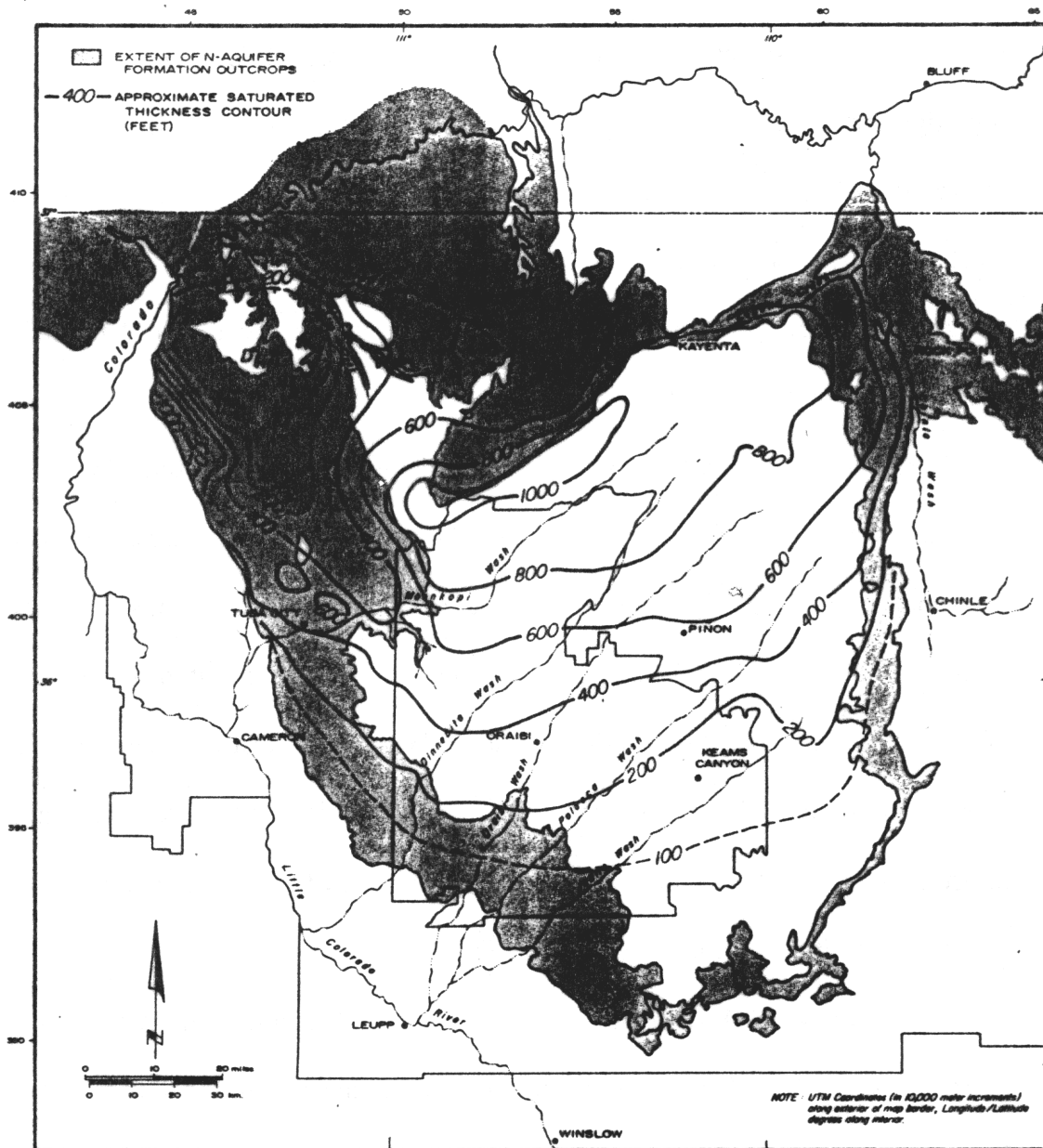


Figure 3-4. Estimated saturated thickness of the N-aquifer, in feet (modified from Eychaner, 1983)

and Hopi Tribe including metalliferous minerals and mineral fuels, nonmetallic minerals, and construction materials (Kiersch, 1955a,b,c); 2) U.S. Geological Survey investigations into the stratigraphy of the uppermost Triassic and Jurassic rocks of the region (Harshbarger et al., 1957); and 3) two unpublished Master's theses from Northern Arizona University (Dulaney, 1989; Luttrell, 1987). To assist the description of the mineralogy, the reader is again referred to the nomenclature chart previously presented in Figure 3-2.

The Lukachukai Member of the Wingate Sandstone is the lowest water-bearing unit in the N-aquifer and is a fine- to very fine-grained sandstone. Harshbarger et al. (1957) reported the absence of platy and micaceous minerals and an invariably low carbonate content. Kiersch (1955b) documented the occurrence of limestone deposits in the undifferentiated Wingate Sandstone. Dulaney (1989) reported sericite in the matrix for three Lukachukai/Wingate samples, identified the feldspars as plagioclase and orthoclase, and found clay fractions to contain 76 to 90 percent smectite with the remainder as illite.

Luttrell (1987) distinguished a subfeldspathic and plutonic feldspathic petrofacies, and a feldspathic volcanoclastic petrofacies within the silty facies of the Kayenta Formation. Quartz grains dominated the plutonic feldspathic petrofacies but it was also rich in feldspars and lithic fragments. The feldspars are mostly orthoclase and microcline, and the lithic fragments are mostly quartzose. For a limited area of northeastern Black Mesa, Luttrell described the subfeldspathic

petrofacies in which quartz comprises about two-thirds of the grains, with lesser percentages of feldspars and lithic fragments. The fine-grained sandstones, siltstones and mudstones in the southwestern study area were reported to contain considerable amounts of smectite, illite, quartz, feldspars and lithic fragments.

Kiersch (1955b) described the Navajo Sandstone as consisting of fine-grained quartz, weakly to firmly cemented with secondary quartz and less amounts of calcite, limonite, and kaolinite. He hypothesized that "the silica cement has been introduced and that it was derived from intrastratal solutions which dissolved silica from the grains at points of contact." On precipitation from solution, silica may have replaced a pre-existing bonding of carbonate. The authigenic silica cement was found to be more abundant at depths of 50-200 feet below the upper contact than for surface samples or for those within ten feet of the upper contact. Microscopic examination of samples from near the top of the formation revealed a greater degree of calcite cementation. He attributed this to either deposition from groundwaters charged with calcium carbonate from the soil horizon or overlying strata, or to a lesser degree, replacement of silica by calcite from intrastratal solutions. Accessory minerals such as plagioclase, varying amounts of limonite, minor magnetite, and biotite are present as "shreds" and subangular grains (Harshbarger et al., 1957).

The occurrence of significant limestone deposits as thin lenses in the Navajo Sandstone was documented by Baker, Dane and Reeside (1936) and later by

Kiersch (1955b). The lenses are usually small in extent, and occur particularly in the upper part of the formation, forming a resistant caprock. They are more abundant in the Navajo Sandstone than in the Wingate Sandstone (Baker, Dane and Reeside, 1936). These deposits consist of high-calcium limestone ranging from 91 to 96 percent pure. The magnesium carbonate content of the limestone is generally less than two percent by weight (Kiersch, 1955b).

Dulaney (1989) performed X-ray diffraction, thin sectioning and petrographic analyses of drill cuttings from 13 wells and seven surface samples from the Navajo Sandstone and Wingate Sandstone. Dulaney reported quartz to be the dominant mineral. Feldspars were also present, mostly plagioclase and orthoclase. Most feldspars showed signs of some alteration, most commonly to sericite, but illite and kaolinite were detected. Dulaney noted calcite as the dominant cement at depth but almost totally lacking in surface samples. However, scattered traces of blocky calcite indicated that calcite cement was once pervasive. Dulaney reported silica cement, primarily as quartz overgrowths, as the more common cement for surface samples. This is contrary to the findings of Kiersch (1955b) who reported silica as the dominant cement at depth. Dulaney detected smectite and illite clays by X-ray diffraction in surface samples and subsurface cuttings from the Navajo Sandstone. In almost all samples, smectite was the dominant clay mineral, with some illite present. Dulaney did not provide details concerning the types of smectite clay.

The Carmel Formation is a sandstone composed of fine-grained subangular quartz with calcareous cement and mica as an accessory mineral. The sandstone within the Carmel Formation contains about 30 percent soluble carbonate minerals. A study of heavy minerals indicates that magnetite is dominant, with muscovite and biotite present in most samples as a small fraction of the total heavy-mineral content (Harshbarger et al., 1957).

### 3.1.3 Groundwater Flow

Within northeastern Arizona, the N-aquifer discharges into three major river basins; the Little Colorado, the San Juan, and the Colorado. The divides that separate the portions of the aquifer that contribute groundwater flow for each of these rivers do not precisely coincide with the surface water drainage basins. Most groundwater in the N-aquifer originates as direct recharge in the eastern portion of the Western Navajo Uplands near Kayenta. Recharge also occurs along a topographical high running from near Kayenta southwest to north of Tuba City (Cooley et al., 1969). North and northwest of Black Mesa, the Navajo Sandstone is well-exposed and exhibits considerable jointing which facilitates recharge. This is also an area of high precipitation relative to other areas. At lower elevations, less precipitation and higher evaporation losses result in little recharge. Such areas include the southern leg of the Western Navajo Uplands where the Navajo Sandstone crops out.

Figure 3-5 shows the generalized potentiometric surface of the N-aquifer and the approximate limit of confined conditions. The source of the water level data used to generate this map was the U.S. Geological Survey's groundwater database. Direction of groundwater flow within the N-aquifer is to the south from areas of recharge, and southwesterly near the southwestern margin of Black Mesa (Cooley et al., 1969; McGavock and Levings, 1973). Discharge within the Little Colorado River Basin occurs as diffuse underflow to adjacent units including valley alluvium, and as surface flow in Moenkopi, Dinnebito, Oraibi, Polacca, and possibly Jadito washes which all lie within canyons or valleys dissecting Black Mesa to the southwest. In the Eastern Navajo Uplands, the aquifer discharges to springs and seeps, and into Laguna Creek and other tributaries to Chinle Wash within the San Juan River Basin. North of the groundwater divide in the Western Navajo Uplands, groundwater flow is to the northwest. Groundwater discharges into Navajo Creek and directly into the Colorado River and Lake Powell as underflow.

McGavock and Levings (1973) reported that evapotranspiration from outcrops represents another form of discharge. Brown and Eychaner (1989) estimated about 6650 AF/Yr is lost from the N-aquifer to evapotranspiration within the Black Mesa area.

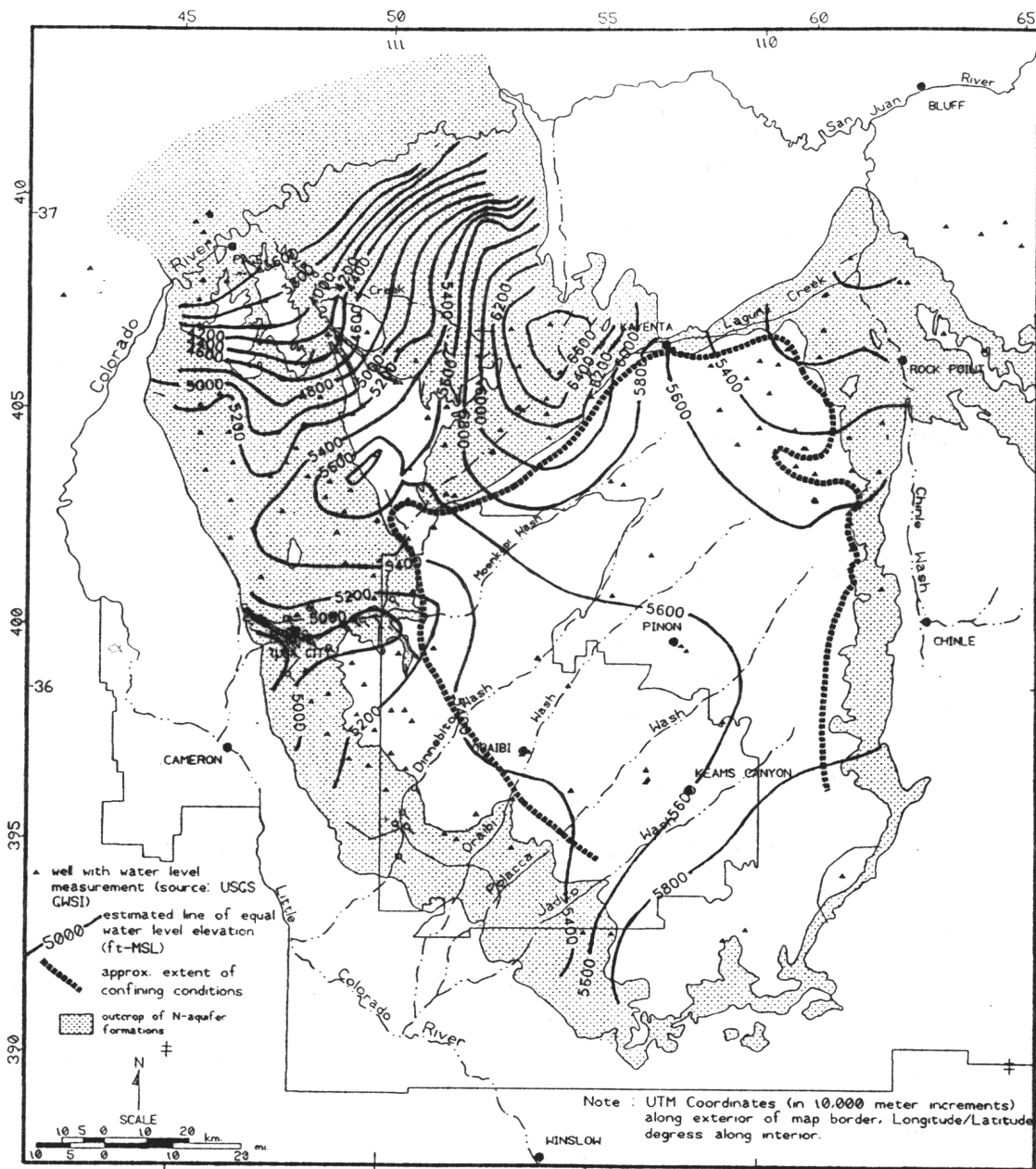


Figure 3-5. Estimated potentiometric surface of the N-aquifer, in feet-MSL

## 3.2 D-aquifer

### 3.2.1 General description

A brief description of the overlying D-aquifer is merited because of its potential hydraulic communication with the N-aquifer. The D-aquifer directly overlies the N-aquifer and is present throughout much of Black Mesa. Compared to the N-aquifer, the D-aquifer generally yields less water, and is smaller in its areal extent. The location of the undifferentiated D-aquifer within the study area is shown in Figure 3-6.

The D-aquifer is considered to include the Dakota Sandstone, the Westwater Canyon Sandstone Member of the Morrison Formation, the Cow Springs Sandstone, and in the northwestern portion of the study area, the Salt Wash Sandstone Member of the Morrison Formation (Cooley et al., 1969). The Morrison Formation is believed to act as an aquitard and bifurcates the water-bearing formations into upper and lower aquifers within the eastern half of Black Mesa subdivision and along the southern leg of the Western Navajo Uplands. Figure 3-7 shows the stratigraphic relationships and water-bearing characteristics of the units associated with the D-aquifer.

The D-aquifer is confined throughout most of its extent. It is separated from overlying water-bearing units by the Mancos Shale which consists of 450 to 650 feet of claystone and mudstone (O'Sullivan et al., 1972). The D-aquifer is underlain by the Carmel Formation and the medial silty member of the Entrada Sandstone

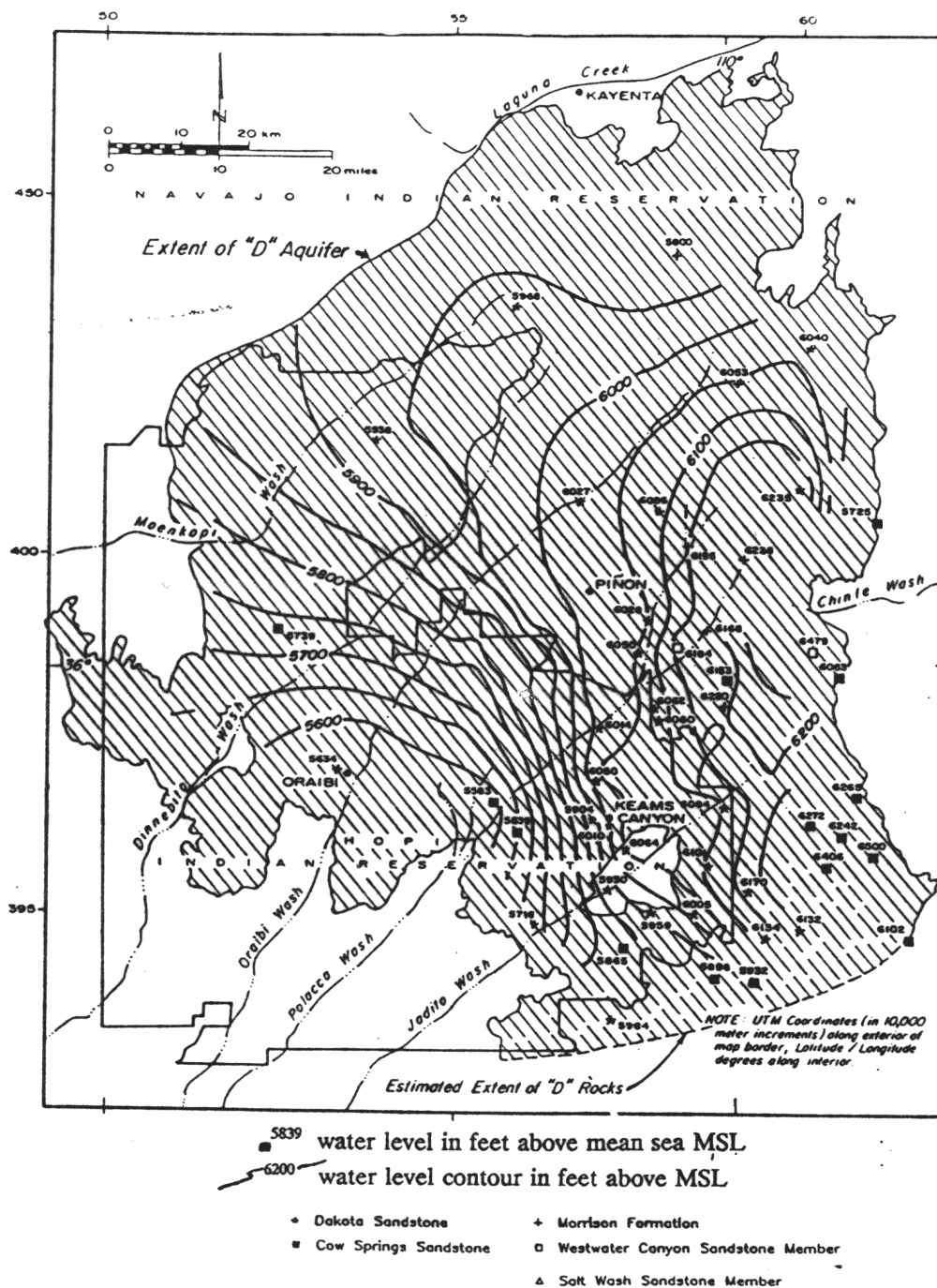


Figure 3-6. Location and estimated potentiometric surface of the D-aquifer, undifferentiated, in feet-MSL (source: Hydro Geo Chem, Inc.)

NOMENCLATURE and WATER-BEARING CHARACTERISTICS for the D-AQUIFER <sup>1</sup>				
SYSTEM	STRATIGRAPHIC UNIT	LITHOLOGY	WATER-BEARING CHARACTERISTICS	
CRETACEOUS	MANCOS SHALE	CHIEFLY CLAYSTONE TO SILTSTONE	UPPER CONFINING UNIT	
	DAKOTA SANDSTONE	SANDSTONES, SILTSTONE, AND COAL	PRIMARY WATER-BEARING UNIT IN THE D-AQUIFER	
JURASSIC	MORRISON FORMATION	BRUSHY BASIN MEMBER	MUDSTONE WITH SANDSTONE LENSES	
		WESTWATER CANYON MEMBER	SANDSTONE AND MINOR SHALY MUDSTONE	
		RECAPTURE MEMBER	SANDSTONE AND SHALY MUDSTONE	
		SALT WASH MEMBER	SANDSTONE AND MUDSTONE	
	COW SPRINGS SANDSTONE	SANDSTONE	SECOND MOST IMPORTANT WATER-BEARING UNIT IN THE D-AQUIFER	
	SAN RAFAEL GROUP	ENTRADA SANDSTONE	UPPER SANDY MEMBER	SANDSTONE
			MEDIAL SILTY MEMBER	SILTY SANDSTONE
LOWER SANDY MEMBER			SANDSTONE	
	CARMEL FORMATION	SANDSTONE AND SILTSTONE	LOWER CONFINING UNIT	

<sup>1</sup> AFTER HARSHBARGER AND OTHERS (1957); COOLEY AND OTHERS (1969)

Figure 3-7. Nomenclature and water-bearing characteristics for the D-aquifer

(Harshbarger et al., 1957). These units consist of 200 to 350 feet of siltstone and silty, very fine-grained sandstone which separate the D-aquifer from the underlying N-aquifer (Eychaner, 1983).

A potentiometric surface map of the undifferentiated D-aquifer is shown in Figure 3-6. Groundwater flow directions are from the east and northeast to the west and southwest. Saturated thickness ranges from 0 to as much as 700 feet, and is greatest to the north near the PCC leasehold. Groundwater discharges from the D-aquifer as underflow to the west and to the southwest into adjacent units. To a lesser degree, the D-aquifer also discharges to the north into adjacent units, and as diffuse seepage and spring flow to washes dissecting the system. The major washes are Jadito, Polacca, Oraibi, Dinnebito and Moenkopi to the west and southwest, and Steamboat Wash to the southeast.

Water level differences between the D- and N-aquifers indicate a downward vertical hydraulic gradient. The difference in head is as much as 600 feet in some areas, most notably within eastern Black Mesa. Near the PCC leasehold, the difference in water levels is about 240 feet. While such a large gradient illustrates the potential for downward leakage, it also implies limited hydraulic communication. Water level differences are smallest along the western limit of the D-aquifer. In this area, the D-aquifer discharges to springs and seeps, and some groundwater flow probably infiltrates to the west beyond the limits of the Carmel Formation and silty facies of the Entrada Sandstone. In these areas, groundwater

that is not lost to evaporation most likely enters the underlying N-aquifer. Localized leakage may also exist, either through mutual fracture and fault systems, by induced vertical gradients from groundwater pumping, or by mechanisms related to well construction.

## CHAPTER 4

### SURFACE WATER HYDROLOGY

The purpose of this chapter is to provide an overview of the surface water hydrology for Moenkopi and Dinnebito washes. Estimates of median baseflow discharge for Moenkopi Wash are derived using available streamflow discharge measurements. The distribution of baseflow and the longitudinal discharge profile is characterized. A more detailed description of the historical data and the statistical approach used to estimate baseflow is provided in Appendix A.

#### 4.1 General Description

Moenkopi Wash drains an area of approximately 2256 square miles and Dinnebito Wash, an area of 722 square miles. The length of the main channel of Moenkopi Wash is about 90 miles from headwaters to the confluence of the Little Colorado River. That of Dinnebito Wash is 95 miles. The Dinnebito Wash watershed is narrow and centers about the main streamcourse. Figure 4-1 shows the watershed areas for each wash.

Streamflow in both drainages is characterized by brief but high peak flows in response to summer monsoons and extended dry periods when evapotranspiration losses and diversions for irrigation and stock watering exceed streamflows. Large-scale winter frontal systems produce long-duration low intensity

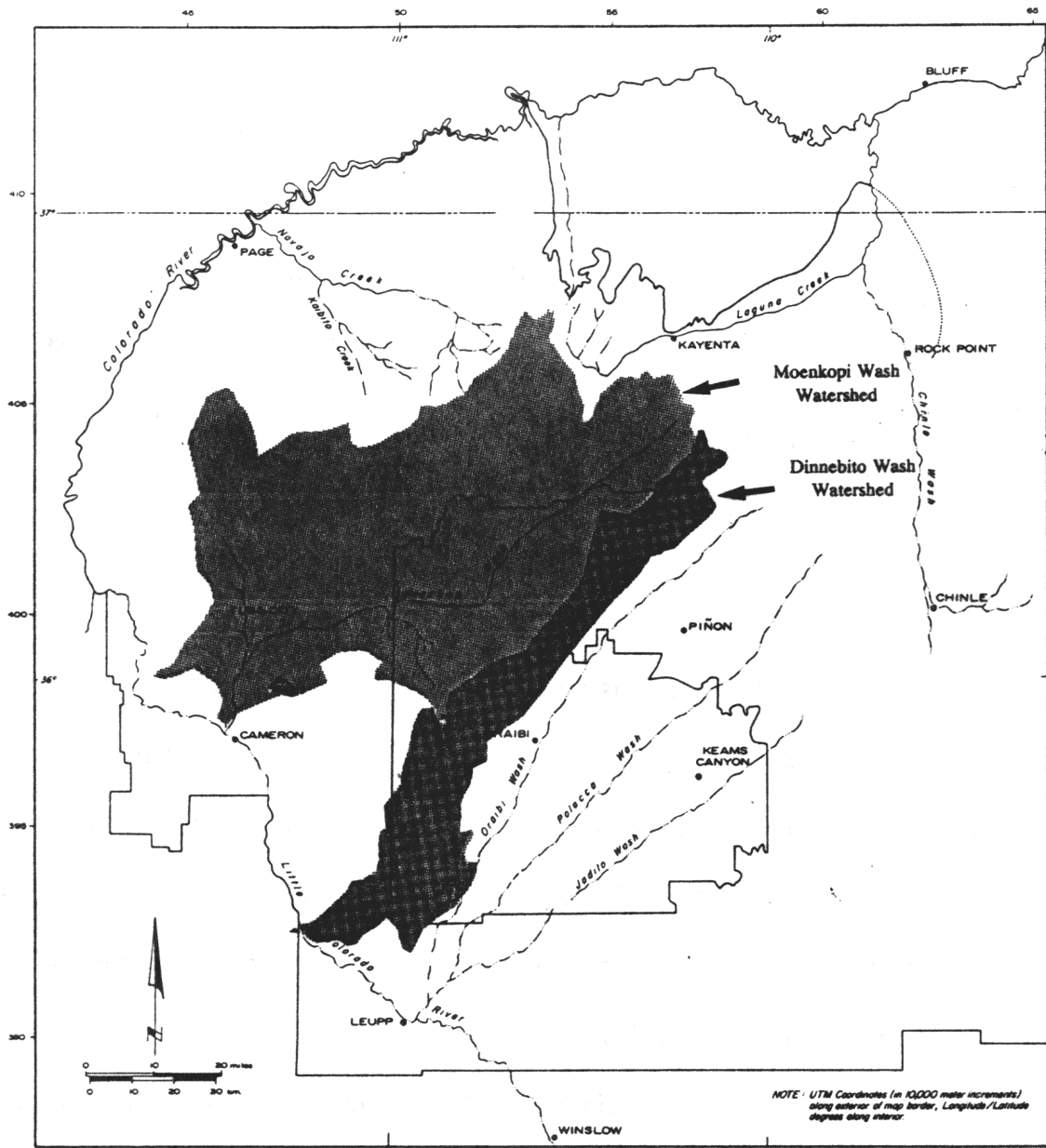


Figure 4-1. Watersheds for Moenkopi Wash and Dinnebito Wash

precipitation, most of which is retained by surficial deposits and permeable bedrock units. During the winter months, low-flows are sustained by regional aquifer discharge responding to hydraulic gradients. Perennial reaches exist along most of these southwestern washes. The length and magnitude of the low-flows depend on seasonal fluctuations in evapotranspiration losses and long-term natural arroyo aggradation and degradation processes.

Storm runoff within these large watersheds may be considered discontinuous for several reasons. Runoff originating in the headwaters typically does not reach the lower basin, with the exception of large storms. Water is removed along the streamcourse by transmission losses from infiltration and evapotranspiration. Storm runoff is also affected by surface water impoundments installed and maintained by PCC. By 1985, approximately 256 square miles of Moenkopi Wash watershed were controlled by 153 surface water impoundments, and 53 square miles were controlled within the Dinnebito Wash watershed (OSMRE, 1989). The small amount of storm water that seeps around the dams and embankments most likely does not reach distant downstream segments. The effect of this diminished streamflow on alluvial water levels, natural channel aggradation and degradation processes, riparian vegetation, and wildlife and stock watering has not been quantified.

Peak discharge for the southwestern washes varies widely as indicated by streamflow records for Moenkopi Wash. Annual peak discharge for the period 1974 to 1989 ranged from 262 cfs in 1978 to 10,100 cfs in 1983. The maximum

recorded flow on Moenkopi Wash for the period of record is 15,100 cfs measured on August 4, 1929 at gauge 1280. The average annual volume discharge is 7600 AF/Yr (gauge 1260). A more complete summary of streamflow statistics for Moenkopi Wash was prepared by the U.S. Geological Survey using streamgauge records and is presented in Appendix B. Records of streamflow discharge could not be located for the other southwestern Black Mesa watersheds located within the study area.

Streamflows along the washes are fed by four processes; direct rainfall to the free water surface, rainfall runoff or overland flow, subsurface stormflow through shallow highly permeable soils, and groundwater discharge. For the purposes of this report, the latter is termed baseflow and is defined as *the component of streamflow that is derived from direct discharge from the regional aquifer*. In areas where the canyons broaden and valley alluvium has formed, an alluvial aquifer may exist. These shallow aquifers are probably in direct hydraulic communication with the regional aquifer and the stream channel where it incises the alluvium. Water levels are sustained by direct regional aquifer discharges to the alluvium and, to a lesser degree, by sporadic lateral or overland infiltration during runoff events that result in elevated stream stage. During baseflow conditions, both direct regional aquifer discharge, alluvial aquifer discharge, and bank-storage releases may contribute to flow. The latter two contributions are small relative to regional aquifer discharges because of the limited areal extent of the alluvial aquifers.

Cooley et al. (1969) discussed the nature of perennial flows within the study area with specific reference to baseflow in the southwestern washes. The perennial reaches were reported to be fed mainly by groundwater from the Navajo and Wingate Sandstones. Although few springs are visible at the stream level, flows in the canyons increase downstream by seepage at the base of the sandstone canyon walls. A similar phenomenon was observed along gaining reaches of both Moenkopi and Dinnebito washes during this investigation. Only one spring, Quicksand Spring (location 22, Plate 1), was observed near the start of baseflow in Moenkopi Wash, and only one for Dinnebito Wash, named Dinnebito Spring (location 30, Plate 1). Along Moenkopi Wash, quicksand was observed near the base of sandstone cliffs as well as in the channel above the confluence with Begashibito Wash. Liquefaction of the alluvial sediment is suggestive of upward and lateral discharge of groundwater and is consistent with the observations by Cooley et al. (1969).

Simple statistical analyses were performed to quantify baseflow using existing streamflow records for Moenkopi Wash. The USGS has operated several streamflow gauging sites along Moenkopi Wash, most near or below the village of Moenkopi. Unfortunately, the reliability of the reported low-flow discharge measurements at these gauges is poor and records for stations without overlapping periods of operation may not be comparable.

An analysis of streamflow records shows that for a period between mid-June and late-September, the wash is dry or streamflow is below the detection limit at the gauge. Only streamflow records for several winter months provide baseflow measurements that do not appear to be influenced by evapotranspiration, storm runoff, snowmelt, or diversions. Streamflows recorded for the months of December, January and February appear to be least affected by the aforementioned processes. The median monthly discharge for these three months is 3.1 cfs for the period of record.

As will be addressed in a later section, baseflow originates along a reach ending about 13 miles upstream of the USGS gauge 1260. Therefore, the estimates of baseflow discharge may reflect some transmission losses. The reader is referred to Appendix A for a more detailed description of the availability and reliability of USGS streamflow records and details of the statistical analysis.

#### 4.2 Distribution of baseflow

Cooley et al. (1969) reported that fluctuations in the stream regimen during historical time included changes in the length of perennial reaches of streams entrenched in arroyos, and a general decline in the magnitude of streamflows. The perennial reach of Moenkopi Wash during 1909-1913 was longer than during 1950 to 1960. Cooley speculated that in some areas the extended reaches were a result of trenching of arroyos below the water table. Perennial reaches were also

observed on Dinnebito, Polacca and Jadito Washes during 1950-1960. The extent of these perennial reaches as reported by Cooley et al. (1969) is shown in Figure 4-2.

Aerial photographs from 1934, 1955 and 1980 were reviewed in order to map the historical distribution of perennial reaches. These photographs are archived at the U.S Bureau of Indian Affairs in Albuquerque, New Mexico. In each photo, the extent of baseflow was remarkably similar. The upstream limit of baseflow in all photos for each wash coincided precisely with the outcrop of the Navajo Sandstone. This observation strongly suggests that the N-aquifer is the principal source of baseflow along these washes.

During the field activities conducted for this investigation, continuous surface flow was observed along Moenkopi Wash from the water caves downstream to below the U.S. I-89 highway overpass. Flow was observed along Dinnebito Wash from one mile upstream of Dinnebito Spring to about six miles downstream of Sand Springs. The start of observed baseflow during the period February to March, 1990 coincides with the outcrop of the Navajo Sandstone as is shown in Plate 3 and Figure 4-3 for Moenkopi and Dinnebito washes, respectively.

Streamflow measurements were taken at most surface water sampling locations along Moenkopi and Dinnebito washes in order to assist the identification of gaining and losing reaches. Velocity and depth of flow measurements were performed with a pygmy meter and wading rod. Velocity measurements were taken

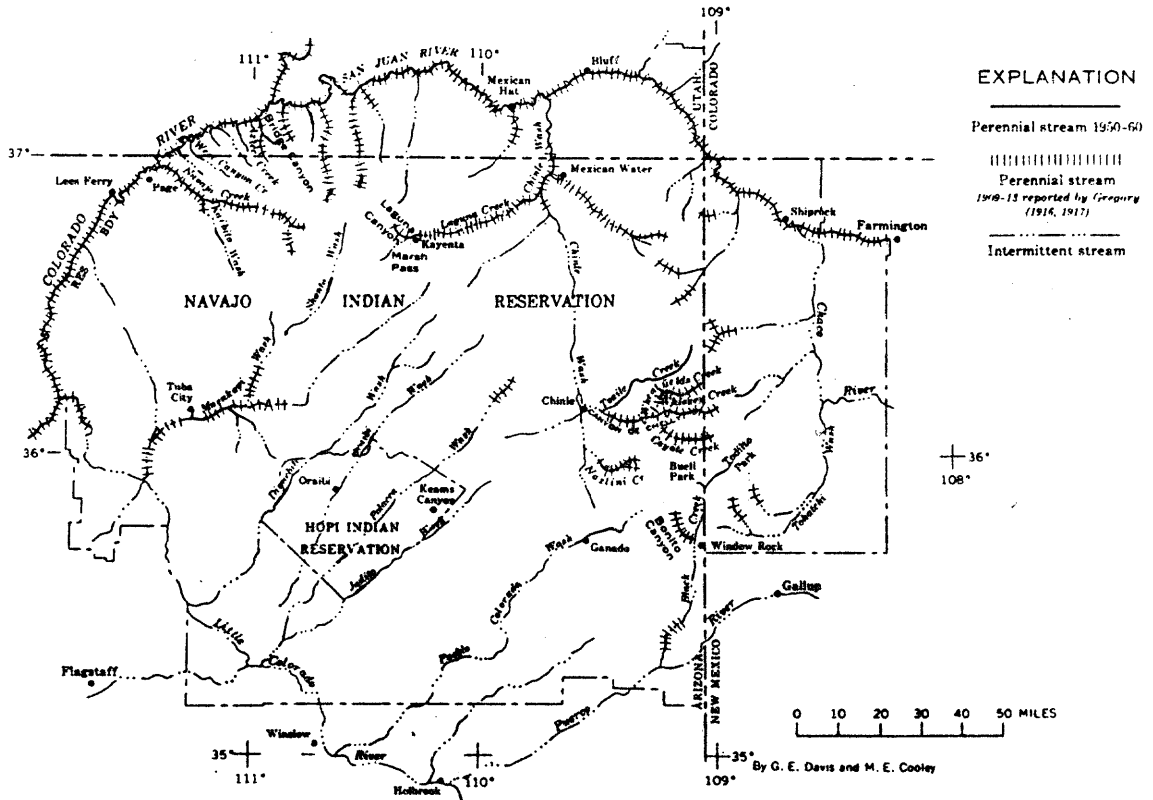


Figure 4-2. Map showing perennial streams during 1903-13 and 1950-60 (from Cooley et al., 1969)

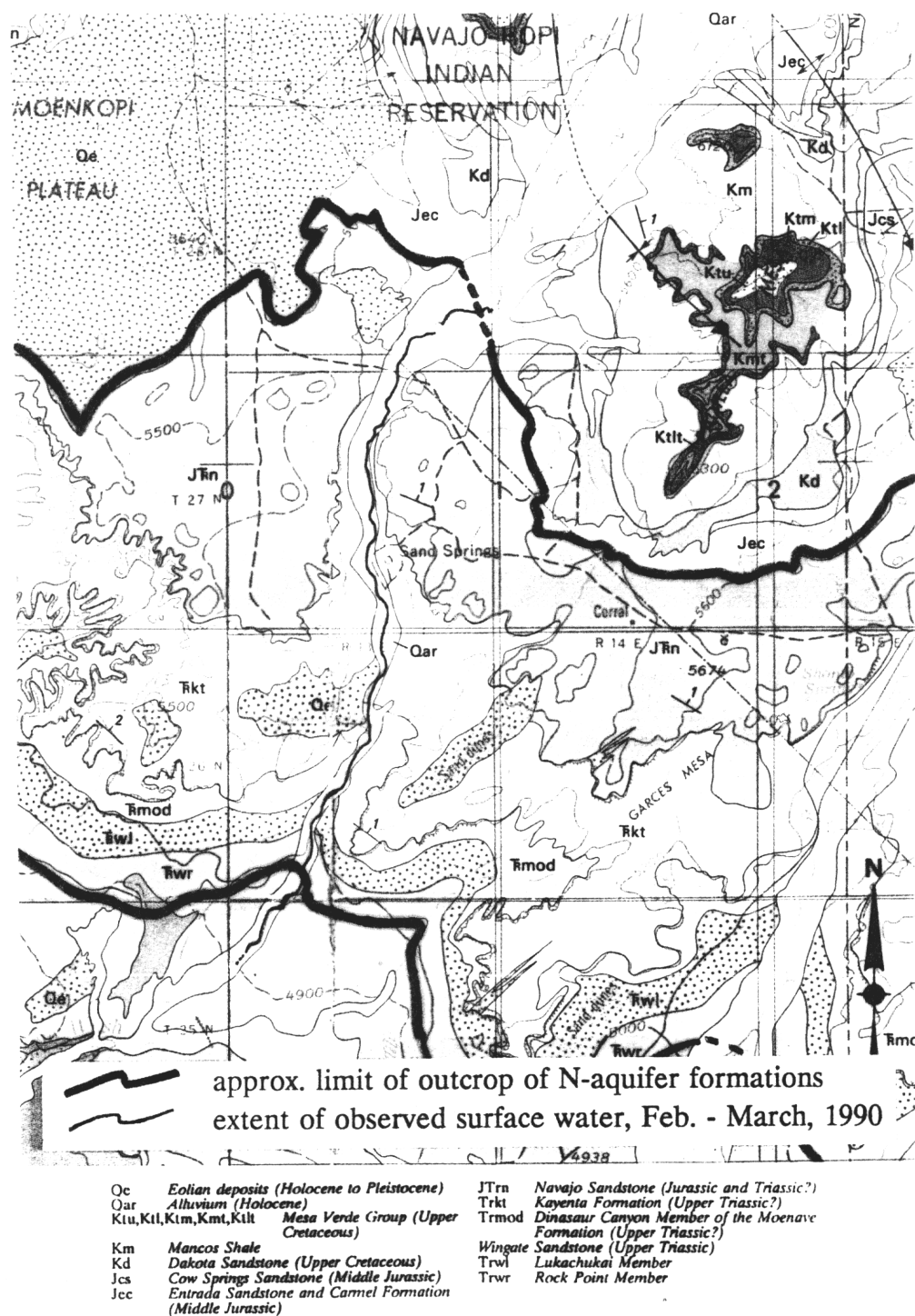


Figure 4-3. Surface geology along Dinnebito Wash  
 (base from Haynes et al., 1978)

at 0.2 and 0.8 times the total depth of flow when possible, and at 0.6 times the depth of flow when shallow. Measurement interval across the stream was typically 0.5 feet. Current meter readings were converted to discharge values using the rating table and the midpoint method. A detailed description of the methods and procedures used for the gauging of streamflow is contained in Hydro Geo Chem (1990).

Streamflow measurement errors for both washes may be attributed largely to channel instability and disturbance during gauging, pygmy meter accuracy, low-flow precision. Occasional ice jamming during early morning measurements may have influenced the rate and volume of flow passing the measurement location. Discharge error is subjectively estimated to be  $\pm 0.5$  cfs.

Figure 4-4 shows the measured streamflow profile along Moenkopi Wash with measurement dates, locations and reported daily mean streamflow for USGS station 1260. Figure 4-4 illustrates that flow along Moenkopi Wash rises sharply below the water caves and continues to increase in discharge to the confluence with Coal Mine Canyon, below which, streamflow gradually declines. Downstream of the highway I-89 overpass below Tuba City, flow diminishes rapidly. The largest gains in baseflow occur within the first six miles of perennial flow. The gain in baseflow along this reach is approximately 0.4 cfs per mile. Only several minor tributaries feed Moenkopi Wash through this reach, and all were dry during the field inspection. Begashibito Wash contributes approximately 0.9 cfs. Assuming

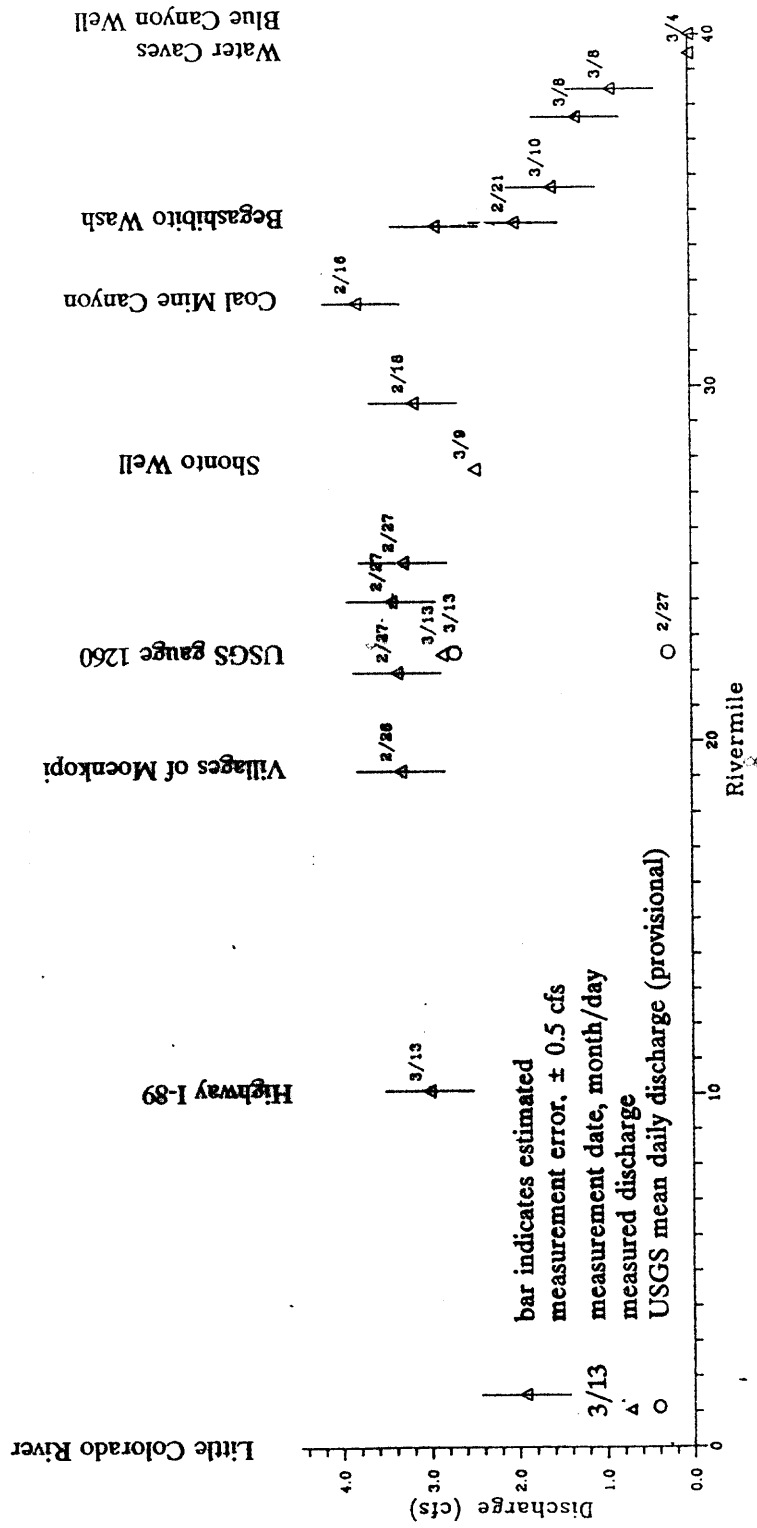


Figure 4-5. Streamflow profile along Moenkopi Wash, February-March, 1990

that the discharge profile in Figure 4-4 depicts representative conditions, the majority of baseflow along Moenkopi Wash is derived above the confluence with Begashibito Wash, and all baseflow is derived above the confluence of Coal Mine Canyon.

The streamflow discharge measurement for March 9, 1990 on Moenkopi Wash at Shonto Well (Figure 4-4) appears to be anomalous and may be affected by measurement error. At this site, the base of the wash is exposed Kayenta Formation. The streamflow profile had a large width and a shallow depth of flow. Much of the area of flow was too shallow for accurate velocity measurements using the pygmy meter and was therefore not gauged. The result is an underestimated value for discharge.

Streamflow discharge measured along Dinnebito Wash was typically less than 1.5 cfs. Low-flows, channel geometry and occasional ice jamming made accurate velocity measurements difficult to obtain. Slumping of the alluvial walls across the wash had impounded sections of the wash and created pools of standing water. Several pools were also located along Dinnebito Wash in aerial photographs from 1980. Streamflow measurements taken during the sampling period downstream of these pools, therefore, are more likely representative of seepage rates through, around and over these natural impoundment structures rather than cumulative upstream discharge from the N-aquifer. For these reasons, an analysis of the longitudinal profile for Dinnebito Wash was not performed.

Whether the streamflow measurements for this investigation are a true representation of baseflow depends on the degree of interference from storm flows, discharge of bank storage, losses to streamflows and temporal variations in N-aquifer discharges. Under ideal circumstances, all streamflow measurements and water samples would have been collected simultaneously to obtain a profile snapshot, but for logistic reasons, measurements were made throughout the course of the sampling period. Nevertheless, interference from storm flows and discharge of bank storage most likely did not significantly affect streamflows along Moenkopi Wash during the sampling period in that only minor variations in streamflow were recorded at the USGS gauge 1260. Also, evapotranspiration losses are minimal during the winter months. Lastly, the temporal variation in discharge from the N-aquifer during the short sampling period is negligible.

In summary, perennial flow along the southwestern washes starts at the outcrop of the Navajo Sandstone. This distribution has not varied significantly since 1934 according to aerial photography. The lack of distinct springs along gaining stream reaches suggests that groundwater discharge to the washes is diffuse.

Baseflow discharge along Moenkopi Wash at the village of Moenkopi was estimated to be about 3.0 cfs based on statistical analysis of streamflow discharge records. However, a streamflow survey conducted for this investigation suggests that the measurements reported for USGS gauging station 1260 may underestimate low flows. A streamflow profile along Moenkopi Wash was generated using

discrete streamflow measurements taken during February to March, 1990. This profile suggests that nearly all the observed baseflow is derived along a gaining reach located above Coal Mine Canyon. No appreciable increase in flow was observed downstream.

## CHAPTER 5

### DATA COLLECTION

Existing water quality data were collected from a variety of sources and an extensive water sampling program was conducted specifically for this investigation. This chapter presents descriptions of historical data sources, the water sampling program for the field investigation, sample identification, and laboratory analysis.

#### 5.1 Historical water quality data

Historical water quality data for groundwater were collected from a variety of sources. Analyses for water samples collected by Hydro Geo Chem, Inc. in 1988 and 1989 were made available for this study. These analyses included major and minor ions, and most samples were analyzed for isotopic composition. Chemical analyses were also available from the USGS WATSTORE database. Additional data were available from a report by Stetson Engineers for a water well on Black Mesa drilled for PCC, results from water sampling at the UMTRA site east of Tuba City, and other miscellaneous reports.

Dulaney collected his own samples for analysis while assisting Hydro Geo Chem during groundwater sampling. The results of chemical analysis presented by Dulaney in his thesis (Dulaney, 1989), although collected at the same time and location, should not be confused with analyses reported by Hydro Geo Chem.

## 5.2 Water sampling

The adequacy of the sampling program is critical to an accurate characterization and analysis of the geochemistry. This chapter outlines the field activities and water sampling program, sample identification and sample analysis. The water sampling protocol and procedures for streamflow discharge measurements employed in this investigation are described in Hydro Geo Chem (1990).

Field activities were completed during a 33 day period from February 15 to March 24, 1990. Travel to sampling sites required the most time. Moenkopi Wash is accessible by vehicle at only several road crossings. Most roads and jeep trails into the watershed are unimproved. Those sites visited along upper Moenkopi Wash required as much as six hours travel time each way. Travel was best accomplished in the early morning when roads were frozen. Remote sections of Moenkopi and Dinnebito washes were reached with the use of three-wheeled all-terrain vehicles. Approximately 55 miles of Moenkopi Wash was traversed in this manner. Most sections of Dinnebito Wash and lower Moenkopi Wash below the bridge for the State Highway 264 were easily reached.

Field analyses included measurements of pH, electrical conductivity (EC), alkalinity, dissolved oxygen and temperature. Alkalinity was measured using the HACH digital titrator, and dissolved oxygen with a HACH DR/2000 Spectrophotometer using manufacturer's recommended procedures. These chemical

parameters were measured for water samples from streams, springs and the shallow drive point wells in the alluvium (a drive point well is described later in this section) at all sites visited regardless of whether or not samples were collected. Field parameters were measured for 50 samples from 35 sites along Moenkopi and Dinnebito washes. Five sites along Moenkopi Wash were revisited for periodic sampling.

A total of 39 water samples were collected for analysis. The sampling locations are shown in Plates 1 and 2. Each sample included separate containers for major and minor cations and anions, and sulfur, oxygen and hydrogen isotopes. Samples were collected at ten locations for future tritium analyses. Sample collection and preservation protocols may be obtained from the author. Of the 39 samples, 26 were collected from flowing surface water, 8 from springs, 4 from drive points, and 1 from a developed spring equipped with a hand pump. Samples were collected at a total of 35 sites along both Dinnebito Wash and along Moenkopi Wash, and also on the following tributaries: Pasture Canyon and Pasture Canyon Reservoir, Coal Mine Canyon, Begashibito Wash, White Ruin Wash, Black Mesa Wash and Horse Corral Tributary (the latter is an unnamed ephemeral wash near Horse Corral Point which enters Moenkopi Wash about 1.5 miles downstream of the water caves).

Drive points were used for measuring vertical hydraulic gradients along the washes and sampling alluvial water along gaining reaches. Drive points consisted

of seven-foot sections of galvanized steel pipe tipped with a solid steel disposable point. These were driven into the ground with a portable post driver and then the pipe was retracted about five inches to allow water to enter. Drive points were installed at 12 sites to depths between three and nine feet within or near the channel. Impenetrable sandstone above the water table was commonly encountered. Water levels were allowed sufficient time to stabilize, requiring typically less than one hour. Field parameters for water samples were measured when drive points could be purged and samples were collected when water levels indicated an upward vertical hydraulic gradient.

The chemical analyses from the groundwater sampling program conducted by Hydro Geo Chem (HGC) were crucial to this investigation. Therefore, a brief description of the HGC sampling procedures is merited. HGC performed serial sampling of pH, EC and temperature with a closed system flow-through cell in order to obtain representative groundwater samples free from human contamination. Grab samples were collected once these parameters had stabilized. Additional parameters measured in the field included sulfate and sulfide, chloride, nitrate and nitrite, fluoride, ferrous iron and total iron, silica, dissolved oxygen and alkalinity. Sampling and analyses were performed for oxygen, sulfur and hydrogen isotopes (deuterium and tritium) and carbon-14. For a detailed discussion of the field measurements and sampling protocols, the reader is referred to Dulaney (1989) who assisted HGC with the groundwater sampling.

The sampling procedures and protocols are unknown for water analyses retrieved from WATSTORE.

#### 5.4 Sample identification

Sites visited and sampled during this study were assigned a location number of 1 through 35 corresponding to the order in which they were first visited. Samples were each assigned a unique name corresponding to the wash, site description, source type, and sample type. For example, a sample collected at location 12, Moenkopi Wash at White Ruin Wash, has a sample identification of MWWRW-X2. The X replaces either a C, A, S, D or T depending on the sample type (Cation, Anion, Sulfur isotopes, Deuterium/oxygen isotopes or Tritium). The 2 refers to the second sample collected at that location. Because specific identification of each sample is not always required nor practical for the plots and diagrams used in this report, samples were assigned a lower-case letter of s, p, or d corresponding to water samples from streams, springs, or drive points, respectively.

The groundwater chemical analyses presented in this report were collected from a wide range of sources with variable reliability. Because the sampling protocols and techniques are unknown for historical chemical analyses obtained from WATSTORE, it is useful to distinguish between sources. Numbering and identification used for chemical analyses was developed to permit this distinction. Groundwater samples collected during the recent HGC investigation (referred to

hereafter as HGC groundwater samples) are numbered between 0 and 100; historical water quality data other than HGC groundwater samples are assigned numbers of 101 or greater. An uppercase "N" is used for graphical representation of HGC samples, and a lowercase "n" is used for all other historical groundwater samples from the N-aquifer. The locations for the N-aquifer groundwater samples used in this study are provided in Appendix C.

### 5.5 Laboratory analysis

Water samples collected during this investigation were analyzed for the anions  $\text{SO}_4^-$ ,  $\text{Cl}^-$ ,  $\text{NO}_3^-$ ,  $\text{Br}^-$ ,  $\text{F}^-$  by the author in HGC's laboratory with a Dionex 2000i Ion Chromatography system following the manufacturer's recommended procedures. Samples were sent to Turner Laboratories (Tucson, Az.) for cation analysis, with duplicates sent to B.C. Laboratories (Bakersfield, Ca.). All HGC groundwater samples were analyzed for ions using the Dionex 2000i by HGC. Results of these analyses for samples from streams, springs and drive points are presented in Table D-1 in Appendix D. Water chemical analyses for the HGC groundwater samples and historical groundwater databases are presented in Table D-2.

Stable isotope ratio analyses for  $^{18}\text{O}/^{16}\text{O}$ ,  $\text{D}/^1\text{H}$  and  $^{34}\text{S}/^{32}\text{S}$  (hereafter denoted  $\delta^{18}\text{O}$ ,  $\delta\text{D}$ , and  $\delta^{34}\text{S}$ , respectively) were performed on all but one of the collected samples. Results are reported in ‰ (per mil) and calculated as:

$$\delta R_{\text{sample}} \text{‰} = \left[ \frac{R_{\text{sample}}}{R_{\text{standard}}} - 1 \right] \times 1000 \quad (1)$$

The standards used were SMOW (Standard Mean Oceanic Water) to calculate  $\delta\text{D}$  and  $\delta^{18}\text{O}$ , and the Cañon Diablo triolite for  $\delta^{34}\text{S}$ . Stable isotopes were analyzed by Geochron Laboratories (Cambridge, Ma.). Duplicates were analyzed at the Laboratory of Isotope Geochemistry, University of Arizona. Results of isotopic analyses for the wash samples are presented in Table D-3, and results from HGC groundwater samples in Table D-4.

Analytical accuracy was evaluated by the correlation between conductivity and total dissolved ions, and by charge balance. The correlation between conductivity and total dissolved ions for Moenkopi Wash and Dinnebito Wash samples together with the HGC groundwater samples is shown in Figure 5-1. Deviation of sample points from the regression line occurs from incomplete or inaccurate ion analyses, or when the sample is dominated by one anion. For example, chloride-dominated samples may plot above the correlation line and sulfate-dominated samples plot below the correlation line (Hem, 1985). Calculated charge balance errors between measured cations and anions for samples from streams, springs and drive points were less than 4 percent for lower Moenkopi Wash, and less than 6.5 percent for Dinnebito. Charge balances for the groundwater samples used in this study are generally better than 5 percent, with

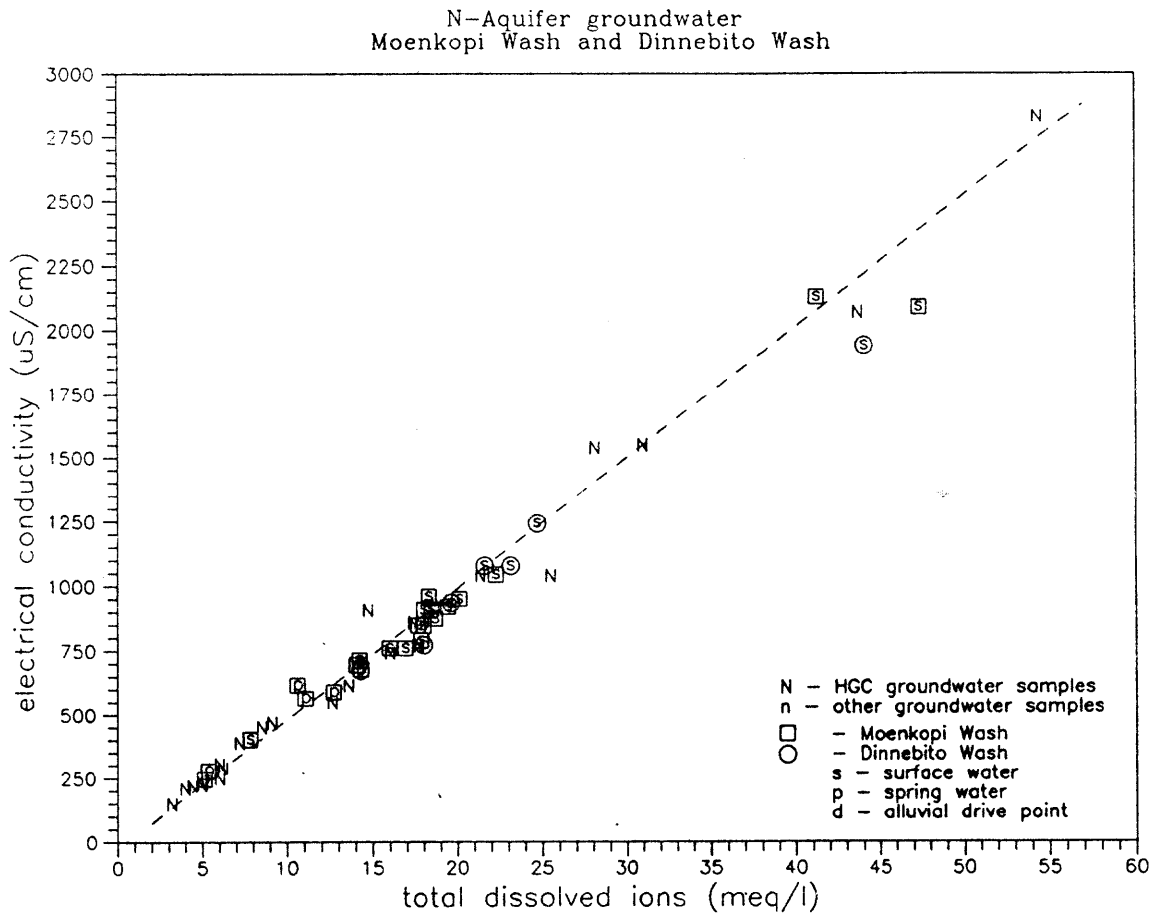


Figure 5-1. Electrical conductivity as a function of total dissolved ions for HGC groundwater samples and wash samples. Total dissolved ions was computed as the sum of equivalents for all measured anions and cations.

only a few exceptions. The computed charge balance error for each analysis is included in Tables D-1 and D-2.

Analytical precision for  $\delta^{18}\text{O}$ ,  $\delta\text{D}$ , and  $\delta^{34}\text{S}$  analyses, including sample preparation, is  $\pm 2\text{‰}$ ,  $\pm 0.2\text{‰}$  and  $\pm 0.4\text{‰}$ , respectively (personal communication, Geochron Laboratories., 1991). Split sample duplicates were submitted to Geochron Laboratories and to the University of Arizona Laboratory of Isotope Geochemistry. University of Arizona reported analytical precision of  $\pm 0.4\text{‰}$  for  $\delta^{18}\text{O}$ , and  $\pm 2.8\text{‰}$  for  $\delta\text{D}$ . Precision for the isotopic analyses for HGC groundwater samples is not known.

## CHAPTER 6

### GROUNDWATER GEOCHEMISTRY

#### 6.1 Introduction

A thorough understanding of the aqueous chemistry of the regional N-aquifer is prerequisite to examining surface water and groundwater interactions. Existing studies, although helpful, are not adequate to achieve the objectives of this thesis, therefore, a regional geochemical analysis for the N-aquifer was performed. This chapter presents an interpretation of the geochemistry of the N-aquifer that is consistent with the observed water quality. The interpretation includes discrimination of water types, and identification and evidence of the dominant reactions and reaction pathways. This chapter is concluded with a brief description of the water quality of the D-aquifer.

#### 6.2 Geochemistry of the N-aquifer

The description of the geochemistry of the N-aquifer is best presented in four sections, much in the order the investigation was performed. The first section is a general description of water chemistry in terms of chemical facies and the areal distribution of specific parameters. The second section describes a generalized conceptual model of the system followed by a more rigorous description of the dominant reactions. In the later, correlations are used in conjunction with the

stoichiometry of the suspected reactions to qualify the existence and role of the dominant reactions. Also, corrections are made to specific constituents in order to distinguish those reactions and processes not readily apparent.

The fourth section presents an analysis of the available isotopic data in the study area for the N-aquifer. This includes a discussion of the observed areal distribution of various isotopes and possible fractionation processes. Description of the quantitative analysis using geochemical modeling is presented separately in Chapter 8.

#### 6.2.1 General description of water quality

The N-aquifer has the lowest degree of mineralization of any major aquifer in the Black Mesa area. EC ranges from 20 to 5130  $\mu\text{S}/\text{cm}$ , with a median value of 363  $\mu\text{S}/\text{cm}$ . The water types vary throughout the aquifer. Four distinct hydrochemical facies are identified in Figure 6-1. The Na-HCO<sub>3</sub> (I) and Ca-HCO<sub>3</sub> (II) water types are dominant. These water types exhibit low EC and correspond to samples collected from the aquifer where confined and unconfined for types I and II, respectively. Type III samples are Ca-SO<sub>4</sub> with moderately high EC ranging from 860 to 1270  $\mu\text{S}/\text{cm}$ . These samples were collected from wells near the periphery of confined conditions and may be influenced by mixing with the overlying D-aquifer. Type IV samples range from Na-SO<sub>4</sub> to Na-Cl, exhibit high EC ranging from 1050-5200  $\mu\text{S}/\text{cm}$ , and may be influenced by localized evaporite

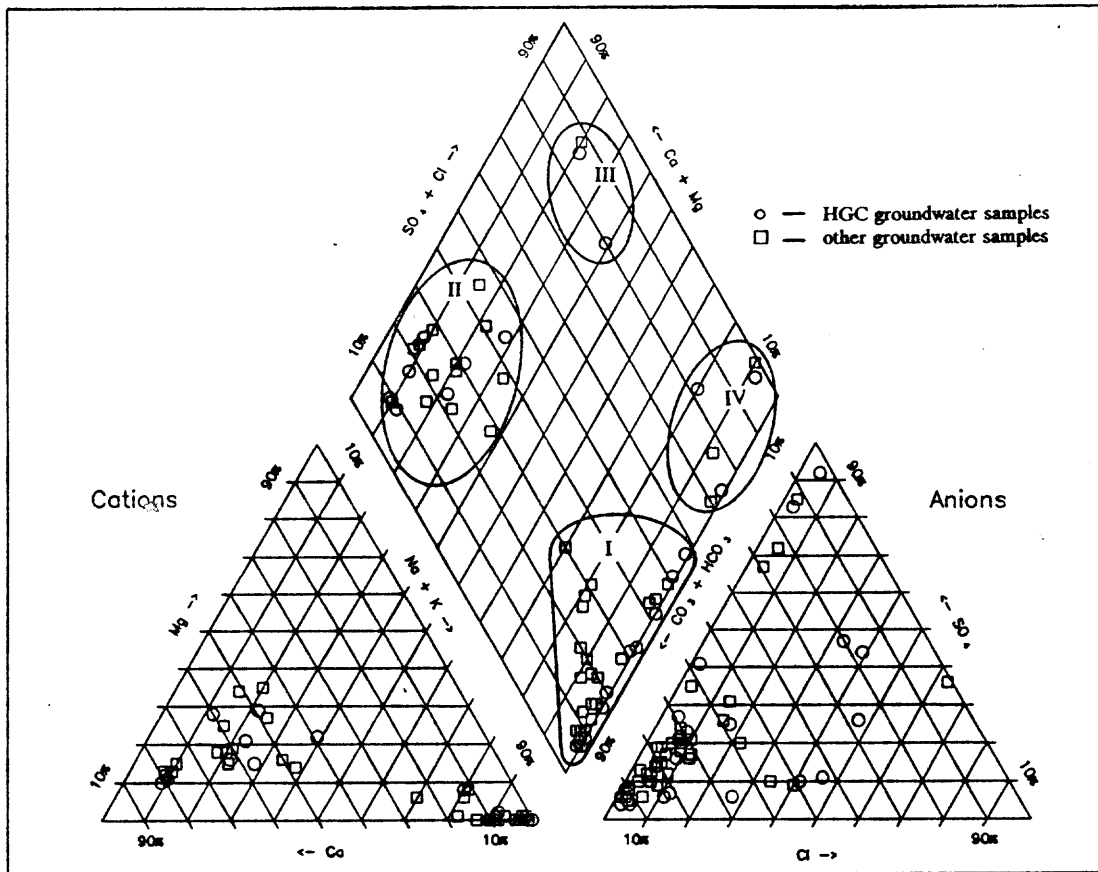


Figure 6-1. Trilinear diagram for N-aquifer groundwater samples. Numbered zones correspond to the four chemical facies.

dissolution or mixing with D-aquifer groundwater. This mixing may occur locally through leakage along fracture and fault systems or from regional discharge along the confined periphery. Type IV samples are anomalous and highly localized.

Appendix D contains maps showing the areal distribution of selected chemical constituents for the N-aquifer. Concentrations for  $\text{Ca}^{2+}$  and  $\text{Mg}^{2+}$  are much smaller in the confined system than in the unconfined system, however, the opposite is true of  $\text{Na}^+$ .  $\text{Na}^+$  in the confined system is typically higher than that found in unconfined areas. No identifiable trends exist in the distribution of  $\text{SO}_4^-$ . Alkalinity appears to increase toward the center of Black Mesa, especially in the vicinity of Keams Canyon. The pH is lowest in the unconfined areas and increases toward the center of Black Mesa and toward the southwestern washes.

### 6.2.2 Qualitative analysis

The following section presents a qualitative analysis of the geochemistry of the N-aquifer. First, a general description of the conceptual geochemical model is presented in order to provide some continuity for subsequent descriptions of individual reactions and processes. Second, specific reactions are examined in greater detail and evidence is presented for their existence and importance.

#### 6.2.2.1 *Conceptual model*

The majority of recharge to the N-aquifer occurs in the Western Navajo Uplands west of Kayenta, Arizona near the Betatakin National Monument. The rain and snowmelt entering the ground infiltrates the soil horizons and percolates to the underlying Navajo Sandstone. The  $\text{CO}_2$  generated by the decay of organic matter and by respiration of plant roots is dissolved by the water during infiltration. The resulting solution is acidic and can rapidly alter soils and geologic materials (Freeze and Cherry, 1979).

Under open system conditions, the total dissolved solids content increases rapidly as the  $\text{CO}_2$ -enriched groundwater dissolves minerals encountered during percolation and along the saturated flow path. From the outset, the water is a  $\text{Ca-HCO}_3$  type (type II, Figure 6-1) with a pH of about 7.5. Alkalinity increases due in part to calcite dissolution. The solution rapidly reaches saturation with respect to calcite. A slight supersaturation early along the flow path may occur due to rapid degassing of  $\text{CO}_{2(\text{aq})}$  deeper in the unsaturated and saturated zones, and increasing temperature which decreases calcite solubility. Kiersch (1955b), Harshbarger (1957) and Dulaney (1989) all reported calcite cement within the Navajo Sandstone.

Early along the flow path, some weathering of silicate minerals occurs, mostly incongruent dissolution of aluminosilicates. The result is, in part, formation of sodic clays, consumption of  $\text{CO}_{2(\text{aq})}$ , rising pH, and precipitation of a silica phase.

This silica phase may replace the preexisting calcite cement in the sandstone matrix (Kiersch, 1955b). The dominant primary mineral is plagioclase which may be altered to produce kaolinite and smectite clays. Kaolinite may also be altered to illite as progressively more  $Mg^{2+}$  is released upon the incongruent dissolution of biotite to kaolinite. This weathering is kinetically controlled under open system conditions, but under confined conditions is also limited by  $CO_2$  availability.

The northern outfacing cliffs of Black Mesa mark the transition of the unconfined to the confined N-aquifer immediately south of the recharge ridge. The top of the Navajo Sandstone dips to nearly 2300 feet below land surface. The aquifer increases in thickness to nearly 1200 feet. Closed system conditions are encountered as groundwater moves south into the confined system and the supply of atmospheric  $CO_2$  is removed. Continued calcite dissolution and, to a lesser degree, silicate weathering consumes additional  $CO_{2(aq)}$  and the partial pressure decreases to  $10^{-4}$  bars. The groundwater temperatures rise with depth to 35 °C.

Ion exchange is the primary process governing changes in the water chemistry beneath Black Mesa. Clays provide the exchange sites and are predominantly sodic, as evidenced by abundant cation exchange for  $Na^+$ . The principal ion exchange reactions are Ca-Na, Mg-Na and Ca-Mg with some additional monovalent exchange. As the Ca- $HCO_3$  type groundwater undergoes ion exchange, both  $Ca^{2+}$  and  $Mg^{2+}$  concentrations drop sharply to typically less than 1 mg/l, with concomitant increases in  $Na^+$  concentrations. These reactions, coupled

with calcite dissolution, result in a Na-HCO<sub>3</sub> water type (type I, Figure 6-1) with high pH's, commonly exceeding nine.

Dissolution of calcite cement also occurs within the confined system. The dissolution reaction is limited by solubility and CO<sub>2</sub> availability. Initially, calcite may be precipitated, most likely driven by a gradual warming of calcite-saturated groundwater. However, Ca-Na and Ca-Mg exchange reduces the activity product of calcite thus permitting continued dissolution. This results in further consumption of CO<sub>2(aq)</sub>, an increase in alkalinity and pH, and continued ion exchange.

Local gypsum dissolution may occur but it is regionally not significant. Most elevated SO<sub>4</sub><sup>=</sup> concentrations are accompanied by a Cl<sup>-</sup> increase indicating mixing with groundwater from the D-aquifer. The irregular distribution of elevated SO<sub>4</sub><sup>=</sup> in the confined system suggests leakage associated with well construction rather than hydrogeologic processes. The SO<sub>4</sub><sup>=</sup> that enters the N-aquifer may be reduced to HS<sup>-</sup> if the environment is sufficiently depleted in oxygen.

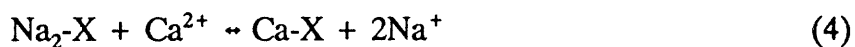
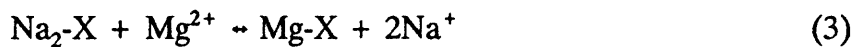
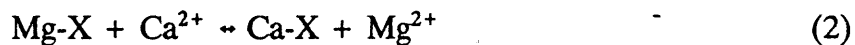
As groundwater leaves closed system conditions and enters the unconfined N-aquifer along the southwestern washes, it may be exposed to the atmosphere, undergo mixing with infiltrating meteoric water, or mix with discharge from the overlying D-aquifer. The atmosphere provides a source for CO<sub>2</sub> to participate in dissolution reactions. Calcite dissolution proceeds to equilibrium, and Ca<sup>2+</sup> and alkalinity rise. Despite these changes, the groundwater retains the high Na<sup>+</sup> concentrations from ion exchange in the confined system. Much of the groundwater

eventually surfaces in the form of springs and baseflow to the southwestern washes. The geochemical processes associated with N-aquifer interaction with the alluvium are discussed in Chapter 8.

Groundwater that does not enter the confined system evolves under open system conditions and remains predominantly a Ca-HCO<sub>3</sub> type. The chemical composition is established early along the flow path. Calcite equilibrium is the dominant process. Without the influence of intensive cation exchange, Na<sup>+</sup> concentrations remain small and are attributable to dissolution of NaCl. The SO<sub>4</sub><sup>=</sup> concentrations are higher than those found in the confined system and due largely to gypsum dissolution. The dominant physical processes in the unconfined system are mixing with atmospheric recharge and evaporative concentration. As compared to the confined system, the unconfined N-aquifer is typically shallower and hydraulic gradients are larger, therefore, residence times are probably smaller.

#### 6.2.2.2 Ion exchange processes

Ion exchange reactions are responsible for the two distinct chemical facies that correspond to the confined and unconfined systems in the N-aquifer. The dominant exchange reactions are represented by the following equations:



where the  $-X$  denotes exchange sites. Additional ion exchange including  $K^+$  may also occur.

Because the sum of reactions 2 through 4 is equal to reaction 4, the presence of these ion exchange reactions should be indicated by a strong relationship between  $Ca^{2+}$  and  $Na^+$  concentrations. However, reactions other than ion exchange affect the concentrations of these constituents and tend to obscure this relationship. For example,  $Na^+$  concentrations are regulated throughout the N-aquifer not only by ion exchange, but also by halite dissolution and weathering of aluminosilicates. To isolate the effects of ion exchange processes, therefore, it was first necessary to identify the influence by other reactions involving mutual constituents. Several assumptions were necessary to derive the corrections. First, the contribution of cations to solution from the weathering of primary silicates is presumed to be small relative to other processes. Second, halite dissolution is assumed to be the sole source for  $Cl^-$  in the N-aquifer, and third,  $Cl^-$  is assumed to be conservative in solution.

Two trends become apparent by comparing  $Ca^{2+}$  to  $Na^+$  as in Figure 6-2. Trend A samples exhibit high  $Na^+$  concentrations with variable  $Ca^{2+}$  and trend B samples exhibit high  $Ca^{2+}$  with variable  $Na^+$  concentrations. As indicated by Figure 6-3, most of the samples from trend B have  $Na^+$  concentrations typically less than 20 mg/l, follow the theoretical halite dissolution line, and are from wells sampled in the unconfined portion of the N-aquifer.

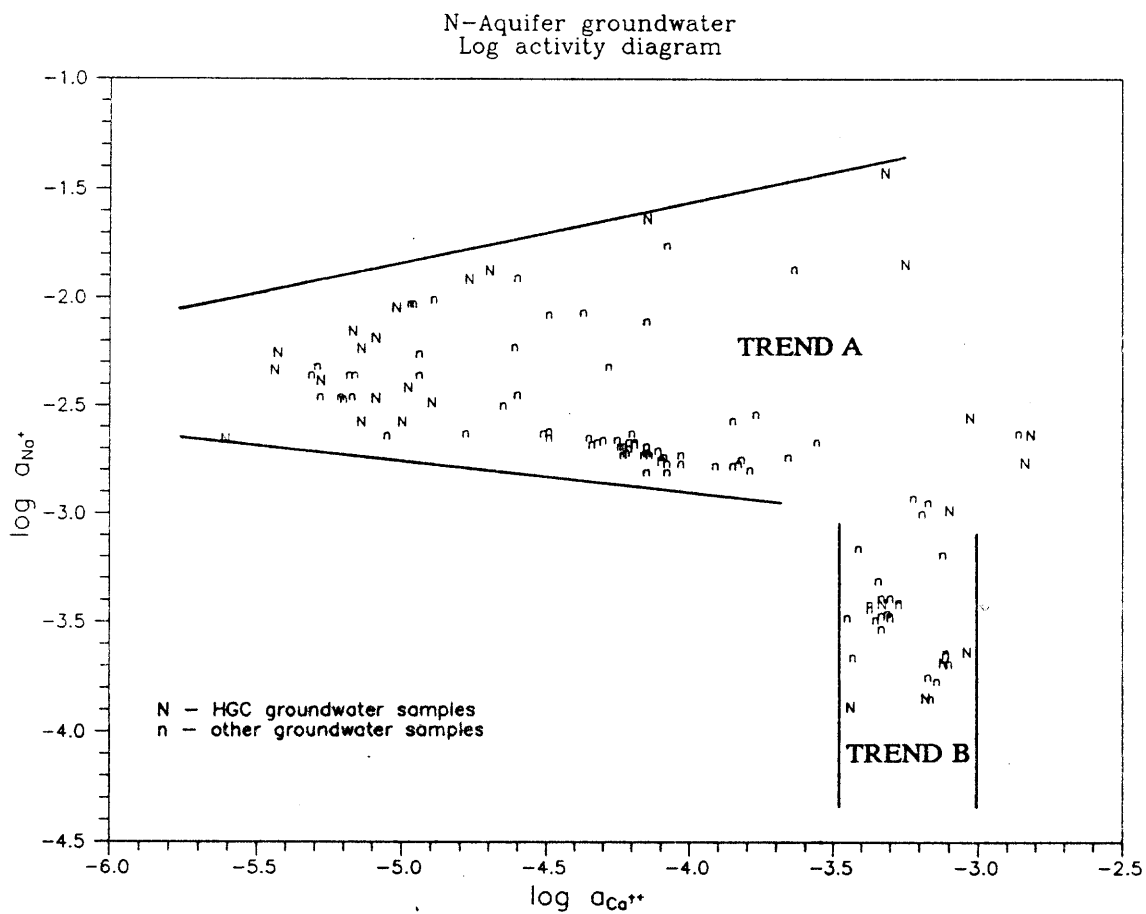


Figure 6-2. Log-activity diagram for  $\text{Na}^+$  as a function of  $\text{Ca}^{2+}$ , N-aquifer. Trends A and B correspond to groundwater samples from the confined and unconfined systems, respectively.

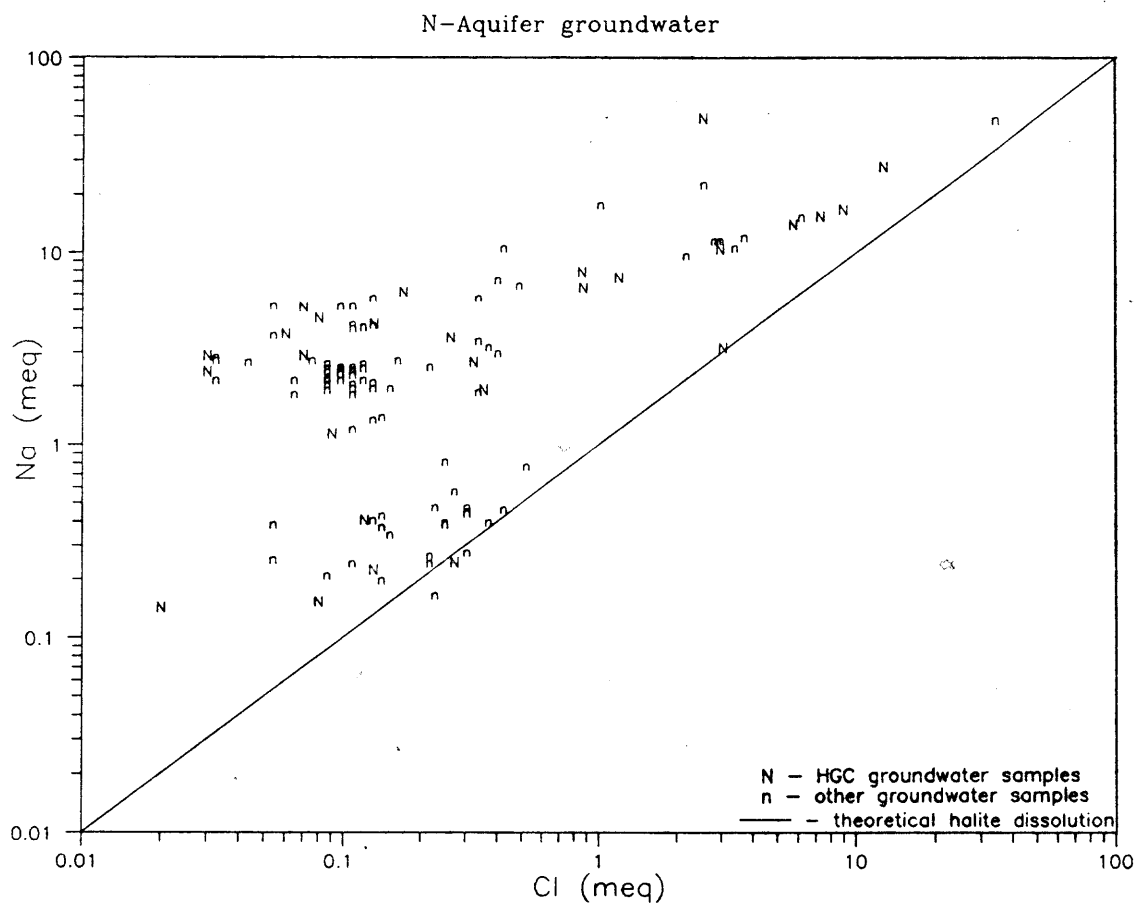


Figure 6-3. Na<sup>+</sup> as a function of Cl<sup>-</sup>, N-aquifer.

Samples along trend A are from the confined aquifer. When compared against an equivalent  $\text{Cl}^-$  concentration,  $\text{Na}^+$  concentrations for this trend are in excess of what may be expected from halite dissolution. To account for this excess, a parameter was introduced and is referred to hereafter as "excess Na". Excess Na is defined as the difference between the measured  $\text{Na}^+$  concentration and an equivalent  $\text{Cl}^-$  concentration and is assumed to be the amount of  $\text{Na}^+$  contributed from ion exchange processes.

By comparing equivalents of excess Na with  $\text{Ca}^{2+}_{\text{corr}}$  as in Figure 6-4, a pronounced 1:1 linear trend appears (the correction denoted by  $_{\text{corr}}$  is for  $\text{Ca}^{2+}$  contributed by calcite and gypsum dissolution and is described in the following section). This trend supports the aforementioned ion exchange reactions and assumptions. Samples with high excess Na (greater than 85 percent of total  $\text{Na}^+$ ) and small  $\text{Ca}^{2+}$  and  $\text{Mg}^{2+}$  concentrations are found only within the confined system and may be attributed to cation exchange with clays, possibly sodium-rich smectite and illite. Halite dissolution appears to contribute only minor  $\text{Na}^+$  in the majority of samples, with only a few localized exceptions.

Ion exchange controls the occurrence of  $\text{Mg}^{2+}$  in the N-aquifer. Mg-Na exchange is the dominant  $\text{Mg}^{2+}$  sink, and Ca-Mg exchange is most likely the dominant  $\text{Mg}^{2+}$  source.  $\text{Mg}^{2+}$  concentrations in the N-aquifer range from less than 0.1 to 57 mg/l. As with  $\text{Ca}^{2+}$ , the smallest concentrations are found in the confined system and are typically less than 0.3 mg/l, suggesting Mg-Na ion exchange. Figure

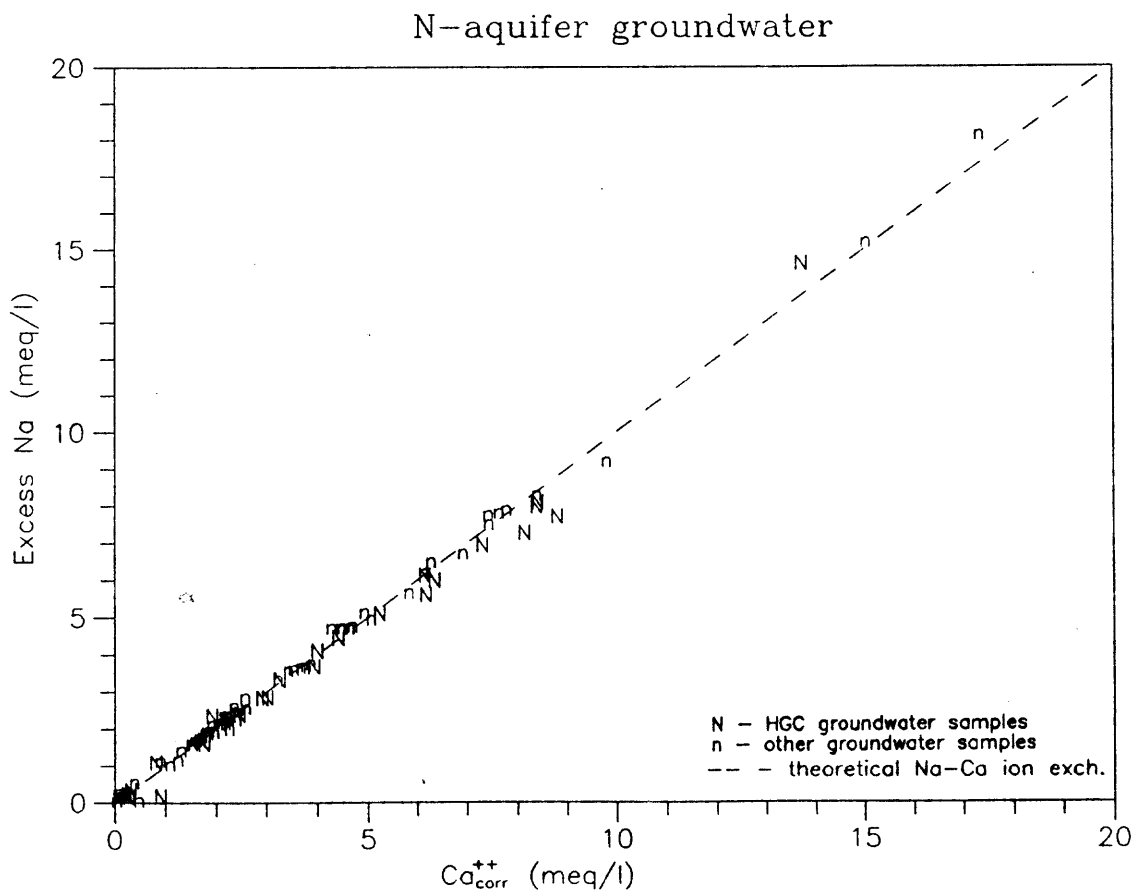


Figure 6-4. Excess Na as a function of corrected  $Ca^{2+}$ , N-aquifer. Corrections are for  $Ca^{2+}$  contributed by calcite and gypsum dissolution.

6-5 is a  $Mg^{2+}$  and  $Ca^{2+}$  log-activity diagram for N-aquifer groundwater samples. The approximate 1:1 linear relationship strongly suggests Ca-Mg ion exchange. Other processes that would produce this relationship include dissolution of dolomite or a high-magnesium calcite, however, these processes are unlikely in the N-aquifer. Dolomite is not known to exist within the study area, and the  $Mg^{2+}$  content of calcite in the N-aquifer formations is invariably low, reported to be typically less than two percent (Kiersch, 1955b).

A correction for the amount of  $Ca^{2+}$  removed from solution by Ca-Mg ion exchange was made by attributing the measured  $Mg^{2+}$  concentration to Ca-Mg cation exchange. This correction to  $Ca^{2+}$  involves the addition of an equivalent measured  $Mg^{2+}$  concentration. Any additional Ca-Mg ion exchange not represented in the measured concentration is accounted for in the excess Na term assuming that Mg-Na is the only significant  $Mg^{2+}$  sink.

As noted earlier, cation exchange reactions are dominant only within the confined system and may be attributed to the following processes. First, over time, the availability of primary minerals may have become depleted in recharge areas relative to the confined system and exchange sites on clays may be occupied. Therefore, silicate weathering could have progressed further along the flow path under Black Mesa. Second, within the confined system, the thickness of the N-aquifer is greater and the hydraulic gradients are smaller than those found in the unconfined areas. Although  $CO_{2(aq)}$  is diminished from that found under open

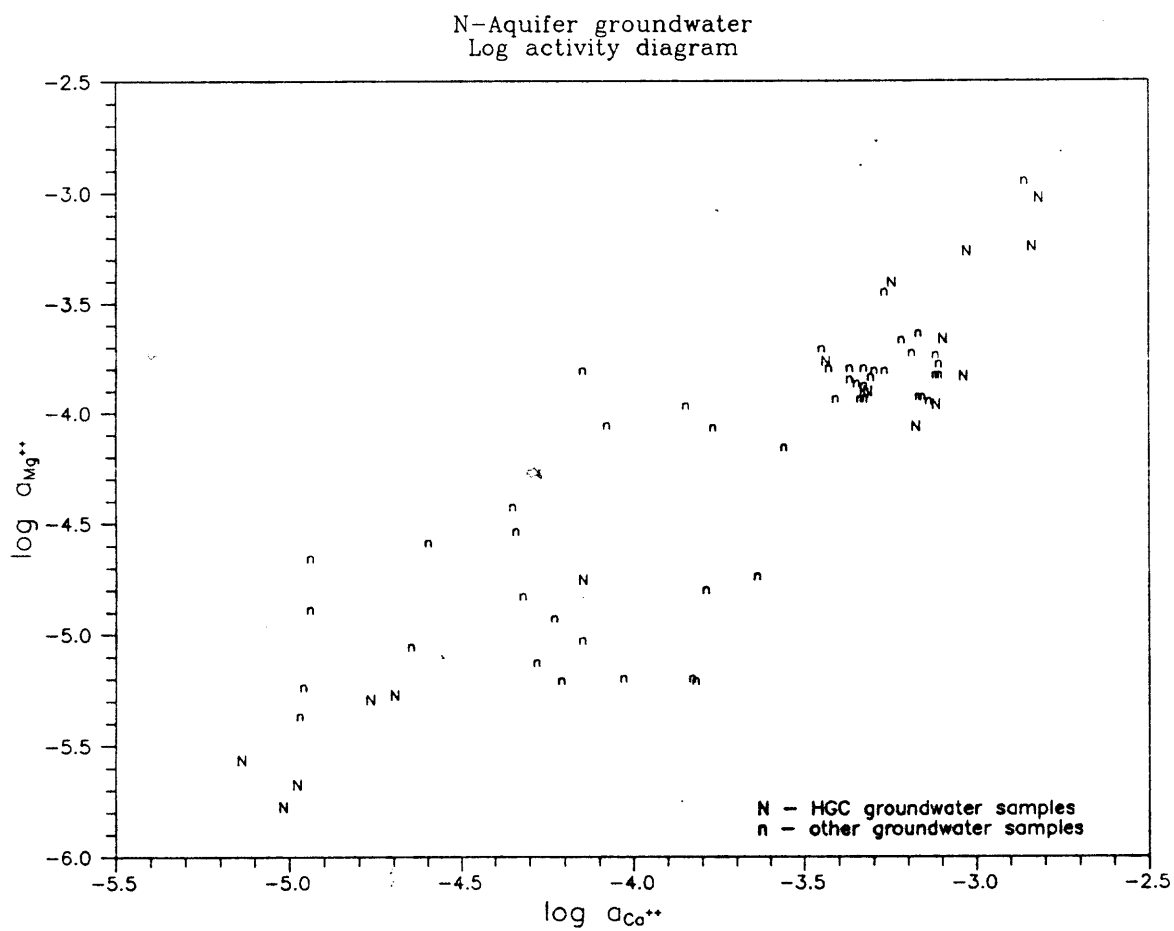


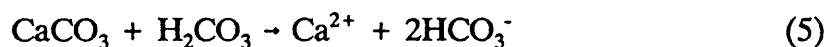
Figure 6-5. Log-activity diagram for  $Mg^{2+}$  as a function of  $Ca^{2+}$ , N-aquifer.

system conditions, a larger source for silicate minerals is available and groundwater residence times are longer.

Dulaney (1989) concluded that cation exchange was not a dominant process controlling  $\text{Na}^+$ ,  $\text{Ca}^{2+}$  or  $\text{Mg}^{2+}$  concentrations in the N-aquifer. When presented with two distinct trends while comparing uncorrected  $\text{Ca}^{2+}$  and  $\text{Mg}^{2+}$  with  $\text{Na}^+$ , Dulaney concluded that the lack of any intermediate samples indicated that one type did not evolve into the other and that little cation exchange was occurring (Dulaney, 1989, page 111). Arguments to the contrary have been presented in this section. Cation exchange is one of the dominant processes not only governing the occurrence of these constituents, but is the key process responsible for the evolution of the two distinct hydrochemical facies present in the unconfined and confined systems.

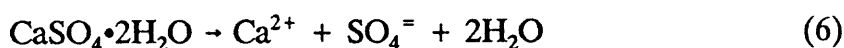
#### 6.2.2.3 *Calcite and gypsum dissolution/precipitation reactions*

Calcite has been identified as a cement in the Navajo Sandstone (Kiersch, 1955b; Harshbarger, 1957; Dulaney, 1989). The dissolution of calcite early along the flow path is suggested by the lack of calcite cement in surface samples (Dulaney, 1989) and rapid increases in  $\text{Ca}^{2+}$  and alkalinity in recharge areas. The dissolution of calcite,



should be supported by a strong correlation between  $\text{Ca}^{2+}$  concentration and

bicarbonate alkalinity. However, gypsum dissolution will also contribute  $\text{Ca}^{2+}$  to solution. The occurrence of  $\text{SO}_4^{=}$ , if attributed to gypsum dissolution,



should be evidenced by a correlation between  $\text{Ca}^{2+}$  and  $\text{SO}_4^{=}$  concentrations.

In order to evaluate these processes in the N-aquifer, corrections were made to concentrations to account for interference from chemical processes involving mutual constituents. For example, deviation from the theoretical dissolution trends for uncorrected  $\text{Ca}^{2+}$  and  $\text{SO}_4^{=}$  could indicate interference from Ca-Na and Ca-Mg ion exchange or from dissolution and precipitation reactions involving  $\text{Ca}^{2+}$ . Dulaney (1989) was unable to detect correlations for calcite and gypsum dissolution without these corrections.

Using a mass balance approach, corrections were made to  $\text{Ca}^{2+}$  concentrations to recover the amount of  $\text{Ca}^{2+}$  removed from solution by ion exchange (Eqns. 2 and 4). The amount of  $\text{Na}^+$  entering solution from ion exchange was estimated from the following mass balance expression:

$$\text{Na}^+(\textit{measured}) = \text{Na}^+(\textit{Na exchange}) + \text{Na}^+(\textit{NaCl dissolution}) \quad (7)$$

where Na ion exchange represents the net contribution from Ca-Na and Mg-Na exchange. The molar quantity of  $\text{Ca}^{2+}$  consumed by these exchange processes is half the molar quantity of excess Na. Equation 7 also assumes that  $\text{Cl}^-$  is contributed only by halite dissolution and is conservative, and that the contribution of major cations from the incongruent dissolution of silicates is negligible.

By further assuming that the  $Mg^{2+}$  concentration in solution is due to Ca-Mg cation exchange, the effect on total  $Ca^{2+}$  (in moles/l) was corrected by the following equation:

$$\text{Corrected } Ca^{2+} = Ca^{2+}(\text{measured}) + \frac{1}{2}(\text{excess Na}) + Mg^{2+} \quad (8)$$

The dissolution of calcite and gypsum both occur simultaneously. One final pair of corrections were applied to account for  $Ca^{2+}$  contributed by gypsum when evaluating calcite dissolution (by subtracting an equivalent amount of  $SO_4^-$ ), and for  $Ca^{2+}$  contributed by calcite when evaluating gypsum dissolution (by subtracting an equivalent  $HCO_3^-$  concentration). With these necessary corrections to account for interferences to the measured  $Ca^{2+}$  concentration, the effects of the dominant reactions can be examined individually.

Figure 6-6 shows alkalinity as a function of measured and corrected  $Ca^{2+}$ . In Figure 6-6a, some samples follow the theoretical calcite dissolution line without  $Ca^{2+}$  correction. These samples are predominantly from the unconfined system. Samples with small  $Ca^{2+}$  concentrations and variable alkalinity are suggestive of interference from Na ion exchange. These samples are exclusively from the confined system. By applying the corrections to  $Ca^{2+}$  for ion exchange and replotting, as in Figure 6-6b, most samples follow theoretical calcite dissolution. Samples that do not follow the theoretical calcite dissolution are influenced by gypsum dissolution. This interference is removed by subtracting an equivalent amount of  $SO_4^-$  for the  $Ca^{2+}$  contributed by gypsum dissolution. With this last

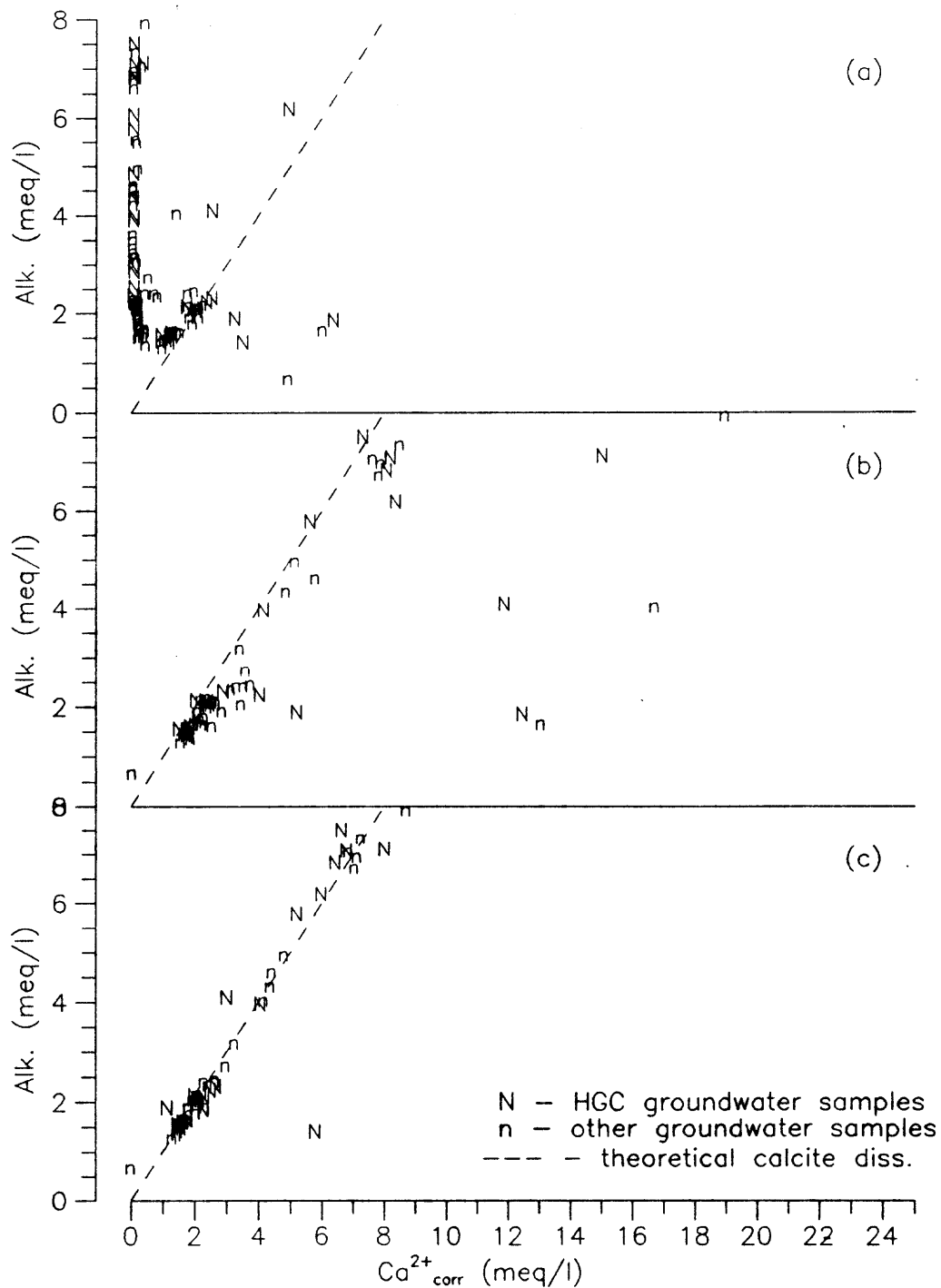


Figure 6-6. Alkalinity as a function of Ca<sup>2+</sup>; uncorrected (a), corrected for ion exchange (b), and corrected for gypsum dissolution (c), N-aquifer.

correction, nearly all samples lie along the theoretical calcite dissolution trend in Figure 6-6c. Scatter about the theoretical is due to analytical errors and interference from other processes.

Calcite dissolution will consume  $\text{CO}_{2(\text{aq})}$  and increase alkalinity along the flow path, as indicated by equation 5. Under closed system conditions, however, the supply of  $\text{CO}_2$  is limited and  $\text{CO}_{2(\text{aq})}$  is expected to decrease along the flow path with an accompanying increase in pH. In addition, Ca-Mg and Ca-Na exchange decreases the  $\text{Ca}^{2+}$  and  $\text{CO}_3^{=}$  activity product which further promotes calcite dissolution. In the confined system, alkalinity is observed to increase only slightly downgradient and is accompanied by a decrease in the partial pressure of  $\text{CO}_{2(\text{aq})}$ , a rise in pH, and a trend toward calcite undersaturation. The computed  $\text{pCO}_{2(\text{aq})}$  decreases from  $10^{-2}$  and  $10^{-3.5}$  in recharge areas to as low as  $10^{-5.3}$  near Oraibi. The pH is observed to increase from about 7.5-8.5 in recharge areas to 8.3-10.0 in the confined system.

From these observations, the conclusion can be made that calcite dissolution is the principal source of alkalinity and  $\text{Ca}^{2+}$ . Most of the calcite dissolution occurs early along the flow path and may involve dissolution of caliche near the surface as well as calcite cement from the sandstone formations. Calcite saturation indices throughout the N-aquifer indicate equilibrium or near-equilibrium conditions (Chapter 8). Under confined conditions, calcite dissolution is most likely limited by the availability of  $\text{CO}_2$  rather than by solubility constraints.

Gypsum dissolution contributes the majority of the  $\text{SO}_4^{=}$  found in the N-aquifer. Sulfate ranges from 6.6 to 2120 mg/l but rarely exceeds 100 mg/l. Saturation indices from speciation modeling range from -0.68 to -5.25 and indicate undersaturation with respect to gypsum. Elevated concentrations appear to be localized, for example in the vicinity of Keams Canyon, and scattered along the border between the confined and unconfined systems. Elevated  $\text{SO}_4^{=}$  concentrations are also found in the confined N-aquifer but are typically isolated and do not consistently increase along the flow path.

The effects of gypsum dissolution can be isolated with the aforementioned corrections to  $\text{Ca}^{2+}$ . Figure 6-7 shows  $\text{SO}_4^{=}$  as a function of measured and corrected  $\text{Ca}^{2+}$ . Without correction, two distinct trends exist (Figure 6-7a). Samples with small  $\text{SO}_4^{=}$  and variable  $\text{Ca}^{2+}$  concentrations correspond to the unconfined system. The trend with variable  $\text{SO}_4^{=}$  and small  $\text{Ca}^{2+}$  concentrations correspond to samples from the confined system and are indicative of Ca ion exchange. By correcting  $\text{Ca}^{2+}$  for interference from ion exchange (Figure 6-7b), and then from calcite dissolution (Figure 6-7c), the gypsum dissolution trend becomes more pronounced. Some scatter about the theoretical line is due to analytical error and unaccounted sources and sinks.

As will be discussed in the next section, an atmospheric source for  $\text{SO}_4^{=}$  in the N-aquifer is indicated by sulfur isotopes, however, the source associated with elevated  $\text{SO}_4^{=}$  in the confined portion and along its periphery is due to either

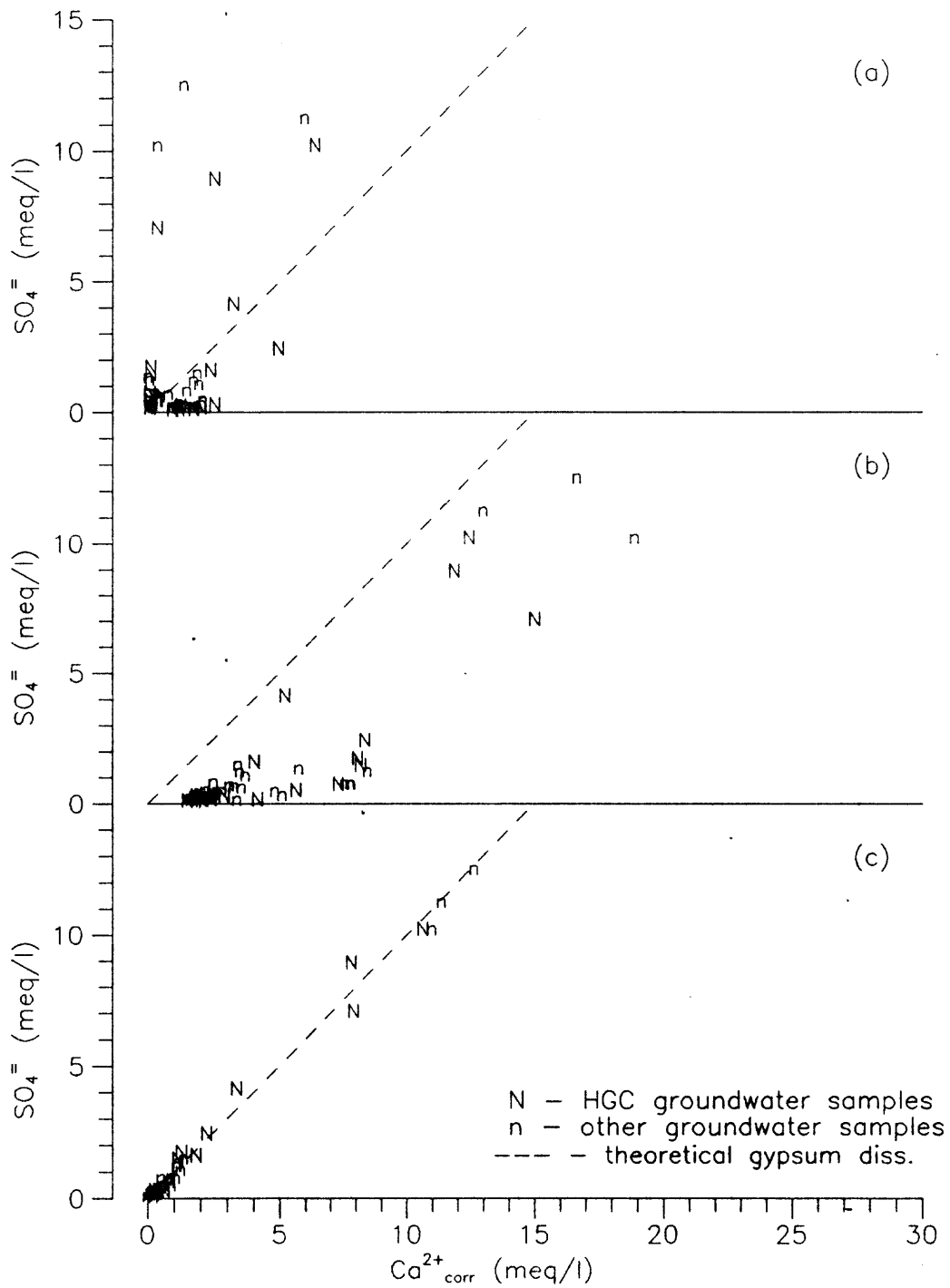


Figure 6-7.  $\text{SO}_4^{2-}$  as a function of  $\text{Ca}^{2+}$ ; uncorrected (a), corrected for ion exchange (b), and corrected for calcite dissolution (c), N-aquifer.

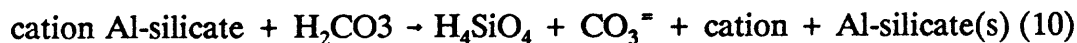
localized dissolution with downgradient dilution or reduction, or leakage from the overlying D-aquifer. Evidence supports leakage from the D-aquifer, most likely associated with well construction. Many of the samples from the confined system with elevated  $\text{SO}_4^-$  are accompanied by high  $\text{Cl}^-$  concentrations, as would be expected from mixing with D-aquifer groundwater. Calculations show that about eight percent mixing with the D-aquifer results in a  $\text{SO}_4^-$  concentration of 37 mg/l (sample 25, NTUA Forest Lake) assuming a background N-aquifer  $\text{SO}_4^-$  concentration of 5 mg/l and 400 mg/l for the D-aquifer. This is also consistent with the sulfur isotope data. The  $\delta^{34}\text{S}$  is light (-9.6 ‰) indicating  $\text{SO}_4^-$  of predominantly marine origin as would be expected in the D-aquifer and the Mancos Shale.

The calcite/gypsum common ion effect is not apparent in the confined system because of small  $\text{SO}_4^-$  concentrations, but may play a role in controlling calcite solubility under open system conditions and in localized areas influenced by the D-aquifer. Without the removal of  $\text{Ca}^{2+}$  by ion exchange in the unconfined system, the activity product for  $\text{Ca}^{2+}$  and  $\text{CO}_3^-$  rises with the contribution of  $\text{Ca}^{2+}$  from gypsum dissolution. Little or no correlation in saturation indices for the two minerals exists, however a trend is suggested where increasing calcite saturation (more positive) is accompanied by a decreasing undersaturation for gypsum (less negative). Saturation indices and this correlation are examined in greater detail in Chapter 8.

#### 6.2.2.4 *Weathering of silicates*

Mineralogic analyses by Dulaney (1989) identified alteration products such as smectite, kaolinite, illite, and muscovite in samples from the N-aquifer formations. Although the role of aluminosilicate hydrolysis in the N-aquifer is small in relation to other reactions, the resulting secondary minerals are an important part in the ion exchange reactions. For continuity in the description of the dominant reactions, some discussion of silicate weathering is merited.

Other than quartz, the minerals identified in the N-aquifer are predominantly feldspars, mainly plagioclase and orthoclase, biotite and muscovite. Dulaney (1989) found as much as 20 percent feldspar in the sandstone samples he analyzed. The feldspars showed signs of alteration, most commonly to sericite but also to kaolinite and illite. The dominant clay fraction was reported as smectite with the remainder as illite. The clays are most likely authigenic, a residual from aluminosilicate hydrolysis as the low TDS, CO<sub>2</sub>-charged groundwater enters the aquifer. A general expression for this weathering reaction is given by;



where the resulting aluminosilicate is a clay (after Stumm and Morgan, 1970).

Aqueous CO<sub>2</sub>, or H<sub>2</sub>CO<sub>3</sub> in equation 10, is most likely responsible for the dissolution of silicate minerals (Freeze and Cherry, 1979). The dissociation of H<sub>2</sub>CO<sub>3</sub> lowers the pH of the groundwater, thereby making the recharged water more aggressive toward the hydrolysis of silicate minerals. As long as acid is added

to the system, the potential exists for consumption of hydrogen ions resulting in an increase in the pH along the flow path.

Although silicate hydrolysis may be partially responsible for the observed pH increases in the confined system, these reactions are not significant in the N-aquifer in terms of contributing cations to solution. Equation 10 implies an increase in the alkalinity during the weathering process as  $H_2CO_3$  changes to bicarbonate, and at higher pH's, bicarbonate to carbonate. Evidence was presented earlier suggesting that the dissolution and precipitation of calcite was largely responsible for the observed variations in alkalinity in the N-aquifer. In the unconfined system, kinetics probably control the degree of silicate weathering.  $CO_2$  availability further limits these reactions in the confined system.

Equation 10 also shows that silica is released during silicate hydrolysis. If saturated or supersaturated conditions of some silica phase exists, then it would precipitate from solution. As will be discussed in chapter 8, groundwater in the confined system is supersaturated with respect to quartz yet undersaturated with respect to amorphous silica. The groundwater is most likely in equilibrium with respect to some intermediate silica phase. Kiersch (1955b) hypothesized that the quartz cement in the sandstone matrix has been introduced and was found to be more abundant at depths of 50-200 feet below the upper contact than for surface samples. On precipitation from solution, this quartz cement may have replaced a pre-existing bonding of carbonate.

Possible reaction sequences consistent with the observed mineralogy include; 1) plagioclase alteration to smectite followed by 2) smectite alteration to kaolinite, and 3) biotite and orthoclase alteration to illite followed by 4) illite alteration to kaolinite.

### 6.2.3 Isotopic Indications

Isotopic data are available for the HGC groundwater samples for the N-aquifer. These data provide useful insights to the groundwater flow regime, the mineralogy of the formations encountered along the flow path, and geochemical processes and sequences. This section presents the isotopic data and a discussion of their indications for the chemical evolution of the groundwater in the N-aquifer.

#### 6.2.3.1 Deuterium and Oxygen-18

Figure 6-8 shows the  $\delta D$  and  $\delta^{18}O$  compositions for the N-aquifer. Most follow the meteoric water line (MWL). Deviations from the MWL may be caused by re-evaporation of rainfall between cloud base and ground, evaporation from the aquifer near the surface, and from mixing effects (IAEA, 1981). The data generally fit into two groups. The group lower along the MWL with lighter compositions in both  $\delta^{18}O$  and  $\delta D$  correspond entirely to samples from the confined portion of the N-aquifer or at the periphery of confining conditions. The isotopically heavier group corresponds to the unconfined system. Possible explanations include mixing

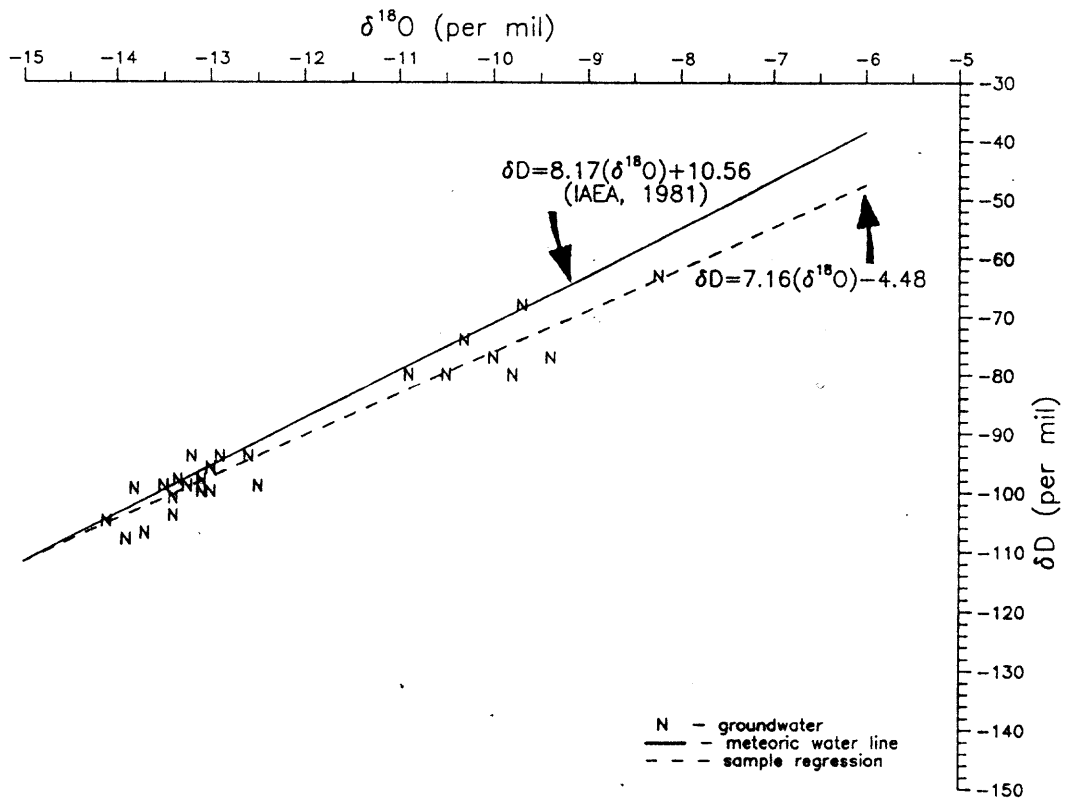


Figure 6-8.  $\delta\text{D}$  as a function of  $\delta^{18}\text{O}$ , N-aquifer.

with leakage from the D-aquifer, the altitude effect, and paleo climate effects. Each of these explanations are examined next.

If recharge to the N-aquifer occurs in part through downward leakage from the overlying D-aquifer, the large concentration dissimilarities between the two aquifers would not persist unless substantial ion stripping occurred within the intermediate Carmel Formation. Brown and Eychaner (1988) determined by numerical modeling that the net vertical leakance was 210 acre-feet out of the 19,400 acre-feet annual budget for the N-aquifer within the Little Colorado River and San Juan River basins. If these figures are accurate, leakage from the overlying D-aquifer could not cause the observing grouping.

Precipitation is typically isotopically lighter with increasing elevation, usually as a function of temperature variations. IAEA (1981) reports correlations of 0.5 to 1.5‰ per 1000 feet for  $\delta^{18}\text{O}$ , and 4.6 to 12.2‰ per 1000 feet for  $\delta\text{D}$ . Recharge areas for the N-aquifer vary in elevation from 3500 feet (MSL) along the Colorado River to over 7500 feet along the northeastern escarpment of Black Mesa. The altitude could explain the observed differences, however, no correlation exists between  $\delta^{18}\text{O}$  and altitude for the samples collected from the unconfined aquifer.

The observed distribution along the MWL is most likely a manifestation of paleoclimatic variations related to the last interglacial stages of the Pleistocene. Generally, paleowaters are depleted in  $^{18}\text{O}$  with respect to recent waters if precipitated under more humid and cooler periods (IAEA, 1981). The lighter

cluster may represent paleowaters bearing the fingerprint of a cold-type recharge while the heavier group is representative of more recent meteoric recharge.

McGavock and Levings (1973) reported an estimate of 15,500 years for the age of groundwater sampled from the PCC wellfield. This wellfield is approximately 40,000 feet downgradient from the recharge area. Three dating techniques were employed, one of which was  $^{14}\text{C}$  (personal communication, Ed McGavock, USGS, 1991). An average linear velocity was calculated using Darcy's Law and published aquifer parameters (Eychaner, 1983); porosity 0.10 to 0.20, and hydraulic conductivity of 0.05 to 2.10 with a mean of 0.65 ft/day. With an average hydraulic gradient equal to 1000 feet per 30 miles, calculated travel times range from 16,000 and 39,000 years for 30 and 55 miles, respectively, downgradient from the recharge area. This suggests that most of the groundwater in the confined system was recharged during the Wisconsin glaciation, the maximum advance of which was about 15,000 to 18,000 years ago (Bloom, 1978).

The distinct grouping of samples in Figure 6-8 is most likely a circumstance of the sampling distribution. Any intermediate samples along the MWL would be located within the deepest and therefore least accessible areas immediately south of the recharge ridge. Unfortunately, such isotopic analyses have not been performed for the PCC wellfield to the knowledge of Ted Smith, Chief Hydrologist, PCC (personal communication, 1990).

### 6.2.3.2. Sulfur-34

An atmospheric origin for the  $\text{SO}_4^{=}$  in the N-aquifer is supported by the relatively low concentrations, high permeability of the N-aquifer formations, and  $\delta^{34}\text{S}$  isotope compositions. Consulting Figure 6-9, the majority of the groundwater samples exhibit a  $\delta^{34}\text{S}$  between +5 and +15‰ which may be due to an atmospheric origin (Holser et al., 1966). Several samples with higher  $\text{SO}_4^{=}$  concentrations and considerably lighter compositions (-9.6 to -13.5 ‰) indicate possible mixing with water having a marine  $\text{SO}_4^{=}$  origin, as with the D-aquifer. Two of these three samples are along the periphery of the confined system where communication with the overlying D-aquifer is likely.

The third sample with an anomalous light  $\delta^{34}\text{S}$  value (-9.6 ‰) was collected from a well in the center of Black Mesa within the confined system (sample 25, NTUA Forest Lake). The  $\text{SO}_4^{=}$  concentration for this sample is higher than most surrounding wells (37 mg/l as opposed to about 5 to 7 mg/l). Using eight percent mixing with D-aquifer groundwater (calculated from  $\text{SO}_4^{=}$  concentrations in section 6.2.2.3) reproduces the light  $\delta^{34}\text{S}$  value for sample 25. This assumes an N-aquifer  $\delta^{34}\text{S}$  of +12 ‰ and a D-aquifer  $\delta^{34}\text{S}$  of about -13 ‰, values consistent with typical ranges for the different sulfur origins. One can conclude, therefore, that some samples collected from within or along the periphery of the confined system with elevated  $\text{SO}_4^{=}$  concentrations are influenced by localized mixing with the D-aquifer,

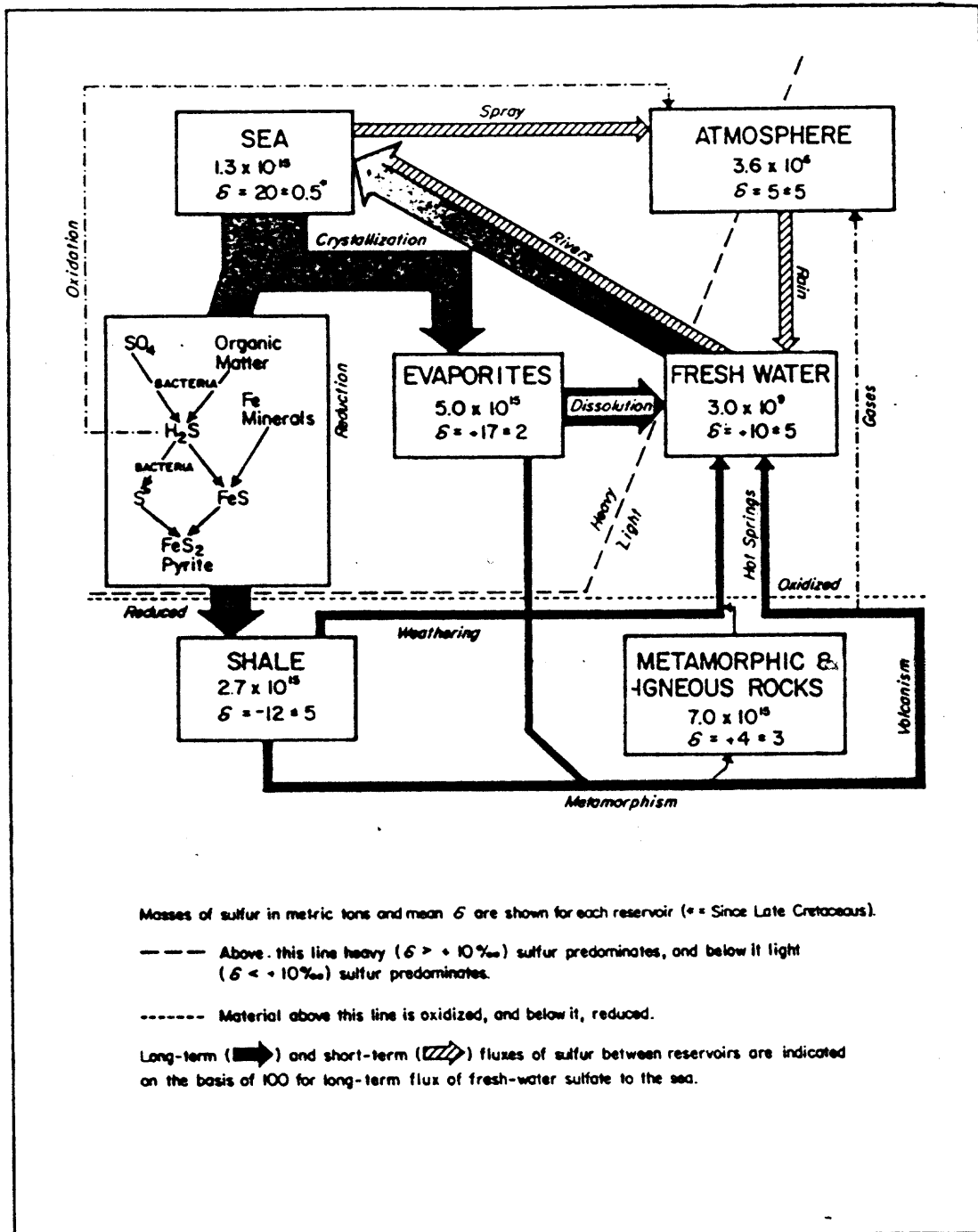


Figure 6-9. Geochemical sulfur cycle (after Holser, et al., 1966).

either through natural hydrogeologic processes, or through processes associated with well construction.

The  $\text{SO}_4^{=}$  concentrations and sulfur isotope data near Keams Canyon do not provide conclusive evidence regarding the  $\text{SO}_4^{=}$  origin. Some wells in the area are old and may allow considerable leakage between the aquifers. Samples strongly influenced by D-aquifer groundwater should exhibit elevated  $\text{SO}_4^{=}$  concentrations with lighter  $\delta^{34}\text{S}$ . Although the lighter isotopes are found for some samples with higher  $\text{SO}_4^{=}$  concentrations, the pattern is not consistent. Both local gypsum dissolution with  $\text{SO}_4^{=}$  of an atmospheric origin and mixing with the D-aquifer may contribute to the observed water quality in the Keams Canyon area.

### 6.3 Water Quality for the D-aquifer

Information has been presented indicating a potential for hydraulic communication between the N-aquifer and the overlying D-aquifer. In addition to natural hydrogeologic processes, samples may be influenced by D-aquifer leakage associated with well construction or samples may have been collected from wells with incorrect information regarding formations encountered or open intervals. This chapter presents a brief characterization of the water quality for the D-aquifer for the purposes of identifying its influence on the N-aquifer and surface water systems.

The water quality summaries used in this section were obtained from HGC and were collected during their preparation for the Little Colorado River system adjudications.

### 6.3.1 General Description of Water Quality

The D-aquifer exhibits a higher degree of mineralization than the underlying N-aquifer, most notably in terms of elevated  $\text{SO}_4^{=}$ ,  $\text{Na}^+$  and  $\text{Cl}^-$  concentrations. The major water types range from Ca- $\text{SO}_4$  to Na- $\text{HCO}_3$  and Na-Cl. EC varies from 400 to 4400  $\mu\text{S}/\text{cm}$  with most samples exceeding 1000  $\mu\text{S}/\text{cm}$ . Average concentrations of selected constituents for samples are listed in Table 6-1. The  $\text{Ca}^{2+}$  concentrations are small throughout the confined system suggesting intensive Ca-Na ion exchange. Large increases in the  $\text{Cl}^-$  and  $\text{Na}^+$  concentrations are observed from east to west along the flow path, possibly as a result of halite dissolution and  $\text{Na}^+$  ion exchange. The  $\text{SO}_4^{=}$  concentrations decrease along the flow path and suggest a reducing environment.

The  $\delta^{34}\text{S}$  composition of the D-aquifer ranges from -22 to +14 ‰. Most samples are isotopically light which may suggest a marine origin for  $\text{SO}_4^{=}$ . It is hypothesized that the origin of  $\text{SO}_4^{=}$  in the D-aquifer is from the oxidation of crystalline pyritic conglomerates found in the overlying Mancos Shale and coal seams within the Dakota Sandstone, Toreva and Wepo Formations (personal communication, Dr. Songlin Cheng, 1989).

Table 6-1  
Average concentrations (mg/l) for selected constituents  
in the D-aquifer  
(source: WATSTORE and Hydro Geo Chem, Inc.)

<u>parameter</u>	<u>average</u> <sup>1</sup>	<u>median</u>	<u>std.dev.</u>
Ca <sup>2+</sup>	41.3	14.5	59
Mg <sup>2+</sup>	11.4	2.6	22
Na <sup>+</sup>	303	265	247
SO <sub>4</sub> <sup>=</sup>	392	225	418
Cl <sup>-</sup>	89	24	154
Alkalinity <sup>2</sup>	302	262	154
pH	8.36	8.30	0.548
EC <sup>3</sup>	2501	2145	1427
TDS	1556	1169	1133

<sup>1</sup> number of samples = 34

<sup>2</sup> as CaCO<sub>3</sub>

<sup>3</sup> units are  $\mu\text{S}/\text{cm}$

#### 6.4 Summary

In summary, the geochemistry of the N-aquifer is dominated by calcite dissolution and cation exchange reactions. Four distinct chemical facies were identified. The dominant water types, Na-HCO<sub>3</sub> and Ca-HCO<sub>3</sub>, correspond to the confined and unconfined systems, respectively. The Ca-HCO<sub>3</sub> evolves rapidly under open system conditions. However, within the confined system, Ca-Mg-Na cation exchange consumes Ca<sup>2+</sup> and Mg<sup>2+</sup>, and increases the Na<sup>+</sup> concentration. Continued calcite dissolution consumes CO<sub>2(aq)</sub> and raises the pH of the groundwater. The result is a distinct Na-HCO<sub>3</sub> water type with elevated Na<sup>+</sup>

concentrations. The exchange sites are most likely clays formed by the alteration of aluminosilicates. The other chemical facies are highly localized and, in several instances, due to leakage from the D-aquifer associated with well construction or natural hydrogeologic processes.

Deuterium and  $^{18}\text{O}$  suggest that most of the groundwater within the confined system was recharged during a colder paleo climate. Groundwater dating and flow calculations indicate that most groundwater within the confined portion of the N-aquifer exceeds 15,000 years and may exceed 39,000 years in areas.

## CHAPTER 7

### SURFACE WATER GEOCHEMISTRY

#### 7.1 Introduction

Understanding the physical processes controlling baseflow along the southwestern Black Mesa washes is essential to predicting the distribution, persistence and natural fluctuations in baseflow, and, ultimately, susceptibility of baseflow to cultural activities such as industrial and municipal groundwater withdrawals. A knowledge of the geochemistry of surface water and groundwater interactions provides insight into the physical processes that cannot be directly observed or easily measured. This chapter presents the results from the geochemical analysis of the surface water, springs and alluvial groundwater along Moenkopi and Dinnebito washes.

Surface water sustained by aquifer discharge will have experienced the same reaction sequence as the groundwater source and therefore should exhibit similar chemical characteristics. However, interaction with the channel alluvium, evapotranspiration, and naturally gaining and losing reaches will vary the chemical and isotopic composition of surface water with time and distance along the streamcourse. The preponderance of chemical and isotopic data collected from surface water, springs and drive points along Moenkopi and Dinnebito washes suggests that baseflow along these washes are sustained largely by N-aquifer

discharge originating from the confined system rather than from locally-recharged, unconfined areas.

A four-level approach was adopted for presenting the geochemical analysis for the washes, similar to the description of the geochemistry of the N-aquifer in the preceding chapter. The first section provides a general description of water quality in terms of chemical facies and distribution of specific parameters. The second section includes a description of the dominant reactions in which correlations are used in conjunction with the stoichiometry of the suspected reactions to qualify the existence and role of the dominant reactions. The third section presents an analysis of the available isotopic data in the study area for the N-aquifer which characterizes the distribution of various isotopes and examines possible fractionation and mixing processes. The fourth and final section describes the surface water interactions with groundwater and the alluvium. A description of the quantitative analysis using geochemical modeling is presented separately in Chapter 8.

### 7.2 General description of water quality

Figure 7-1 is a trilinear diagram for samples collected from surface water, springs and drive points along Moenkopi and Dinnebito washes. Most samples are a Ca-SO<sub>4</sub> type although springs and tributaries range from Na-Cl to Ca-HCO<sub>3</sub>. With the exception of springs and Pasture Canyon Reservoir, most samples do not

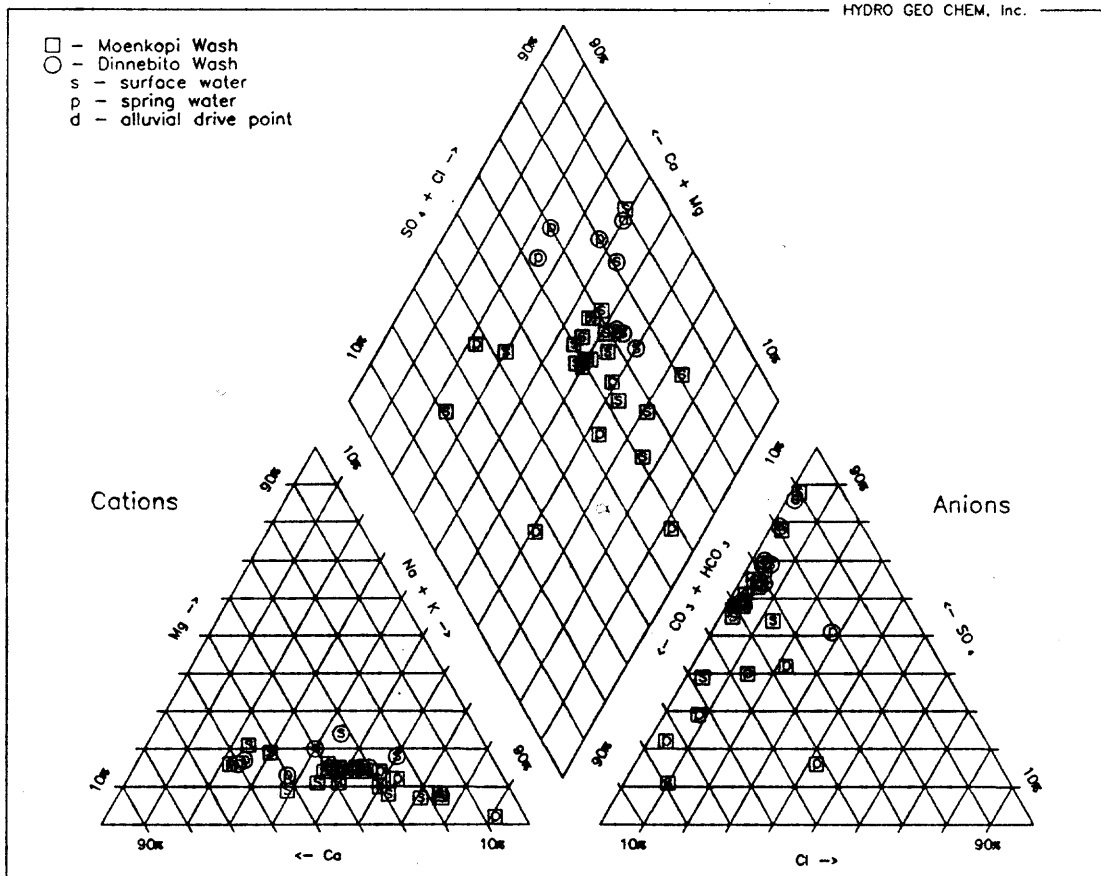


Figure 7-1. Trilinear diagram for wash samples.

fit neatly into any of the dominant water types prevalent in the N-aquifer but clear trends do exist. This may suggest continued chemical evolution including groundwater and surface water interaction with channel alluvium, and mixing with storm runoff, alluvial groundwater or the D-aquifer.

Overall, baseflow samples from both washes exhibit higher levels of mineralization relative to the N-aquifer as indicated by EC (median 363  $\mu\text{S}/\text{cm}$  for the N-aquifer groundwater samples). EC ranges from 246 to 2130  $\mu\text{S}/\text{cm}$  with a median of 790  $\mu\text{S}/\text{cm}$  for Moenkopi Wash, and a range of 674 to 2090  $\mu\text{S}/\text{cm}$  with a median of 1079  $\mu\text{S}/\text{cm}$  for Dinnebito Wash. Samples obtained by drive point from the alluvial aquifer exhibit EC ranging from 351 to 2190  $\mu\text{S}/\text{cm}$  for Moenkopi Wash with one value of 2080  $\mu\text{S}/\text{cm}$  for Dinnebito Wash. In general,  $\text{SO}_4^-$  and  $\text{Ca}^{2+}$  concentrations for baseflow and drive point samples are elevated relative to the N-aquifer.

The distribution of selected parameters and chemical constituents for samples from surface water, springs and drive points is presented in Appendix F for Moenkopi Wash, and in Appendix G for Dinnebito Wash. Most changes in the chemical composition of baseflow along Moenkopi Wash are restricted to the gaining reach above the confluence with Begashibito Wash. These changes typically are increases in concentration. The chemical composition of spring samples along Moenkopi Wash is significantly different from that of baseflow. Typically, spring

samples exhibit higher  $\text{Cl}^-$  and  $\text{NO}_3^-$  concentrations and lower  $\text{SO}_4^{2-}$  and  $\text{Ca}^{2+}$  concentrations. There are no discernable trends along Dinnebito Wash.

Spring samples with elevated  $\text{NO}_3^-$  concentrations were collected along both the northern and southern cliffs of Moenkopi Wash. While baseflow  $\text{NO}_3^-$  concentrations are typically less than 1 mg/l,  $\text{NO}_3^-$  in spring samples was measured as high as 22 mg/l which exceeds the range for most natural waters (Davis and DeWiest, 1966). A potential source of  $\text{NO}_3^-$  contamination is the UMTRA site to the north of Moenkopi Wash near sampling location 24 (Plate 1). Prior to closing the processing facility, ammonium and nitric acids were used as resin strippers in an acid-leaching process.  $\text{NO}_3^-$  concentration reported for contaminated groundwater at the site ranges from 64 to 1800 mg/l and averages 928 mg/l for 15 analyses (USDOE, 1989).

If elevated  $\text{NO}_3^-$  concentrations in spring samples are due to past operations at the UMTRA site, then wind dispersal from tailings, sludge and slime piles is the most likely transport mechanism. Elevated  $\text{NO}_3^-$  concentrations were found in springs from both sides of Moenkopi Wash but not in spring samples collected along Dinnebito Wash, about 25 miles to the south. A plume of contaminated groundwater from the leaching pits was identified but it was not reported to have reached Moenkopi Wash at the time the springs were sampled (USDOE, 1989). The plume also contains high concentrations of other constituents that were not observed in the spring samples. In addition, the spring along south Kerley Valley

(location 15) with elevated  $\text{NO}_3^-$  would not be affected by the plume given existing patterns of groundwater flow.

Most spring samples exhibit  $\text{Cl}^-$  concentrations that exceed those typically measured from baseflow samples and groundwater samples from the regional N-aquifer. For example, Sand Spring (location 32) has a  $\text{Cl}^-$  content of 93 mg/l as compared to less than 20 mg/l for baseflow. The elevated  $\text{Cl}^-$  concentrations suggest that either springs are contaminated by past operations at the UMTRA site, or the N-aquifer is subject to evaporative concentration near points of discharge.

One baseflow sample requires specific mention. The sample from Moenkopi Wash at the I-89 highway overpass (location 28) was the furthest downstream sample collected. This sample has a high  $\text{Cl}^-$  concentration relative to other upstream baseflow samples. The  $\text{Cl}^-$  to  $\text{Br}^-$  ratio for this sample is greater than four times the average of the other surface water and spring samples. Through Kerley Valley, effluent from single family residences, treated effluent from a sewage treatment facility, irrigation return flows, and refuse disposal in the wash may all contribute to the observed water quality at the I-89 sampling location.

### 7.3 Qualitative analysis

Stoichiometric relationships were used to qualify the existence and role of the dominant reactions in Chapter 6. The next two sections apply this same approach to examine the geochemistry of the surface water systems. The reader

should note that the chemical composition of the baseflow and spring samples reflects not only reactions along the streamcourse, but the geochemistry of the source water.

### 7.3.1 Ion exchange processes

Elevated  $\text{Na}^+$  concentrations are limited to the confined system of the N-aquifer and are attributed to Na cation exchange. Baseflow  $\text{Na}^+$  concentrations are typically greater than 80 mg/l and exceed the average concentration for the unconfined N-aquifer.  $\text{Na}^+$  concentrations for Moenkopi Wash range from 34.8 mg/l at Quicksand Spring (location 22) to 348 mg/l for Coal Mine Canyon (location 4). Concentrations range from 35 to 216 mg/l along Dinnebito Wash.

Figure 7-2 shows  $\text{Na}^+$  as a function of  $\text{Cl}^-$ . The baseflow samples have substantial excess Na concentrations, accounting for an average of 93 percent of measured  $\text{Na}^+$ . Spring samples and Pasture Canyon Reservoir have smaller concentrations of excess Na and lie closer to the theoretical halite dissolution line. On this basis, NaCl dissolution contributes typically less than 10 percent of the measured  $\text{Na}^+$  concentrations for baseflow samples.

Cation exchange is responsible for the observed  $\text{Na}^+$  concentrations in the surface water samples. Figure 7-3 is a log activity diagram with  $\text{Ca}^{2+}$  and  $\text{Na}^+$  for N-aquifer groundwater samples and surface water samples along Moenkopi and Dinnebito washes. The wash samples are at the intersection of the two trends

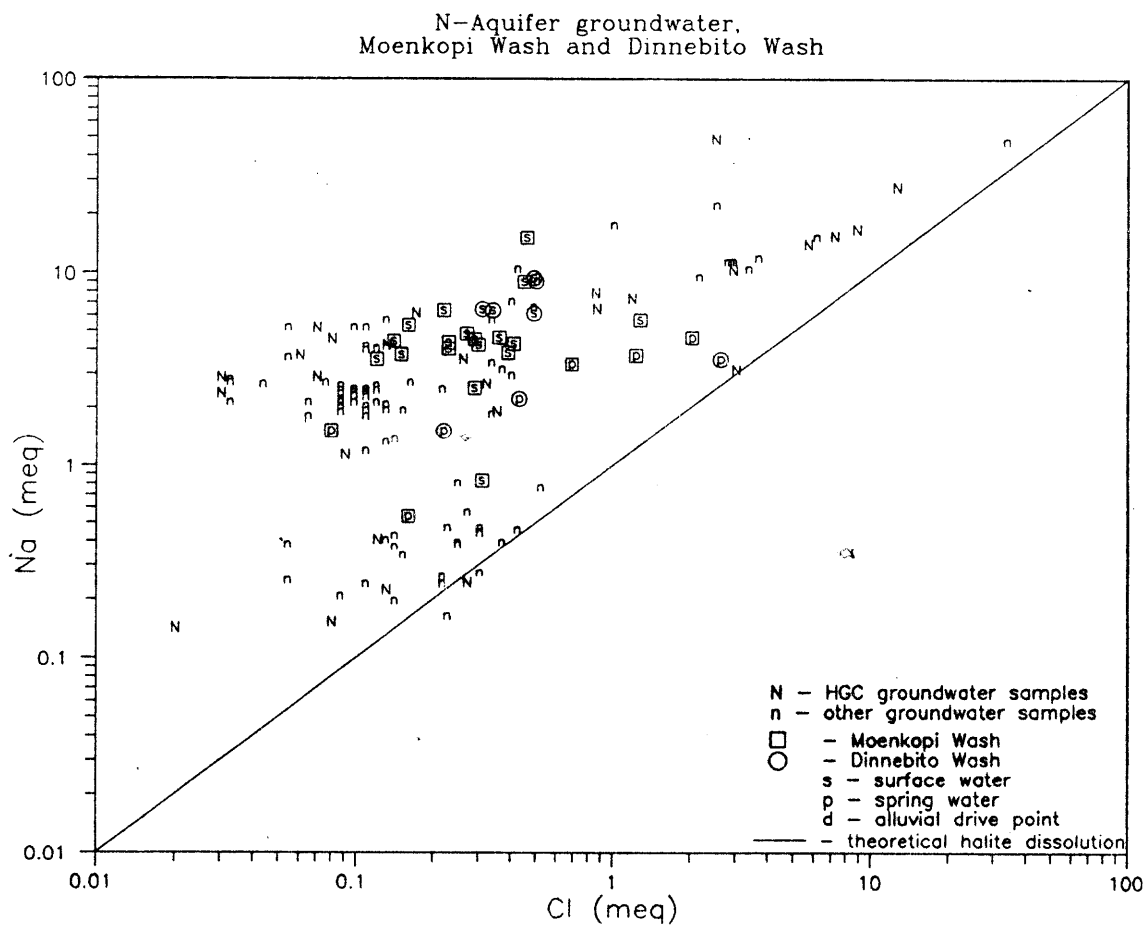


Figure 7-2.  $\text{Na}^+$  as a function of  $\text{Cl}^-$  for N-aquifer and wash samples.

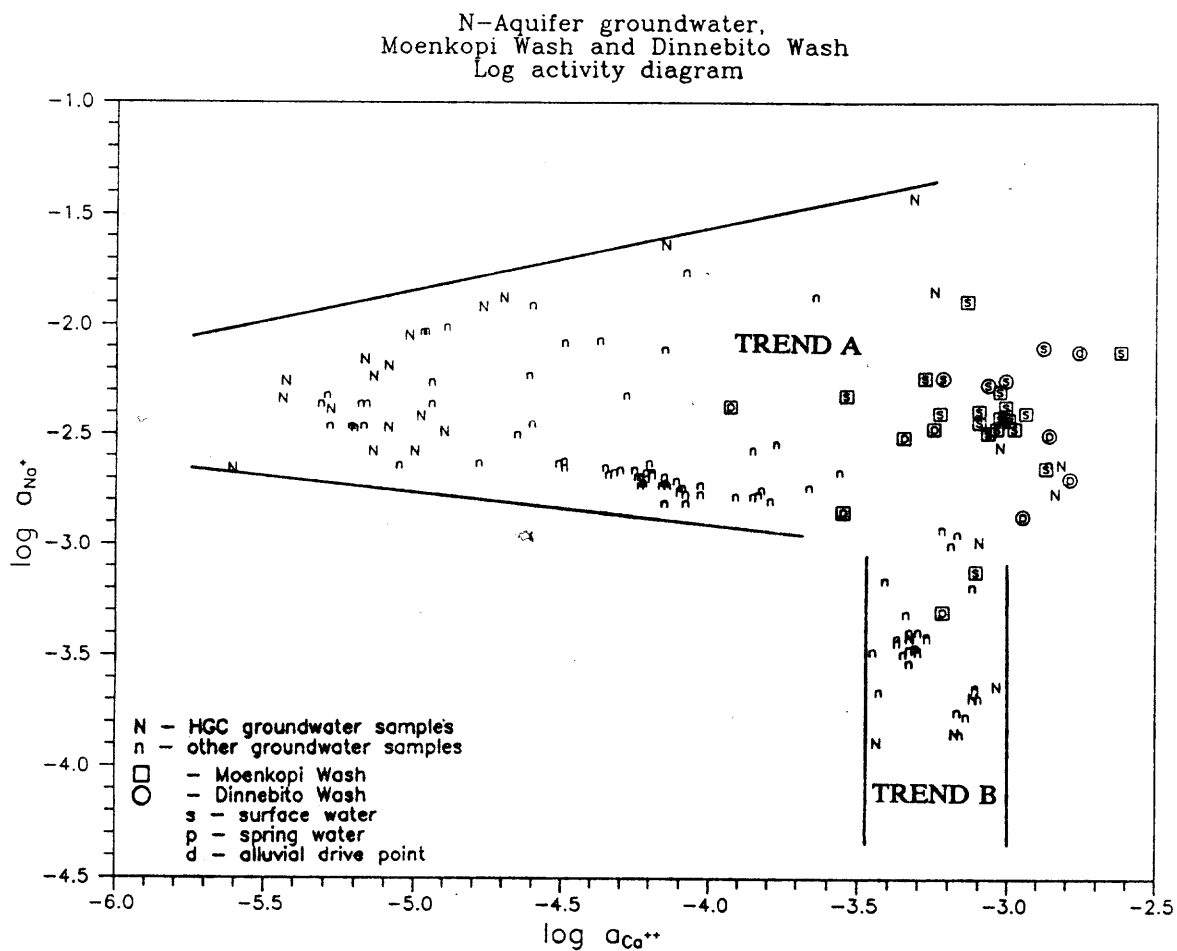


Figure 7-3. Log-activity diagram for  $\text{Na}^+$  as a function of  $\text{Ca}^{2+}$  for N-aquifer and wash samples. Trends A and B correspond to groundwater samples from the confined and unconfined N-aquifer systems, respectively.

identified for the N-aquifer.  $\text{Ca}^{2+}$  concentrations are consistent with open system calcite dissolution in that they lie along trend B with groundwater samples from the unconfined N-aquifer.  $\text{Na}^+$ , however, is elevated to concentrations comparable to samples from the confined N-aquifer. With corrections to measured  $\text{Ca}^{2+}$  for interferences from calcite and gypsum dissolution and Ca-Mg ion exchange, Figure 7-4 shows a pronounced 1:1 linear relationship between excess Na and  $\text{Ca}^{2+}_{\text{corr}}$ . This relationship strongly supports cation exchange.

The distinct Na- $\text{HCO}_3$  water type found in the confined N-aquifer was shown to evolve from a Ca- $\text{HCO}_3$  water type as the result of Na cation exchange. Evidence for exchange reactions in baseflow supports a confined N-aquifer origin. Inasmuch as clays exist in the alluvial sediment, cation exchange could occur by interaction with alluvial sediment and baseflow could potentially originate from the unconfined N-aquifer if followed by rapid and intensive cation exchange with alluvial clays. However, with intensive cation exchange, excess Na would be expected to increase in the downstream direction as surface flow interacts with alluvial sediment. This increase is not observed in the profiles along either wash. As will be discussed in section 7.5, the isotopic composition of baseflow samples identify the confined N-aquifer as the dominant source for baseflow discharge.

The  $\text{Mg}^{2+}$  concentrations for samples from surface water, springs and drive points are similar to those from the unconfined N-aquifer. Magnesium concentrations range from 1.1 to 25.2 for Moenkopi Wash, and from 13.9 to 61.7

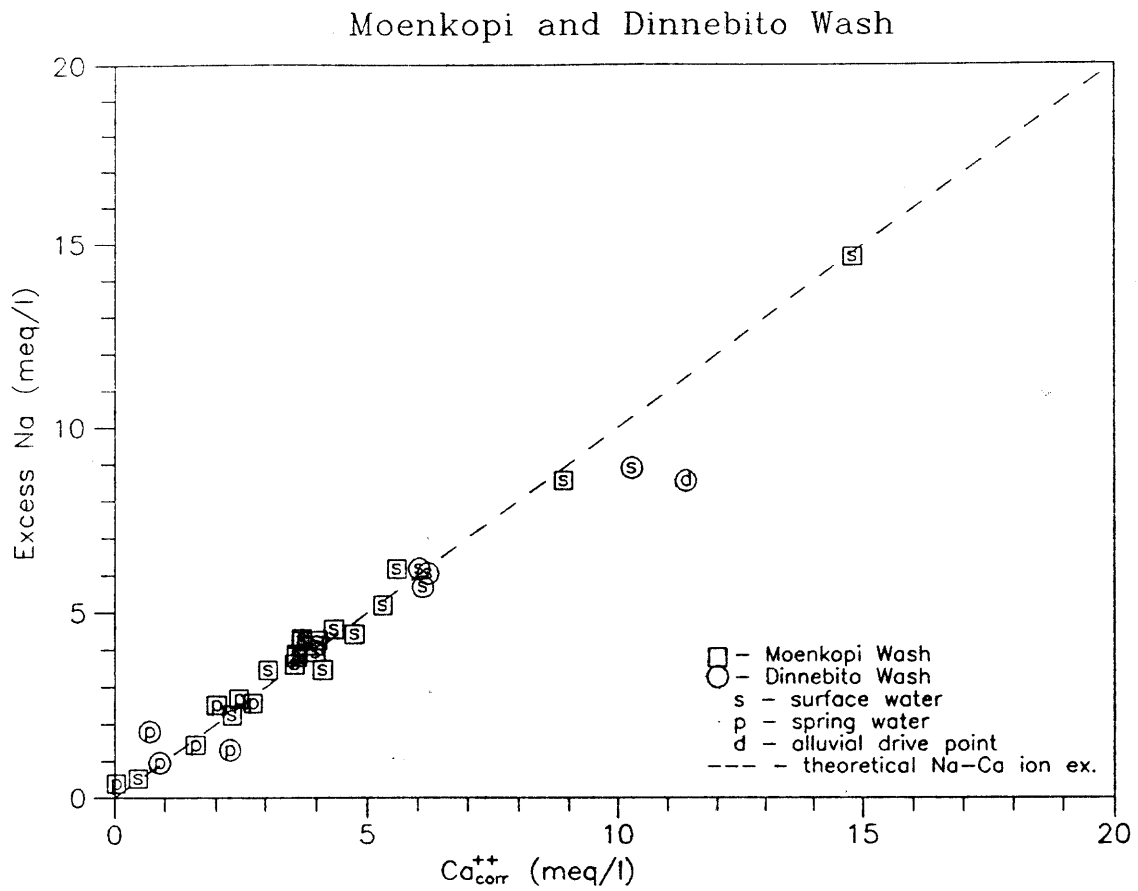


Figure 7-4. Excess Na as a function of corrected Ca<sup>2+</sup> for wash samples. Corrections are for Ca<sup>2+</sup> contributed by calcite and gypsum dissolution.

mg/l for Dinnebito Wash as compared to less than 0.3 mg/l in the confined N-aquifer. When compared to  $\text{Ca}^{2+}$  in a log-activity diagram (Figure 7-5), they fall along a 1:1 linear trend which suggests Ca-Mg exchange.

### 7.3.2. Calcite and gypsum dissolution/precipitation reactions

Both calcite and gypsum dissolution play an important role in the evolution of baseflow along the washes. In general, groundwater entering open system conditions accepts  $\text{CO}_2$  and dissolves calcite from the N-aquifer formations and the alluvial sediment. Gypsum is also dissolved from the alluvial sediment along the washes, resulting in supersaturated conditions with respect to calcite from the common ion effect.

The same approach was followed as with the N-aquifer in Chapter 6 to examine the role of calcite dissolution and precipitation reactions in the surface water system. Figure 7-6a shows total alkalinity as a function of the uncorrected  $\text{Ca}^{2+}$  concentration. The locations of samples along the abscissa represent the net concentration of  $\text{Ca}^{2+}$  contributed by calcite and gypsum dissolution and lost through ion exchange. Figure 7-6b shows alkalinity as a function of  $\text{Ca}^{2+}$  corrected for the effects of cation exchange. The  $\text{Ca}^{2+}$  concentration in spring samples is controlled largely by calcite solubility. Most baseflow samples have  $\text{Ca}^{2+}$  concentrations in excess of what may be expected from calcite dissolution and may be attributed to gypsum dissolution. By adding an equivalent amount of  $\text{SO}_4^-$  to

N-Aquifer groundwater,  
Moenkopi Wash and Dinnebito Wash  
Log activity diagram

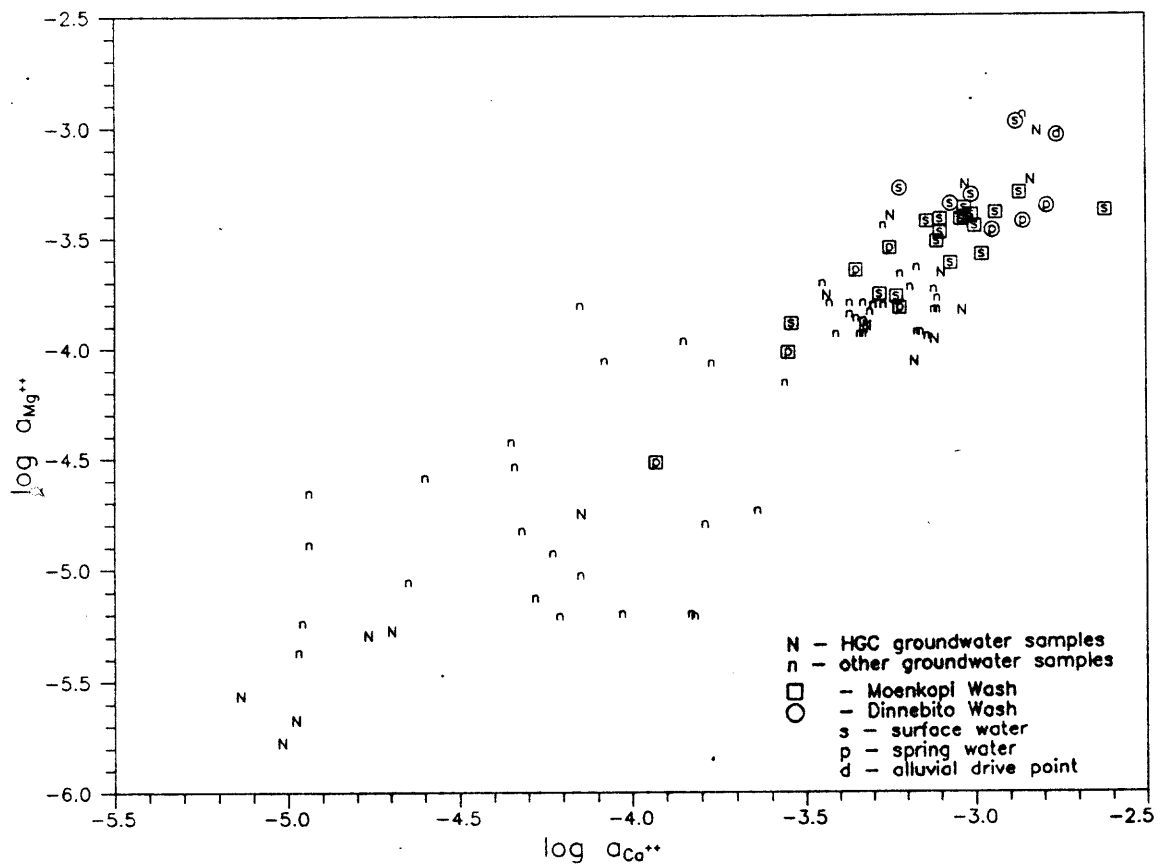


Figure 7-5. Log-activity diagram for  $Mg^{2+}$  as a function of  $Ca^{2+}$  for N-aquifer and wash samples.

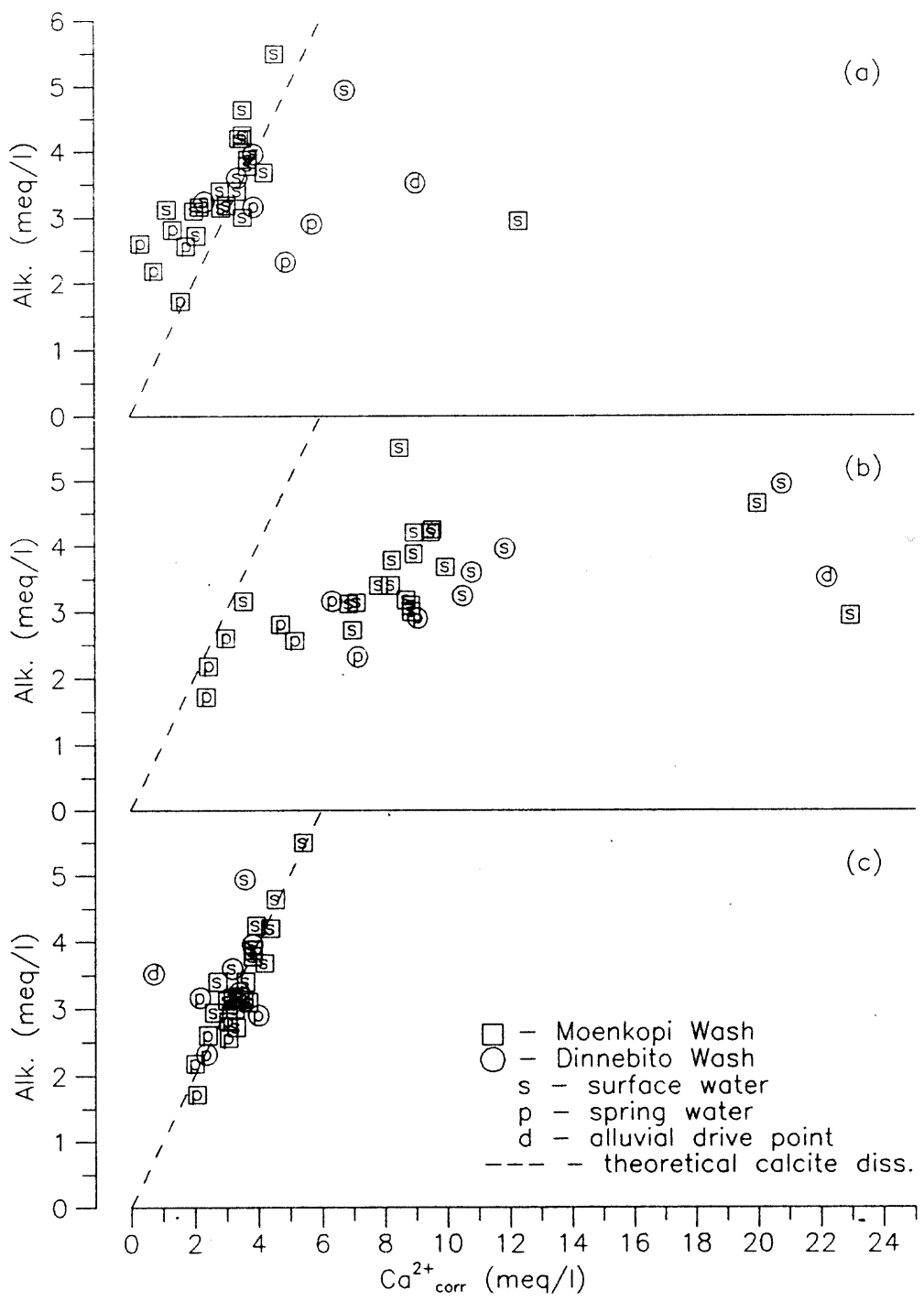


Figure 7-6. Alkalinity as a function of  $Ca^{2+}$ ; uncorrected (a), corrected for ion exchange (b), and corrected for gypsum dissolution (c), for wash samples.

account for the effects of gypsum dissolution, nearly all samples lie along the theoretical calcite dissolution line in Figure 7-6c. Samples that deviate from this line are possibly affected by analytical error or unidentified reactions.

Most calcite dissolution occurs during or shortly after groundwater discharge. Alkalinity rises from the water caves to the confluence with Begashibito Wash, below which, it remains relatively constant. The results of speciation calculations in chapter 8 show that samples are saturated to supersaturated with respect to calcite and therefore, calcite would be expected to precipitate from solution. Calcite saturation indices range from -0.22 to 1.37 for Moenkopi Wash and -0.07 to 1.30 for Dinnebito Wash. The trend for baseflow samples is toward increased supersaturation in the downstream direction.

Calcite is abundant in the alluvial sediment. During the field investigation, large areas along the banks were encrusted with a white crystalline substance that effervesced when dilute hydrochloric acid was applied. The substance was more prevalent along banks located in direct sunlight (northern banks) and typically extended to several feet above baseflow stage. One explanation is that storm runoff enters bank storage during elevated stream stage and dissolves calcite from the alluvial sediment. Once the flood stage recedes, bank storage discharges to the wash and calcite precipitates from solution due to evaporation or increasing water temperature.

Gypsum dissolution contributes the majority of the total  $\text{Ca}^{2+}$  in surface water samples and influences calcite solubility by the common ion effect. The  $\text{SO}_4^{=}$  concentrations for baseflow samples exceed those for the regional N-aquifer and typically fall between 180 to 250 mg/l. The concentration increases slightly in the downstream direction. Samples for Horse Corral Tributary and Coal Mine Canyon, both tributaries along the gaining reach of Moenkopi Wash, contain high  $\text{SO}_4^{=}$  concentrations, measuring 977 and 741 mg/l, respectively.

As with the examination of calcite dissolution, corrections to the measured  $\text{Ca}^{2+}$  concentration were employed to isolate the effects of gypsum dissolution. Figure 7-7a shows  $\text{SO}_4^{=}$  as a function of uncorrected  $\text{Ca}^{2+}$  and illustrates the effects of competing reactions involving  $\text{Ca}^{2+}$ . By correcting for cation exchange reactions, Figure 7-7b provides a measure of the relative  $\text{Ca}^{2+}$  contribution from both calcite and gypsum dissolution. With all the corrections, samples lie along the theoretical gypsum dissolution line in Figure 7-7c. Dinnebito Wash samples typically lie higher along the theoretical line indicating a greater degree of gypsum dissolution than for Moenkopi Wash.

Gypsum dissolution is consistent with calculated saturation indices described in Chapter 8. Baseflow samples are undersaturated to saturated with respect to gypsum. Saturation is approached in the downstream direction indicating that a source for gypsum must exist beyond the gaining reach above Begashibito Wash. As shown in Appendix F,  $\text{Ca}^{2+}$  concentrations remain relatively constant in the

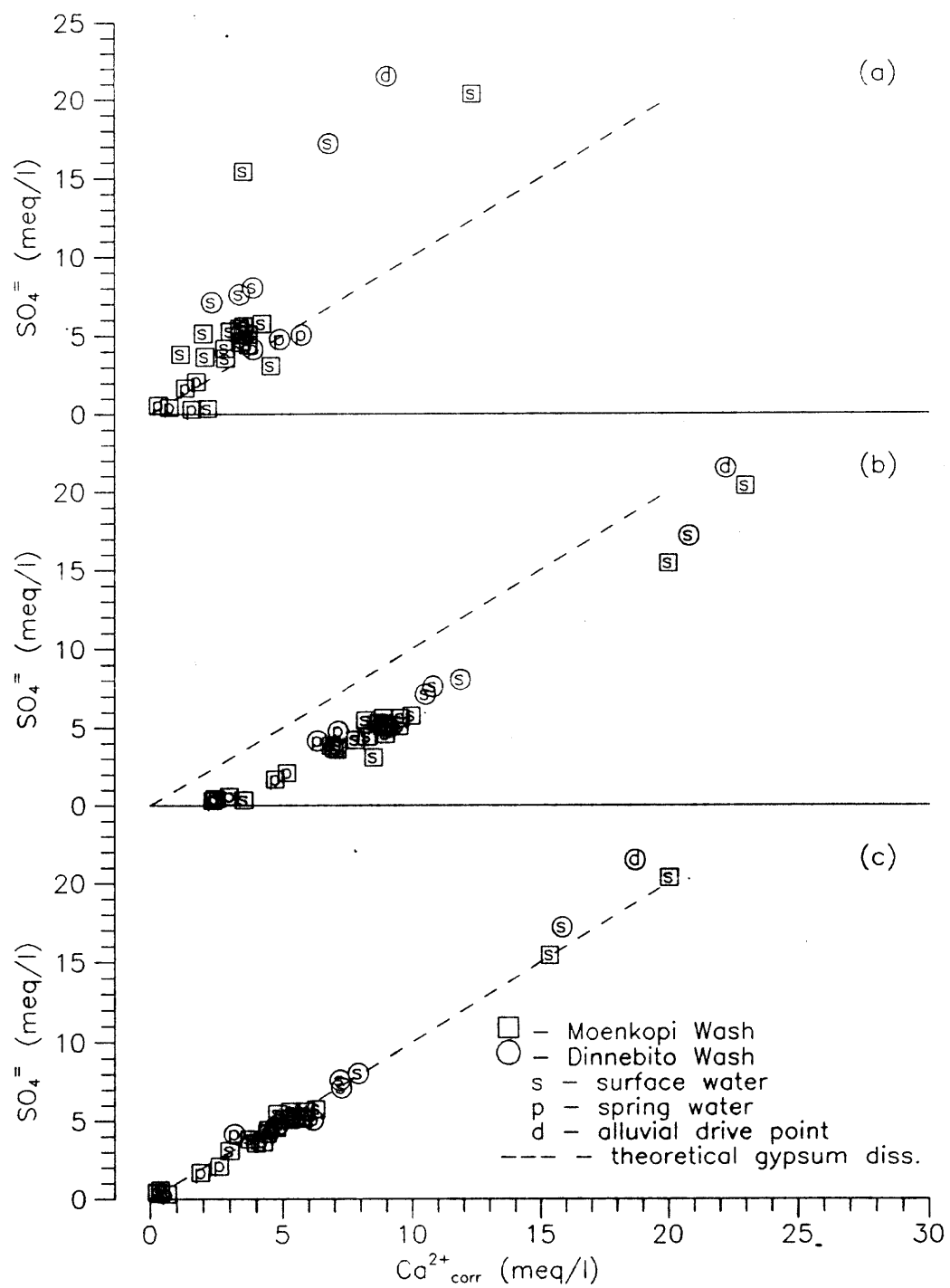


Figure 7-7.  $SO_4^{2-}$  as a function of  $Ca^{2+}$ ; uncorrected (a), corrected for ion exchange (b), and corrected for calcite dissolution (c), for wash samples.

downstream direction while the  $\text{SO}_4^-$  concentration and gypsum saturation index increase. The  $\text{SO}_4^-$  source is most likely from the dissolution of gypsum from the alluvial sediment. The alluvial sediment is probably derived, in part, from weathering of gypsiferous formations upstream. The analysis of sulfur isotopes presented in the next section supports a  $\text{SO}_4^-$  of marine origin for baseflow as opposed to an atmospheric origin.

#### 7.4 Isotopic Indications

Hydrogen and oxygen and sulfur isotopes can be valuable in distinguishing processes not readily apparent from chemical analyses. For example, the ionic composition of samples from baseflow suggest dissolution of gypsum to be the dominant source of elevated  $\text{SO}_4^-$ . The sulfur isotopic composition suggests that the  $\text{SO}_4^-$  may be of marine shale origin, and therefore, would be due to the weathering of upstream Cretaceous formations with deposition as channel alluvium along the perennial reaches. In this section, the isotopic composition of springs, surface water and alluvial groundwater from Moenkopi and Dinnebito washes are analyzed. Section 7.5 describes in greater detail isotopic indications regarding surface water and alluvial interactions.

#### 7.4.1. Deuterium and Oxygen-18

Figure 7-8 shows  $\delta D$  as a function of  $\delta^{18}O$  for Moenkopi Wash and the N-aquifer. All samples plot to the right of the MWL indicating that one or more processes are affecting the isotopic composition. Baseflow samples plot along a line sub-parallel to the MWL with a slope of 5.4 and an intercept on the MWL of  $\delta^{18}O = -17.3\text{‰}$ ,  $\delta D = -151\text{‰}$ . The seven lightest water samples from Moenkopi Wash correspond to the gaining reach above the confluence with Begashibito Wash and exhibit  $\delta^{18}O$  concentrations equal to those of the confined N-aquifer paleowater. The profiles for  $\delta D$  and  $\delta O^{18}$  for Moenkopi Wash are provided in Appendix F.

Figure 7-9 shows  $\delta D$  as a function of  $\delta^{18}O$  for Dinnebito Wash. A standard linear regression for baseflow samples has a slope of 2.59, and an intercept on the MWL of  $\delta^{18}O = -13.6\text{‰}$ , and  $\delta D = -100.5\text{‰}$ . If the regression represents an evaporation line, then the MWL is intersected at the paleowater cluster for the N-aquifer suggesting that the sampled baseflow originates entirely from the confined N-aquifer. The  $\delta^{18}O$  and  $\delta D$  profiles for Dinnebito Wash are provided in Appendix G.

Evaporative enrichment is suggested as the primary process responsible for the observed shift from the MWL. In semi-arid zones the water loss by evaporation assumes importance, often with the result that the heavy isotope species in the groundwater are enriched relative to those of precipitation, shifting the isotopic composition of groundwater away from the meteoric water line along evaporation

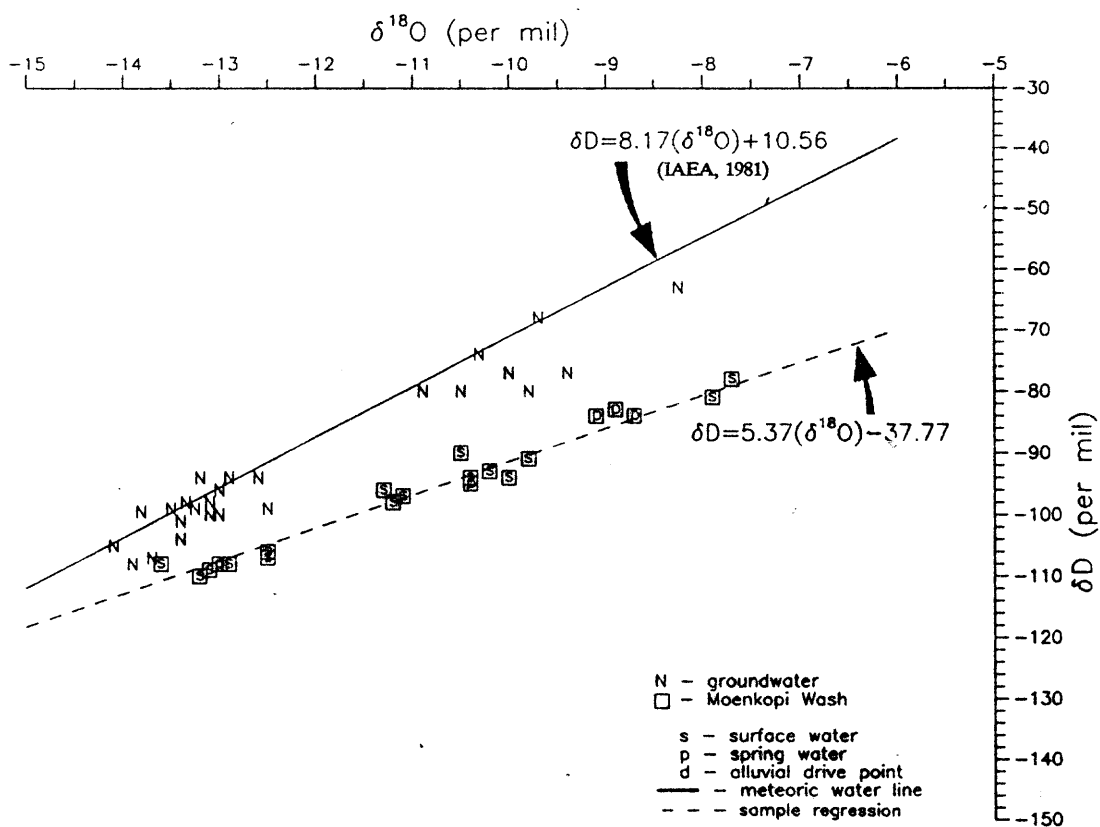


Figure 7-8.  $\delta\text{D}$  as a function of  $\delta^{18}\text{O}$  for N-aquifer and Moenkopi Wash samples.

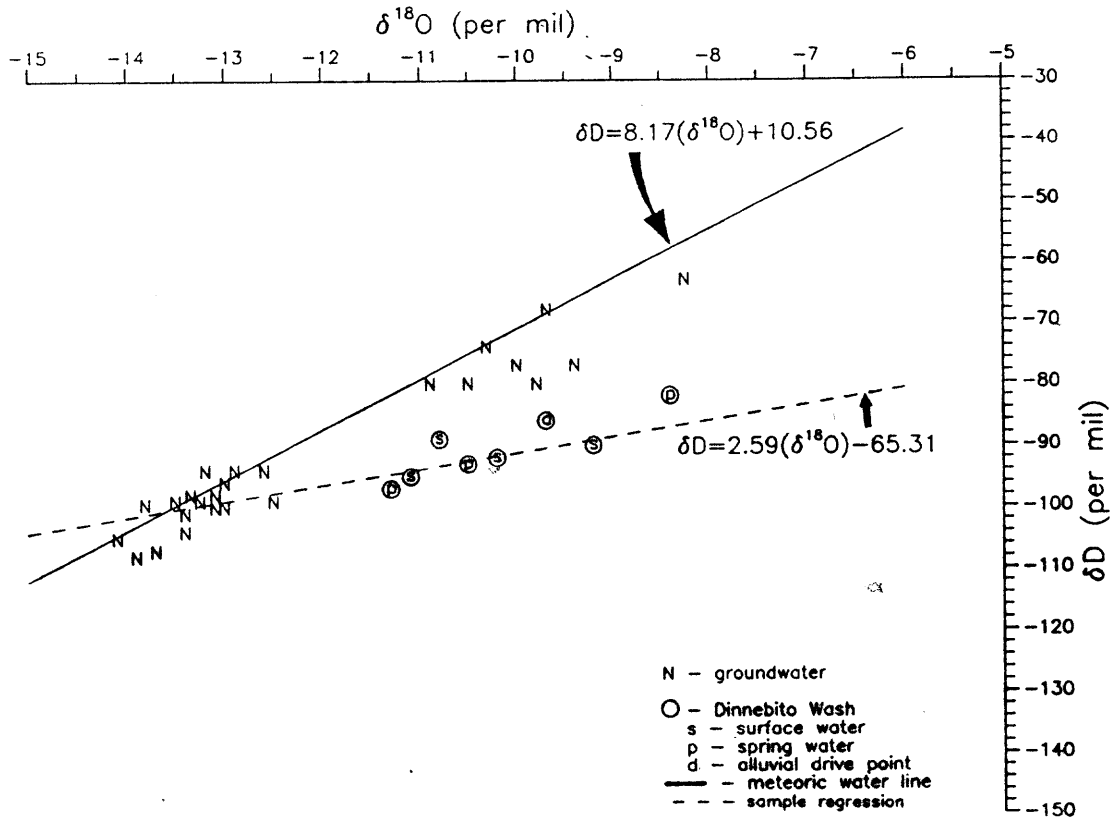


Figure 7-9.  $\delta\text{D}$  as a function of  $\delta^{18}\text{O}$  for N-aquifer and Dinnebito wash samples.

lines (IAEA, 1981). Samples were collected during the winter months when evaporation and transpiration were minimal, however, most surface water samples lie along what appears to be one or more evaporation trends.

The gradient representing evaporative enrichment of  $\delta D$  with respect to  $\delta^{18}O$  was estimated from the isotopic composition of samples from Pasture Canyon Spring and Pasture Canyon Reservoir (the former feeds into the latter). The computed slope of the evaporation line is 4.3. This assumes that the spring sample is representative of inflow to the reservoir, and that the reservoir sample represents the average isotopic composition. For comparison, the slope of a linear regression using the first seven upstream baseflow samples from Moenkopi Wash above Begashibito Wash is 4.4. These values compare well and fall within the range of 3.5 to 6.0 for slopes of evaporation trends reported in the literature (IAEA, 1981). If the actual slope of the evaporation line is about 5.4, the isotopic shift along Moenkopi Wash may be explained entirely by evaporative enrichment.

In summary,  $\delta D$  and  $\delta^{18}O$  compositions for baseflow samples indicate predominantly a paleowater origin for the baseflow along the upper perennial reaches. Both  $\delta D$  and  $\delta^{18}O$  become gradually heavier in the downstream direction which suggests limited mixing and/or exchange with water in the alluvium. The increasing differential enrichment of  $\delta^{18}O$  with respect to  $\delta D$  in the downstream direction indicates intensive evaporation. A description of the physical processes associated with the different mixing scenarios is presented in Section 7-5.

#### 7.4.2. Sulfur-34

Gypsiferous formations are not known to be abundant in the units which comprise the N-aquifer. Possible mechanisms to explain the elevated  $\text{SO}_4^-$  concentrations in baseflow samples include 1) local N- and D-aquifer mixing, 2) dissolution of sulfur-bearing alluvial minerals, 3) atmospheric input with evaporative enrichment, and 4) other unidentified sources.

For Moenkopi Wash,  $\delta^{34}\text{S}$  for baseflow samples ranges from -2.5 to -20‰, and -7.9 to +1.0‰ for spring samples. For Dinnebito Wash,  $\delta^{34}\text{S}$  for baseflow samples ranges from -8.9 to -9.7‰, and -9.4 to +8.4‰ for spring samples.  $\text{SO}_4^-$  increases slightly and  $\delta^{34}\text{S}$  become heavier (from -15 to -10‰) in the downstream direction along Moenkopi Wash. Appendices F and G provide  $\delta^{34}\text{S}$  profiles along Moenkopi Wash and Dinnebito Wash, respectively.

Observations along Moenkopi Wash suggest that interaction with alluvial sediment may be the source for  $\text{SO}_4^-$  in baseflow samples. The isotopically lightest baseflow samples occur along the gaining reach between the water caves and the confluence with Begashibito Wash.  $\text{SO}_4^-$  concentrations and  $\delta^{34}\text{S}$  values downstream of the confluence with Coal Mine Canyon remain constant where streamflow remains constant or declines. Because discharge from the N-aquifer to the washes is diffuse, gypsiferous materials may be dissolved during flow through the alluvium and, to a lesser degree, by downstream interaction with alluvial sediment.

Figure 7-10 shows  $\delta^{34}\text{S}$  against the reciprocal of the  $\text{SO}_4^{=}$  concentrations for Moenkopi Wash together with N-aquifer samples. Most groundwater samples exhibit variable  $\text{SO}_4^{=}$  concentrations but, overall, exhibit a heavy  $\delta^{34}\text{S}$  composition. The heavier values suggest an atmospheric origin for  $\text{SO}_4^{=}$ , given the lack of mineralogic evidence for evaporite deposits. The trend toward higher  $\text{SO}_4^{=}$  concentrations generally follows a confined flow path (analyses for sulfur isotopes were not performed for samples collected from the unconfined N-aquifer). Analysis of sulfur isotopes for spring samples suggests a mixed atmospheric/marine gypsum source and may be typical for the regional unconfined N-aquifer.

Alluvial sediment near the water caves and for a distance downstream is most likely derived from weathering of upstream Cretaceous formations. These formations would be an abundant source of sulfur-bearing minerals, mostly of marine shale origin. This sediment would exhibit a light  $\delta^{34}\text{S}$ . Although all baseflow samples typically exhibit a  $\delta^{34}\text{S}$  of marine shale origin, a trend toward heavier  $\delta^{34}\text{S}$  with increasing  $\text{SO}_4^{=}$  is apparent in the downstream direction. This trend is most likely a result of gypsum dissolution from the alluvium. Downstream, the alluvium is likely to contain an increasing degree of isotopically-heavier  $\text{SO}_4^{=}$  from the Jurassic formations.

Several samples are worth individual mention. Stream samples were collected at Horse Corral Tributary to the north (location 26) and Coal Mine Canyon to the south (location 4), both tributaries to Moenkopi Wash which dissect

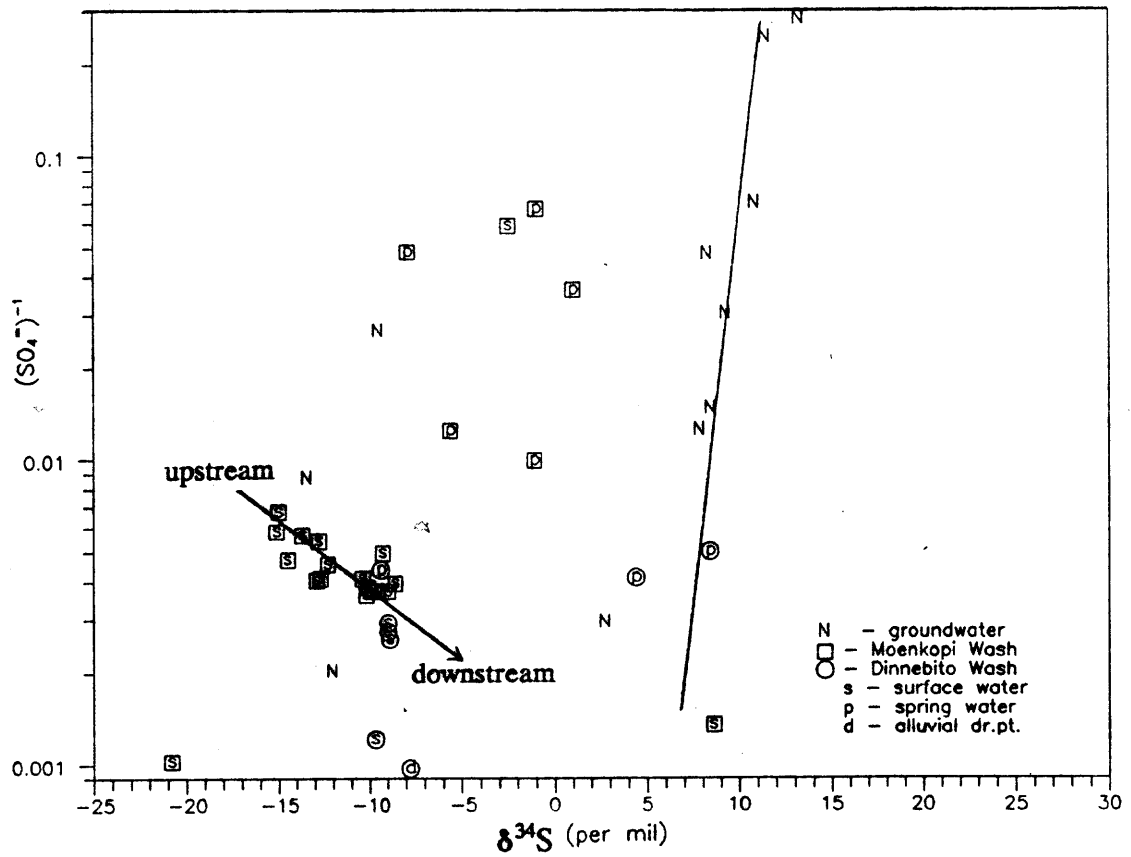


Figure 7-10. The inverse of  $SO_4^{2-}$  as a function of  $\delta^{34}S$  for N-aquifer and wash samples.

the N-aquifer and upper Jurassic and Cretaceous units. Although their contribution to baseflow discharge is small, they are illustrative of the geochemical heterogeneities within system. The washes follow steep and narrow gorges with narrow alluvial deposits. Both samples exhibit elevated  $\text{SO}_4^-$  concentrations measuring 977 and 741 mg/l, however, the water types and isotopic compositions are strikingly different. Horse Corral Tributary is a  $\text{Ca-SO}_4$  water type with a heavy  $\delta^{34}\text{S}$  value suggestive of a marine shale origin (-20.8‰). Coal Mine Canyon is a  $\text{Na-SO}_4$  water type with a light  $\delta^{34}\text{S}$  value (+8.6‰). Both washes were found to be dry a short distance upstream of each confluence. The chemical composition of baseflow in each canyon is most likely a result of interactions with sediment derived from different formations.

### 7.5 Surface water and groundwater interactions

The preponderance of data suggests that the majority of the baseflow sampled along the washes is initially derived from N-aquifer groundwater discharges originating from the confined system. However, as discussed in the previous sections, downstream variations of certain ionic species and isotopes in baseflow samples suggest some limited interaction with channel alluvium, and/or mixing with other sources. The purpose of this section is to describe the surface water and groundwater interactions in terms of the observed water quality along the washes,

and where possible, to distinguish between the effects of groundwater mixing and interaction with alluvial sediment.

The conceptual model for the surface water and groundwater interactions includes only limited mixing with water from sources other than the confined N-aquifer. Baseflow is derived largely, if not completely, from N-aquifer discharges originating from the confined system. The chemical signature of baseflow is established during groundwater discharge through the channel alluvium, and thereafter, from interaction of baseflow with the channel alluvium. This interaction involves some mixing of baseflow with the alluvial groundwater which plays an important role in the geochemistry.

Water sources for mixing include infiltrating storm runoff, discharges from the unconfined N-aquifer and direct precipitation. The alluvial valley begins at the confluence of Coal Mine Canyon (refer to Plate 3) and all discharging groundwater from the N-aquifer and springs must enter the valley alluvium. In the conceptual model, transpiration by phreatophytes and evaporation from bare soils depletes the alluvial aquifer at a rate exceeding the combined recharge from infiltrating storm runoff, discharge from the N-aquifer, and direct precipitation. The alluvium is a sink for all but the winter months. The shallow aquifer is subject to intense evaporation during all but the winter months resulting in a highly-mineralized groundwater that is differentially enriched in  $\delta^{18}\text{O}$  with respect to  $\delta\text{D}$ . The trend in baseflow, therefore, is gradually toward an isotopically heavier and enriched

water in the downstream direction as a result of mixing or exchange with alluvial groundwater.

The aforementioned concept of an alluvial sink is supported by examining the EC measured for groundwater from alluvial drive points along Moenkopi Wash. Figure 7-11 shows the EC profile along Moenkopi Wash with standard linear regressions for samples from drive points and baseflow. Field measurements of groundwater samples from the four Moenkopi Wash drive points show that EC increases sharply, at a rate of nearly 100  $\mu\text{S}/\text{cm}/\text{mile}$  in the downstream direction. The increase in EC for alluvial groundwater in the downstream direction is most likely the result of evaporative concentration and mineralization. The effects of mixing on baseflow composition are not apparent. Inasmuch as the alluvial EC levels rise downstream, the lack of the baseflow EC response, only 2.5  $\mu\text{S}/\text{cm}/\text{mile}$ , indicates very limited mixing with alluvial groundwater.

The  $\delta\text{D}$  and  $\delta^{18}\text{O}$  isotope data support limited mixing and/or evaporative concentration, although the ionic composition of baseflow along Moenkopi and Dinnebito washes does not change appreciably with distance along the streamcourse. Mixing calculations were performed for Moenkopi Wash to determine what percentage of mixing with additional water sources was required to achieve the observed isotopic shift. These calculations were based on the  $\delta\text{D}$  and  $\delta^{18}\text{O}$  isotopic compositions of springs, groundwater, and baseflow samples, and precipitation. The first approach involved mixing spring water with the initial

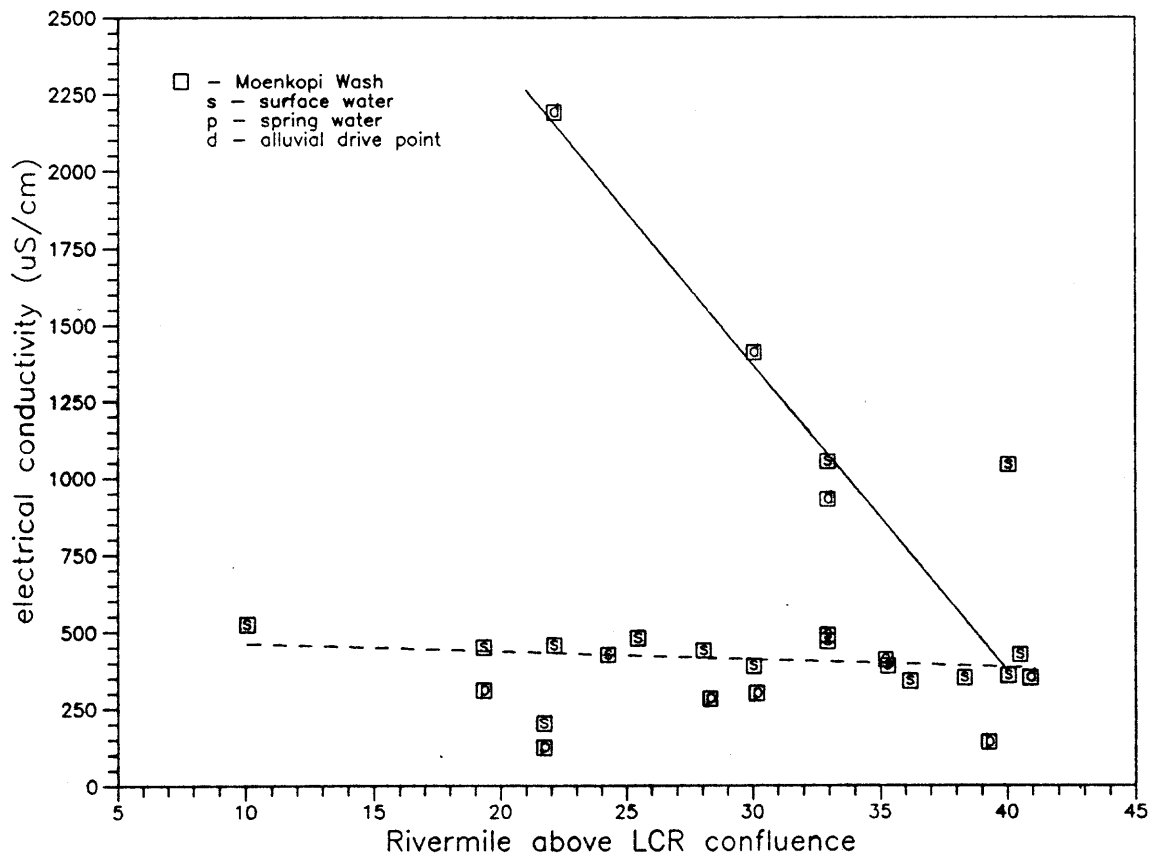


Figure 7-11. Electrical conductivity as a function of distance along Moenkopi Wash. Lines for surface water and drive point samples calculated with linear regression analysis.

baseflow composition to derive the observed downstream isotope ratios. The second and third approaches evolved baseflow along evaporative fractionation gradients with subsequent mixing of representative unconfined N-aquifer groundwater and precipitation. Calculations were constrained only by isotope data. The results of these calculations are presented in Table 7-1. Mixing ratios were not computed for Dinnebito Wash because the computed slope using regression analysis for baseflow samples is below the range for evaporation.

Without evaporation, the observed isotopic shift could not be reproduced by mixing either with N-aquifer groundwater or with precipitation. With evaporative enrichment, however, estimates of contributions from the unconfined N-aquifer range from 19 to 35 percent and 11 and 22 percent from precipitation. The isotopic constraints were also satisfied if 61 percent of the measured baseflow along Moenkopi Wash is derived from water similar in isotopic composition to the sampled springs. This degree of mixing with spring water, however, is inconsistent with the measured  $\text{Cl}^-$  and  $\text{NO}_3^-$  concentrations and with the observed streamflow profile.

If baseflow is sustained by N-aquifer discharges originating in the confined system, then evapotranspiration losses along Moenkopi Wash downstream of Begashibito Wash must equal or exceed discharges from the unconfined system. Calculations were performed to estimate the amount of groundwater discharging from the unconfined portion of the N-aquifer into Moenkopi Wash valley and the

Table 7-1

Hypothetical mixing and evaporative enrichment  
along Moenkopi Wash  
(concentrations are in per mil)

Mixing Scenario	Components		Results					
	$\delta^{18}\text{O}$	$\delta\text{D}$	$\delta^{18}\text{O}^2$	Mixed <sup>3</sup>	$\delta^{18}\text{O}$	Mixed	$\delta^{18}\text{O}$	Mixed
	A. Upstream baseflow		-12.6		-110			
	B. Downstream baseflow		-10.0		-93			
	C. N-aquifer springs		-8.8		-82			
	D. N-aquifer (unconfined)		-10.0		-76			
	E. Precipitation <sup>1</sup>		-7.5		-60			
1. A+C			-10.3	61%				
2. A+D (#B)								
3. A+E (#B)								
			gradient = 3.0		Evaporation <sup>4</sup> gradient = 4.0		gradient = 5.0	
4. A-EVAP+D			-10.0	35%	-10.0	27%	-10.0	19%
5. A-EVAP+E			-9.5	22%	-9.6	17%	-9.7	11%

<sup>1</sup> estimates for precipitation from Flagstaff, Az. IAEA/WMO station;  $\delta^{18}\text{O} = -8.62$ ,  $\delta\text{D} = -66.7$  reported weighted mean composition; corrected for altitude effect with  $-0.26\text{‰}(\delta^{18}\text{O})/100$  meters (IAEA, 1981).

<sup>2</sup> calculated by mixing to  $\delta\text{D}$  value

<sup>3</sup> percentage of mixing as volume of alternate source to volume of baseflow

<sup>4</sup> gradients represent evaporative fractionation of  $\delta\text{D}$  with respect to  $\delta^{18}\text{O}$

amount of evapotranspiration losses from the alluvium. A detailed geologic cross-section and aquifer properties were available for the UMTRA Tuba City site (USDOE, 1989). Groundwater flow normal to the wash was computed using Darcy's law in one-dimension. Evapotranspiration losses from phreatophytes and bare soil were determined using a procedure by Rantz (1968) adapted by the Arizona Department of Water Resources (1989). This procedure is outlined in Appendix H.

Groundwater flow and ET loss estimates are based on the following assumptions:

- phreatophyte density along the wash averages 25 percent of alluvial area
- phreatophyte communities consist of 20 percent willow and cottonwoods, and 80 percent tamarisk
- consumptive use coefficient for cottonwoods and willows is 1.5 and 1.6 for tamarisk (ADWR, 1989)
- the sum of the mean monthly temperatures and percent of daytime hours during the year for the growing season is similar for Winslow, Arizona
- average evaporation from bare soils along the valley alluvium is one ft/yr
- the reported geometric mean of hydraulic conductivity values (163 ft/yr) calculated from slug and aquifer tests at the UMTRA Tuba City site (USDOE, 1989) is representative of the N-aquifer in the vicinity of Moenkopi Wash
- the representative hydraulic gradient for N-aquifer groundwater north of Moenkopi Wash is 0.007 ft/ft (USDOE, 1989)

- total saturated thickness of the N-aquifer north of Moenkopi Wash is 360 feet (USDOE, 1989)
- the alluvial valley is 1000 feet wide

Calculated ET losses exceed groundwater inflow to Moenkopi Wash valley by a factor of nearly 2.5. Total groundwater flow to the valley alluvium was calculated to be 1.1 ft<sup>2</sup>/day for a unit length along the wash. The ET and bare-soil evaporation (weighted by area) was estimated to be 2.7 ft<sup>2</sup>/day and is considered a conservative estimate. In many areas the tamarisk density exceeds 25 percent of the alluvial area, and the calculations do not include evaporation losses from spring discharges nor from the Navajo Sandstone where the water table is near the surface.

Without ET losses, the total potential groundwater discharge to the Moenkopi Wash valley is estimated to be about 585 AF/Yr from the unconfined N-aquifer between the confluence of Coal Mine Wash and Tuba City, a distance of about 12 miles. This is a maximum of 25 percent of the total 2245 AF/Yr of baseflow (assuming an average annual baseflow of 3.1 cfs). This value agrees with the mixing calculations performed for  $\delta D$  and  $\delta^{18}O$  which estimated 27 percent mixing with groundwater from the unconfined system (assuming evaporative fractionation with a gradient of 4.0). The sampling was conducted during winter months when ET losses were minimal, therefore, this mixing ratio represents an upper limit.

## 7.6 Summary

In summary, baseflow exhibits the chemical and isotopic signature of the confined N-aquifer. Surface water samples have high- $\text{Na}^+$  from Ca-Mg-Na cation exchange. Baseflow samples also have a light  $\delta\text{D}$  and  $\delta^{18}\text{O}$  composition indicative of paleowaters recharged during a cooler and more humid environment. Gypsum dissolution from the alluvial sediment and calcite dissolution are the dominant reactions during groundwater discharge. Calcite is dissolved under open system conditions, and gypsum is dissolved as groundwater discharges through the alluvium. The common ion effect from gypsum dissolution creates supersaturated conditions with respect to calcite.

Evidence supports only minor interaction and mixing of baseflow with various water sources along Moenkopi Wash downstream of Coal Mine Canyon. Although the ionic composition of baseflow does not vary appreciably along the streamcourse, deuterium and  $^{18}\text{O}$  isotopes show some limited mixing or exchange with a heavier and evaporatively-enriched water source. A conceptual model of downstream interactions is presented and tested with various mixing scenarios and computed estimates of groundwater flow and ET losses.

## CHAPTER 8

### GEOCHEMICAL MODELING

The purpose of this chapter is to further evaluate and quantify the geochemistry for the N-aquifer and the surface water systems with the use of geochemical models. This chapter is divided into two sections. The first section describes the application and results of thermodynamic speciation modeling. The second section describes the development, application and results of mass balance and reaction path models for the N-aquifer and Moenkopi Wash.

#### 8.1 Thermodynamic speciation calculations

A description of geochemical reactions is facilitated by the use of ion activities and saturation indices (SI). Ion activities are best suited for representing solute concentrations because they are the thermodynamically effective concentration available to participate in the reaction. SI's are also useful in that they permit the comparison of the status of a sample to thermodynamic equilibrium conditions. In this report, the SI is defined as the product of the ion activities divided by the equilibrium constant for a particular mineral. A SI greater than zero represents an excess of ionic constituents or supersaturation with respect to that mineral. A SI less than zero represents undersaturation.

Speciation calculations were performed with the computer program PHREEQE (Parkhurst et al., 1980). As used in this investigation, PHREEQE calculates solution speciation and saturation states of the aqueous phase with respect to various minerals given the analytical concentrations and sample pH. PHREEQE was also used to simulate different reaction paths by specifying the addition or subtraction of various reactants to or from solution. PHREEQE computed the pH, total concentrations of the elements, amounts of minerals transferred, the distribution of aqueous species and the saturation state of the aqueous phase for various minerals during a reaction simulation.

Computed ion activities, SI's for water with respect to calcite, gypsum, quartz, and several silica phases, and the partial pressure of  $\text{CO}_2$  for sample analyses used in this investigation are listed in Tables D-5 through D-6 in Appendix D. The following two sections provide a general description of the results of the speciation calculations for groundwater samples from the N-aquifer and samples from streams, springs and drive points for Moenkopi and Dinnebito washes.

#### 8.1.1 N-aquifer

Figure 8-1 shows the saturation indices for calcite and gypsum for N-aquifer groundwater samples. Figures showing the areal distribution of these parameters are provided in Appendix C. Most groundwater samples are near or at equilibrium with respect to calcite and are undersaturated with respect to gypsum which is

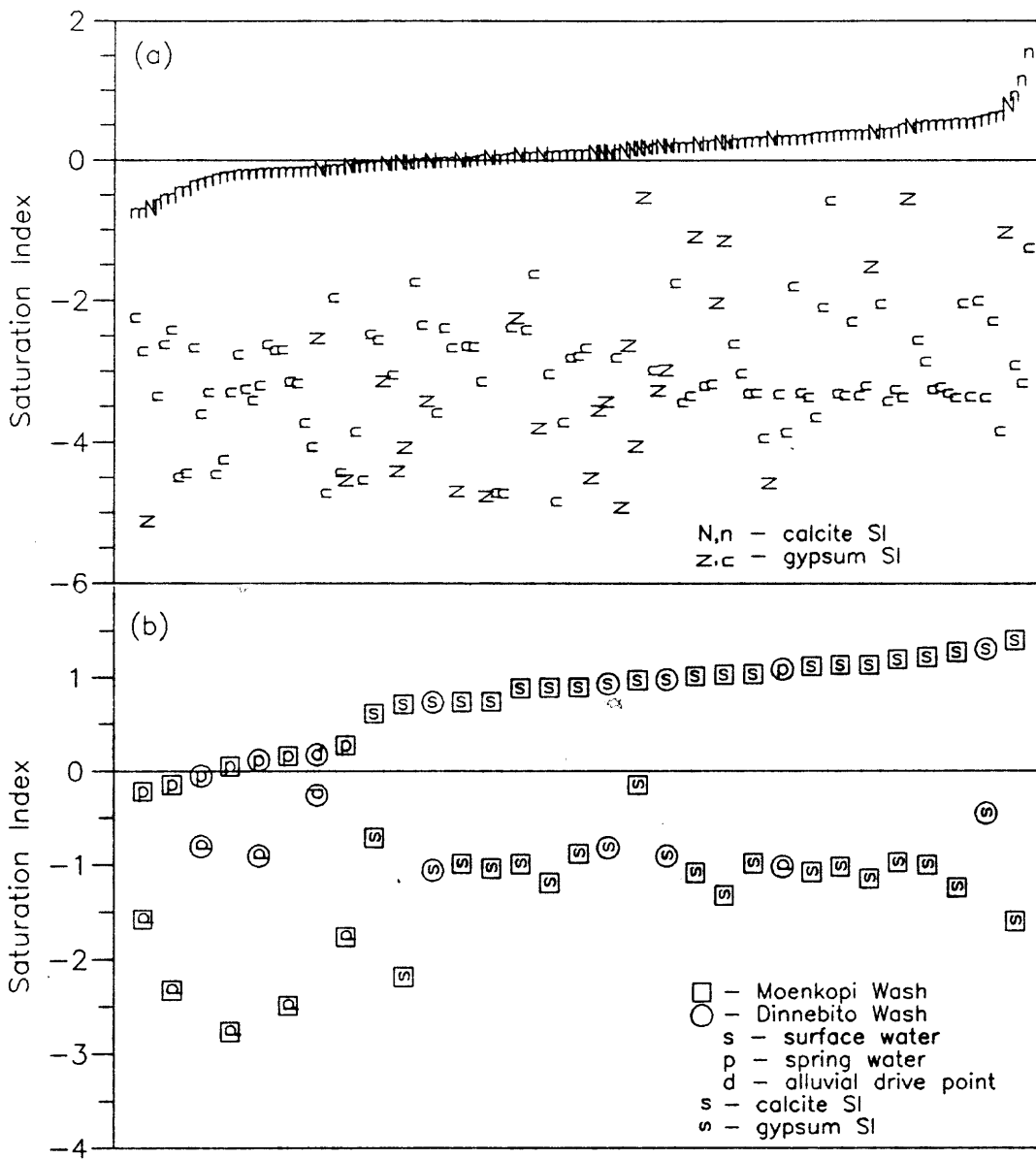


Figure 8-1. Calcite and gypsum saturation indices for samples from the N-aquifer (a) and Moenkopi Wash and Dinnebito Wash (b).

consistent with the N-aquifer geochemistry presented in Chapter 6. Calcite is abundant as cement in the N-aquifer formations and, therefore, is readily dissolved and precipitated from solution. Gypsum undersaturation supports gypsum as a source for  $\text{SO}_4^-$  and  $\text{Ca}^{2+}$  which may be expected to dissolve when encountered. The large degree of undersaturation suggests that gypsum dissolution is controlled by its occurrence rather than by solubility constraints. Consulting Figure 8-1a, the common ion effect does not appear to be a significant process in the N-aquifer. Figure 8-1 was generated by plotting saturation indices for both calcite and gypsum for each sample. Samples were sorted by calcite SI in ascending order. Increasing calcite supersaturation (more positive SI) is not accompanied by a consistent trend of decreasing gypsum undersaturation (less negative SI). Also, alkalinity is not observed to decrease along the flow path, as would be expected with calcite precipitation.

The silica phase in equilibrium is not readily apparent. Most groundwater samples are supersaturated with respect to quartz and approach equilibrium with respect to quartz further along the confined flow path. This may be attributed to increased silica solubility with increasing pH and temperature, or precipitation of some intermediate silica phase that replaces the preexisting calcite cement at depth.

The areal distribution of the computed  $\text{pCO}_2$  for the N-aquifer is included in Appendix C. Where unconfined, partial pressures range from  $10^{-1.9}$  to  $10^{-3.6}$  bars and are typically above the  $\text{pCO}_2$  of the earth's atmosphere ( $10^{-3.5}$  bars). This

suggests that the groundwater is charged with  $\text{CO}_2$  during infiltration through soil zones. Partial pressures are smallest in the confined system, as low as  $10^{-4.9}$  bars, which is consistent with a closed system.  $\text{CO}_{2(\text{aq})}$  is consumed by the dissolution of calcite and, to a lesser degree, by the dissolution of aluminosilicates. Ca-Na ion exchange promotes additional calcite dissolution within the confined system. Those areas within the confined system with the lowest  $\text{pCO}_2$  exhibit a slight undersaturation with respect to calcite.

#### 8.1.2. Moenkopi and Dinnebito washes

SI profiles for Moenkopi and Dinnebito washes are included in Appendices F and G, respectively. The surface water samples show increased calcite saturation and supersaturation (more positive SI) and less undersaturation with respect to gypsum (less negative SI) when compared to the N-aquifer. Spring samples tend to be more undersaturated with respect to gypsum and nearer to calcite equilibrium.

Baseflow becomes less undersaturated with respect to gypsum in the downstream direction along Moenkopi Wash indicating gypsum dissolution from the channel alluvium. The water sample from a drive point collected along Dinnebito Wash is at saturation with respect to gypsum and also suggests that the channel alluvium is a source for  $\text{SO}_4^-$ . The largest increase in this SI is along the gaining reach above the confluence with Begashibito Wash indicating that most of the  $\text{SO}_4^-$

content of baseflow is derived during groundwater discharge through the alluvium. Supersaturation with respect to calcite may be attributed, in part, to the common ion effect from gypsum dissolution.

The computed  $p\text{CO}_2$  profile for Moenkopi and Dinnebito washes are also included in Appendices F and G. For Moenkopi Wash, the lowest  $p\text{CO}_2$  for baseflow samples occurs furthest upstream along the gaining reach and supports a confined N-aquifer origin. Most downstream baseflow and spring samples approximate atmospheric  $p\text{CO}_2$ . Dinnebito Wash baseflow samples also average about  $10^{-3.5}$  bars for the exception of spring samples which typically exhibit a greater  $p\text{CO}_2$ .

## 8.2 Reaction path modeling

This section details the methodology, techniques, assumptions and results of the quantitative analysis using reaction path modeling. Incorporating the results of the first three sections, mass transfer and thermodynamic reaction models were developed to define the plausible reaction paths and quantify the minerals dissolving or precipitating along flow paths. Simply stated, the chemical evolution of groundwater is simulated between known compositions along a flow path for specific sets of reaction phases and constraints. This final analysis incorporates speciation calculations, groundwater flow patterns and isotopic data to identify those models that are consistent with the data.

Each set of reactions was compared against three criteria in order to examine the proposed reaction pathways. First, a set of reactions had to be consistent with the observed stoichiometric relationships presented in Chapters 6 and 7. Second, each set of reactions had to yield a mass transfer consistent with the observed changes in chemical composition along the flow path, thereby satisfying conservation of mass. And third, the set of reactions had to be thermodynamically feasible, that is, agree with calculated saturation states of various mineral phases and, for the N-aquifer, accurately reproduce the observed changes in pH.

Mass transfer calculations were performed with the computer program BALNINPT, a modification of the program BALANCE by Parkhurst et al. (1982). Required inputs include the chemical compositions of an initial and final end member (i.e. the upgradient and downgradient water samples), and a set of reaction phases that match the number of chemical species. The user may also specify a second initial member for mixing. BALNINPT simultaneously solves the set of linear equations and computes the amount of reactant phases entering or leaving the solution using the constraints of the known compositions. The number of solutions is limited by the users knowledge of geochemical processes, the mineralogy, and the groundwater flow patterns.

When the number of suspected phases exceeded the number of chemical species, mass balance calculations were performed with the linear programming feature in Quattro Pro, version 3.0 (Borland International, Inc., 1991). Similar to

BALNINPT, Quattro Pro can solve a set of linear equations (provided as a matrix) within specified constraints. The advantage of this technique is that the number of phases considered in any reaction set can exceed the number of species provided that the amount added or lost to the solution was specified for the additional phases, and the amount of any phase added or removed could be constrained within specified minima and maxima.

A limitation of mass balance calculations is that several different sets of reactions may satisfy the imposed constraints resulting in solutions that are not unique. Therefore, to limit the number of solutions, each reaction path was tested for thermodynamic feasibility. The program PHREEQE (Parkhurst et al., 1980) was used to perform the thermodynamic calculations.

Two tests were used to evaluate thermodynamic feasibility. First, sets of reaction phases used in the mass transfer modeling were eliminated if they were inconsistent with calculated saturation indices. For example, if speciation calculations indicated that both end members were undersaturated with respect to calcite, then sets of reaction phases that include calcite precipitation were considered unlikely. The second test examined the effect of the reaction set on pH. Starting with the chemical composition of the initial end member, phases were added or removed according to the amounts computed by the mass transfer calculations. For a reaction set to be thermodynamically feasible, the pH of the

evolved water computed by PHREEQE must have agreed with the measured pH of the final end member.

The pH modeling with PHREEQE was not used to evaluate thermodynamic feasibility for the surface water reactions. Without a supply of CO<sub>2</sub> under closed system conditions, the final simulated pH was entirely a function of the reaction set. Under open system conditions, however, the CO<sub>2(aq)</sub> derived from soil gas and the atmosphere would need to be represented in the model. Specifying the pCO<sub>2</sub> in PHREEQE during thermodynamic modeling of the surface water geochemistry is equivalent to specifying the pH of the final end member, and the test, therefore, becomes valueless.

Certain assumptions were made for the geochemical modeling and are stated as follows:

- samples used for end members occur along the same flow path
- groundwater flow is steady-state between end members
- the geochemistry is steady-state between end members
- analytical data are complete and accurate
- samples chosen as end members were not affected by leakage from the D-aquifer or from anthropogenic contamination
- all significant tributary, seep or spring inflows are accounted for and streamflow samples are not affected by anthropogenic contamination
- dispersion is not a significant process
- REDOX reactions are not significant

- the thermodynamic data used in PHREEQE are accurate
- phases are kinetically and thermodynamically feasible

The phases used for the reaction path modeling are listed in Table 8-1. The list should not be considered complete. This list of reactions was developed based on the previously presented analyses and on the known mineralogy of the formations. The intent was to include the dominant geochemical reactions. The evolution of rainfall and snowmelt to the composition of groundwater from the N-aquifer was not explicitly modeled and is not considered pertinent to the objectives of this study. The stoichiometry of the reactions input to PHREEQE are consistent with the mass transfer calculations. The moles of reaction or phases entering or leaving solution input to PHREEQE were derived by the mass transfer calculations.

Calcite was assumed to dissolve and precipitate as pure  $\text{CaCO}_3$ . The  $\text{Mg}^{2+}$  composition of calcite was reported as invariably low in mineralogic analyses, typically less than two percent (Kiersch, 1955b). Calcite was added or removed from solution by equilibrating the final solution to the saturation index calculated by PHREEQE for the end member. Gypsum was assumed to exist as pure  $\text{CaSO}_4 \cdot 2\text{H}_2\text{O}$ .

Lastly, incongruent dissolution of aluminosilicates in the N-aquifer was represented with plagioclase. Plagioclase (undifferentiated) was identified as the

Table 8-1

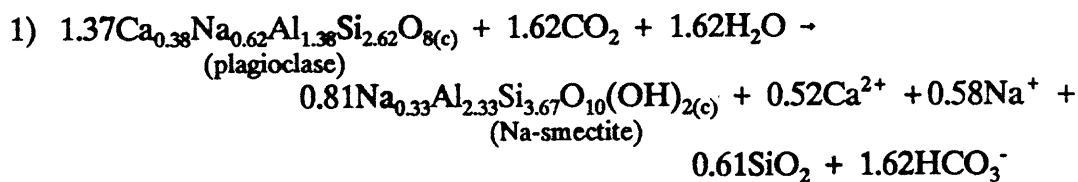
## Phases considered in reaction path modeling

## A. Congruent dissolution and precipitation

- 1)  $\text{CaCO}_{3(c)} + \text{H}_2\text{O} \leftrightarrow \text{Ca}^{2+} + \text{CO}_3^{=} + \text{H}_2\text{O}$  (calcite)
- 2)  $\text{CaSO}_4 \cdot 2\text{H}_2\text{O}_{(c)} \leftrightarrow \text{Ca}^{2+} + \text{SO}_4^{=} + 2\text{H}_2\text{O}$  (gypsum)
- 3)  $\text{NaCl}_{(c)} + \text{H}_2\text{O} \leftrightarrow \text{Na}^+ + \text{Cl}^- + \text{H}_2\text{O}$  (halite)
- 4)  $\text{SiO}_{2(c)} + 2\text{H}_2\text{O} \leftrightarrow \text{H}_4\text{SiO}_4$  (silica)
- 5)  $\text{H}_2\text{CO}_3 \leftrightarrow \text{H}_2\text{O} + \text{CO}_{2(g)}$  (carbonic acid)
- 6)  $\text{CaF}_{2(c)} + \text{H}_2\text{O} \leftrightarrow \text{Ca}^{2+} + \text{F}^- + \text{H}_2\text{O}$  (fluorite)

where (c) denotes solid phase

## B. Incongruent dissolution of aluminosilicates



## C. Ion Exchange Reactions

- 1)  $\text{Na}_2\text{-X} + \text{Ca}^{2+} \leftrightarrow \text{Ca-X} + 2\text{Na}^+$
- 2)  $\text{Na}_2\text{-X} + \text{Mg}^{2+} \leftrightarrow \text{Mg-X} + 2\text{Na}^+$
- 3)  $\text{Ca-X} + \text{Mg}^{2+} \leftrightarrow \text{Mg-X} + \text{Ca}^{2+}$
- 4)  $\text{Na-X} + \text{K}^+ \leftrightarrow \text{K-X} + \text{Na}^+$
- 5)  $\text{K}_2\text{-X} + \text{Ca}^{2+} \leftrightarrow \text{Ca-X} + 2\text{K}^+$

where -X denotes clay

dominant mineral other than quartz. A sodium plagioclase was assumed because strong evidence exists for cation exchange for  $\text{Na}^+$  in the confined system.

### 8.2.1 N-aquifer

Reaction path modeling was performed for the N-aquifer to examine the reaction pathways described in Chapter 6 and to determine if these reactions could reproduce the different water types and pH's between the confined and unconfined N-aquifer. Geochemical models were developed for four sets of groundwater samples; sets A and B were used to model the chemical evolution from the unconfined system to the confined system under Black Mesa, and two sets further along the same flow path through the confined system. The initial end members (samples 26 and 122) are in the principal recharge area in the Navajo Uplands. About 10 to 15 miles downgradient to the south is the PCC wellfield in the confined N-aquifer. These wells were represented as a single value derived from 32 samples from the six PCC wells (median of samples numbered 128 through 133). Sets C and D were used to evolve the groundwater further along the flow path toward the town of Oraibi and include samples 28 and 2 as the final end members. The sample sets and results of the reaction path modeling for the N-aquifer are listed in Table 8-2. The locations of these samples and the simulated flow paths are shown in Figure 8-2.

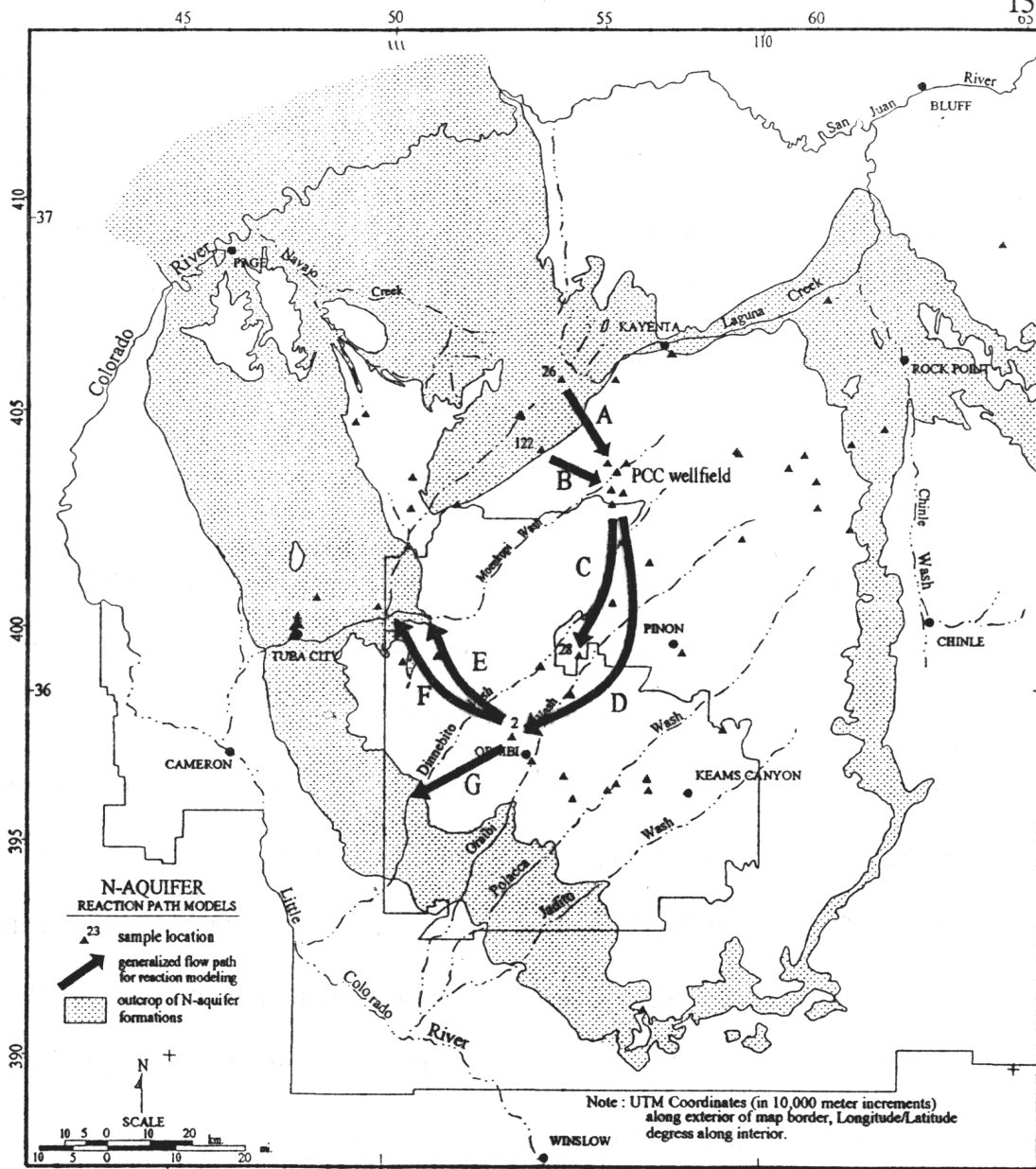


Figure 8-2. Simulated reaction path models for the N-aquifer. Lettered arrows refer to sample sets in Tables 8-2 and 8-3 in text.

Table 8-2 includes the mass difference in ion and silica concentrations for end members and the computed amount of each phase added or removed from solution by mass transfer calculations. Also listed are measured pH and temperature values for each sample and simulated pH from the thermodynamic model. Computed and simulated values for  $p\text{CO}_2$  are also provided.

The results of the N-aquifer reaction path modeling are consistent with the conceptual geochemical model for the N-aquifer presented in Chapter 6. With each of the sample sets, mass was conserved and the reaction phases proved to be thermodynamically feasible. The dominant reactions responsible for the evolution of distinct chemical facies between the unconfined and the confined systems are Ca-Mg-Na ion exchange and calcite equilibrium. Ca-Mg ion exchange was not explicitly simulated in the confined system because it is accounted for in the net effect of Ca-Na and Mg-Na exchange. Reaction path modeling indicated that gypsum and halite dissolution are not significant reactions in the N-aquifer.

The observed pH change between the confined and unconfined systems is due largely to calcite dissolution under closed system conditions but also may be due, in part, to minor dissolution of aluminosilicates early along the flow path. Alkalinity decreases from the unconfined to confined systems which is consistent with saturation to supersaturation with respect to calcite for the PCC wellfield samples. Even though ion exchange and reactions involving calcite and gypsum would adequately reproduce downgradient compositions, they could not fully

reproduce the observed pH changes for sets A and B. The observed increase in pH from 8 to 9 and decrease in  $p\text{CO}_2$  between end members was simulated by plagioclase dissolution. The alkalinity and  $\text{SiO}_2$  added to solution were removed by calcite and  $\text{SiO}_2$  precipitation.

The weathering of aluminosilicates results in the formation of clays and releases silica into solution. The modeling indicated that  $\text{SiO}_2$  or some other silica phase may be precipitated along the flow path. This precipitation is consistent with Kiersch (1955b) who reported quartz cement to be more abundant at depth. He conjectured that the quartz cement was derived from solution which dissolved silica from the grains and may have replaced calcite as the preexisting cement. Inasmuch as Dulaney (1989) reported that feldspars comprise as much as 20 percent of the sandstone matrix in some samples, the weathering of silicates is probably controlled more by kinetics and  $\text{CO}_2$  availability than by abundance.

The continued chemical evolution within the confined system is dominated by cation exchange, as is shown by simulations with sets C and D. This cation exchange promotes calcite dissolution, thereby increasing alkalinity, raising the pH and consuming additional  $\text{CO}_{2(\text{aq})}$ . Sets C and D show a net increase in alkalinity downgradient from the PCC wellfield. Calcite dissolution alone adequately reproduced the observed pH increases and  $p\text{CO}_2$  was consumed within the constraints of the measured alkalinity changes. Calcite dissolution is also consistent

Table 8-2  
Results of mass transfer and pH modeling, N-aquifer

	<i>Samples</i>			
	set A Betatakin Nat.Mon. (sample 26) to PCC Wellfield (median values)	set B BM-4 USGS Well (sample 122) to PCC Wellfield (median values)	set C PCC Wellfield (median values) to Hardrock (sample 28)	set D PCC Wellfield (median values) to Hoteville Sch. 2 (sample 2)
<i>Measured change in concentration (final-initial in mmoles/l)</i>				
Ca <sup>2+</sup>	-0.752	-0.802	-0.076	-0.081
Mg <sup>2+</sup>	-0.107	-0.148	-0.004	-0.004
Na <sup>+</sup>	+1.740	+1.740	+0.948	+0.931
SO <sub>4</sub> <sup>-</sup>	+0.107	+0.010		
K <sup>+</sup>	-0.010	-0.015	-0.002	-0.007
Si	+0.240	+0.100	-0.098	+0.068
Cl <sup>-</sup>	+0.011			
F <sup>-</sup>	+0.011	+0.005	+0.010	-0.008
C	-0.205	-0.225	+0.566	+0.615
<i>Reaction phases added(+) or removed(-) from solution (mmoles/l)</i>				
Mg/Na Ex.	+0.107	+0.148	+0.004	+0.004
Ca/Na Ex.	+0.607	+0.570	+0.469	+0.458
Calcite	-0.437	-0.422	+0.398	+0.380
Halite	+0.011			
Gypsum		+0.010		
SiO <sub>2</sub>	-0.992	-1.118	-0.098	+0.068
K/Na Ex.	+0.010	+0.015	+0.002	+0.007
Plagioclase	+0.470	+0.465		
CO <sub>2</sub>	+0.232	+0.197	+0.167	+0.234
Fluorite	+0.005	+0.003		-0.004
<i>Saturation indices</i>				
calcite				
starting	+0.17	-0.04	+0.08	+0.08
ending	+0.08	+0.08	+0.08	-0.03
gypsum				
starting	-3.02	-2.37	-3.33	-3.33
ending	-3.33	-3.33	-4.54	-4.73
<i>pH</i>				
measured				
starting	8.10	7.90	9.00	9.00
ending	9.00	9.00	9.64	9.81
modeled	9.00	9.00	9.62	9.59
<i>log pCO<sub>2</sub></i>				
starting	-3.09	-2.92	-3.85	-3.85
ending	-3.85	-3.85	-4.58	-4.83
modeled	-3.94	-3.99	-4.58	-4.60
<i>Temperature (°C)</i>				
measured				
starting	13.4	14.0	32.0	32.0
ending	32.0	32.0	32.5	26.0

with the results of speciation of the end members which indicated a slight undersaturation with respect to calcite further along the confined flow path.

Although plagioclase was selected for modeling as a representative aluminosilicate, it is not necessarily the only viable mineral for this system. For comparison, identical results were obtained for the first sample set using sepiolite ( $\text{Mg}_4(\text{Si}_2\text{O}_5)_3(\text{OH})_2 \cdot 6\text{H}_2\text{O}$ ).

#### 8.2.2. Moenkopi Wash and Dinnebito Wash

Mass transfer models using BALNINPT were developed to simulate chemical changes from the N-aquifer to Moenkopi Wash and Dinnebito Wash, and along the washes themselves. The groundwater sample at Hoteville Sch. 2 (location 2) was used as the starting composition because the  $\delta\text{D}$  and  $\delta^{18}\text{O}$  composition of baseflow indicates a confined N-aquifer origin. This sample was assumed to be representative of N-aquifer groundwater from the confined system.

The geochemical evolution of groundwater discharge from the confined portion of the N-aquifer to the washes was simulated using several approaches. Sample set E in Table 8-3 was used to evolve groundwater between Hoteville Sch. 2 and Moenkopi Wash at Horse Corral Tributary (HCT). Set F was used to evolve N-aquifer groundwater from Hoteville Sch. 2 to the Moenkopi Wash baseflow composition at the confluence with Begashibito Wash. For Dinnebito Wash, groundwater was evolved to the baseflow composition at Sweetwater Well with

sample set G. The locations of sample sets and simulated flow paths that include the N-aquifer for reaction path modeling are shown in Figure 8-2. The location of wash samples used in the reaction path modeling are shown in Plates 1 and 2.

The simulated chemical evolution from the N-aquifer to the washes was dominated by gypsum dissolution and cation exchange. In Table 8-3, the computed gypsum dissolution for Dinnebito Wash is greater than for Moenkopi Wash and may be due to a larger alluvial valley through which groundwater must flow before entering the wash. Similarly, groundwater discharge to a downstream location on Moenkopi Wash (set F) required more gypsum dissolution than for the upstream sample (set E). This may also be attributed to gypsum dissolution along the channel. For all sets, the gypsum SI approaches saturation (becomes less negative). Calcite is also dissolved along each reaction path which is consistent with a trend from equilibrium to supersaturated conditions. As open system conditions are established,  $\text{CO}_2$  is available to dissolve calcite. However, subsequent gypsum dissolution creates supersaturated conditions with respect to calcite. As will be shown with the next three sample sets, nearly all the mass transfer occurs prior to and during groundwater discharge with only minor transfer occurring from interaction with channel sediment and alluvial groundwater.

Reaction path modeling along Moenkopi Wash was simulated using sample sets H, I and J in Table 8-3. For set H, baseflow at HCT was evolved to baseflow at the confluence with Begashibito Wash by various reaction phases and mixing with

groundwater from the confined N-aquifer, represented by sample 2 at Hoteville Sch.

2. BALNINPT calculated the mass transfer for different phases and the amount of each initial sample. Set I used the baseflow composition at Begashibito Wash with Begashibito Wash inflows (added manually) and Coal Mine Canyon tributary inflows as initial end members, and Moenkopi Wash downstream of Coal Mine Canyon as the final end member. Again BALNINPT was used to calculate the contribution of each initial member. Lastly, set J was used to simulate mass transfer between Moenkopi Wash at Coal Mine Canyon to just upstream of the village of Moenkopi. The locations of individual wash samples are shown in Plate 1.

The results of mass transfer modeling along Moenkopi Wash for sets H, I and J are presented in Table 8-3. Based on chemical composition and the specified reactions phases, BALNINPT computed about 34 percent of baseflow at Begashibito Wash confluence from the N-aquifer above the confluence with HCT, and approximately 66 percent between Begashibito Wash and HCT. This distribution is consistent with the streamflow profile presented in Chapter 4. Gypsum dissolution is the dominant phase and is most likely due to groundwater discharging through the channel alluvium. Considerably less gypsum is dissolved along the losing reach indicating limited interaction with channel alluvium. Mass transfer calculations estimated that Coal Mine Canyon increases baseflow in Moenkopi Wash by about nine percent. This estimate is probably the upper limit;

Table 8-3  
Results of mass transfer modeling, N-aquifer,  
Moenkopi Wash and Dinnebito Wash

	<i>Samples</i>		
	set E	set F	set G
	Hoteville Sch. 2 (sample 2) to Moenkopi Wash at Horse Corral Trib. (location 28)	Hoteville Sch. 2 (sample 2) to Moenkopi Wash at Begashibito confl. (location 8)	Hoteville Sch. 2 (sample 2) to Dinnebito Wash at Sweetwater Well (location 29)
<i>Measured change in concentration (final-initial in mmoles/l)</i>			
Ca <sup>2+</sup>	+0.576	+1.846	+1.158
Mg <sup>2+</sup>	+0.247	+0.459	+0.996
Na <sup>+</sup>	+2.527	+0.994	+3.658
SO <sub>4</sub> <sup>-</sup>	+1.878	+2.159	+3.514
K <sup>+</sup>	+0.051	+0.081	+0.074
Si	-0.230	-0.289	-0.211
Cl <sup>-</sup>	+0.127	+0.122	+0.277
C	-0.219	+0.110	-0.160
<i>Reaction phases added(+) or removed(-) from solution (mmoles/l)</i>			
Ca/Mg Ex.	+0.247	+0.459	+0.996
Ca/Na Ex.	+1.200	+0.411	+1.691
Ca/K Ex.	+0.026	+0.041	+0.037
Calcite	+0.171	+0.598	+0.376
Halite	+0.127	+0.122	+0.277
Gypsum	+1.878	+2.159	+3.514
SiO <sub>2</sub>	-0.230	-0.290	-0.211
CO <sub>2</sub>	-0.391	-0.188	-0.527
<i>Saturation indices</i>			
calcite			
starting	-0.03	-0.03	-0.03
ending	+1.39	+1.13	+0.73
gypsum			
starting	-4.73	-4.73	-4.73
ending	-1.60	-1.02	-1.06
<i>pH</i>			
measured			
starting	9.81	9.81	9.80
ending	9.80	8.76	8.71
<i>log pCO<sub>2</sub></i>			
starting	-4.83	-4.83	-4.83
ending	-4.90	-3.62	-3.67
<i>temperature (°C)</i>			
measured			
starting	26.0	26.0	26.0
ending	11.6	6.4	3.1

Table 8-3 (continued)  
Results of mass transfer modeling, N-aquifer,  
Moenkopi Wash and Dinnebito Wash

	<i>Samples</i>					
	set H			set I		
	Moenkopi Wash at Horse Corral Tributary (location 26) plus Hoteville Sch. 2 (location 2) to Moenkopi Wash at Begashibito Wash confl. (location 8)			Moenkopi Wash downstream of Begashibito confl. (location 8 + location 7) plus Coal Mine Canyon trib. inflows (location 4) to Moenkopi Wash at Coal Mine Canyon (location 2)		
<i>Measured concentrations (mmoles/l)</i>						
	init.1	init.2	final	init.1	init.2	final
Ca <sup>2+</sup>	0.591	0.015	1.861	1.970	1.778	1.772
Mg <sup>2+</sup>	0.247	0.000	0.459	0.560	0.872	0.699
Na <sup>+</sup>	5.350	2.823	3.767	3.439	15.137	4.828
SO <sub>4</sub> <sup>=</sup>	1.926	0.048	2.207	2.031	7.714	2.540
K <sup>+</sup>	0.062	0.011	0.092			
Si	0.171	0.401	0.112	0.123	0.102	0.109
Cl <sup>-</sup>	0.158	0.031	0.153	0.189	0.459	0.274
C	1.559	1.778	1.888	2.116	2.318	2.098
<i>Reaction phases added(+) or removed(-) from solution (mmoles/l)</i>						
initial 1			+0.343			+0.910
initial 2			+0.658			+0.090
Ca/Mg Ex.			+0.374			+0.111
Ca/Na Ex.						+0.140
Ca/K Ex.			+0.032			
Calcite			+0.538			+0.070
Halite			+0.078			+0.061
Gypsum			+1.516			
SiO <sub>2</sub>			-0.212			-0.013
CO <sub>2</sub>			-0.354			-0.106
<i>Saturation indices</i>						
	init.1	init.2	final	init.1	init.2	final
calcite	+1.39	-0.03	+1.13		+0.61	+0.74
gypsum	-1.60	-4.73	-1.02		-0.72	-0.99
<i>pH</i>						
measured	9.80	9.81	8.76		8.29	8.40
<i>log pCO<sub>2</sub></i>						
calculated	-4.90	-4.83	-3.62		-3.05	-3.26
<i>Temperature (°C)</i>						
measured	11.6	26.0	6.4		7.4	1.3

Table 8-3 (continued)  
Results of mass transfer modeling, N-aquifer,  
Moenkopi Wash and Dinnebito Wash

*Samples*

set J

Moenkopi Wash at  
Coal Mine Canyon  
(location 2) to  
Moenkopi Wash upstream  
of Moenkopi (location 18)

*Measured change in concentration (final-initial in mmoles/l)*

Ca <sup>2+</sup>	-0.200
Na <sup>+</sup>	+0.261
SO <sub>4</sub> <sup>-</sup>	+0.348
K <sup>+</sup>	+0.003
Si	-0.027
Cl <sup>-</sup>	+0.129
C	-0.510

*Reaction phases added(+) or removed(-) from solution (mmoles/l)*

Ca/Na Ex.	+0.067
Na/K Ex.	+0.003
Calcite	-0.481
Halite	+0.129
Gypsum	+0.348
SiO <sub>2</sub>	-0.027
CO <sub>2</sub>	-0.029

*Saturation indices*

calcite	
starting	+0.74
ending	+1.12
gypsum	
starting	-0.99
ending	-1.08

*pH*

measured	
starting	8.40
ending	8.76

*log pCO<sub>2</sub>*

starting	-3.26
ending	-3.58

*Temperature (°C)*

starting	1.3
ending	19.4

gypsum would be dissolved from the channel sediment between Begashibito Wash and Coal Mine Canyon. For the last modeled segment along Moenkopi Wash, a net loss in alkalinity occurs and calcite was removed from solution.

### 8.3 Summary

Mass transfer and reaction path modeling were used to quantitatively evaluate the geochemical pathways for groundwater in the N-aquifer and in baseflow along the washes. The results of the analysis support the conclusions of the qualitative analyses presented in Chapters 6 and 7. In summary, reaction models for the N-aquifer support calcite dissolution and Ca-Mg-Na ion exchange to account for observed changes between the unconfined and confined portions of the N-aquifer. Some alteration of aluminosilicates may occur between the transition from recharge areas to the PCC wellfield in that the confined system pH's could not be reproduced by calcite dissolution alone.

Mass balance calculations for reactions during groundwater discharge to streams suggest gypsum dissolution is the dominant reaction. Discharge of groundwater to the washes results in initial calcite dissolution once open system conditions are encountered, followed by gypsum dissolution during passage through the alluvial sediment. The mass transfer for baseflow occurs almost entirely along gaining reaches and may be attributed to groundwater interaction with alluvial sediment.

These reactions are consistent with mineral SI's and mass transfer calculations, and can be shown to be thermodynamically feasible. Baseflow interaction with alluvial sediment plays only a minor role in the chemical evolution of baseflow along Moenkopi Wash below Coal Mine Canyon.

## CHAPTER 9. SUMMARY AND CONCLUSIONS

The aqueous chemistry of individual components in a hydrologic system were examined in this investigation to indirectly evaluate surface water and groundwater interactions. This approach was applied to the perennial reaches of two Black Mesa drainages located in northern Arizona. Moenkopi and Dinnebito washes receive groundwater discharging from the regional N-aquifer. In general, the geochemistry provided valuable insight to the physical and chemical processes governing the surface water and groundwater interactions.

Existing water quality, isotope and streamflow data were collected from different sources and compiled. An extensive sampling program was designed and implemented to measure streamflow discharge and collect water samples from surface water, springs and the alluvial groundwater. Samples were analyzed for major and minor ions and selected isotopes.

Baseflow was defined as the component of surface flow that is derived from groundwater discharge. The spatial distribution of baseflow along the washes was examined by field inspection and measurement, literature review and aerial photography. The temporal distribution of baseflow was quantified statistically from historical streamflow records.

The geochemistry of the N-aquifer and the perennial reaches was characterized by integrating hydrologic, geologic, physiographic and major ion and

stable isotope data. Distinct chemical facies were identified. Stoichiometric relationships and corrections to specific ions were developed to isolate the effects of individual reactions. As a result, interference from competing reactions was quantified and the dominant geochemical reactions were identified. Computer programs were used to perform aqueous speciation and mass transfer calculations in order to quantitatively evaluate the suspected reactions pathways against known chemical compositions and parameters. Both pH modeling and computed saturation states of mineral phases were used to test the reaction pathways for thermodynamic feasibility.

The isotope chemistry for the major components in the system was characterized and interpreted. Explanations were offered for the different isotopic signatures found between the confined and unconfined N-aquifer, and gaining and losing stream reaches.

Surface water and groundwater interactions were examined directly by streamflow measurements and indirectly by comparing the chemical and isotopic composition of the different components in the system. A conceptual model of the interactions was described and data and observations were presented in support of the model. Mixing calculations were performed to quantify the influence on the composition of baseflow from mixing with water of various sources. Estimates were computed for groundwater flow to the Moenkopi Wash valley alluvium and for losses due to plant transpiration and bare soil evaporation.

The conclusions from this investigation are summarized below:

- 1) The areal and temporal distribution of baseflow along the southwestern Black Mesa washes has not varied significantly since 1935. The upstream start of perennial flow along Moenkopi and Dinnebito washes coincides with the outcrop of the Navajo Sandstone. The measured streamflow profile along Moenkopi Wash suggests that nearly all the observed baseflow is derived from the discharging N-aquifer above the confluence with Coal Mine Canyon.
- 2) The long-term median of measured baseflow along Moenkopi Wash was calculated from historical USGS streamgauging records to be 3.0 cfs. However, the streamflow survey conducted for this investigation suggests that some of the reported low-flow measurements at USGS gauging station 1260 are in error.
- 3) The dominant geochemical reactions for the N-aquifer are calcite dissolution and cation exchange. Halite and gypsum dissolution occur but are not quantitatively significant. Minor dissolution of aluminosilicates, possibly plagioclase alteration to a smectite clay, consumes  $\text{CO}_{2(\text{aq})}$ , raises the pH, and provides sites for cation exchange.

4) Four distinct chemical facies in the N-aquifer were identified. The two dominant water types, Ca-HCO<sub>3</sub> and Na-HCO<sub>3</sub>, correspond to the unconfined and confined systems, respectively. The latter evolves from the former as a result of Ca-Mg-Na cation exchange and closed system calcite dissolution. The other chemical facies appear to be isolated and may be attributed to local mineralogy, or to leakage from the overlying D-aquifer by processes associated with well construction or local geologic heterogeneities. The geochemistry of the N-aquifer does not support significant leakage from the D-aquifer on a regional scale.

5) Deuterium and <sup>18</sup>O data suggest that most of the groundwater within the confined N-aquifer was recharged during a different paleo climate. Beneath Black Mesa, groundwater exhibits a δD and δ<sup>18</sup>O composition lighter than recent meteoric water suggesting recharge during a colder and more humid environment. Groundwater dating and flow calculations indicate that the age of groundwater within the confined system is predominantly 15,000 years or older, and could exceed 39,000 years.

6) The baseflow geochemistry is dominated by open system calcite and gypsum dissolution as groundwater interacts with the channel alluvium. The largest chemical changes occur upstream of Coal Mine Canyon with no appreciable changes downstream. Mass balance calculations indicate that nearly all the mass

transferred to baseflow along Moenkopi Wash occurs along the gaining reach with only a minor amount of mass transferred downstream of Coal Mine Canyon. Baseflow possesses a high- $\text{Na}^+$  signature that was attributed to cation exchange.

7) A light  $\delta\text{D}$  and  $\delta^{18}\text{O}$  composition in baseflow along the gaining reach of Moenkopi Wash suggests a confined N-aquifer origin. In the downstream direction, however, these isotopes become heavier and shift from the MWL as  $\delta^{18}\text{O}$  is differentially enriched with respect to  $\delta\text{D}$ . Mixing calculations for baseflow with unconfined N-aquifer groundwater, springs and storm runoff indicate that evaporative enrichment exhibits a strong influence on the surface water composition. With evaporation, the isotopic composition of downstream baseflow samples could be reproduced by mixing with 19 to 35 percent unconfined N-aquifer groundwater, or 11 to 22 percent with precipitation.

8) The results of streamflow profiles, stable isotopes, mixing calculations and geochemical modeling suggest that nearly all the sampled baseflow along the washes is derived from groundwater originating from the confined N-aquifer. The small observed changes in chemical composition of baseflow along the streamcourse were attributed to interaction with channel alluvium or minor exchange with alluvial groundwater.

APPENDIX A

Analysis of streamflow data for Moenkopi Wash

## APPENDIX A

### Analysis of streamflow data for Moenkopi Wash

Appendix A provides a summary of the historic streamflow data for Moenkopi Wash, and a description of the reliability of streamflow data and the statistical analysis used to quantify baseflow discharge.

#### A-1. Historical Data and Reliability

Continuous recording streamflow gauges have been in operation along lower Moenkopi Wash since 1926 at five different locations. Streamflows have not been gauged on the other southwestern washes. As shown in Table A-1, periods of record do overlap sufficiently to establish reliable correlations for equivalent flows at different stations. Although backwater calculations for storm runoff may be used to estimate coincident discharges at other locations, such a technique cannot account for the routing losses, diversions, diffuse contributions and inaccuracies typically influencing low-flows and their measurement. Therefore, the absolute measured baseflow during different time frames for different stations along Moenkopi Wash are not necessarily equivalent nor comparable.

Records from stations 1280, 1400, 1250, and 1260 were analyzed. Station 1500 near Cameron was located near the confluence with the Little Colorado River. The routing losses which occur beyond Kerley Valley to the confluence typically

exceed baseflow discharge, thus the gauge did not provide measurements useful to this analysis. Records for stations 1239 and 1226 were also not used. These stations gauge streamflows on ephemeral reaches within the headwaters of Moenkopi Wash, approximately 40 miles upstream of the water caves.

Table A-1

U.S. Geological Survey stream gauging stations,  
Moenkopi Wash, Arizona

<u>Station No.</u>	<u>Dates</u>	<u>Location</u>
09401280	7/26-9/40	Moenkopi Wash at Tuba City, Az.
09401400	10/40-12/53, 2/65-9/78	Moenkopi Wash near Tuba City, Az.
09401500	11/53-1/65	Moenkopi Wash near Cameron, Az.
09401250	10/73-6/76	Moenkopi Wash near Moenkopi, Az.
09401260	7/76-present	Moenkopi Wash at Moenkopi, Az.
09401239	5/78-10/83	Coal Mine Wash near Nr. Mouth N r . Shonto, Az.
09401226	10/78-9/81	Coal Mine Wash Trib. Nr. Kayenta

Streamflow records from other gauging stations are available within the Moenkopi Wash watershed: USGS Station No. 09401240, Moenkopi Wash near Shonto, Arizona, and USGS Station No. 09401248, Begashibito Wash near Tonalea, Arizona. These were crest-stage partial-record stations that operated between 1974 and 1977 and measured maximum peak discharge. PCC operates stream gauges and flumes within their leasehold to assess the effects of impoundment structures

on surface water runoff and alluvial groundwater flow and water quality.

Sites for the present and historical USGS stream gauging stations along lower Moenkopi Wash were visited during the field activities and notes made regarding the location, channel configuration and stability. The channel foundation for most stations was exposed hardrock. The foundation for the active station (No. 1260, located at the Arizona State Highway 264 overpass) is exposed Kayenta Formation across which a typical baseflow discharge is 1-3 inches in depth. The rating for this gauge is reported to extend to zero flow (personal communication, Don Bills, October 16, 1990).

The streamflow survey conducted during this investigation provides some measure of the accuracy and reliability of low-flow measurements by the active gauge at station 1260. Streamflow measurements were collected at most water quality sample locations using a Pygmy flow meter and wading rod. Measurements were made at approximately 2.6 and 1.4 miles upstream of the gauge (location 9 at the abandoned USGS Station No. 1250, and location 18, respectively), and at 0.6 and 3.6 miles downstream (locations 17 and 16, respectively). An additional measurement was taken 300 feet downstream of the gauge. Table A-2 lists these streamflow data.

USGS gauge readings at 15-minute resolution were reviewed for each day a discrete discharge measurement was taken. For all but one instance, the USGS stream gauge registered flow which was less than 20 percent of the discrete

measurement. It is not likely that the discharge profile varies as much as 3.2 cfs within the distances from the gauge to the sampling locations, nor were such variations observed along the reach during field activities.

Table A-2

Comparison of streamflow discharge measurements  
and reported discharges for the USGS station 1260 (cfs)

<u>discharge measurements (pygmy meter)</u>			<u>USGS gauge measurements</u>		
date	location	discharge	min	max	mean
2/22/90	9	3.28	0.60	0.60	0.60
2/26/90	16	3.32	0.17	0.17	0.17
2/27/90	17	3.36	0.27	0.60	0.27
	18	3.42			
3/13/90	at gauge	2.84	2.1	2.8	2.7

Irrigated fields exist along the reach where these measurements were taken, however, the fields remained fallow during the sampling period and pre-season irrigation had not begun. No other diversions or contributions were observed. It may be concluded, therefore, that the current stream gauge USGS Station No. 1260 provided unreliable low-flow measurements for those days for which discrete streamflow measurements were taken.

#### A-2. Baseflow Determination

Baseflow was quantified using stream gauge records and a statistical approach to separate baseflow from storm runoff. Although the reported minimum

daily average flow would insure that storm runoff and bank storage effects would typically be excluded, upstream diversions and, as demonstrated earlier, problems with the low-flow stream gauge reliability, prohibited such an approach. The hydrograph separation technique, commonly referred to as baseflow-recession, was not appropriate for this application. Baseflow resulting from regional groundwater discharge is the result of a slow response to changes in the groundwater flow system induced by long-term variations in areal recharge and is not dependent on recharge and subsequent discharge along the streamcourse during fluctuating stages. The only baseflow variations which would be observed from storm runoff could be attributed to the discharging of the free bank storage from the shallow alluvial aquifer bounding the wash. These minor variations are overshadowed by the quality and reliability of the low-flow gauge measurements.

The median of the average daily values for each month was determined to be the optimal estimator of baseflow. The median approach was chosen because it is less subjective than hydrograph separation techniques and would minimize the effect of erroneous low-flow measurements, assuming that the latter did not exceed 50 percent of the month. When streamflow records for a month were dominated by storm runoff, adjustments were made by using a subjective lower percentile value.

Reported USGS average daily discharges were compiled for each of the gauges along the wash and median and mean baseflow values were calculated for

each month. Low-flows during late March to mid-November are influenced by evapotranspiration while December, January, and February are least affected (Figure A-1). Storm or snowmelt runoff is indicated during February, and some evapotranspiration losses are apparent in late March. Long-term mean and median monthly baseflow for December, January and February is summarized in Table A-3.

Table A-3  
Long-term mean and median monthly  
baseflow at Moenkopi, Arizona 1926-present (cfs)  
USGS Stations 1280, 1400, 1250, 1260

Month	Median	Mean
December	3.00	3.24
January	3.00	3.32
February	3.25	4.00

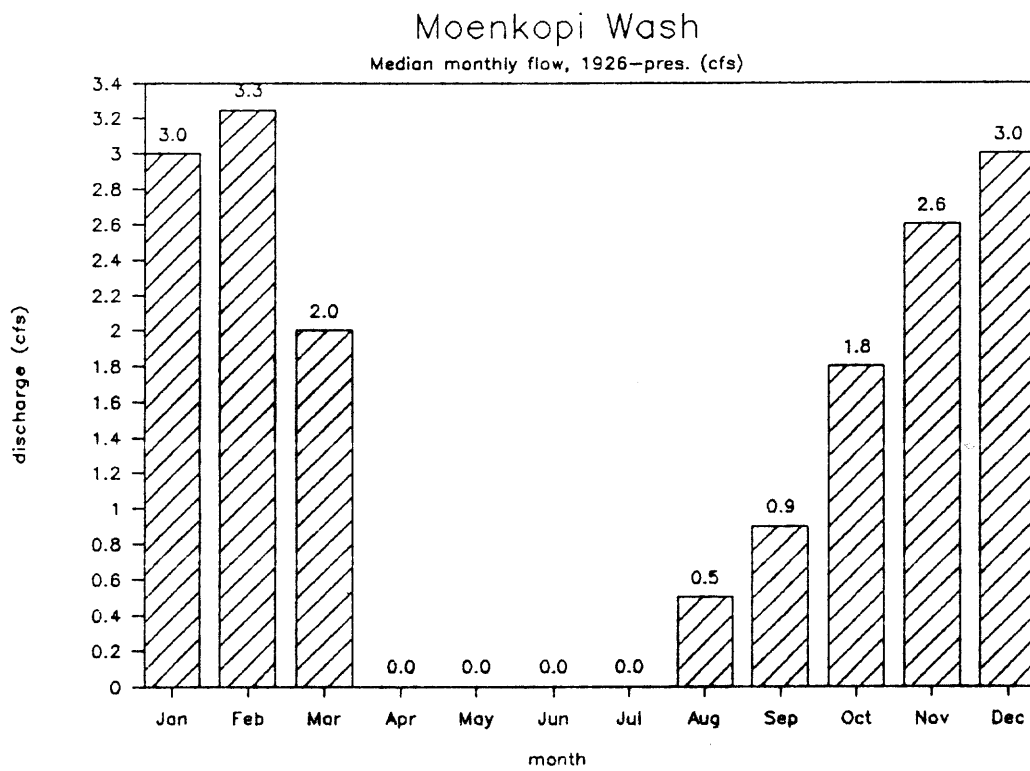


Figure A-1. Median monthly streamflows for Moenkopi Wash from USGS gauging stations 1280, 1400, 1250 and 1260, 1926-1991.

**APPENDIX B**

**Statistical streamflow summary for Moenkopi Wash  
(source: U.S. Geological Survey, Tucson office)**

PRELIMINARY DRAFT--SUBJECT TO REVISION AZ09900-678 11/2/89.1  
 FINDOC2.WM STATIONS 4007 TO 4249

## LITTLE COLORADO RIVER BASIN

09401260 MOENKOPI WASH AT MOENKOPI, AZ

LOCATION.--Lat 36°06'18", long 111°12'04", in MNWEX sec.3, T.31 N., R.11 E., Coconino County, Hydrologic Unit 15020018, in Navajo Indian Reservation on right bank 100 ft upstream from bridge on State Highway 264, 1.3 mi southeast of Moenkopi, 2.5 mi downstream from former gaging station 09401250, and 12.5 mi downstream from Begashibito Wash.

DRAINAGE AREA.--1,629 mi<sup>2</sup>, including all closed basins entirely within the drainage area.

## ANNUAL PEAK DISCHARGE

WATER YEAR	DATE	ANNUAL PEAK DISCHARGE (FT <sup>3</sup> /S)
1974	07-19-74	2,340
1975	09-13-75	2,380
1976	09-25-76	5,420
1977	07-21-77	4,120
1978	09-25-78	262
1979	11-12-78	330
1980	09-10-80	1,740
1981	07-14-81	4,640
1982	10-02-81	8,010
1983	09-30-83	10,100
1984	08-18-84	9,030
1985	09-12-85	520
1986	09-09-86	7,970
1987	08-24-87	3,990
1988	08-27-88	7,280
1989	08-01-89	3,380

## BASIN CHARACTERISTICS

MAIN CHANNEL SLOPE (FT/MI)	STREAM LENGTH (MI)	MEAN BASIN ELEVATION (FT)	FORESTED AREA (PERCENT)	SOIL INDEX	MEAN ANNUAL PRECIPITATION (IN)	RAINFALL INTENSITY, 24-HOUR	
						2-YEAR (IN)	50-YEAR (IN)
24.8	87.1	5,850	47.2	3.0	9.5	1.3	2.6

LITTLE COLORADO RIVER BASIN  
09401260 MOENKOPI WASH AT MOENKOPI, AZ--Continued

MEAN MONTHLY AND ANNUAL DISCHARGES 1977-89

MONTH	MAXIMUM (FT <sup>3</sup> /S)	MINIMUM (FT <sup>3</sup> /S)	MEAN (FT <sup>3</sup> /S)	STAN- DARD DEVI- ATION (FT <sup>3</sup> /S)	COEFFI- CIENT OF VARI- ATION	PERCENT OF ANNUAL RUNOFF
OCTOBER	82	0.25	11	22	2.0	8.5
NOVEMBER	71	1.1	9.9	19	1.9	7.7
DECEMBER	14	0.62	4.1	3.2	0.78	3.2
JANUARY	9.2	2.0	4.3	2.1	0.48	3.4
FEBRUARY	29	2.2	7.4	8.0	1.1	5.8
MARCH	10	2.0	3.8	2.2	0.57	3.0
APRIL	8.5	1.0	2.5	1.9	0.76	1.9
MAY	11	0.31	1.9	2.7	1.4	1.5
JUNE	11	0.00	0.90	2.9	3.3	0.7
JULY	92	0.00	17	28	1.6	13.4
AUGUST	129	0.00	34	37	1.1	26.4
SEPTEMBER	134	0.00	32	38	1.2	24.7
ANNUAL	19	2.2	11	6.0	0.56	100

MAGNITUDE AND PROBABILITY OF ANNUAL LOW FLOW  
BASED ON PERIOD OF RECORD 1978-89

PERIOD (CON- SEC- TIVE DAYS)	DISCHARGE, IN FT <sup>3</sup> /S, FOR INDICATED RECURRENCE INTERVAL, IN YEARS, AND NON-EXCEEDANCE PROBABILITY, IN PERCENT					
	2 50%	5 20%	10 10%	20 5%	50† 2%	100† 1%
1						
3						
7						
14						
30	0.00	0.00	0.00	0.00	0.00	0.00
60	0.00	0.00	0.00	0.00	0.00	0.00
90	0.67	0.39	0.30	0.24	0.19	0.16
120	1.8	0.77	0.44	0.27	0.15	0.09
183	3.5	1.6	1.0	0.72	0.49	0.38

MAGNITUDE AND PROBABILITY OF ANNUAL HIGH FLOW  
BASED ON PERIOD OF RECORD 1977-89

PERIOD (CON- SEC- TIVE DAYS)	DISCHARGE, IN FT <sup>3</sup> /S, FOR INDICATED RECURRENCE INTERVAL, IN YEARS, AND EXCEEDANCE PROBABILITY, IN PERCENT					
	2 50%	5 20%	10 10%	25 4%	50† 2%	100† 1%
1	766	1,830	2,750	4,080	5,170	6,310
3	406	844	1,140	1,480	1,710	1,910
7	198	397	521	653	734	800
15	104	209	276	351	398	438
30	61	114	145	179	199	215
60	34	66	89	117	138	158
90	25	48	64	83	98	111

MAGNITUDE AND PROBABILITY OF INSTANTANEOUS PEAK FLOW  
BASED ON PERIOD OF RECORD 1974-89

DISCHARGE, IN FT <sup>3</sup> /S, FOR INDICATED RECURRENCE INTERVAL IN YEARS, AND EXCEEDANCE PROBABILITY, IN PERCENT						
2 50%	5 20%	10 10%	25 4%	50† 2%	100† 1%	
3,970	7,040	9,330	12,400	14,800	17,300	
WEIGHTED SKEW (LOGS)= -0.27						
MEAN (LOGS)= 3.58						
STANDARD DEV. (LOGS)= 0.31						

DURATION TABLE OF DAILY MEAN FLOW FOR PERIOD OF RECORD 1977-89

DISCHARGE, IN FT <sup>3</sup> /S, WHICH WAS EQUALED OR EXCEEDED FOR INDICATED PERCENT OF TIME																	
1%	5%	10%	15%	20%	30%	40%	50%	60%	70%	80%	90%	95%	98%	99%	99.5%	99.9%	
173	20	8.0	5.3	4.3	3.2	2.5	2.1	1.5	0.77	0.12	0.00	0.00	0.00	0.00	0.00	0.00	0.00

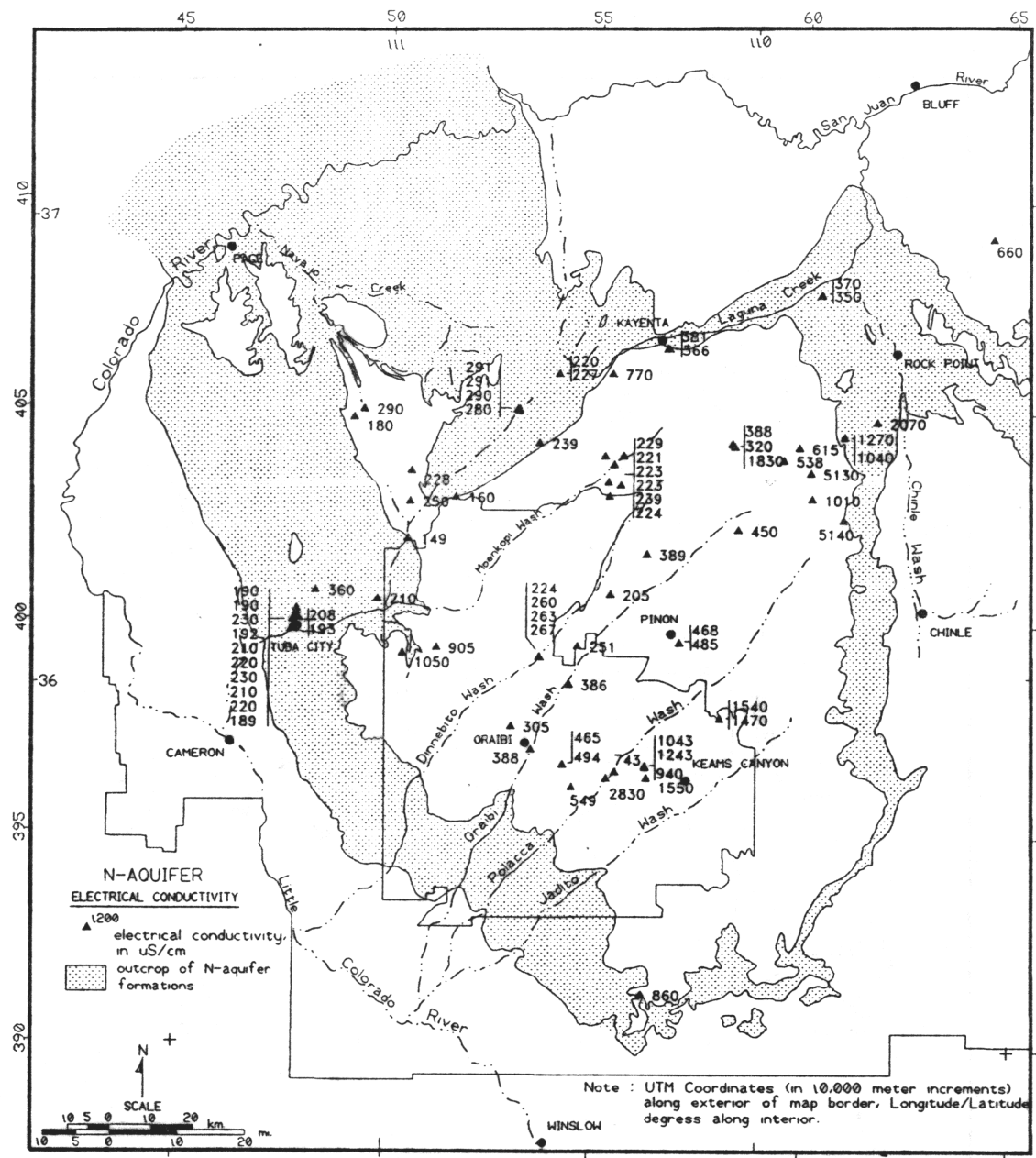
† Reliability of values in column is uncertain, and potential errors are large.

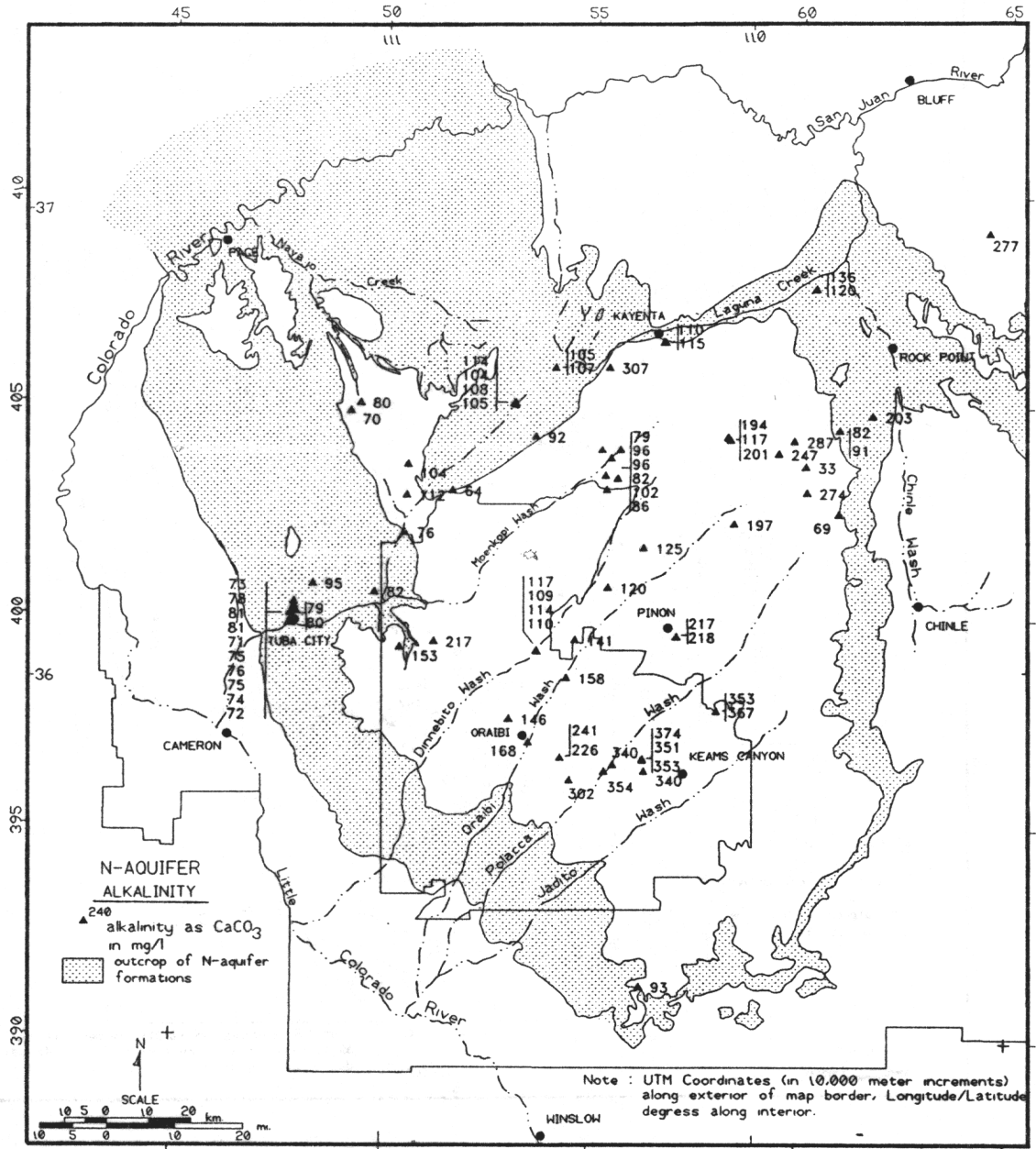
APPENDIX C

Areal distribution of selected chemical constituents, N-aquifer



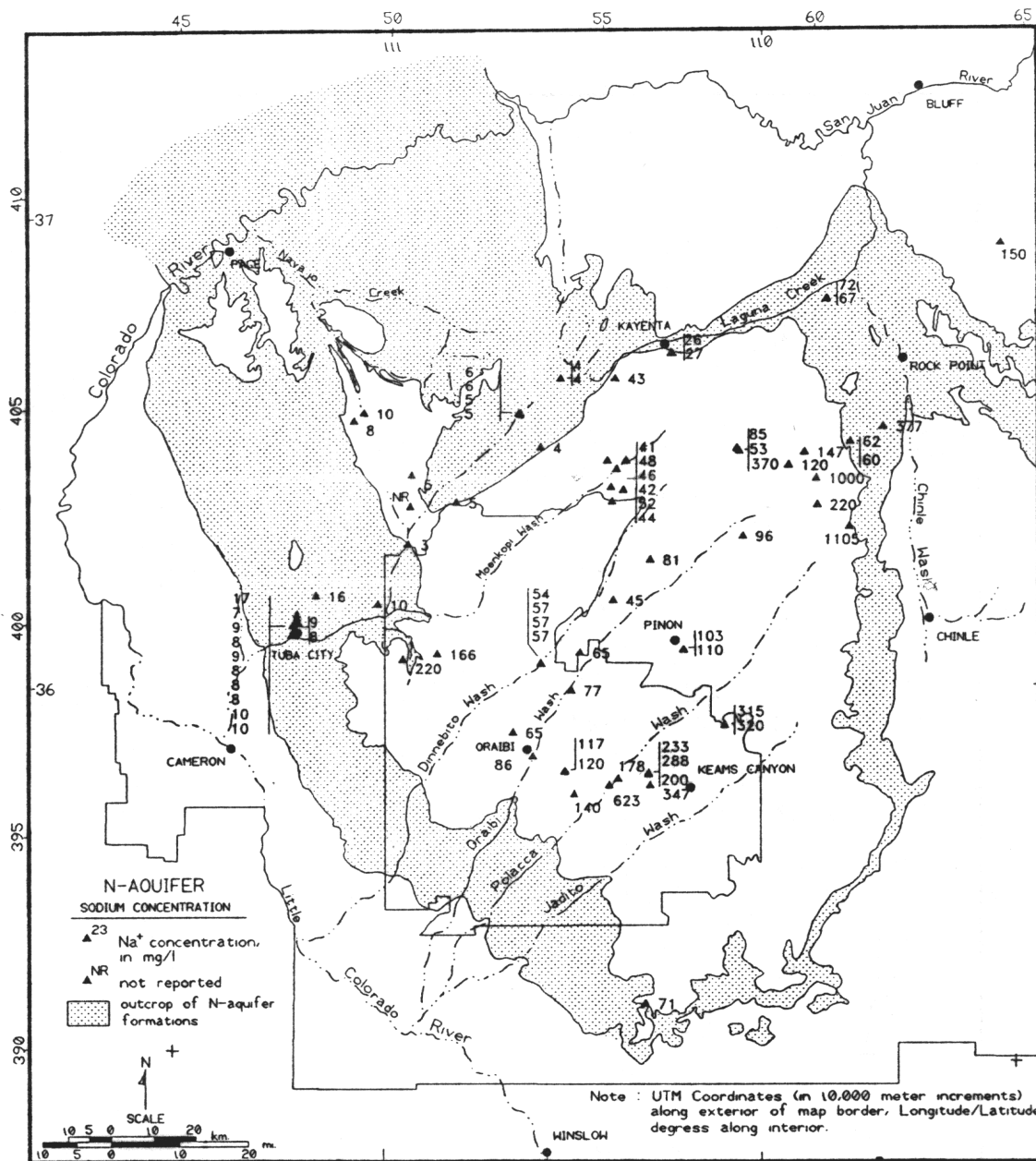




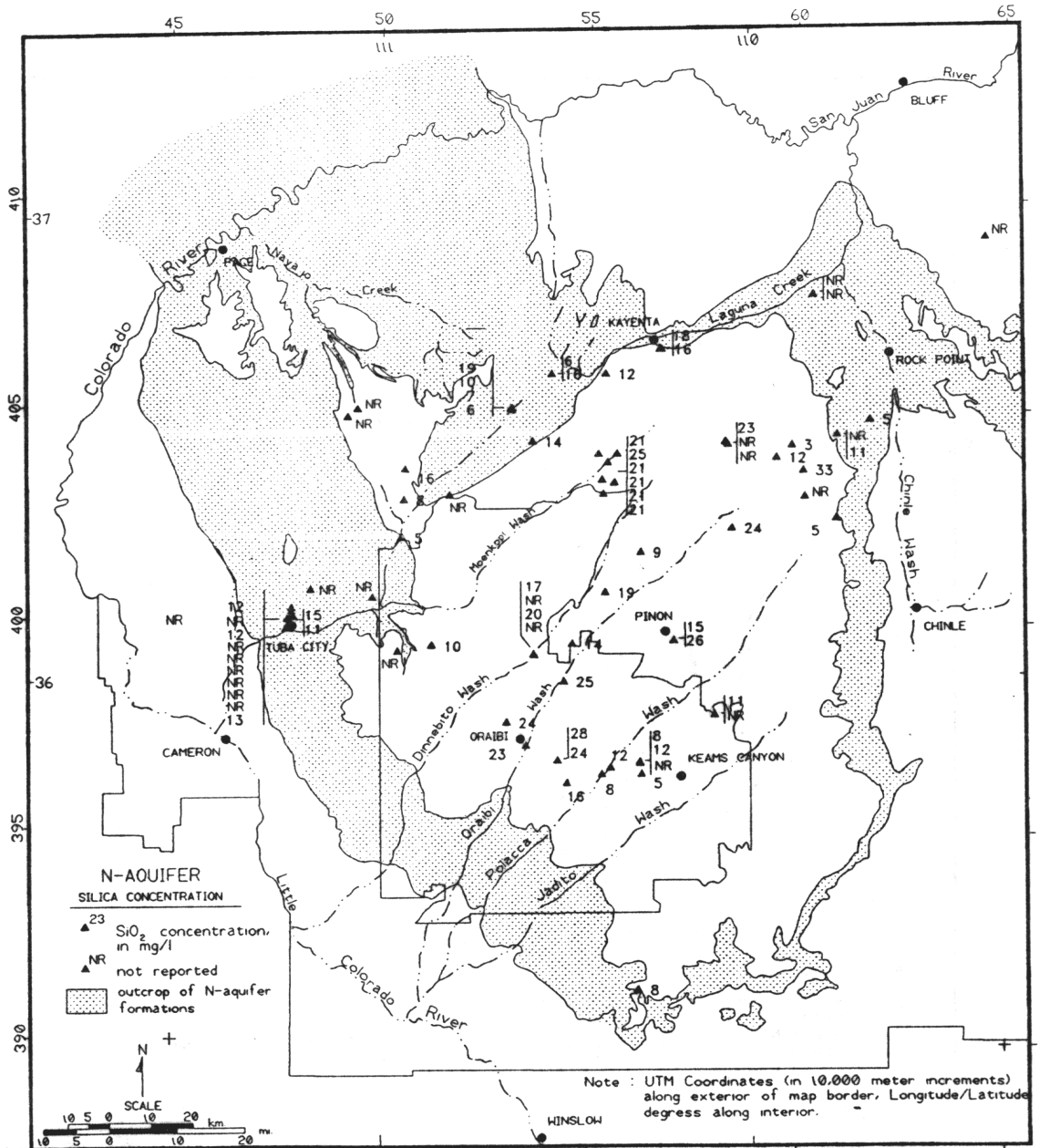




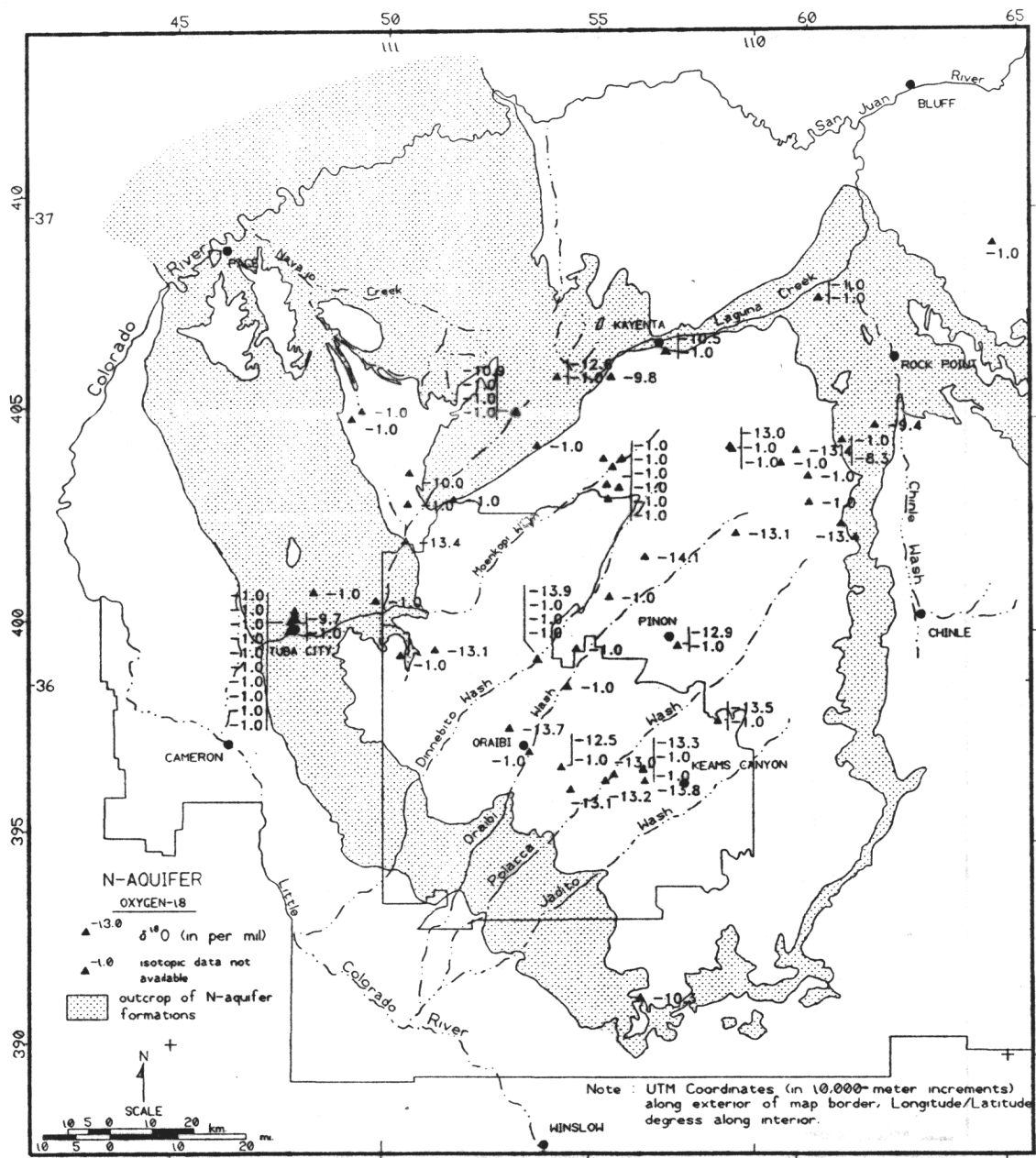












45

50

55

60

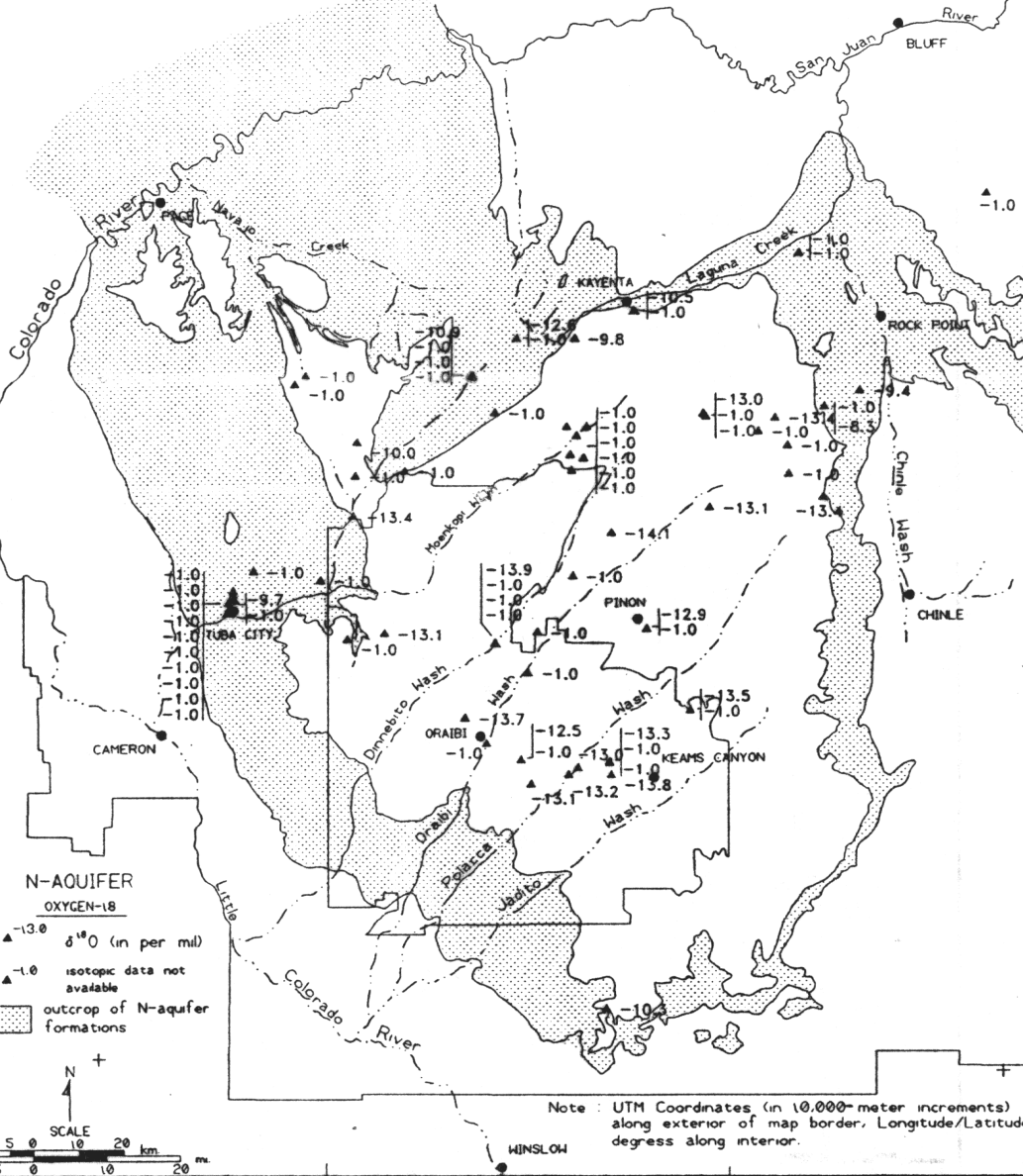
65

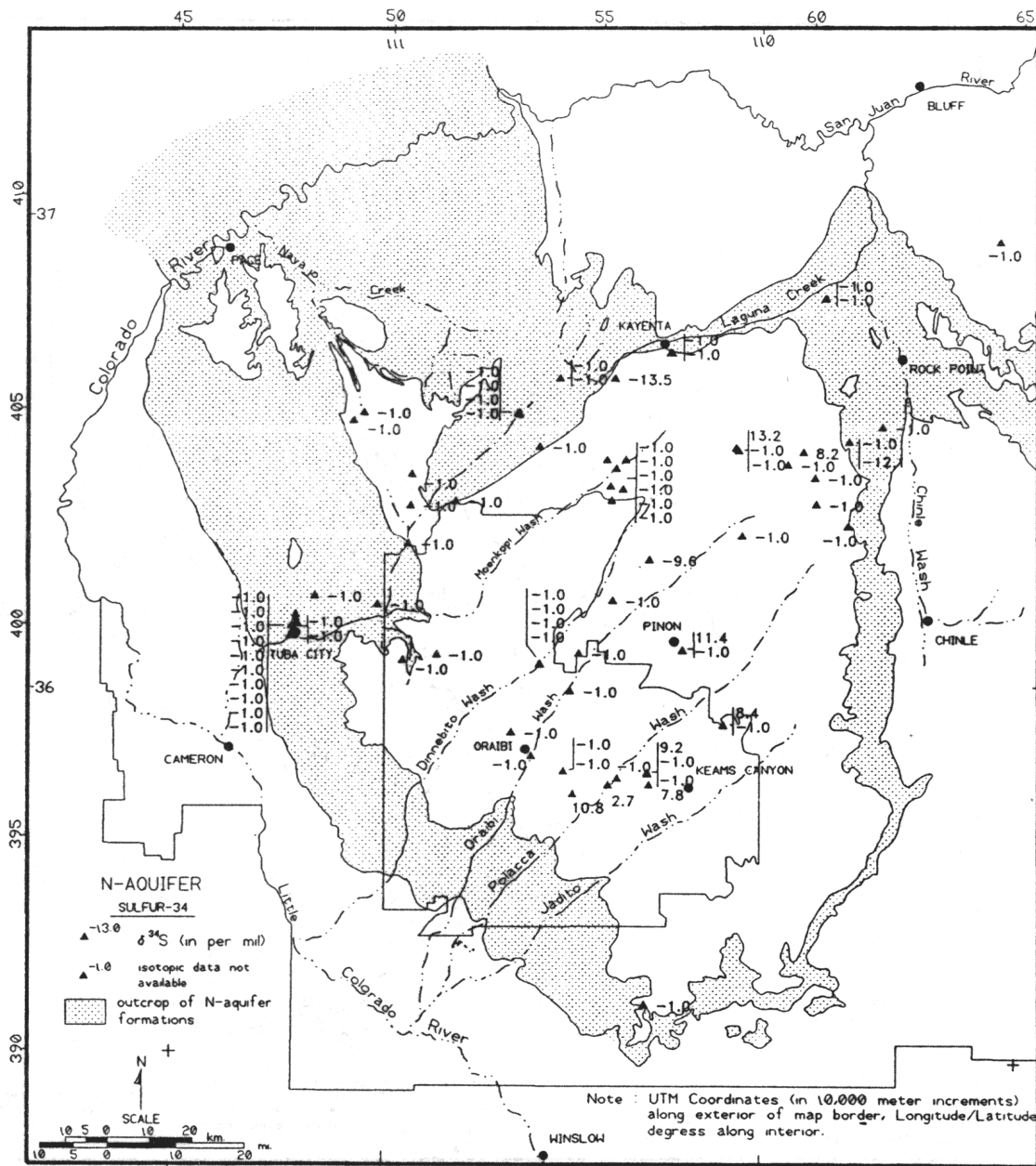
37

36

395

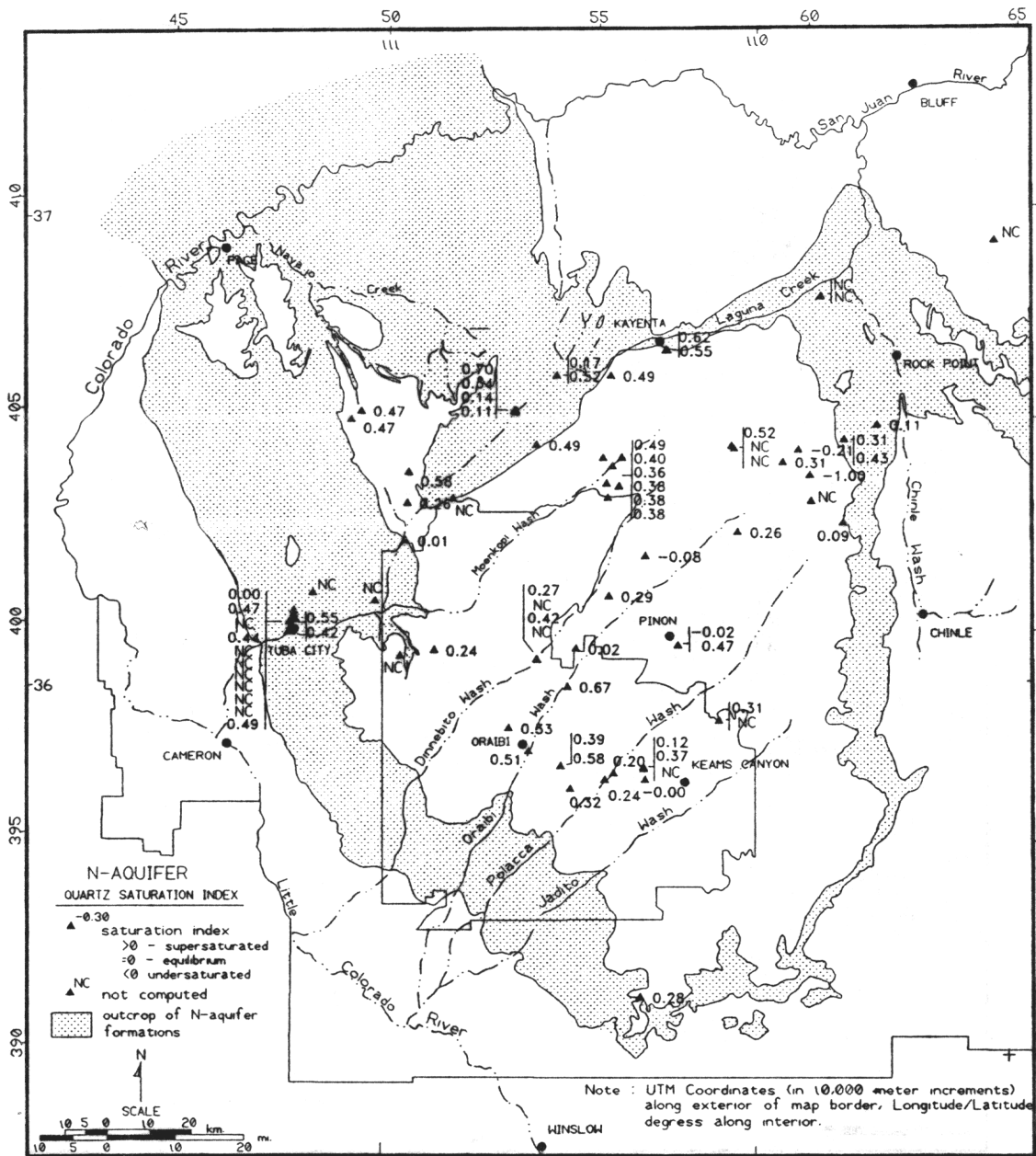
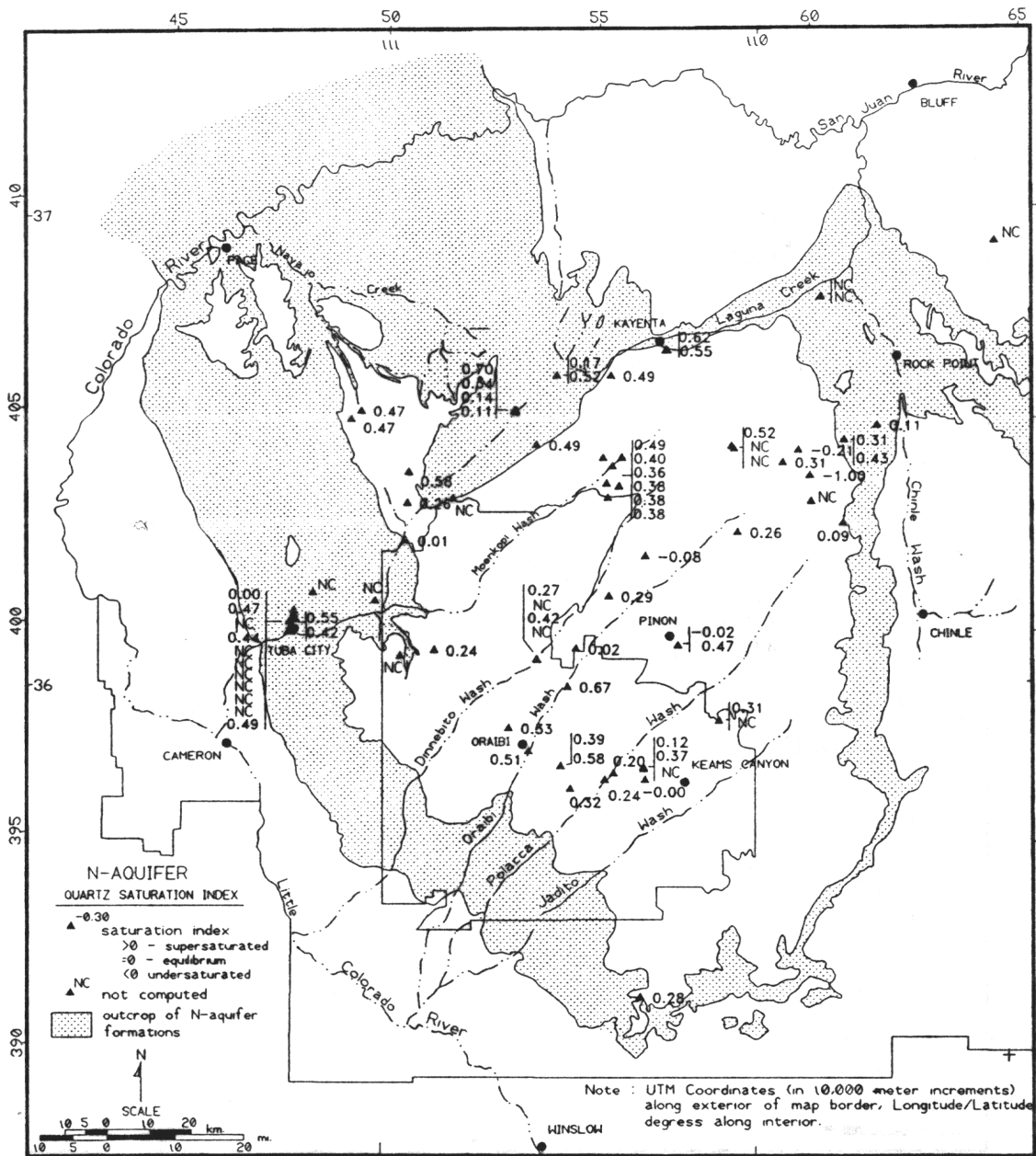
390

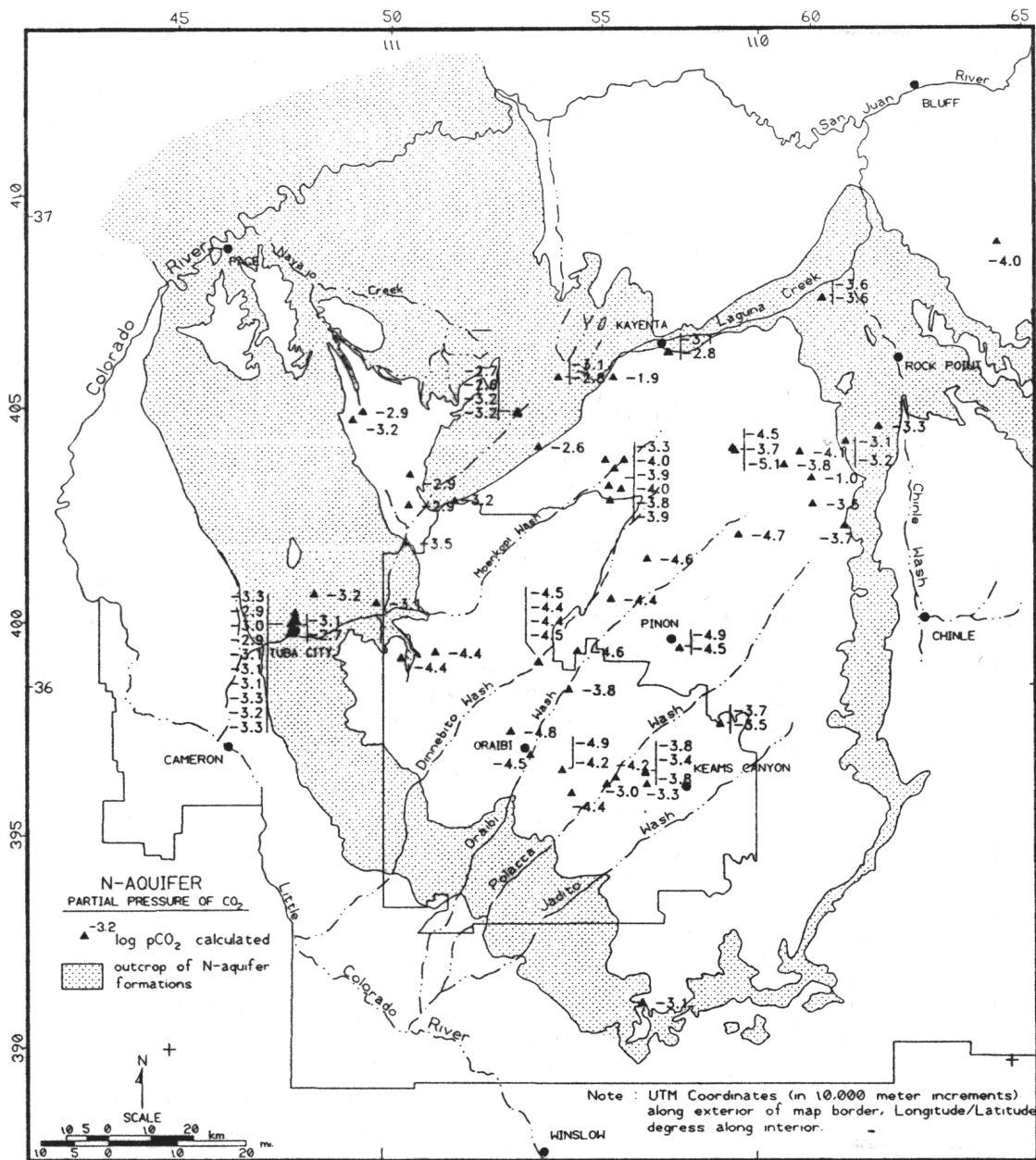












APPENDIX D  
Water quality data

Table D-1. Chemical composition of groundwater samples from the N-aquifer

SAMPLE NAME	SAMPLE NO.	AQ.	UTM COORDINATES EAST	UTM COORDINATES NORTH	SAMPLE DATE (M/D/YR)	TEMP (C°)	pH	EC (µs/cm)	DO	ALK. (as CaCO <sub>3</sub> )	Na*	EXCESS NA	K*	Li*	Ca <sup>2+</sup>	Mg <sup>2+</sup>
ROCKY PM2	1	N	536845	3991774	27.4	9.55	224	4.9	117.3	53.9	53.2	0.36	0.043	0.2		
HOTEVILLA SCH 2	2	N	530200	3975600	26.0	9.81	305	5.6	146.0	64.9	64.2	0.41	0.038	0.6		
HOPI CULT. CTR.	3	N	542720	3966629	22.8	10.20	465	1.2	241.1	117.3	115.6	0.50	0.052	0.4		
2ND MESA SCH 2	4	N	545000	3961300	20.2	9.73	569	0.7	302.0	140.2	136.4	0.49	0.038	0.4		
POLACCA 6	5	N	553300	3963500	19.3	8.56	2830	0.6	354.3	623.1	334.5	2.81		6.5	0.9	
POLACCA SCH 2	6	N	555350	3965100	21.8	9.61	743	1.6	339.6	178.2	158.6	0.89		0.7		
KEANS CYN #2	7	N	562541	3966193	19.8	9.27	1043	0.2	374.0	232.9	165.8	0.62		0.8	0.1	
HOPI HIGH SCH #3	8	N	562900	3963600	20.3	8.81	1550	0.1	339.6	347.0	182.2	0.78		1.6	0.2	
9Y-92	9	N	609004	4044579	14.7	8.11	1040	13.8	91.0	60.2	52.7	3.26		126.7	45.8	
8T-518	10	N	598191	4041984	16.4	9.47	615	2.5	287.1	147.2	127.3	0.52		0.6	0.1	
CHLCHN PM3	11	N	582230	4042750	20.2	9.66	388	8.1	193.6	84.6	83.2	0.42	0.041	0.6		
8T-522	12	N	553613	4058909	13.2	7.37	770	2.8	307.1	43.3	35.3	2.67		98.2	22.8	
KAYENTA SCH 2	13	N	566600	4065000	16.2	8.17	381	7.8	109.9	25.8	23.7	1.26	0.023	46.6	7.6	
SHONTO SCH #2	14	N	530684	4050292	13.8	7.78	291	8.6	114.0	5.6	-0.6	1.21	0.018	49.8	4.7	
2K-319	15	N	505401	4035603	15.4	7.97	228	7.2	104.2	5.0	1.9	1.14	0.034	39.7	3.5	
1K-214	16	N	505181	4028301	15.6	8.02	250	6.6	111.5							
RED LAKE SCH PM1	17	N	504800	4019450	16.8	8.36	149	7.7	76.3	3.1	2.7	1.90	0.021	18.1	5.2	
TUBA CITY SCH PM5	18	N	477706	3998935	16.6	7.99	208	6.8	78.7	9.3	6.4	1.10		24.1	3.7	
10R 111	19	N	608928	4024774	16.3	8.46	5140	9.5	68.9	1105.4	1048.0	4.95	0.453	69.3	10.1	
9K215	20	N	616665	4048193	15.3	8.51	2070	4.3	202.6	377.4	176.0	12.80		50.0	20.3	
PINON PM6	21	N	570310	3995553	27.0	10	468	5.3	216.5	102.7	100.8	0.09		0.5		
LOW MTN PM2	22	N	580173	3977890	20.3	9.16	1540	0.2	352.7	314.7	185.0	0.34		1.4	0.2	
KITSILLIE	23	N	583990	4022290	28.7	9.81	450	5.3	196.8	96.0	93.0	0.28		0.9	0.1	
3M156	24	N	512004	3993800	16.5	9.61	905	0.5	216.5	166.4	139.4	0.44		0.7		
NTUA FOREST LAKE	25	N	562300	4016450	28.9	9.63	389	5.7	125.1	81.0	75.1	0.07		0.9	0.1	
NAVAJO NAT.M.(BET.)	26	N	540681	4058776	13.4	8.1	220	8.0	105.0	3.5	1.7	1.07		34.0	2.7	
DILKON BIA 2	27	N	562420	3912610	15.1	8.04	860	7.5	92.7	71.3	2.5	3.76		64.4	22.3	
IHS HARD ROCK-N	28	N	546000	3994500	32.5	9.64	251		141.1	65.3	63.6	0.62		0.8		

(all concentrations are in mg/l unless stated otherwise)

Table D-1. Chemical composition of groundwater samples from the M-aquifer (continued)

SAMPLE NAME	SAMPLE NO.	AQ.	UTM COORDINATES	SAMPLE DATE (M/D/YR)	TEMP (C°)	pH	EC (µs/cm)	DO	ALK. (as CaCO <sub>3</sub> )	Na <sup>+</sup>	EXCESS NA	K <sup>+</sup>	Li <sup>+</sup>	Ca <sup>2+</sup>	Mg <sup>2+</sup>
3T-333	111	n	477803 3997764	09/16/65	8.2	190			73	17.0	11.7	1.30		20.0	3.6
3T-54	112	n	478416 4002815	10/19/71	15.5	7.8	190		78	7.1	4.0	1.00		24.0	4.1
3T-508	113	n	478960 4000534	09/16/65	8.0	230			81	9.4	3.0	1.20		28.0	4.9
3T-528	114	n	482846 4007088	09/16/65	8.2	360			95	16.0	5.0	1.30		42.0	6.1
KAI SCH 4	115	n	491451 4048115	06/24/69	8.1	180			70	8.0	6.8	4.70		18.0	6.1
KAIBIT PM3	116	n	493838 4050023	06/26/59	7.9	290			80	9.7	0.6	0.80		30.0	12.0
3K-323	117	n	497652 4005284	05/06/68	8.1	210			82	10.0	5.2	0.60		26.0	4.9
3K-330	118	n	503802 3992406	05/06/68	9.5	1050			153	220.0	210.9			3.0	
1P-511	119	n	516163 4029454	02/01/71	8.1	160			64	5.3	4.1	1.20		19.0	4.9
SHONTO PM2	120	n	530684 4050292	08/07/73	8.1	280			106	5.5	0.9	1.60		42.0	4.9
SHONTO PM2	120	n	530684 4050292	05/20/86	14.0	7.1	302		101	5.7	-0.8	1.60		41.0	5.4
ORAIPI PM4	121	n	534980 3970138	10/11/68	9.8	400			158	88.0	85.7	0.40		2.0	
ORAIPI PM4	121	n	534980 3970138	11/23/72	9.3	368			162	84.0	81.7	0.80		0.4	
ORAIPI PM4	121	n	534980 3970138	07/29/82	22.0	385			167	85.0	82.4	0.40		0.4	0.0
ORAIPI PM4	121	n	534980 3970138	08/15/83	22.0	400			180	87.0	84.3	0.50		0.5	0.2
ORAIPI PM4	121	n	534980 3970138	08/14/84	21.0	385			174	86.0	83.4	0.40		0.4	0.0
BM 4; 2T-514	122	n	536059 4042455	06/16/72	14.0	7.9	236		95	3.5	-1.4	1.30		36.0	3.7
BM 4; 2T-514	122	n	536059 4042455	06/16/72	7.3	242			89	4.2	1.2	1.10		38.0	3.6
ROCKY PM2	125	n	536845 3991774	06/24/69	9.4	260			109	57.0	55.4	0.80		1.0	
BETKN N M	126	n	540681 4058776	00/00/72	7.9	227			107	4.4	2.5	1.20		35.0	3.7
4T-519	127	n	544055 3985553	11/23/72	9.0	386			158	77.0	75.8	1.50		1.3	0.3
PEABODY 2	128	n	552017 4039517	10/19/71	8.7	211			81	40.0	38.2	1.10		7.5	0.1
PEABODY 2	128	n	552017 4039517	09/10/75	31.0	230			84	41.0	37.8	0.80		7.8	0.2
PEABODY 2	128	n	552017 4039517	11/17/76	30.0	260			79	41.0	38.7	0.70		4.9	
PEABODY 2	128	n	552017 4039517	08/09/79	31.0	220			82	43.0	40.8	0.80		8.2	0.2
PEABODY 2	128	n	552017 4039517	08/19/80	30.5	225			67	39.0	31.9	0.70		8.5	0.5
PEABODY 4	129	n	552900 4033422	09/10/75	34.0	220			84	41.0	38.8	0.70		4.9	0.2
PEABODY 4	129	n	552900 4033422	11/17/76	32.0	240			76	40.0	38.1	0.80		7.0	0.1
PEABODY 4	129	n	552900 4033422	08/09/79	32.0	220			85	45.0	42.5	0.70		5.1	0.1
PEABODY 4	129	n	552900 4033422	08/19/80	32.0	230			84	44.0	41.2	0.70		4.6	0.1
PEABODY 4	129	n	552900 4033422	03/25/86	32.0	205			80	41.0	38.3	0.70		4.9	0.0

(all concentrations are in mg/l unless stated otherwise)

Table D-1. Chemical composition of groundwater samples from the M-aquifer (continued)

SAMPLE NAME	SAMPLE NO.	AQ.	UTM COORDINATES	SAMPLE DATE	TEMP (C°)	PH	EC (µs/cm)	DO	ALK. (as CaCO <sub>3</sub> )	Na <sup>+</sup>	EXCESS NA	K <sup>+</sup>	Li <sup>+</sup>	Ca <sup>2+</sup>	Mg <sup>2+</sup>
PEABODY 7	130	n	553220 4030003	09/10/75	33.0	8.5	220		88	46.0	44.1	0.70		3.8	0.3
PEABODY 7	130	n	553220 4030003	11/18/76	32.0	9.2	240		86	45.0	42.9	0.70		4.2	0.1
PEABODY 7	130	n	553220 4030003	08/09/79	32.0	8.7	225		95	48.0	45.8	0.70		4.3	0.1
PEABODY 7	130	n	553220 4030003	08/19/80	33.5	9.1	210		75	38.0	35.6	0.70		4.0	
PEABODY 5	131	n	554219 4037559	06/12/68	31.5	9.2	224		103	51.0	48.7	0.90		2.8	1.0
PEABODY 5	131	n	554219 4037559	08/18/71		9.0	226		94	45.0	43.6	1.80		3.9	
PEABODY 5	131	n	554219 4037559	09/10/75	34.0	8.5	240		99	52.0	49.4	0.70		3.5	0.1
PEABODY 5	131	n	554219 4037559	01/18/77	32.0	9.2	220		95	45.0	43.1	0.60		3.5	0.4
PEABODY 5	131	n	554219 4037559	08/23/77	33.0	9.3	220		110	47.0	45.1	0.70		3.8	
PEABODY 5	131	n	554219 4037559	08/09/79	31.0	8.7	220		85	43.0	41.1	0.70		4.3	0.1
PEABODY 5	131	n	554219 4037559	08/19/80	32.0	9.1	210		84	42.0	40.1	0.80		4.5	0.1
PEABODY 3	132	n	555842 4032762	04/29/68	31.0	8.2	236		104	55.0	52.4	0.90		2.4	1.2
PEABODY 3	132	n	555842 4032762	10/19/71		9.2	247		99	53.0	50.7	0.80		3.0	
PEABODY 3	132	n	555842 4032762	09/10/75	31.0	8.5	240		99	52.0	50.2	0.70		3.3	0.2
PEABODY 3	132	n	555842 4032762	11/18/76	32.0	9.2	250		101	50.0	48.1	0.70		3.5	
PEABODY 3	132	n	555842 4032762	08/23/77	32.0	9.3	230		110	49.0	46.9	0.70		3.9	
PEABODY 3	132	n	555842 4032762	08/09/79	32.0	8.5	240		110	53.0	50.9	0.70		3.1	0.1
PEABODY 3	132	n	555842 4032762	08/19/80	32.0	9.1	230		90	50.0	47.7	0.70		3.4	0.1
PEABODY 6	133	n	556420 4039606	06/29/68	34.0	9.0	201		108	52.0	50.1	0.90		2.8	0.5
PEABODY 6	133	n	556420 4039606	08/23/77	34.0	9.3	240		98	51.0	48.9	0.80		4.0	0.1
PEABODY 6	133	n	556420 4039606	08/19/80	32.0	8.9	260		100	50.0	47.7	0.80		4.0	
PEABODY 6	133	n	556420 4039606	01/23/86	33.5	9.1	182		76	38.0	36.5	0.80		4.7	0.0
KEAMS CYN2	134	n	562541 3966193	05/14/70		8.5	2090		396	470.0	416.2			8.0	4.9
KEAMS CYN2	134	n	562541 3966193	11/23/72		8.8	937		343	240.0	181.0	1.10		0.8	0.1
KEAMS CYN2	134	n	562541 3966193	09/01/82	19.0	9.0	1010		348	240.0	179.0	0.80		0.8	0.3
KEAMS CYN2	134	n	562541 3966193	08/23/83	19.0	9.1	1120		330	250.0	172.2	1.00		1.0	0.1
KEAMS CYN2	134	n	562541 3966193	08/13/84	19.0	9.3	1060		336	240.0	177.7	0.70		0.9	0.2
8K-416	135	n	565994 4064950	10/18/71		7.9	367		102	25.0	22.7	1.40		38.0	6.6
8K-416	135	n	565994 4064950	09/28/82	17.5	7.8	360		120	29.0	26.1	1.30		35.0	7.5
8K-416	135	n	565994 4064950	08/16/84	16.0	8.0	370		122	28.0	25.3	1.30		39.0	8.0

(all concentrations are in mg/l unless stated otherwise)

Table D-1. Chemical composition of groundwater samples from the N-aquifer (continued)

SAMPLE NAME	SAMPLE NO.	AQ.	UTM COORDINATES	SAMPLE DATE (M/D/YR)	TEMP (C°)	PH	EC (µs/cm)	DO	ALK. (as CaCO <sub>3</sub> )	Na <sup>+</sup>	EXCESS NA	K <sup>+</sup>	Li <sup>+</sup>	Ca <sup>2+</sup>	Mg <sup>2+</sup>
PINON PM 6	136	n	570310	3995553	05/29/70	9.8	490		216	110.0	108.8			1.0	0.6
PINON PM 6	136	n	570310	3995553	11/23/72	9.5	455		218	110.0	107.9	0.60		0.5	
PINON PM 6	136	n	570310	3995553	09/16/82	25.5	485		228	110.0	107.6	0.50		0.6	
PINON PM 6	136	n	570310	3995553	08/16/83	24.5	505		210	110.0	107.7	0.50		0.6	0.1
PINON PM 6	136	n	570310	3995553	08/14/84	27.0	490		220	110.0	107.6	0.40		0.5	0.0
L MTN PM2	137	n	580173	3977890	04/27/72	9.0	1470		367	320.0	190.3			2.0	1.2
CHLCHN PM3	138	n	582390	4042589	08/13/73	8.8	320		117	53.0	48.5	0.78		16.0	2.4
81-540	139	n	582892	4042131	05/19/73	10.0	1830		201	370.0	348.6	22.00		28.0	1.2
81-537	140	n	594518	4038984	05/24/72	21.0	538		247	120.0	112.9	1.10		3.7	0.3
81-511	141	n	600998	4035976	04/17/63	20.5	5130		33	1000.0	286.6			98.0	1.3
10T-251	142	n	601369	4029817	10/19/70	8.9	1010		274	220.0	148.7			3.0	
8K-403	143	n	602906	4078035	07/25/69	8.8	370		136	72.0	64.9	4.00		10.0	3.0
8K-521	144	n	603028	4078191	07/30/64	8.7	350		120	67.0	59.2	0.80		8.0	3.7
9Y-92	145	n	609004	4044579	08/23/71	8.0	1270		82	62.0	53.6	0.80		120.0	57.0
9Y-12	146	n	631046	4094296	03/11/55	14.5	630		230	140.0	129.6	0.80		0.8	0.9
RD MES SCH	147	n	644121	4091765	02/29/72	9.4	660		277	150.0	141.6			2.0	
ROCKY	148	n	536644	3991897	03/09/76	9.6	270		113	57.0	53.6	1.20		4.0	
ROCKY	148	n	536644	3991897	09/02/82	26.0	255		114	56.0	55.1	0.50		0.5	
ROCKY PM1	149	n	536569	3991865	11/30/67	9.4	280		110	59.0	58.3	0.60		2.0	
ROCKY PM1	149	n	536569	3991865	11/23/70	9.6	260		111	57.0	56.3			2.0	
ROCKY PM1	149	n	536569	3991865	02/11/71	9.5	260		109	55.0	53.2			2.0	
SHNT PM3	150	n	531008	4050015	08/07/73	8.3	290		108	5.0	0.4	1.60		44.0	4.9
SHONTO PM4	151	n	531106	4050478	08/07/73	8.3	280		105	5.0	2.7	1.60		42.0	4.9
NTUA 3	152	n	478462	4001151	11/09/71	16.0	193		80	7.8	4.8	1.00		23.0	4.2
KEAMS CYN3	153	n	562464	3966531	01/22/76	9.3	940		353	200.0	154.0	2.00		6.0	7.3
HOPI A & C	154	n	542720	3966629	11/23/72	9.5	494		226	120.0	117.2	0.50		0.4	
BM 6	155	n	553762	4006867	08/30/77	30.0	205		120	45.0	44.2	0.60		14.0	0.1
3T-546	156	n	478414	4002045	09/17/71	17.0	192		81	8.4	5.5	1.00		25.0	4.4
3T-511	157	n	477410	4000168	09/16/65	8.0	210		71	9.2	2.8	1.20		22.0	4.9
3GS-77-2	158	n	477983	3999488	09/16/65	8.0	220		75	8.0	2.8	1.20		26.0	4.9
3GS-77-3	159	n	477983	3999427	09/16/65	8.0	230		76	8.3	0.5	1.20		26.0	4.9

(all concentrations are in mg/l unless stated otherwise)

Table D-1. Chemical composition of groundwater samples from the N-aquifer (continued)

SAMPLE NAME	SAMPLE NO.	AQ.	UTM COORDINATES		SAMPLE DATE (M/D/YR)	TEMP (C°)	PH	EC (µs/cm)	DO	ALK. (as CaCO <sub>3</sub> )	Na*	EXCESS NA	K*	Li*	Ca <sup>2+</sup>	Mg <sup>2+</sup>
			EAST	NORTH												
3K-318-1	160	n	478281	3998779	09/16/65		8.2	210		75	8.3	3.0	1.20		24.0	3.6
3K-318-2	161	n	477706	3998935	09/16/65		8.1	220		74	10.0	3.6	1.20		24.0	4.9
3T-222	162	n	477079	3997765	05/09/55	16.0	8.2	188		74	8.9	6.0	2.20		22.0	4.4
3T-222	163	n	477079	3997765	09/16/65		8.2	190		69	12.0	6.2	1.20		24.0	3.6

(all concentrations are in mg/l unless stated otherwise)

Table D-1. Chemical composition of groundwater samples from the N-aquifer (continued)

SAMPLE NAME	SAMPLE NO.	AQ.	UTM COORDINATES		F <sup>-</sup>	Cl <sup>-</sup>	Br <sup>-</sup>	NO <sub>3</sub> <sup>-</sup>	SO <sub>4</sub> <sup>2-</sup>	SiO <sub>2</sub>	COMPUTED BALANCE
			EAST	NORTH							
ROCKY PM2	1	N	536845	3991774	0.04	1.0	0.04	6.27	5.0	17.4	-4.3%
HOTEVILLA SCH 2	2	N	530200	3975600	0.06	1.1	0.01	5.13	4.6	24.1	-4.4%
HOPI CULT. CTR.	3	N	542720	3966629	0.02	2.6		0.03	19.2	28.4	-1.5%
2ND MESA SCH 2	4	N	545000	3961300	0.04	5.9	0.022	0.03	14.2	15.6	-2.9%
POLACCA 6	5	N	553300	3963500	2.25	445.0	0.11	0.48	336.0	8.4	1.5%
POLACCA SCH 2	6	N	555350	3965100	0.62	30.3	0.01		24.5	11.8	-2.3%
KEAMS CYN #2	7	N	562541	3966193	1.46	103.4	0.04		32.8	7.6	-4.5%
HOPI HIGH SCH #3	8	N	562900	3963600	1.88	254.0		0.09	79.5	5.1	-1.6%
9Y-92	9	N	609004	4044579	1.17	11.5	0.09	18.80	488.0	10.7	0.5%
8T-518	10	N	598191	4041984	0.108	30.7	0.064	5.17	20.9	3.2	-4.9%
CHLCHN PM3	11	N	582230	4042750	0.13	2.1		5.69	3.5	23.2	-4.7%
8T-522	12	N	553613	4058909	0.28	12.3	0.16	4.80	114.0	11.6	-1.3%
KAYENTA SCH 2	13	N	566600	4065000	0.07	3.3		4.35	73.8	17.5	2.6%
SHOWTO SCH #2	14	N	530684	4050292		9.6	0.11	15.70	11.5	19.4	1.8%
2K-319	15	N	505401	4035603	0.01	4.7	0.03	11.00	5.5	15.7	0.2%
1K-214	16	N	505181	4028301	0.3	3.2		2.90	12.0	7.6	
RED LAKE SCH PM1	17	N	504800	4019450	0.018	0.7	0.019	6.07	1.7	4.5	-4.9%
TUBA CITY SCH PMS	18	N	477706	3998935	0.012	4.4	0.073	8.10	10.5	15.1	-2.7%
10R 111	19	N	608928	4024774	2.24	88.5	0.2	4.23	2120	5.2	4.3%
9K215	20	N	616665	4048193	0.442	310.6	1.18	64.68	426.0	5.4	-4.2%
PINON PM6	21	N	570310	3995553	0.17	2.9	0.005	7.16	4.0	14.6	-1.3%
LOW MTN PM2	22	N	580173	3977890	3.39	200.0	0.005	0.22	67.7	11.4	-1.8%
KITSILLIE	23	N	583990	4022290	0.55	4.6	0.01	6.16	4.4	24.2	-0.5%
3M156	24	N	512004	3993800	2	41.7	0.001	0.33	87.3	9.9	-1.0%
NTUA FOREST LAKE	25	N	562300	4016450	0.33	9.2	0.13	3.50	37.4	9.1	-0.5%
NAVAJO NAT.M.(BET.)	26	N	540681	4058776		2.7	0.055	4.23	2.7	5.6	-4.7%
DILKON BIA 2	27	N	562420	3912610	0.034	106.2	0.198	10.65	195.5	7.7	-4.9%
IHS HARD ROCK-N	28	N	546000	3994500	0.01	2.5	0.017	7.39	5.2	14.1	-3.7%

(all concentrations are in mg/l unless stated otherwise)

Table D-1. Chemical composition of groundwater samples from the M-aquifer (continued)

SAMPLE NAME	SAMPLE NO.	AQ.	UTM COORDINATES			F <sup>-</sup>	Cl <sup>-</sup>	Br <sup>-</sup>	NO <sub>3</sub> <sup>-</sup>	SO <sub>4</sub> <sup>=</sup>	SiO <sub>2</sub>	COMPUTED BALANCE
			EAST	NORTH								
3T-333	111	n	477803	3997764	0.2	8.2		6.50	10		1.3%	
3T-54	112	n	478416	4002815	0.2	4.8			8	12.0	-0.0%	
3T-508	113	n	478960	4000534	0.1	9.9		5.60	14		-1.0%	
3T-528	114	n	482846	4007088	0.2	17.0		22.00	23		1.6%	
KAI SCH 4	115	n	491451	4048115	0.1	1.8		8.10	10		2.0%	
KAIBIT PM3	116	n	493838	4050023	0.2	14.0		6.20	39		0.2%	
3K-323	117	n	497652	4005284		7.4		7.70	14		-2.5%	
3K-330	118	n	503802	3992406	0.3	14.0		1.10	330		-3.2%	
1P-511	119	n	516163	4029454	0.2	1.8		5.00	11		-1.1%	
SHONTO PM2	120	n	530684	4050292		7.1		14.00	20	6.3	-3.2%	
SHONTO PM2	120	n	530684	4050292		10.0			14	14.0	3.5%	
ORAIBI PM4	121	n	534980	3970138	0.1	3.6		4.30	39		-2.6%	
ORAIBI PM4	121	n	534980	3970138	0.2	3.6		3.40	10	23.0	1.1%	
ORAIBI PM4	121	n	534980	3970138	0.2	4.0			10	23.0	0.9%	
ORAIBI PM4	121	n	534980	3970138	0.2	4.1			10	23.0	-1.2%	
ORAIBI PM4	121	n	534980	3970138	0.2	4.0			10	22.0	-0.4%	
BM 4; 2T-514	122	n	536059	4042455		7.6		2.90	12	14.0	-2.6%	
BM 4; 2T-514	122	n	536059	4042455	0.1	4.6		11.00	10	13.0	2.3%	
ROCKY PM2	125	n	536845	3991774	0.1	2.5		6.20	14		-1.8%	
BETKN N M	126	n	540681	4058776	0.1	3.0		2.20	4	16.0	-1.7%	
4T-519	127	n	544055	3985553	0.2	1.8		4.10	7	25.0	0.8%	
PEABODY 2	128	n	552017	4039517	0.2	2.8		3.40	18	20.0	0.3%	
PEABODY 2	128	n	552017	4039517	0.2	5.0			20	20.0	-0.8%	
PEABODY 2	128	n	552017	4039517	0.2	3.6			16	22.0	0.5%	
PEABODY 2	128	n	552017	4039517	0.1	3.4			24	22.0	1.7%	
PEABODY 2	128	n	552017	4039517	0.2	11.0			20	21.0	2.4%	
PEABODY 4	129	n	552900	4033422	0.2	3.4			13	21.0	0.2%	
PEABODY 4	129	n	552900	4033422	0.2	2.9			19	21.0	2.7%	
PEABODY 4	129	n	552900	4033422	0.2	3.9			19	23.0	0.5%	
PEABODY 4	129	n	552900	4033422	0.2	4.3			13	21.0	2.1%	
PEABODY 4	129	n	552900	4033422	0.2	4.2			12	20.0	1.8%	

(all concentrations are in mg/l unless stated otherwise)

Table D-1. Chemical composition of groundwater samples from the M-aquifer (continued)

SAMPLE NAME	SAMPLE NO.	AG.	UTM COORDINATES EAST NORTH	F <sup>-</sup>	Cl <sup>-</sup>	Br <sup>-</sup>	NO <sub>3</sub> <sup>-</sup>	SO <sub>4</sub> <sup>-2</sup>	SiO <sub>2</sub>	COMPUTED BALANCE
PEABODY 7	130	n	553220 4030003	0.2	3.0			15	20.0	1.5%
PEABODY 7	130	n	553220 4030003	0.2	3.2			13	21.0	2.4%
PEABODY 7	130	n	553220 4030003	0.2	3.4			20	22.0	-1.9%
PEABODY 7	130	n	553220 4030003	0.2	3.7			11	20.0	0.7%
PEABODY 5	131	n	554219 4037559		3.5		2.90	16		-0.5%
PEABODY 5	131	n	554219 4037559	0.2	2.1			12	21.0	-1.1%
PEABODY 5	131	n	554219 4037559	0.2	4.0			18	20.0	-0.3%
PEABODY 5	131	n	554219 4037559	0.2	3.0			13	21.0	-1.9%
PEABODY 5	131	n	554219 4037559	0.2	3.0			12	21.0	-6.1%
PEABODY 5	131	n	554219 4037559	0.2	2.9			15	21.0	0.2%
PEABODY 5	131	n	554219 4037559	0.2	2.9			10	21.0	2.8%
PEABODY 3	132	n	555842 4032762	0.6	4.0		4.00	17	30.0	-0.1%
PEABODY 3	132	n	555842 4032762	0.2	3.5		3.00	17	19.0	-0.3%
PEABODY 3	132	n	555842 4032762	0.5	2.8			14	19.0	1.8%
PEABODY 3	132	n	555842 4032762	0.4	3.0			11	17.0	0.3%
PEABODY 3	132	n	555842 4032762	0.5	3.2			12	20.0	-4.5%
PEABODY 3	132	n	555842 4032762	0.4	3.3			17	21.0	-3.5%
PEABODY 3	132	n	555842 4032762	0.4	3.5			14	20.0	3.5%
PEABODY 6	133	n	556420 4039606	0.4	3.0		2.60	13	34.0	-2.2%
PEABODY 6	133	n	556420 4039606	0.2	3.2			13	22.0	2.4%
PEABODY 6	133	n	556420 4039606	0.3	3.5			15	20.0	-0.6%
PEABODY 6	133	n	556420 4039606	0.2	2.3			10	22.0	3.2%
KEAMS CYN2	134	n	562541 3966193	4.8	83.0		2.50	490		1.2%
KEAMS CYN2	134	n	562541 3966193	1.4	91.0		0.10	46	12.0	0.3%
KEAMS CYN2	134	n	562541 3966193	1.4	94.0			35	13.0	0.5%
KEAMS CYN2	134	n	562541 3966193	1.5	120.0			42	12.0	0.1%
KEAMS CYN2	134	n	562541 3966193	1.3	96.0			36	12.0	1.3%
8K-416	135	n	566994 4064950	0.2	3.6		2.90	71	15.0	-1.6%
8K-416	135	n	566994 4064950	0.2	4.5			58	17.0	-1.1%
8K-416	135	n	566994 4064950	0.2	4.2			51	16.0	3.0%

(all concentrations are in mg/l unless stated otherwise)

Table D-1. Chemical composition of groundwater samples from the N-aquifer (continued)

SAMPLE NAME	SAMPLE NO.	AG.	UTM COORDINATES EAST NORTH	F <sup>-</sup>	Cl <sup>-</sup>	Br <sup>-</sup>	NO <sub>3</sub> <sup>-</sup>	SO <sub>4</sub> <sup>2-</sup>	SiO <sub>2</sub>	COMPUTED BALANCE
PINON PM 6	136	n	570310 3995553	0.3	1.8		5.60	22		-0.5%
PINON PM 6	136	n	570310 3995553	0.2	3.2		5.00	5	25.0	1.9%
PINON PM 6	136	n	570310 3995553	0.2	3.7			5	27.0	0.5%
PINON PM 6	136	n	570310 3995553	0.2	3.6			5	27.0	4.5%
PINON PM 6	136	n	570310 3995553	0.2	3.7			5	26.0	2.1%
L MTN PM2	137	n	580173 3977890	3.2	200.0		-4.00	59		-0.7%
CHLCHN PM3	138	n	582390 4042589	0.2	7.0		6.20	33		-0.1%
8T-540	139	n	582892 4042131	0.4	33.0		0.62	600		1.9%
8T-537	140	n	594518 4038984	0.4	11.0			15	12.0	-1.1%
8T-511	141	n	600998 4035976	1.6	1100.0		0.30	860	33.0	-1.2%
10T-251	142	n	601369 4029817	3.2	110.0		5.00	45		-0.2%
8K-403	143	n	602906 4078035	0.2	11.0		9.00	29		2.5%
8K-521	144	n	603028 4078191	0.2	12.0		4.40	31		2.5%
9Y-92	145	n	609004 4044579	1.2	13.0		9.30	540		-0.2%
9Y-12	146	n	631046 4094296	0.3	16.0		0.50	64	11.0	-1.4%
RD MES SCH	147	n	644121 4091765	0.6	13.0		0.12	33		0.0%
ROCKY	148	n	536644 3991897	0.3	5.3		1.50	4		3.5%
ROCKY	148	n	536644 3991897	0.1	1.4			6	20.0	0.5%
ROCKY PM1	149	n	536569 3991865	0.1	1.1		5.20	23		-2.0%
ROCKY PM1	149	n	536569 3991865	0.1	1.1		5.60	12		-0.3%
ROCKY PM1	149	n	536569 3991865	0.2	2.8		5.60	6		0.3%
SHNT PM3	150	n	531008 4050015		7.1		12.00	24	6.8	-3.3%
SHONTO PM4	151	n	531106 4050478		3.6		12.00	23	6.4	-2.0%
NTUA 3	152	n	478462 4001151	0.2	4.6			9	11.0	-1.9%
KEAMS CYN3	153	n	562464 3966531	1.1	71.0			36		-1.1%
HOP1 A & C	154	n	542720 3966629	0.2	4.3		0.20	20	24.0	1.8%
BM 6	155	n	553762 4006867	0.1	1.2			6	19.0	2.4%
3T-546	156	n	478414 4002045	0.2	4.4			2	12.0	5.5%
3T-511	157	n	477410 4000168	0.1	9.9		6.10	8		-1.0%
3GS-77-2	158	n	477983 3999488	0.2	8.0		6.20	12		-0.1%
3GS-77-3	159	n	477983 3999427	0.1	12.0		5.00	10		-1.4%

(all concentrations are in mg/l unless stated otherwise)

Table D-1. Chemical composition of groundwater samples from the M-aquifer (continued)

SAMPLE NAME	SAMPLE NO.	AQ.	UTM COORDINATES		F <sup>-</sup>	Cl <sup>-</sup>	Br <sup>-</sup>	NO <sub>3</sub> <sup>-</sup>	SO <sub>4</sub> <sup>2-</sup>	SiO <sub>2</sub>	COMPUTED BALANCE
			EAST	NORTH							
3K-318-1	160	n	478281	3998779	0.1	8.2		6.10	6		-2.0%
3K-318-2	161	n	477706	3998935	0.1	9.9		6.20	8		0.8%
3T-222	162	n	477079	3997765	0.1	4.5		6.40	9	13.0	-0.0%
3T-222	163	n	477079	3997765	0.1	8.9		6.80	16		-0.8%

(all concentrations are in mg/l unless stated otherwise)

Table D-2. Chemical composition of water samples from streams, springs and drive points, Moenkopi and Dinnebito washes

LOC. ID	SITE DESCRIPTION	SAMPLE TYPE	SAMPLE ID.	SAMPLES COLLECTED	DATE (M/D/YR)	TEMP (°C)	PH	EC (µS/cm)	DO	ALK. (as CaCO <sub>3</sub> )	Na*	EXCESS NA	K*	Li*	Ca <sup>2+</sup>	Mg <sup>2+</sup>
MOENKOPI WASH																
1	MW; old USGS gauging station	s		none	02/15/90	7.7	8.59	1200								
2	MW; at Coal Mine Canyon	s	CMC-X1	CASD	02/16/90	2.3	8.39	960	13.0	210.0	100.0	95	3.10	0.03	69.0	17.0
2	MW; at Coal Mine Canyon	s	CMC-X2	CASD	02/17/90	1.3	8.40	920	13.2	210.0	111.0	105	2.90	0.01	71.0	17.0
3	MW; at Coal Mine Canyon	d		none	02/17/90	11.2	7.83	930								
4	MW; Coal Mine Wash	s	CMW-X1	CASD	02/17/90	7.4	8.29	2130	11.7	232.0	348.0	337	8.56	0.04	71.2	21.2
5	MW; Springs W. of LDSK	p	WLDK-X1	CASD	02/17/90	14.4	7.68	590	8.3	128.0	86.1	58	1.40	0.03	35.7	10.6
6	MW; at Lechee Da Si Kaid	d		none	02/18/90	12.0	8.00	1410	7.6							
6	MW; at Lechee Da Si Kaid	s	MLDSK-X1	CASD	02/18/90	6.7	8.93	760	12.8	170.0	93.0	88	2.60	0.01	57.0	14.0
7	MW; Begashibito Wash	s	BMC-X1	CASD	02/21/90	1.2	8.43	790	11.7	275.0	58.1	51	5.22	0.03	91.5	20.6
8	MW; MW at Begashibito	s	BMWC-X1	CASD	02/21/90	6.4	8.76	760	9.5	189.0	86.6	83	3.59	0.01	74.6	11.1
9	MW; at Falls	s	MMF-X1	CASD	02/22/90	1.7	8.55	950	12.4	184.0	104.0	97	4.61	0.02	84.8	18.1
13	MW; springs, Pasture Canyon	p	PCS-X1	CASD	02/25/90	15.5	7.87	246	6.9	86.0	12.4	9	1.60	<0.01	32.0	4.95
15	MW; springs S. Kerley Valley	p	SKVS-X1	CASD	02/26/90	10.4	8.70	617	8.7	130.0	106.0	59	3.68	0.05	6.8	1.1
16	MW; in Kerley Valley	s	MMKV-X1	CASD	02/26/90	10.4	8.93	910	12.0	150.0	98.6	89	5.36	0.02	71.2	17.5
17	MW; at Moenkopi	s	MMW-X1	CASD	02/27/90	8.5	8.57	909	11.5	170.0	88.5	79	4.77	0.02	67.8	16.5
17	MW; at Moenkopi	d		none	02/28/90	8.8	7.71	2190	3.6	596.0						
17	MW; at Moenkopi	s		none	03/09/90	8.5	8.58	929	11.2	189.9						
18	MW; upstream of Moenkopi	s	MMJSM-X1	CASD	02/27/90	19.4	8.76	848	10.6	159.0	106.0	98	3.20	0.02	61.0	17.0
20	MW; at water caves	s	MMWC-X1	CASDT	03/08/90	11.1	9.28	849	11.0	155.0	147.0	142	2.66	0.02	40.7	8.0
21	MW; at Sand Springs	s	MMSS-X1	CASD	03/08/90	17.7	8.89	695	8.8	136.0	102.0	99	1.60	0.01	42.0	7.1
22	MW; at Quicksand Spring	s		none	03/10/90	7.8	8.84	762								
22	MW; Quicksand Spring	p		none	03/10/90	7.3	9.63	692								
22	MW; Quicksand Spring	p	QSS-X1	CASDT	03/08/90	17.4	8.38	279	7.2	109.0	34.8	33	1.82	0.01	15.3	3.1
22	MW; at Quicksand Spring	s		none	03/08/90	13.7	9.40	730	9.0	125.0						
23	MW; Shonto Well springs	p	SHS-X1	CASD	03/09/90	15.3	8.23	566	8.2	140.8	77.4	62	3.00	0.02	27.3	8.3

(all concentrations are in mg/l unless stated otherwise)

SAMPLE TYPES: s - surface water sample  
p - spring water sample  
d - drive point sample

C - cations  
A - anions  
S - sulfur isotopes

D - deuterium/oxygen isotopes  
T - tritium

Table D-2. Chemical composition of water samples from streams, springs and drive points, Moenkopi and Dinnebito washes (continued)

LOC. ID	SITE DESCRIPTION	SAMPLE TYPE	SAMPLE ID.	SAMPLES COLLECTED	DATE (M/D/YR)	TEMP (°C)	pH	EC (µS/cm)	DO	ALK. (as CaCO <sub>3</sub> )	Na <sup>+</sup>	EXCESS NA	K <sup>+</sup>	Li <sup>+</sup>	Ca <sup>2+</sup>	Mg <sup>2+</sup>
MOENKOPI WASH (continued)																
24	MW; at Shonto Well	s	MWSW-X1	CASD	03/09/90	13.5	8.76	875	10.1	194.4	97.3	90	4.72	0.02	74.6	15.7
25	MW; at campfire	s	MWCF-X1	CASD	03/10/90	10.9	8.61	679	9.7	157.3	82.2	79	2.95	0.01	57.6	9.7
26	MW; Horse Corral Trib.	s	HCT-X1	CASD	03/10/90	10.6	8.30	2090	7.9	147.0	207.0	197	5.22	0.06	247.0	25.2
26	MW; at Horse Corral Trib.	s	MWHCT-X1	CASDT	03/10/90	11.6	9.80	714	10.8	156.0	123.0	119	2.43	0.01	23.7	6.0
27	MW; Pasture Canyon Res.	s	PCR-X1	CASD	03/13/90	6.4	8.51	403	8.5	158.0	19.0	12	4.81	0.02	44.1	10.2
28	MW; at I-89	s	MW189-X1	CASD	03/13/90	6.7	8.65	1045	12.0	212.9	131.0	102	8.31	0.02	71.2	19.2
DINNEBITO WASH																
29	DW; Sweetwater Well	p	SW-X1	CASD	03/14/90	8.6	8.73	674	10.1	158.0	34.8	30	6.90	0.03	78.0	13.9
29	DW; at Sweetwater Well	s	DWSW-X1	CASD	03/14/90	3.1	8.71	1079	12.3	162.0	149.0	142	3.30	0.02	47.0	24.2
30	DW; at Dinnebito Spring	s	DWDS-X1	CASD	03/14/90	12.8	8.65	1939	10.8	247.4	216.0	205	4.31	0.03	136.0	61.7
31	DW; at Sand Valley	s	DWSV-X1	CASD	03/15/90	1.2	8.64	1243	13.1	198.0	147.0	139	4.74	0.03	78.0	23.2
32	DW; spring at Sand Spring	p	SSS-X1	CASD	03/15/90	9.5	7.76	935	9.1	116.0	82.2	22	3.86	0.04	98.3	15.7
33	DW; near Whisky Spring	p	WS-X1	CASD	03/15/90	3.6	7.51	773	3.2	145.0	51.2	41	3.36	0.03	115.0	18.6
34	DW; at Sand Spring	s	DWSS-X1	CASD	03/15/90	9.1	8.68	1079	9.6	180.2	142.0	131	3.95	0.02	67.8	21.0
34	DW; at Sand Spring	d	DWSS-X2	CASD	03/15/90	7.8	7.59	2090	3.6	176.0	208.0	197	3.10	0.04	181.0	56.1

(all concentrations are in mg/l unless stated otherwise)

SAMPLE TYPES: s - surface water sample  
 p - spring water sample  
 d - drive point sample

C - cations  
 A - anions  
 S - sulfur isotopes

D - deuterium/oxygen isotopes  
 T - tritium

Table D-2. Chemical composition of water samples from streams, springs and drive points, Moenkopi and Dinnebito washes (continued)

LOC. ID	SITE DESCRIPTION	SAMPLE TYPE	SAMPLE ID.	SAMPLES COLLECTED	F <sup>-</sup>	Cl <sup>-</sup>	Br <sup>-</sup>	NO <sub>3</sub> <sup>-</sup>	SO <sub>4</sub> <sup>-2</sup>	SiO <sub>2</sub>	COMPUTED BALANCE
MOENKOPI WASH											
1	MW; old USGS gauging station	s		none							
2	MW; at Coal Mine Canyon	s	CMC-X1	CASD	0.47	8.03	0.06	0.60	220	6.9	1.3%
2	MW; at Coal Mine Canyon	s	CMC-X2	CASD	0.63	9.71	0.07	0.68	244	6.4	1.3%
3	MW; at Coal Mine Canyon	d		none							
4	MW; Coal Mine Wash	s	CMW-X1	CASD	1.00	16.27	0.10	0.03	741	6.1	0.2%
5	MW; Springs V. of LDSK	p	WLDSK-X1	CASD	0.89	43.52	0.41	21.10	101	16.0	1.3%
6	MW; at Lechee De Si Kaid	d		none							
6	MW; at Lechee De Si Kaid	s	MWLDK-X1	CASD	0.53	8.21	0.04	0.58	202	6.6	1.5%
7	MW; Begashibito Wash	s	BWC-X1	CASD	0.56	10.25	0.12	0.48	148	9.3	0.1%
8	MW; MW at Begashibito	s	MBWC-X1	CASD	0.54	5.41	0.03	2.01	212	6.7	0.5%
9	MW; at Falls	s	MWF-X1	CASD	0.65	10.22	0.09	0.22	277	6.7	3.0%
13	MW; spring, Pasture Canyon	p	PCS-X1	CASD	0.18	5.82	0.08	21.62	15	8.2	0.5%
15	MW; springs S. Kerley Valley	p	SKVS-X1	CASD	0.78	72.38	0.49	13.65	28	9.8	-3.2%
16	MW; in Kerley Valley	s	MWKV-X1	CASD	0.58	14.40	0.12	0.02	269	4.0	2.1%
17	MW; at Moenkopi	s	MMW-X1	CASD	0.64	13.92	0.11	0.04	263	4.7	-3.2%
17	MW; at Moenkopi	d		none							
17	MW; at Moenkopi	s		none							
18	MW; upstream of Moenkopi	s	MMUSM-X1	CASD	0.71	12.59	0.12	0.06	253	5.3	1.6%
20	MW; at water caves	s	MMWC-X1	CASDT	0.52	7.69	0.05	0.32	248	9.1	3.6%
21	MW; at sand Springs	s	MWSS-X1	CASD	0.51	4.84	0.02	0.50	176	8.7	1.8%
22	MW; at Quicksand Spring	s		none							
22	MW; Quicksand Spring	p		none							
22	MW; Quicksand Spring	p	QSS-X1	CASDT	0.17	2.85	0.06	5.83	21	13.4	-4.0%
22	MW; at Quicksand Spring	s		none							
23	MW; Shonto Well springs	p	SWS-X1	CASD	0.73	24.36	0.29	21.87	81	10.6	-0.7%

(all concentrations are in mg/l unless stated otherwise)

SAMPLE TYPES: s - surface water sample

p - spring water sample

d - drive point sample

C - cations

A - anions

S - sulfur isotopes

D - deuterium/oxygen isotopes

T - tritium

Table D-2. Chemical composition of water samples from streams, springs and drive points, Moenkopi and Dinnebito washes (continued)

LOC. ID	SITE DESCRIPTION	SAMPLE TYPE	SAMPLE ID.	SAMPLES COLLECTED	F <sup>-</sup>	Cl <sup>-</sup>	Br <sup>-</sup>	NO <sub>3</sub> <sup>-</sup>	SO <sub>4</sub> <sup>2-</sup>	SiO <sub>2</sub>	COMPUTED BALANCE
MOENKOPI WASH (continued)											
24	MW; at Shonto Well	s	MWSM-X1	CASD	0.70	10.57	0.07	0.03	245	6.3	0.3%
25	MW; at campfire	s	MWCF-X1	CASD	0.50	4.43	0.04	0.27	172	8.1	2.3%
26	MW; Horse Corral Trib.	s	HCT-X1	CASDT	0.65	16.00	0.06	0.68	977	9.7	-0.5%
26	MW; at Horse Corral Trib.	s	MWHCT-X1	CASDT	0.48	5.59	0.01	0.04	185	10.3	-0.4%
27	MW; Pasture Canyon Res.	s	PCR-X1	CASD	0.46	10.90	0.14	0.02	17	9.5	1.9%
28	MW; at I-89	s	MWI89-X1	CASD	0.84	45.42	0.12	3.14	270	6.9	-0.9%
DINNEBITO WASH											
29	DW; Sweetwater Well	p	SW-X1	CASD	0.46	7.65	0.03	0.11	199	15.7	-5.8%
29	DW; at Sweetwater Well	s	DWSM-X1	CASD	0.81	10.91	0.13	0.04	342	11.4	0.9%
30	DW; at Dinnebito Spring	s	DWDS-X1	CASD	0.82	17.27	0.14		825	16.5	-2.9%
31	DW; at Sand Valley	s	DWSV-X1	CASD	0.92	12.02	0.13	0.01	386	9.4	-0.3%
32	DW; spring at Sand Spring	p	SSS-X1	CASD	0.45	93.14	0.26	0.68	229	9.1	0.6%
33	DW; Whisky Spring (adjacent	p	WS-X1	CASD	0.50	15.14	0.08	0.20	243	11.5	6.5%
34	DW; at Sand Spring	d	DWSS-X2	CASD	0.86	17.62	0.15	0.05	1032	14.7	-5.7%
34	DW; at Sand Spring	s	DWSS-X1	CASD	1.08	17.27	0.03	0.004	366	10.1	-1.6%

(all concentrations are in mg/l unless stated otherwise)

SAMPLE TYPES: s - surface water sample

p - spring water sample

d - drive point sample

C - cations

A - anions

S - sulfur isotopes

D - deuterium/oxygen isotopes

T - tritium

Table D-3. Isotopic composition of groundwater samples from the N-aquifer

SAMPLE NAME	SAMPLE		UTM COORDINATES		$\delta^{18}\text{O}$	$\delta\text{D}$	$\delta^{34}\text{S}$
	NO.	AQ.	EAST	NORTH			
ROCKY PM2	1	N	536845	3991774	-13.90	-108.0	
HOTEVILLA SCH 2	2	N	530200	3975600	-13.70	-107.0	
HOPI CULT. CTR.	3	N	542720	3966629	-12.50	-99.0	
2ND MESA SCH 2	4	N	545000	3961300	-13.10	-100.0	10.8
POLACCA 6	5	N	553300	3963500	-13.20	-94.0	2.7
POLACCA SCH 2	6	N	555350	3965100	-13.00	-100.0	
KEAMS CYN #2	7	N	562541	3966193	-13.25	-99.0	9.2
HOPI HIGH SCH #3	8	N	562900	3963600	-13.81	-99.5	7.8
9Y-92	9	N	609004	4044579	-8.25	-63.0	-12.1
8T-518	10	N	598191	4041984	-13.40	-101.0	8.2
CHLCHN PM3	11	N	582230	4042750	-13.00	-96.0	13.2
8T-522	12	N	553613	4058909	-9.80	-80.0	-13.5
KAYENTA SCH 2	13	N	566600	4065000	-10.50	-80.0	
SHOWTO SCH #2	14	N	530684	4050292	-10.90	-80.0	
2K-319	15	N	505401	4035603	-10.00	-77.0	
RED LAKE SCH PM1	17	N	504800	4019450	-13.40	-104.0	
TUBA CITY SCH PM5	18	N	477706	3998935	-9.70	-68.0	
10R-111	19	N	608928	4024774	-13.35	-98.0	
9K-215	20	N	616665	4048193	-9.40	-77.0	
PINON PM6	21	N	570310	3995553	-12.90	-94.0	11.4
LOW MTN PM2	22	N	580173	3977890	-13.50	-99.0	8.4
KITSILLIE	23	N	583990	4022290	-13.10	-98.0	
3M-156	24	N	512004	3993800	-13.10	-98.0	
NTUA FOREST LAKE	25	N	562300	4016450	-14.10	-105.0	-9.6
NAVAJO NAT.M.(BET.)	26	N	540681	4058776	-12.60	-94.0	
DILKON BIA 2	27	N	562420	3912610	-10.31	-74.0	

(all concentrations are in per mil)

Table D-4. Isotopic Composition of samples from streams, springs and drive points, Moenkopi and Dinnebito washes

SAMPLE ID	LOCAT. NO.	SITE DESCRIPTION	SAMPLES T COLLECT.	SAMPLE DATE (M/D/YR)	TEMP. (°C)	$\delta D$	$\delta^{18}O$	$\delta^{34}S$	
MOENKOPI WASH									
CMC-X1	2	MW at Coal Mine Canyon	s	CASD	02/16/90	2.3	-96	-11.3	-12.3
CMC-X2	2	MW at Coal Mine Canyon	s	CASD	02/17/90	1.3	-98	-11.2	-12.7
CMW-X1	4	Coal Mine Wash	s	CASD	02/17/90	7.4	-94	-10.0	8.6
WLDSK-X1	5	Springs at Lechee Da Si Kaid	p	CASD	02/17/90	14.4	-83	-8.9	-1.1
MWLDSK-X1	6	MW at Lechee Da Si Kaid	s	CASD	02/18/90	6.7			-9.3
BWC-X1	7	Begashibito Wash	s	CASD	02/21/90	1.2	-90	-10.5	-15.0
MBWC-X1	8	MW at Begashibito	s	CASD	02/21/90	6.4	-107	-12.5	-14.5
MWF-X1	9	MW at Falls	s	CASD	02/22/90	1.7	-97	-11.1	-10.2
PCS-X1	13	Pasture Canyon spring	p	CASD	02/25/90	15.5	-84	-9.1	-1.0
SKVS-X1	15	Springs, S. Kerley Valley	p	CASD	02/26/90	10.4	-95	-10.4	1.0
MWKV-X1	16	MW in Kerley Valley	s	CASD	02/26/90	10.4	-93	-10.2	-9.6
MWM-X1	17	MW at Moenkopi	s	CASD	02/27/90	8.5	-94	-10.4	-10.1
MWJSM-X1	18	MW upstream of Moenkopi	s	CASD	02/27/90	19.4	-91	-9.8	-8.6
MWMC-X1	20	MW at water caves	s	CASDT	03/08/90	11.1	-108	-13.6	-12.9
MWSS-X1	21	MW at Sand Springs	s	CASD	03/08/90	17.7	-110	-13.2	-13.7
QSS-X1	22	Quicksand Spring	p	CASDT	03/08/90	17.4	-108	-13.0	-7.9
SWS-X1	23	Shonto Well springs	p	CASD	03/09/90	15.3	-84	-8.7	-5.6
MWSW-X1	24	MW at Shonto Well	s	CASD	03/09/90	13.5	-94	-10.0	-10.4
MWCF-X1	25	MW at campfire	s	CASD	03/10/90	10.9	-106	-12.5	-15.1
MWHCT-X1	26	MW at Horse Corral Trib.	s	CASDT	03/10/90	11.6	-109	-13.1	-12.8
HCT-X1	26	Horse Corral Trib.	s	CASDT	03/10/90	10.6	-108	-12.9	-20.8
PCR-X1	27	Pasture Canyon Res.	s	CASD	03/13/90	6.4	-78	-7.7	-2.5
MW189-X1	28	MW at I-89	s	CASD	03/13/90	6.7	-81	-7.9	-9.0
DINNEBITO WASH									
SW-X1	29	Sweetwater Well	p	CASD	03/14/90	8.6	-97	-11.3	8.4
DWSW-X1	29	DW at Sweetwater Well	s	CASD	03/14/90	3.1	-95	-11.1	-9.0
DWDS-X1	30	DW at Dinnebito Spring	s	CASD	03/14/90	12.8	-89	-10.8	-9.7
DWSV-X1	31	DW at Sand Valley	s	CASD	03/15/90	1.2	-90	-9.2	-8.9
SSS-X1	32	Spring at Sand Spring	p	CASD	03/15/90	9.5	-82	-8.4	-9.4
WS-X1	33	near Whisky Spring	p	CASD	03/15/90	3.6	-93	-10.5	4.4
DWSS-X2	34	DW at Sand Spring	d	CASD	03/15/90	7.8	-86	-9.7	-7.8
DWSS-X1	34	DW at Sand Spring	s	CASD	03/15/90	9.1	-92	-10.2	-9.0

(all concentrations are in per mil)

SAMPLE TYPES: s - surface water sample  
p - spring water sample  
d - drive point sample

C - cations      D - deuterium/oxygen isotopes  
A - anions      T - tritium  
S - sulfur isotopes

Table D-5. Computed activities and saturation indices for groundwater samples from the N-aquifer

SAMPLE NAME	SAMPLE NO.	AG.	UTM COORDINATES		NORTH	[Ca]	[LOG ACTIVITIES]		[Na]	CALCITE	GYPSUM	HALITE	QUARTZ	SiO <sub>2</sub> (A,C)	I N D I C E S	SiO <sub>2</sub> (A,P)	FLUORITE	pCO <sub>2</sub>
			EAST	WEST			[Mg]	[Mg]										
ROCKY PM2	1	N	536845	3991774	5.6133	-2.6579	-0.7212	-5.1556	-8.8059	0.2651	-1.0143	-1.0143	-1.0143	-6.0852	-4.5418			
HOTEVILLA SCH 2	2	N	530200	3975600	-5.1407	-2.5812	-0.0278	-4.7272	-8.7166	0.3330	-0.9555	-0.9555	-0.9555	-5.2502	4.8298			
HOPI CULT. CTR.	3	N	542720	3966629	-5.4399	-2.3332	-0.0634	-4.4442	-8.0860	0.3898	-0.9201	-0.9201	-0.9201	-6.4414	4.9221			
2ND MESA SCH 2	4	N	545000	3961300	-5.4301	-2.2588	-0.1092	-4.5738	-7.6444	0.3185	-1.0090	-1.0090	-1.0090	-5.8241	-4.4198			
POLACCA 6	5	N	553300	3963500	-4.1506	-1.6407	0.2181	-2.0732	-5.1829	0.2422	-1.0914	-1.0914	-1.0914	-1.1198	-3.0259			
POLACCA SCH 2	6	N	555350	3965100	-5.1672	-2.1589	0.1386	-4.0932	-6.8439	0.1976	-1.1190	-1.1190	-1.1190	-3.2289	-4.2056			
KEAMS CYN #2	7	N	562541	3966193	-5.0179	-5.7778	-2.0450	-3.8366	-6.1969	0.1245	-1.2057	-1.2057	-1.2057	-2.3208	-3.7513			
HOPI HIGH SCH #3	8	N	562900	3963600	-4.6994	-1.8781	-0.0805	-3.1714	-5.6490	-0.0044	-1.3315	-1.3315	-1.3315	-1.8039	-3.2820			
9Y-92	9	N	609004	4044579	-2.8204	-3.0318	-2.6435	-0.5912	-7.7480	0.4316	-0.9344	-0.9344	-0.9344	-0.3198	-3.1916			
8T-518	10	N	598191	4041984	-5.1382	-2.2355	-0.0560	-4.1125	-6.8988	-0.2139	-1.5676	-1.5676	-1.5676	-4.6452	-4.1151			
CHLCHN PM3	11	N	582230	4042750	-5.0868	-2.4684	0.0070	-4.8013	-8.3070	0.5157	-0.8118	-0.8118	-0.8118	-4.4625	-4.5069			
8T-522	12	N	553613	4058909	-2.8350	-3.2512	-2.7748	-1.1890	-7.8364	0.4933	-0.8829	-0.8829	-0.8829	-1.5230	-1.9137			
KAYENTA SCH 2	13	N	566600	4065000	-3.1048	-3.6688	-2.9856	-1.5593	-8.6131	0.6163	-0.7387	-0.7387	-0.7387	-2.9911	-3.1234			
SHONTO SCH #2	14	N	530684	4050292	-3.0359	-3.8407	-3.6426	-2.2841	-8.7952	0.7039	-0.6680	-0.6680	-0.6680	-2.9911	-2.7295			
2K-319	15	N	505401	4038603	-3.1221	-3.9663	0.1280	-2.6728	-9.1591	0.5843	-0.7763	-0.7763	-0.7763	-4.6699	-2.9417			
1K-214	16	N	505181	4028301	-3.1221	-3.9663	0.1280	-2.6728	-9.1591	0.5843	-0.7763	-0.7763	-0.7763	-4.6699	-2.9417			
RED LAKE SCH PM1	17	N	504800	4019450	-3.4425	-3.7666	-3.8901	-3.4652	-10.2045	0.0111	-1.3398	-1.3398	-1.3398	-4.4868	-3.4541			
TUBA CITY SCH PMS	18	N	477706	3998935	-3.3288	-3.9226	-3.4177	-2.5712	-8.9067	0.5463	-0.8059	-0.8059	-0.8059	-4.7259	-3.0675			
10R 111	19	N	608928	4024774	-3.3240	-3.9147	-1.4254	-0.1599	-5.6899	0.0927	-1.2617	-1.2617	-1.2617	-0.3144	-3.6923			
9K215	20	N	616665	4048193	-3.2492	-3.4101	-1.8545	-0.7679	-5.5389	0.1142	-1.2472	-1.2472	-1.2472	-1.5932	-3.2538			
PINON PM6	21	N	570310	3995553	-5.2816	-3.4101	-2.3917	-4.9562	-8.1005	-0.0181	-1.3001	-1.3001	-1.3001	-4.5110	-4.9494			
LOW Mtn PM2	22	N	580173	3977890	-4.7749	-5.3044	-1.9196	-3.3073	-5.7924	0.3086	-1.0181	-1.0181	-1.0181	-1.3641	-3.6558			
KITTSILLIE	23	N	583990	4022290	-4.9849	-5.6795	-2.4182	-4.6165	-7.9282	0.2629	-1.0080	-1.0080	-1.0080	-3.2109	-4.7018			
3M156	24	N	512004	3993800	-5.0919	-6.1927	-2.1855	-0.0392	-3.4570	-6.7181	-1.1126	-1.1126	-1.1126	-2.0702	-4.4252			
NTUA FOREST LAKE	25	N	562300	4016450	-4.9000	-5.9174	-2.4875	-3.5939	-7.6961	-0.0835	-1.3531	-1.3531	-1.3531	-3.5677	-4.6246			
NAVAJO NAT.M.(BET.)	26	N	540681	4058776	-3.1818	-4.0734	-3.8475	-0.1730	-3.0192	0.1703	-1.2045	-1.2045	-1.2045	-3.5677	-3.0865			
DILKON BIA 2	27	N	562420	3912610	-3.0345	-3.2689	-2.5578	-0.2047	-1.1329	0.2778	-1.0850	-1.0850	-1.0850	-3.5745	-3.0910			
IHS HARD ROCK-N	28	N	546000	3994500	-5.0026	-3.2689	-2.5795	-0.0806	-4.5424	0.0178	-1.2287	-1.2287	-1.2287	-6.7417	-4.5750			

Table D-5. Computed activities and saturation indices for groundwater samples from the H-aquifer

SAMPLE NAME	SAMPLE NO. Aq. EAST		UTM COORDINATES		[LOG ACTIVITY]	S A T U R A T I O N		I N D I C E S		pCO <sub>2</sub>					
	NO.	Aq.	EAST	NORTH		[Ca]	[Mg]	[Na]	QUARTZ		SiO <sub>2</sub> (A.C)	SiO <sub>2</sub> (A.P)	FLUORITE		
3T-333	111	n	477803	3997764	-3.4110	-3.9374	-3.1561	-0.0150	-2.6727	-8.3856	0.0000	0.0000	0.0000	-2.4055	-3.2833
3T-54	112	n	478416	4002815	-3.3262	-3.8767	-3.5348	-0.3629	-2.6842	-8.9857	0.4660	-0.8940	-0.8940	-2.2653	-2.8890
3T-508	113	n	478960	4000534	-3.2729	-3.8116	-3.4154	-0.0313	-2.4062	-8.5651	0.4660	-0.8940	-0.8940	-2.8762	-3.0377
3T-528	114	n	482846	4007088	-3.1203	-3.7388	-3.1894	0.3787	-2.0703	-8.1093	0.4660	-0.8940	-0.8940	-2.1341	-3.1803
KAI SCH 4	115	n	491451	4048115	-3.4532	-3.7050	-3.4828	-0.1729	-2.7142	-9.3701	0.4660	-0.8940	-0.8940	-3.0522	-3.1990
KALBIT PM3	116	n	493838	4050023	-3.2669	-3.4452	-3.4060	-0.1347	-1.9803	-8.4093	0.4660	-0.8940	-0.8940	-2.2861	-2.9471
3K-323	117	n	497652	4005284	-3.3045	-3.8107	-3.3882	0.0414	-2.4340	-8.6638	0.4660	-0.8940	-0.8940	-2.2861	-3.1335
3K-330	118	n	503802	3992406	-4.4211	-3.8107	-2.0754	0.3612	-2.3165	-7.0999	0.4660	-0.8940	-0.8940	-3.2972	-4.4320
1P-511	119	n	516163	4029454	-3.4263	-3.7967	-3.6607	-0.1837	-2.6413	-9.5470	0.4660	-0.8940	-0.8940	-2.4195	-3.2369
SHONTO PM2	120	n	530684	4050292	-3.1141	-3.8281	-3.6517	0.3368	-2.1177	-8.9492	0.1108	-1.2180	-1.2180	-2.4195	-3.0285
SHONTO PM2	120	n	530684	4050292	-3.1133	-3.7770	-3.6351	-0.7632	-2.2629	-8.7685	0.5594	-0.8112	-0.8112	-2.4195	-2.0942
ORAIPI PM4	121	n	534980	3970138	-4.5986	-3.7770	-2.4531	0.4982	-3.2758	-8.0483	0.5594	-0.8112	-0.8112	-4.2030	-4.7825
ORAIPI PM4	121	n	534980	3970138	-5.2042	-3.7770	-2.6684	-0.4499	-4.4584	-8.0603	0.6013	-0.7275	-0.7275	-4.2000	-4.1251
ORAIPI PM4	121	n	534980	3970138	-5.2127	-5.9948	-2.4647	-0.2707	-4.4711	-8.0162	0.5186	-0.7966	-0.7966	-4.2337	-4.3509
ORAIPI PM4	121	n	534980	3970138	-5.1747	-5.4142	-2.4561	-0.1331	-4.4459	-7.9978	0.4903	-0.8250	-0.8250	-4.1978	-4.4513
ORAIPI PM4	121	n	534980	3970138	-5.2837	-6.3512	-2.4622	-0.0961	-4.5567	-8.0126	0.3813	-0.9407	-0.9407	-4.2954	-4.8984
BM 4; 2T-514	122	n	536059	4042455	-3.1636	-3.9346	-3.8450	-0.0422	-2.3661	-9.0957	0.5573	-0.8132	-0.8132	-4.2954	-2.9229
BM 4; 2T-514	122	n	536059	4042455	-3.1400	-3.9461	-3.7662	-0.5533	-2.4360	-9.2497	0.4298	-0.8990	-0.8990	-2.7444	-2.2926
ROCKY PM2	125	n	536845	3991774	-4.7823	-3.9461	-2.6327	-0.1060	-3.8737	-8.3790	0.4298	-0.8990	-0.8990	-4.3725	-4.4031
BETKN N M	126	n	540681	4058776	-3.1743	-3.9328	-3.7454	0.0883	-2.8274	-9.4140	0.5175	-0.8113	-0.8113	-2.7773	-2.8167
4T-519	127	n	544055	3985553	-4.6539	-5.0616	-2.5045	-0.1653	-4.0851	-8.3962	0.6745	-0.6543	-0.6543	-3.6480	-3.7907
PEABODY 2	128	n	552017	4039517	-3.8474	-5.5010	-2.7839	0.0769	-2.8296	-8.4790	0.5972	-0.7316	-0.7316	-2.8327	-3.7551
PEABODY 2	128	n	552017	4039517	-3.8318	-5.2011	-2.7741	-0.2094	-2.7804	-8.2431	0.4386	-0.8175	-0.8175	-2.9464	-3.1422
PEABODY 2	128	n	552017	4039517	-4.0342	-5.2011	-2.7728	-0.0699	-3.0694	-8.3809	0.4793	-0.7832	-0.7832	-3.1341	-3.5916
PEABODY 2	128	n	552017	4039517	-3.8195	-5.2081	-2.7540	0.0783	-2.6910	-8.3909	0.4689	-0.7872	-0.7872	-3.5371	-3.4669
PEABODY 2	128	n	552017	4039517	-3.7866	-4.7972	-2.7953	-0.7609	-2.7349	-7.9204	0.4749	-0.7843	-0.7843	-2.8957	-2.7349
PEABODY 4	129	n	552900	4033422	-4.0318	-5.1971	-2.7729	-0.1707	-3.1608	-8.4146	0.4070	-0.8300	-0.8300	-3.1767	-3.3313
PEABODY 4	129	n	552900	4033422	-3.9092	-5.5211	-2.7848	0.4976	-2.8761	-8.4918	0.3695	-0.8802	-0.8802	-3.0332	-4.1669
PEABODY 4	129	n	552900	4033422	-4.0346	-5.5137	-2.7339	0.1704	-3.0016	-8.3128	0.4503	-0.7994	-0.7994	-3.1593	-3.7687
PEABODY 4	129	n	552900	4033422	-4.0933	-5.5215	-2.7433	0.3630	-3.2218	-8.2792	0.3695	-0.8802	-0.8802	-3.2167	-4.1175
PEABODY 4	129	n	552900	4033422	-4.0785	-5.9275	-2.7738	0.5078	-3.2399	-8.3195	0.3041	-0.9456	-0.9456	-3.2009	-4.3874

Table D-5. Computed activities and saturation indices for groundwater samples from the M-aquifer

SAMPLE NAME	SAMPLE UTM COORDINATES		[LOG ACTIVITIES]		S A T U R A T I O N		I N D I C E S		FLUORITE	pCO <sub>2</sub>						
	NO. Aq.	EAST NORTH	[Ca]	[Mg]	[Na]	QUARTZ	SiO <sub>2</sub> (A.C)	SiO <sub>2</sub> (A.P)								
PEABODY 7	130	n	553220	4030003	-4.1486	-5.0264	-2.7237	-0.1871	-3.2163	-8.4182	0.3962	-0.8471	-0.8471	-0.9192	-3.2826	-4.1321
PEABODY 7	130	n	553220	4030003	-4.1431	-5.5287	-2.7359	0.4024	-3.2715	-8.3982	0.3494	-0.9003	-0.9003	-0.9003	-3.2667	-4.2282
PEABODY 7	130	n	553220	4030003	-4.1099	-5.5155	-2.7045	0.0548	-3.0562	-8.3456	0.4400	-0.8097	-0.8097	-0.8097	-3.2357	-3.6090
PEABODY 7	130	n	553220	4030003	-4.1458	-5.5155	-2.8055	0.2815	-3.3409	-8.4084	0.3210	-0.9192	-0.9192	-0.9192	-3.2826	-4.1603
PEABODY 5	131	n	554219	4037559	-4.3389	-4.5445	-2.6816	0.2982	-3.3837	-8.3077	0.3210	-0.9192	-0.9192	-0.9192	-3.2826	-4.1321
PEABODY 5	131	n	554219	4037559	-4.1633	-4.5445	-2.7338	0.2627	-3.3269	-8.5812	0.3861	-0.8636	-0.8636	-0.8636	-3.2871	-3.9477
PEABODY 5	131	n	554219	4037559	-4.1943	-5.5120	-2.6719	-0.1677	-3.1882	-8.2450	0.3806	-0.8564	-0.8564	-0.8564	-3.3426	-3.3658
PEABODY 5	131	n	554219	4037559	-4.2300	-4.9323	-2.7345	0.3616	-3.3596	-8.4272	0.3493	-0.9004	-0.9004	-0.9004	-3.3549	-4.1821
PEABODY 5	131	n	554219	4037559	-4.2218	-4.9323	-2.7171	0.5230	-3.3901	-8.4130	0.3048	-0.9385	-0.9385	-0.9385	-3.3588	-4.2381
PEABODY 5	131	n	554219	4037559	-4.0979	-5.5053	-2.7526	0.0054	-3.1625	-8.4571	0.4361	-0.8199	-0.8199	-0.8199	-3.2097	-3.6613
PEABODY 5	131	n	554219	4037559	-4.0990	-5.5178	-2.7628	0.3584	-3.3610	-8.4691	0.3696	-0.8801	-0.8801	-0.8801	-3.2211	-4.1163
PEABODY 3	132	n	555842	4032762	-4.3498	-4.4292	-2.6479	-0.6353	-3.3697	-8.2151	0.6147	-0.6414	-0.6414	-0.6414	-2.4997	-3.0501
PEABODY 3	132	n	555842	4032762	-4.3031	-4.4292	-2.6646	0.2959	-3.3196	-8.2895	0.3247	-0.9314	-0.9314	-0.9314	-3.4185	-4.1657
PEABODY 3	132	n	555842	4032762	-4.2129	-5.2063	-2.6712	-0.2292	-3.3119	-8.3923	0.4053	-0.8508	-0.8508	-0.8508	-2.5314	-3.3810
PEABODY 3	132	n	555842	4032762	-4.2352	-5.2063	-2.6893	0.3875	-3.4390	-8.3826	0.2574	-0.9923	-0.9923	-0.9923	-2.7583	-4.1509
PEABODY 3	132	n	555842	4032762	-4.2082	-5.2063	-2.6991	0.5249	-3.3768	-8.3650	0.3036	-0.9461	-0.9461	-0.9461	-2.5387	-4.2406
PEABODY 3	132	n	555842	4032762	-4.2480	-5.5139	-2.6639	-0.2046	-3.2662	-8.3166	0.4330	-0.8167	-0.8167	-0.8167	-2.7729	-3.3303
PEABODY 3	132	n	555842	4032762	-4.2313	-5.5273	-2.6886	0.2577	-3.3294	-8.3146	0.3482	-0.9015	-0.9015	-0.9015	-2.7540	-4.0847
PEABODY 6	133	n	556420	4039606	-4.3230	-4.8337	-2.6728	0.1831	-3.4588	-8.3711	0.5598	-0.6772	-0.6772	-0.6772	-2.8705	-3.8862
PEABODY 6	133	n	556420	4039606	-4.1925	-5.5484	-2.6815	0.5081	-3.3274	-8.3514	0.3050	-0.9321	-0.9321	-0.9321	-3.3407	-4.2917
PEABODY 6	133	n	556420	4039606	-4.1523	-5.5484	-2.6890	0.2149	-3.2231	-8.3155	0.3784	-0.8713	-0.8713	-0.8713	-2.9258	-3.8065
PEABODY 6	133	n	556420	4039606	-4.0752	-5.9109	-2.8055	0.3551	-3.3304	-8.6148	0.3624	-0.8778	-0.8778	-0.8778	-3.2122	-4.1573
KEAMS CYN2	134	n	562541	3966193	-4.0838	-4.0635	-1.7611	0.2922	-1.8214	-6.0294	0.3624	-0.8778	-0.8778	-0.8778	-0.3978	-2.9031
KEAMS CYN2	134	n	562541	3966193	-4.9557	-5.6278	-2.0298	-0.3334	-3.6253	-6.2369	0.3702	-0.9586	-0.9586	-0.9586	-2.2961	-3.2569
KEAMS CYN2	134	n	562541	3966193	-4.9623	-5.2417	-2.0299	-0.1666	-3.7495	-6.2204	0.4079	-0.9278	-0.9278	-0.9278	-2.2906	-3.4771
KEAMS CYN2	134	n	562541	3966193	-4.8944	-5.5043	-2.0134	-0.0361	-3.6072	-6.0990	0.3633	-0.9724	-0.9724	-0.9724	-2.1648	-3.6145
KEAMS CYN2	134	n	562541	3966193	-4.9667	-5.3710	-2.0310	0.0667	-3.7426	-6.2127	0.3366	-0.9990	-0.9990	-0.9990	-2.3598	-3.8395
8K-416	135	n	566994	4064950	-3.1877	-3.7268	-2.9980	0.0473	-1.6491	-8.5938	0.4896	-0.8392	-0.8392	-0.8392	-2.2845	-2.8444
8K-416	135	n	566994	4064950	-3.2173	-3.6665	-2.9331	-0.0473	-1.7624	-8.4260	0.5849	-0.7611	-0.7611	-0.7611	-2.2036	-2.6938
8K-416	135	n	566994	4064950	-3.1685	-3.6370	-2.9485	0.1828	-1.7730	-8.4678	0.5818	-0.7747	-0.7747	-0.7747	-2.1374	-2.9038

Table D-5. Computed activities and saturation indices for groundwater samples from the H-aquifer

SAMPLE NAME	SAMPLE NO.	AC. EAST	UTM NORTH	[Ca]	[LOG ACTIVITYIES]	[Mg]	[Na]	CALCITE	GYPSUM	MALITE	QUARTZ	SiO <sub>2</sub> (A,C)	SiO <sub>2</sub> (A,P)	FLUORITE	PCO <sub>2</sub>
PINON PM 6	136	n	570310	3995553	-4.9434	-4.8916	-2.3595	0.2845	-3.8807	-8.2584	0.5818	-0.7747	-0.7747	-3.5993	-4.6514
PINON PM 6	136	n	570310	3995553	-5.1755	-4.8916	-2.3562	-0.1452	-4.7396	-8.0034	0.5971	-0.7318	-0.7318	-4.1793	-4.2490
PINON PM 6	136	n	570310	3995553	-5.1636	-4.8916	-2.3589	0.0135	-4.7436	-7.9565	0.4792	-0.8127	-0.8127	-4.2338	-4.3417
PINON PM 6	136	n	570310	3995553	-5.1799	-5.8150	-2.3583	-0.0098	-4.7322	-7.9651	0.4659	-0.8326	-0.8326	-4.2378	-4.5213
PINON PM 6	136	n	570310	3995553	-5.3080	-6.7205	-2.3622	0.0657	-4.8589	-7.9641	0.2328	-1.0492	-1.0492	-4.3972	-4.9570
L MTN PM2	137	n	580173	3977890	-4.6048	-4.5893	-1.9119	0.2174	-3.1985	-5.7840	0.2328	-1.0492	-1.0492	-1.2417	-3.4570
CHLCHN PM3	138	n	582390	4042589	-3.5559	-4.1553	-2.6680	0.6137	-2.3111	-7.9713	0.2328	-1.0492	-1.0492	-2.8073	-3.7098
8T-540	139	n	582892	4042131	-3.6370	-4.7439	-1.8664	1.5313	-1.2795	-6.5333	0.2328	-1.0492	-1.0492	-2.0204	-5.1109
8T-537	140	n	594518	4038984	-4.2803	-5.1287	-2.3202	0.5805	-3.3890	-7.4356	0.3141	-1.0079	-1.0079	-2.6990	-3.8251
8T-511	141	n	600998	4035976											
10T-251	142	n	601369	4029817	-4.3744	-5.1287	-2.0661	0.2437	-3.0486	-6.1894	0.3141	-1.0079	-1.0079	-0.9941	-3.4612
8K-403	143	n	602906	4078035	-3.7673	-4.0651	-2.5364	0.4685	-2.5798	-7.6449	0.3141	-1.0079	-1.0079	-2.7718	-3.6436
8K-521	144	n	603028	4078191	-3.8541	-3.9657	-2.5664	0.2358	-2.6323	-7.6360	0.3141	-1.0079	-1.0079	-2.8574	-3.5894
9Y-92	145	n	609004	4044579	-2.8402	-2.9512	-2.6328	0.3397	-0.6014	-7.6986	0.3141	-1.0079	-1.0079	-0.4214	-3.0793
9Y-12	146	n	631046	4094296	-4.9441	-4.6568	-2.2557	-0.2025	-3.4280	-7.1958	0.3996	-0.9674	-0.9674	-3.5392	-3.9053
RD MES SCH	147	n	644121	4091765	-4.6056	-4.6568	-2.2279	0.4512	-3.3851	-7.2722	0.3996	-0.9674	-0.9674	-2.6669	-4.0225
ROCKY	148	n	536644	3991897	-4.2024	-4.6568	-2.6331	0.6316	-3.8638	-8.0532	0.3996	-0.9674	-0.9674	-2.8390	-4.6453
ROCKY	148	n	536644	3991897	-5.0540	-4.6568	-2.6395	-0.4510	-4.5134	-8.6504	0.4423	-0.8463	-0.8463	-4.7128	-4.1196
ROCKY PM1	149	n	536569	3991865	-4.4883	-4.6568	-2.6188	0.1889	-3.3691	-8.7226	0.4423	-0.8463	-0.8463	-4.7128	-4.4022
ROCKY PM1	149	n	536569	3991865	-4.5065	-4.6568	-2.6333	0.3234	-3.6668	-8.7364	0.4423	-0.8463	-0.8463	-4.0973	-4.6495
ROCKY PM1	149	n	536569	3991865	-4.4873	-4.6568	-2.6477	0.2646	-3.9599	-8.3441	0.4423	-0.8463	-0.8463	-3.4743	-4.5274
SHIT PM3	150	n	531008	4050015	-3.0995	-3.8328	-3.6936	0.5526	-2.0270	-8.9916	0.1409	-1.1879	-1.1879	-3.4743	-3.2273
SHONTO PM4	151	n	531106	4050478	-3.1169	-3.8301	-3.6930	0.5239	-2.0590	-9.2853	0.1146	-1.2142	-1.2142	-3.4743	-3.2385
NTUA 3	152	n	478462	4001151	-3.3453	-3.8649	-3.4941	-0.5620	-2.6423	-8.9647	0.4208	-0.9357	-0.9357	-2.2908	-2.6718
KEAMS CYN3	153	n	562464	3966531	-4.1487	-3.8122	-2.1097	0.9122	-2.9300	-6.4239	0.4208	-0.9357	-0.9357	-1.7051	-3.8184
HOP1 A & C	154	n	542720	3966629	-5.2852	-3.8122	-2.3204	-0.2417	-4.2630	-7.8409	0.5790	-0.7498	-0.7498	-4.2924	-4.2358
BM 6	155	n	553762	4006867	-3.6630	-5.5611	-2.7370	1.1375	-3.1833	-8.8254	0.2942	-0.9683	-0.9683	-3.3724	-4.3553
3T-546	156	n	478414	4002045	-3.3064	-3.8442	-3.4618	-0.3046	-3.3161	-8.9542	0.4415	-0.9080	-0.9080	-2.2651	-2.8590
3T-511	157	n	477410	4000168	-3.3670	-3.8013	-3.4227	-0.1798	-2.7193	-8.5704	0.4415	-0.9080	-0.9080	-2.9659	-3.0922
3GS-77-2	158	n	477983	3999488	-3.3004	-3.8070	-3.4845	-0.0909	-2.4951	-8.7257	0.4415	-0.9080	-0.9080	-2.2995	-3.0699
3GS-77-3	159	n	477983	3999427	-3.2998	-3.8065	-3.4686	-0.0848	-2.5742	-8.5339	0.4415	-0.9080	-0.9080	-2.9013	-3.0643

Table D-5. Computed activities and saturation indices for groundwater samples from the N-aquifer

SAMPLE NAME	SAMPLE NO. Aq.		UTM COORDINATES		[LOG ACTIVITIES]	S A T U R A T I O N		I N D I C E S	pCO <sub>2</sub>						
	EAST	NORTH	[Ca]	[Mg]		[Na]	QUARTZ			SiO <sub>2</sub> (A.C)	SiO <sub>2</sub> (A.P)	FLUORITE			
3K-318-1	160	n	478281	3998779	-3.3293	-3.9350	-3.4672	0.0780	-2.8022	-8.6965	0.4415	-0.9080	-0.9080	-2.9259	-3.2721
3K-318-2	161	n	477706	3998935	-3.3323	-3.8041	-3.3871	-0.0298	-2.6889	-8.5354	0.4415	-0.9080	-0.9080	-2.9325	-3.1769
3T-222	162	n	477079	3997765	-3.3664	-3.8476	-3.4367	-0.0246	-2.6672	-8.9169	0.4894	-0.8671	-0.8671	-2.9141	-3.3132
3T-222	163	n	477079	3997765	-3.3366	-3.9417	-3.3081	0.0336	-2.4007	-8.5027	0.4894	-0.8671	-0.8671	-2.9348	-3.3092

Table D-6. Computed activities and saturation indices for water samples from streams, springs and drive points, Moenkopi Wash and Dinnebito Wash

LOC. ID	SITE DESCRIPTION	T	SAMPLE ID	[LOG ACTIVITIES]	[Ca]	[Mg]	[Na]	CALCITE	GYPSUM	HALITE	QUARTZ	SiO <sub>2</sub> (A,C)	SiO <sub>2</sub> (A,P)	FLUORITE	PCO <sub>2</sub>
<b>MOENKOPI WASH</b>															
2	MW; at Coal Mine Canyon	s	CMC-X1	-3.0110	-3.3968	-2.4114	0.7382	-1.0408	-7.6299	0.4510	-1.0056	-1.0916	-1.0056	-1.0916	-3.2325
2	MW; at Coal Mine Canyon	s	CMC-X2	-3.0063	-3.4042	-2.3674	0.7369	-0.9940	-7.5022	0.4365	-1.0277	-0.8206	-1.0277	-0.8206	-3.2565
4	MW; Coal Mine Wash	s	CMW-X1	-3.1371	-3.4307	-1.8928	0.6135	-0.7151	-6.8388	0.3093	-1.1090	-0.6684	-1.1090	-0.6684	-3.0452
5	MW; Springs W. of LDSK	p	WLDSK-X1	-3.2455	-3.5222	-2.4683	-0.2208	-1.5786	-6.9761	0.6103	-0.7574	-0.9135	-0.7574	-0.9135	-2.5816
6	MW; at Lechee Da Si Kaid	s	MWLDK-X1	-3.0977	-3.4798	-2.4406	1.1333	-1.1506	-7.6588	0.3407	-1.0828	-1.1268	-1.0828	-1.1268	-3.8426
7	MW; Begashibito Wash	s	BWC-X1	-2.8719	-3.3000	-2.6462	1.0145	-1.0861	-7.7554	0.6003	-0.8647	-0.7883	-0.8647	-0.7883	-3.1731
8	MW; MW at Begashibito	s	MBWC-X1	-2.9819	-3.5832	-2.4728	1.1323	-1.0246	-7.8721	0.3581	-1.0676	-0.9919	-1.0676	-0.9919	-3.6184
9	MW; at Falls	s	MWF-X1	-2.9392	-3.3850	-2.3971	0.8941	-0.8842	-7.5118	0.4477	-1.0135	-0.7353	-1.0135	-0.7353	-3.4673
13	MW; springs, Pasture Canyon	p	PCS-X1	-3.2185	-3.8159	-3.2964	-0.1481	-2.3270	-8.6678	0.3004	-1.0596	-2.2582	-1.0596	-2.2582	-2.9219
15	MW; springs S. Kerley Valle	p	SKVS-X1	-3.9322	-4.5179	-2.3711	0.0498	-2.7666	-6.6416	0.4531	-0.9433	-1.6386	-0.9433	-1.6386	-3.6454
16	MW; in Kerley Valley	s	MWKV-X1	-3.0260	-3.4056	-2.4193	1.1913	-0.9800	-7.4062	0.0557	-1.3407	-1.0364	-1.3407	-1.0364	-3.8701
17	MW; at Moenkopi	s	MWV-X1	-3.0360	-3.4233	-2.4655	0.8828	-0.9947	-7.4618	0.1709	-1.2393	-0.9336	-1.2393	-0.9336	-3.4411
18	MW; upstream of Moenkopi	s	MWU-X1	-3.0968	-3.4206	-2.3879	1.1192	-1.0804	-7.4547	0.0277	-1.3052	-1.0466	-1.3052	-1.0466	-3.5795
20	MW; at water caves	s	MWMC-X1	-3.2825	-3.7560	-2.2445	1.2683	-1.2421	-7.5038	0.3740	-1.0173	-1.3833	-1.0173	-1.3833	-4.2397
21	MW; at Sand Springs	s	MWSS-X1	-3.2261	-3.7683	-2.3982	1.0293	-1.3256	-7.8698	0.2648	-1.0799	-1.4194	-1.0799	-1.4194	-3.7895
22	MW; Quicksand Spring	p	QSS-X1	-3.5458	-4.0240	-2.8476	0.1592	-2.4914	-8.5330	0.4766	-0.8701	-2.6525	-0.8701	-2.6525	-3.3182
23	MW; Shonto Well springs	p	SWS-X1	-3.3524	-3.6486	-2.5118	0.2728	-1.7644	-7.2710	0.4125	-0.9489	-1.1956	-0.9489	-1.1956	-3.0859
24	MW; at Shonto Well	s	MWSH-X1	-3.0039	-3.4518	-2.4251	1.2162	-1.0037	-7.5543	0.2051	-1.1691	-0.8908	-1.1691	-0.8908	-3.5417
25	MW; at campfire	s	MWCF-X1	-3.0745	-3.6222	-2.4921	0.8895	-1.1941	-7.9865	0.3641	-1.0287	-1.2033	-1.0287	-1.2033	-3.4856
26	MW; Horse Corral Trib.	s	HCT-X1	-2.6222	-3.3776	-2.1237	0.9691	-0.1519	-7.0903	0.4555	-0.9394	-0.3565	-0.9394	-0.3565	-3.2369
26	MW; at Horse Corral Trib.	s	MWHT-X1	-3.5416	-3.8929	-2.3179	1.3947	-1.5997	-7.7127	0.3222	-1.0655	-1.7069	-1.0655	-1.7069	-4.8965
27	MW; Pasture Canyon Res.	s	PCR-X1	-3.1061	-3.5245	-3.1163	0.7122	-2.1845	-8.1975	0.5140	-0.9117	-1.2286	-0.9117	-1.2286	-3.4144
28	MW; at I-89	s	MWI89-X1	-3.0269	-3.3698	-2.2986	1.0347	-0.9887	-6.7805	0.3684	-1.0551	-0.6726	-1.0551	-0.6726	-3.4519

SAMPLE TYPES: s - surface water sample  
 p - spring water sample  
 d - drive point sample

C - cations  
 A - anions  
 S - sulfur isotopes

D - deuterium/oxygen isotopes  
 T - tritium

Table D-6. Computed activities and saturation indices for water samples from streams, springs and drive points, Moerkopi Wash and Dinnebito Wash

LOC. ID	SITE DESCRIPTION	T	SAMPLE ID	[LOG ACTIVITIES]	[Ca]	[Mg]	[Na]	HALITE	GYPSUM	QUARTZ	SiO <sub>2</sub> (A,G)	SiO <sub>2</sub> (A,P)	FLUORITE	PCO <sub>2</sub>
DINNEBITO WASH														
29	DW; Sweetwater Well	p	SW-X1	-2.9516	-3.4747	-2.8665	1.0874	-1.0205	-8.1187	0.6891	-0.7204	-0.7204	-1.1290	-3.6412
29	DW; at Sweetwater Well	s	DWSW-X1	-3.2176	-3.2780	-2.2430	0.7341	-1.0619	-7.3349	0.6505	-0.8000	-0.8000	-0.8463	-3.6717
30	DW; at Dinnebito Spring	s	DWS-X1	-2.8752	-2.9824	-2.1028	1.3031	-0.4583	-7.0394	0.6408	-0.7383	-0.7383	-0.6849	-3.3599
31	DW; at Sand Valley	s	DWSV-X1	-3.0095	-3.3087	-2.2519	0.9302	-0.8222	-7.2994	0.6031	-0.8619	-0.8619	-0.5069	-3.5398
32	DW; spring at Sand Spring	p	SSS-X1	-2.8604	-3.4327	-2.4987	0.1144	-0.9045	-6.6741	0.4480	-0.9549	-0.9549	-1.0831	-2.7689
33	DW; near Whisky Spring	p	WS-X1	-2.7886	-3.3570	-2.7033	-0.0522	-0.8058	-7.6516	0.6529	-0.7938	-0.7938	-0.8401	-2.4883
34	DW; at Sand Spring	d	DWSS-X2	-2.7622	-3.0361	-2.1226	0.1739	-0.2593	-7.0410	0.6885	-0.7269	-0.7269	-0.4631	-2.4610
34	DW; at Sand Spring	s	DWSS-X1	-3.0736	-3.3533	-2.2662	0.9759	-0.9093	-7.1760	0.4904	-0.9154	-0.9154	-0.5370	-3.5326

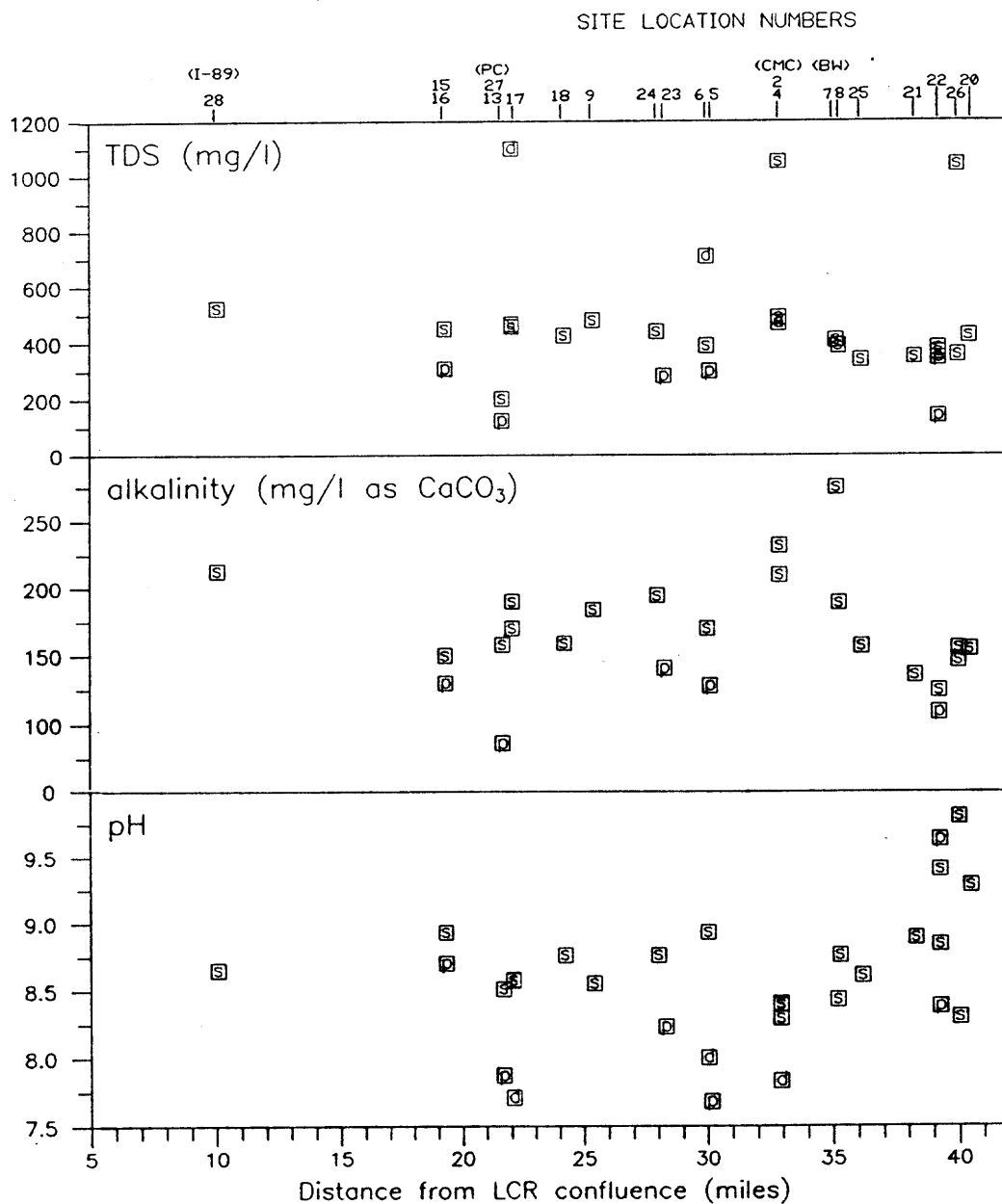
SAMPLE TYPES: s - surface water sample  
p - spring water sample  
d - drive point sample

C - cations  
A - anions  
S - sulfur isotopes

D - deuterium/oxygen isotopes  
T - tritium

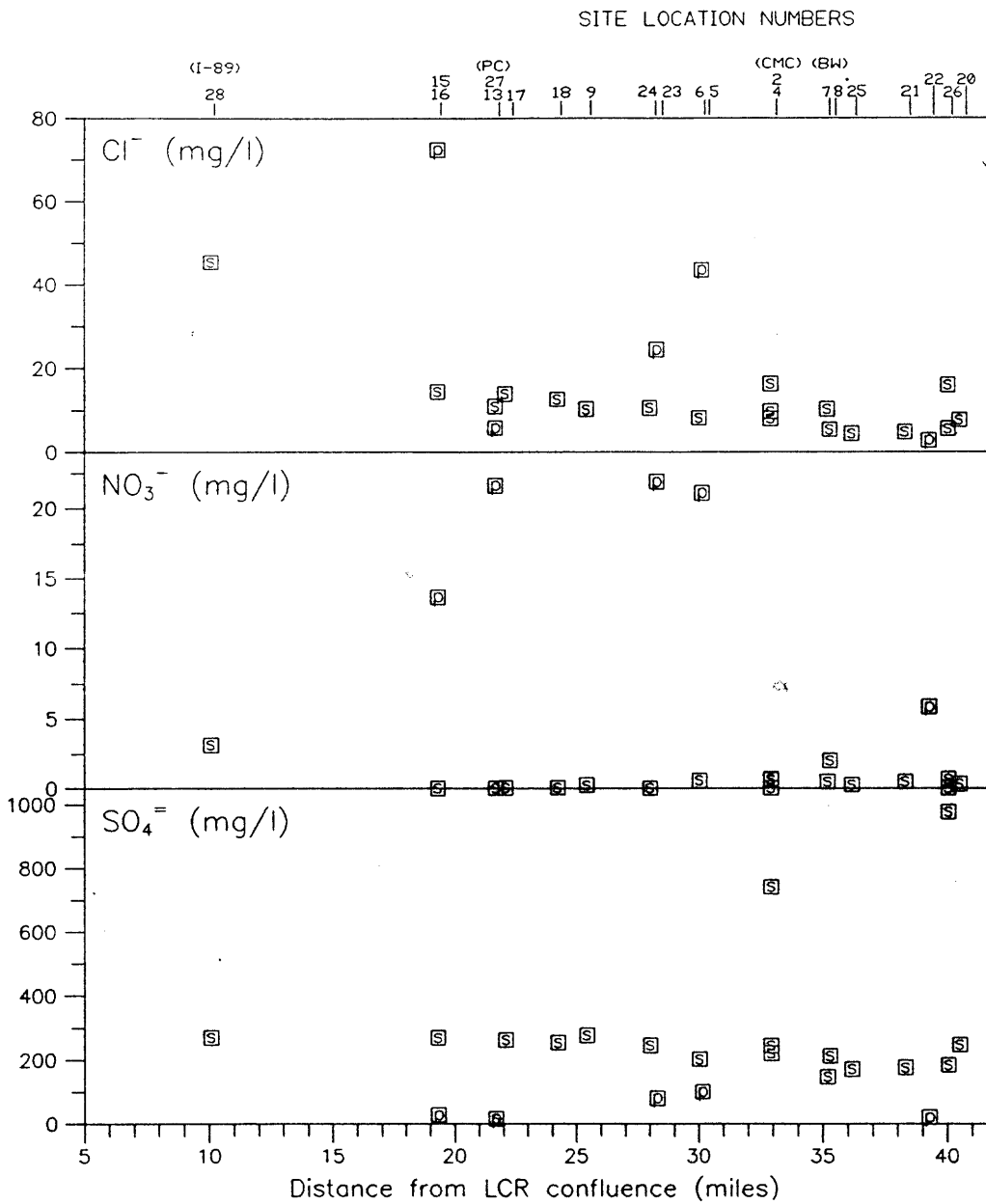
APPENDIX E

Profiles for selected chemical constituents and isotopes,  
Moenkopi Wash



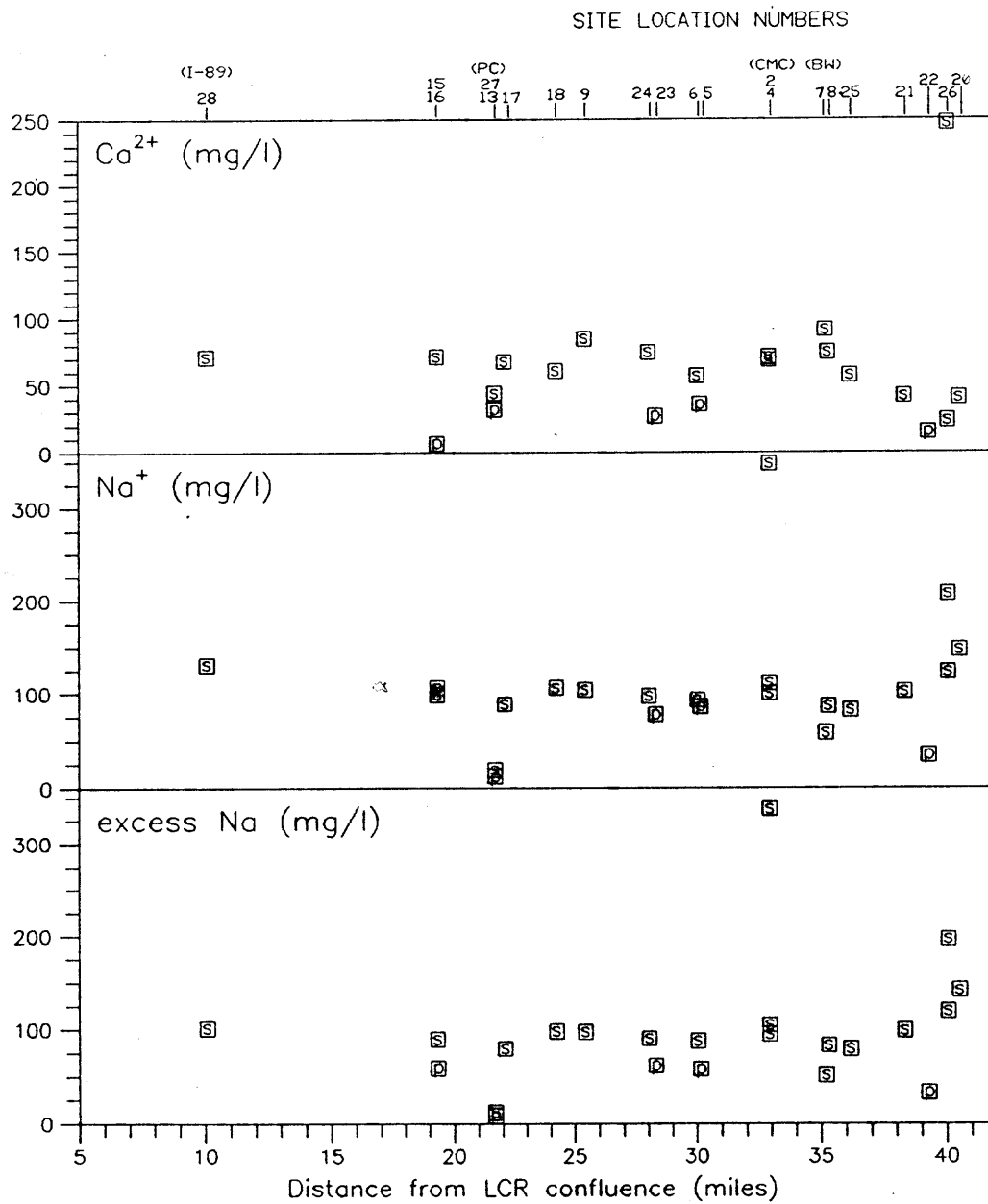
MOENKOPI WASH

- ☐ - surface water
- ☐ - spring water
- ☐ - alluvial drive point
- I-89 - Highway I-89
- PC - Pasture Canyon
- CMC - Coal Mine Canyon
- BW - Begashibito Wash



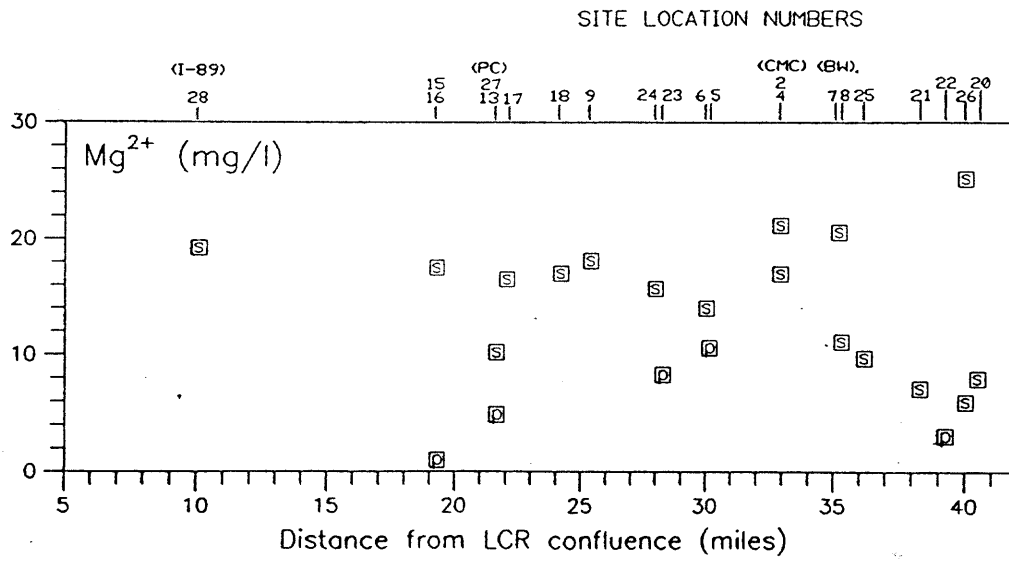
MOENKOPI WASH

- ☐ - surface water
- ☐ - spring water
- ☐ - alluvial drive point
- I-89 - Highway I-89
- PC - Pasture Canyon
- CMC - Coal Mine Canyon
- BW - Begashibito Wash

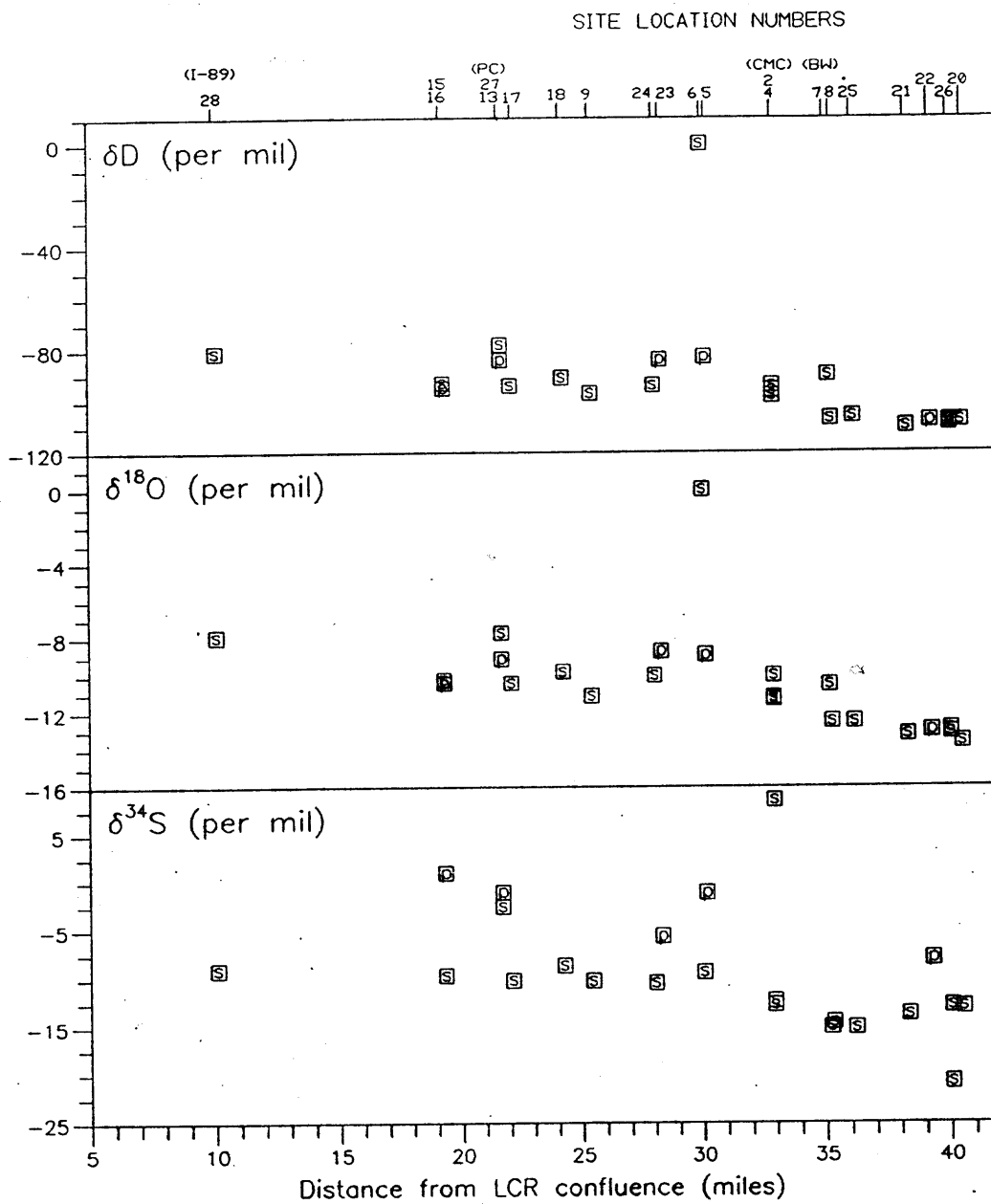


MOENKOPI WASH

- |   |                        |      |                    |
|---|------------------------|------|--------------------|
| □ | - surface water        | I-89 | - Highway I-89     |
| ◻ | - spring water         | PC   | - Pasture Canyon   |
| ◻ | - alluvial drive point | CMC  | - Coal Mine Canyon |
|   |                        | BW   | - Begashibito Wash |

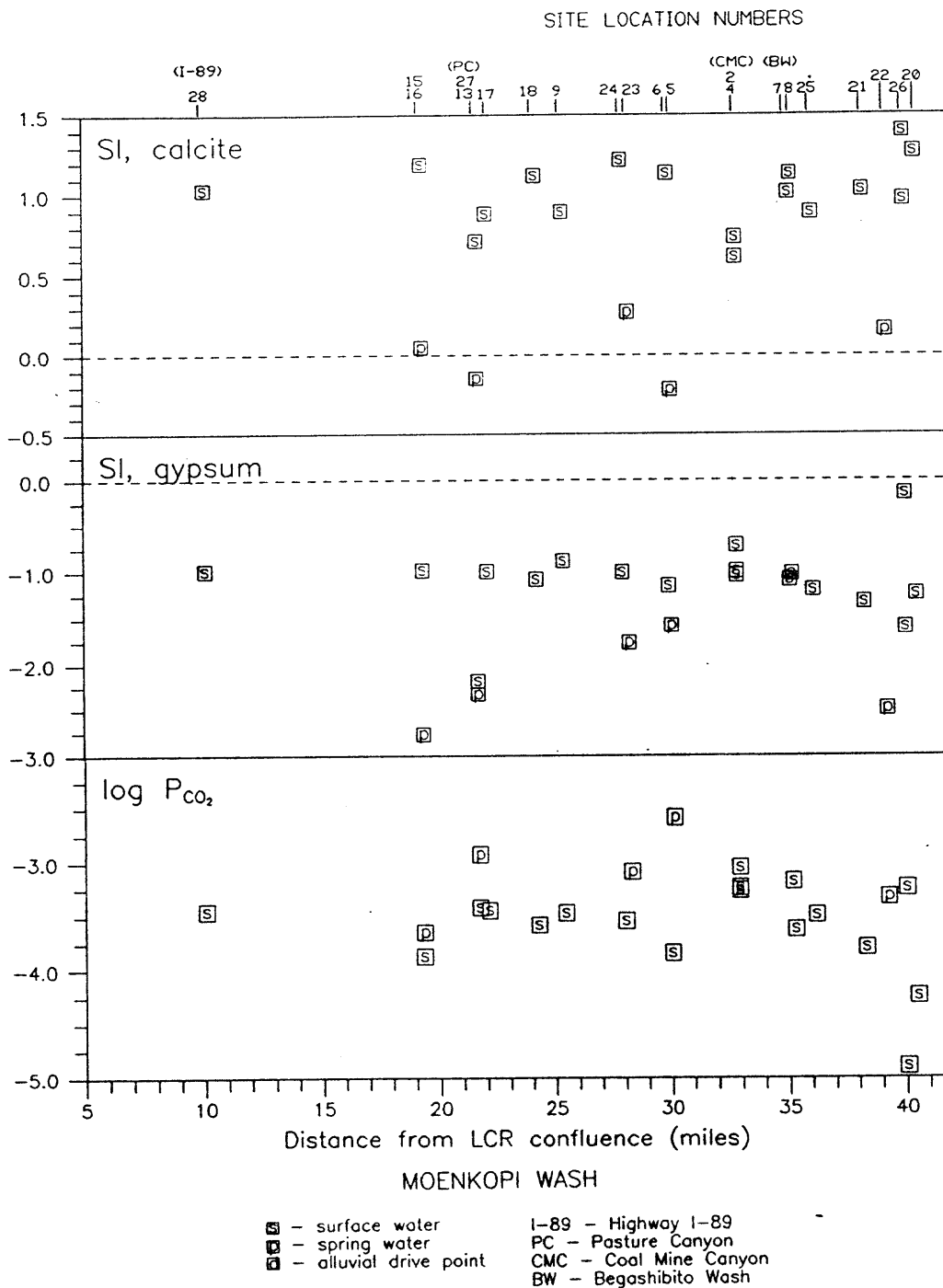


- ☐ - surface water
- ◻ - spring water
- ◻ - alluvial drive point
- I-89 - Highway I-89
- PC - Pasture Canyon
- CMC - Coal Mine Canyon
- BW - Begashibito Wash



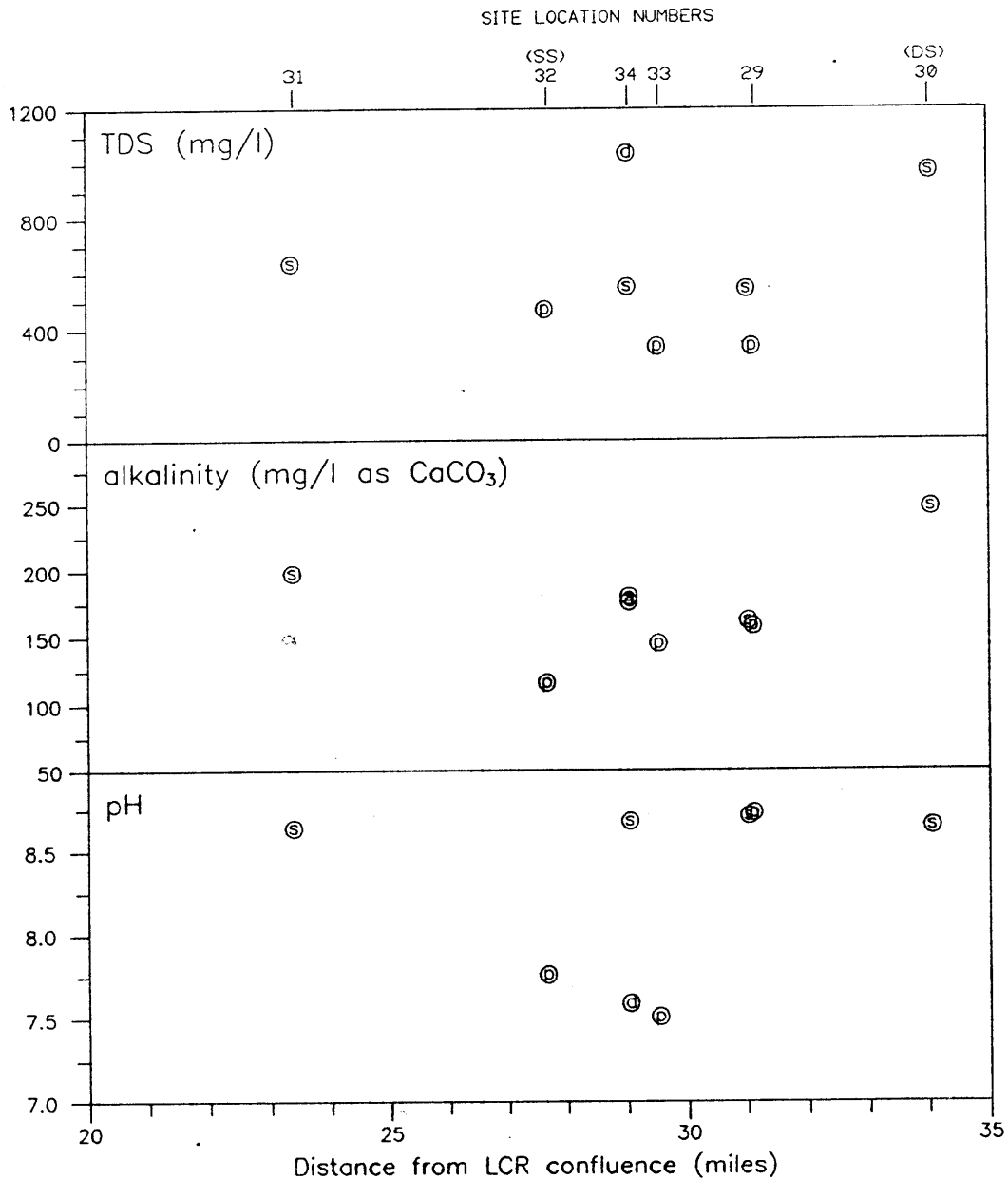
MOENKOPI WASH

- |   |   |
|---|---|
| <ul style="list-style-type: none"> <li>□ - surface water</li> <li>○ - spring water</li> <li>◇ - alluvial drive point</li> </ul> | <ul style="list-style-type: none"> <li>I-89 - Highway I-89</li> <li>PC - Pasture Canyon</li> <li>CMC - Coal Mine Canyon</li> <li>BW - Begashibito Wash</li> </ul> |
|---|---|



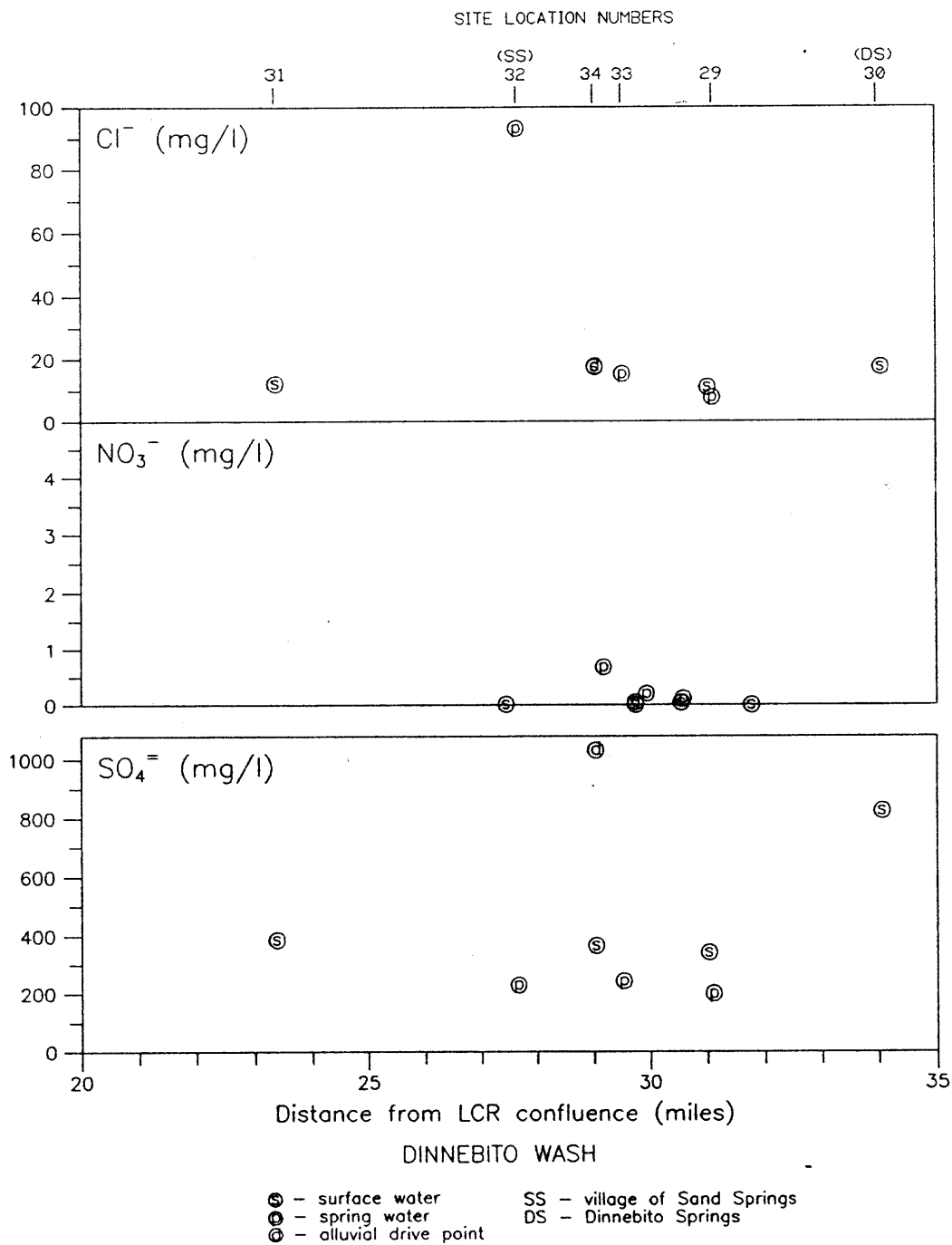
APPENDIX F

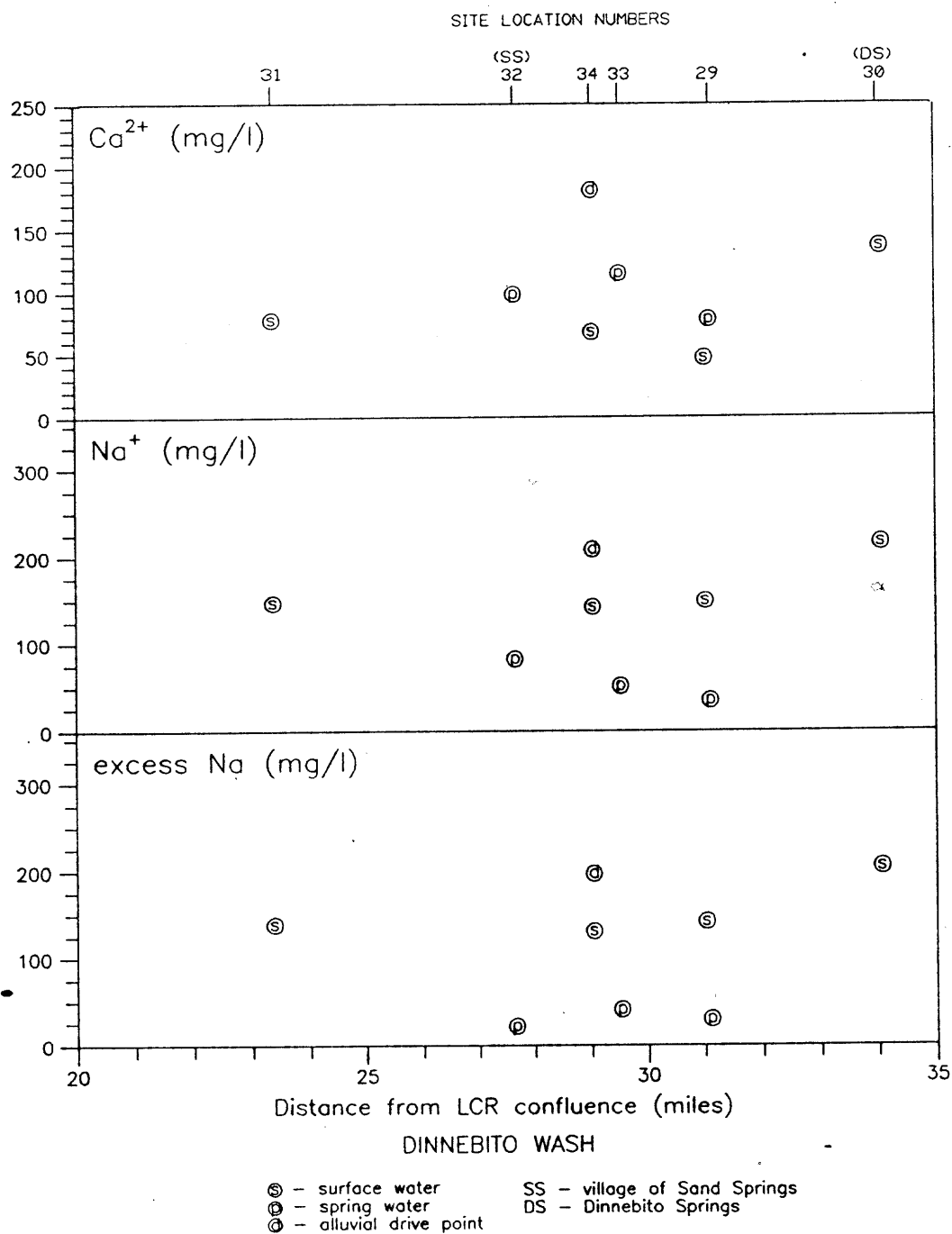
Profiles for selected chemical constituents and isotopes,  
Dinnebito Wash

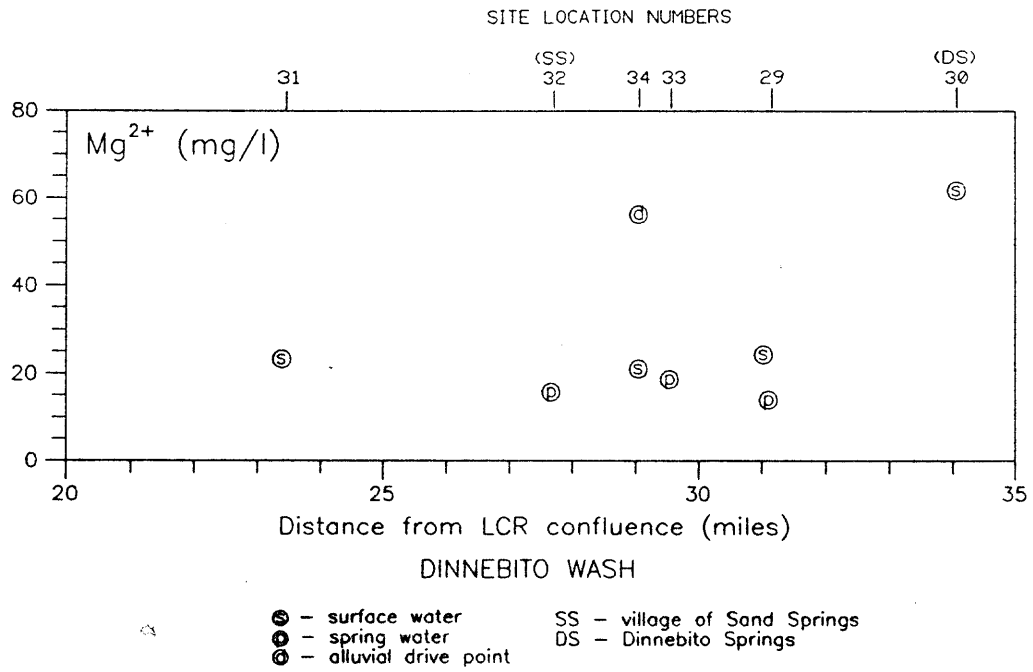


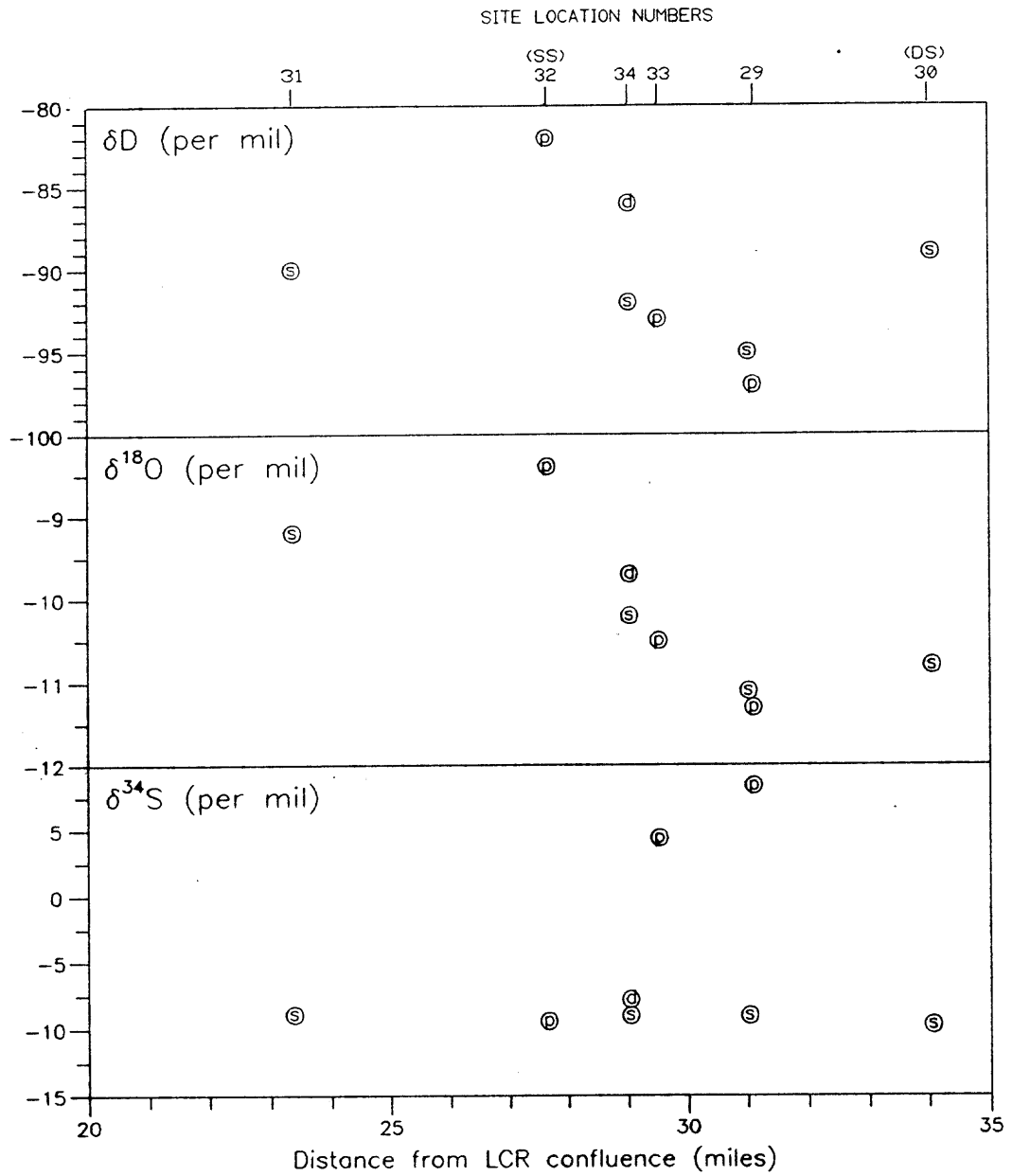
DINNEBITO WASH

- ⊙ - surface water
- ⊖ - spring water
- ⊕ - alluvial drive point
- SS - village of Sand Springs
- DS - Dinnebito Springs



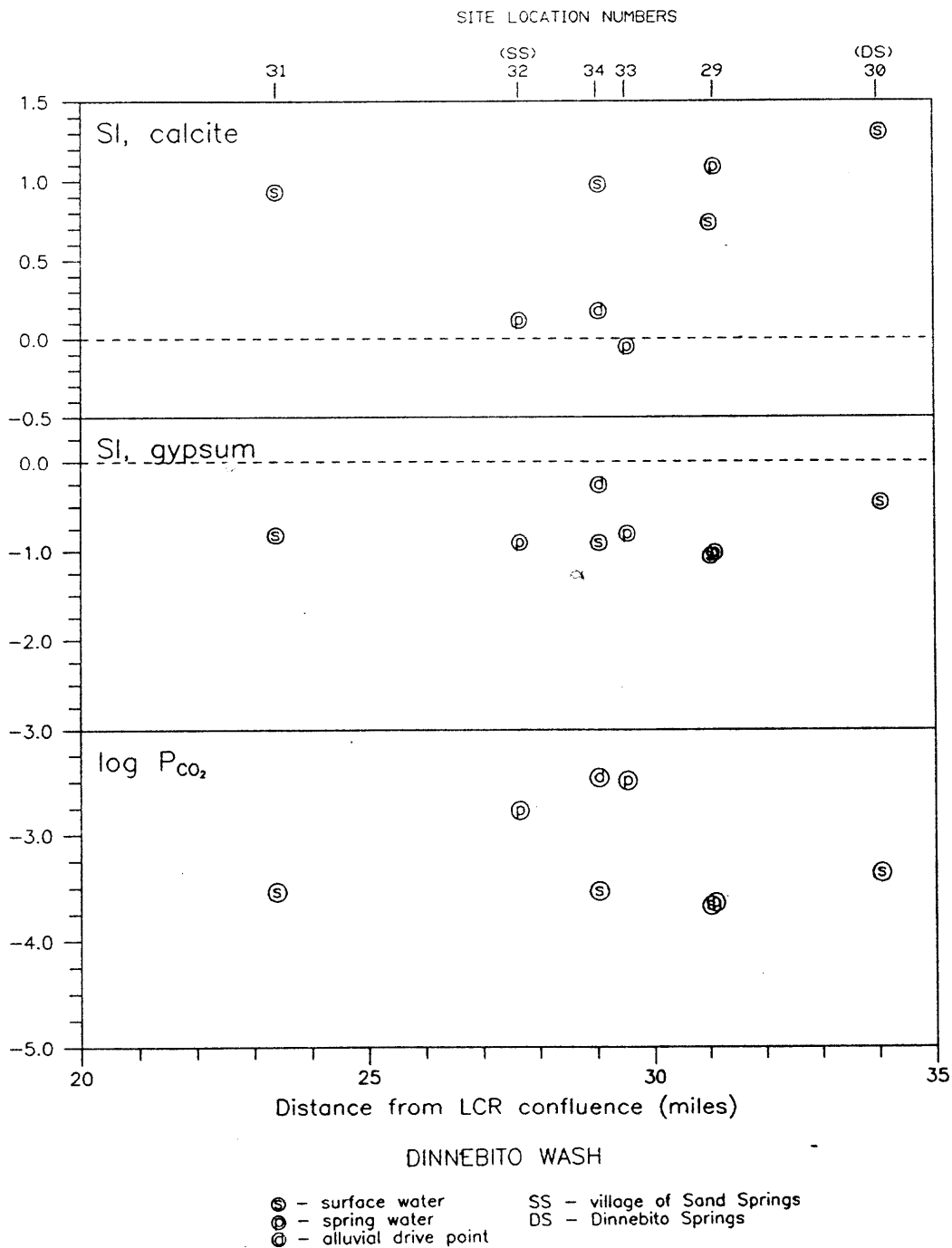






DINNEBITO WASH

- Ⓢ - surface water
- Ⓟ - spring water
- Ⓞ - alluvial drive point
- SS - village of Sand Springs
- DS - Dinnebito Springs



**APPENDIX G**

**Procedures for determining transpiration from phreatophytes  
and evaporation from bare alluvial soils (from APPENDIX F, ADWR, 1989)**

PROCEDURES FOR DETERMINING TRANSPIRATION FROM PHREATOPHYTES AND  
EVAPORATION FROM BARE ALLUVIAL SOILS

In order to assess the transpiration and evaporation losses from alluvial soils, the following information is necessary: (1) the areal extent of the floodplain, (2) the availability of groundwater, (3) the climate, and (4) the extent, density, species composition, and potential water use of the phreatophyte community.

The procedure utilized to evaluate evapotranspiration (ET) was modified from Rantz (1968). The technique is based on the Blaney-Criddle method for determining consumptive use of crops. The equation is  $U = KF$ , where  $U$  is the annual ET,  $F$  is the annual consumptive use factor, and  $K$  is the consumptive use coefficient for each species. The  $K$  for dense vegetation relates primarily to the individual species and the depth to water. The  $F$  is the sum of the products of mean monthly temperature and percent of daytime hours of the year for the growing season at a given location.

1. The extent of floodplain for each major tributary of the Little Colorado River system was ascertained using aerial photography. Polygons were sketched on maps which correspond to the USGS quads produced by the Department outlining the alluvium. For areas where the alluvium is not as extensive, the extent of alluvium was estimated by assuming an average width and multiplying by the channel length measured from USGS quads.
2. The depth to groundwater within the alluvium was assumed to be three feet for most of the Little Colorado River System. The only exceptions were the reach of the Little Colorado from Zion Reservoir to the confluence with Silver Creek where the depth was assumed to be five feet, and the Little Colorado River from the headwaters to

Springerville which was estimated to have groundwater depths of only two feet below the surface of the alluvium.

3. For each riparian reach, the climate of a nearby community was assumed to be representative of the climate along the river. For each zone, the F values were based on Blaney and Harris (1951) published monthly consumptive use factors for the community within the zone or calculated from the raw climatic data (US West Optical Publishing, 1988) for communities not included in Blaney and Harris' report. Table F.1 gives the F value for each zone.

TABLE F.1. ANNUAL CONSUMPTIVE USE VALUES (F) FOR EACH CLIMATIC ZONE AND GEOGRAPHIC COMMUNITY

<u>CLIMATE ZONE</u>	<u>COMMUNITY</u>	<u>F</u>
1	Winslow	36.28
2	Holbrook	36.86
3	St. Johns	34.22
4	Springerville	25.03
5	Snowflake	28.15
6	Sanders	27.47
7	Chevelon Ranger Station	27.81
8	Alpine	14.95
9	Greer	17.31

- 4a. Landsat scenes from June 1983 were obtained. Ratios between the near infrared and red band reflections were established to aid in determining the extent and relative density of vegetation in the basin. Classes of vegetation densities were established based on the near IR - red band ratio and plotted on the 1:24000 maps which correspond to USGS 7.5 minute quads. These were the maps on which the alluvial polygons were sketched.
- 4b. Spot field checks were conducted throughout the Little Colorado River system to determine the species composition of the phreatophyte community, and to provide field rectification of the vegetation density information. The mean density for the vegetation

classes was used in the ET calculations. Table F.2 shows the range and mean density for each class.

TABLE F.2. GROUND COVER RANGE AND MEAN VALUES FOR VEGETATION CLASSES

<u>VEGETATION CLASS</u>	<u>GROUND COVER RANGE</u>	<u>MEAN GROUND COVER</u>
Dense	80 to 100%	90%
Moderate	40 to 80%	60%
Sparse	10 to 40%	30%
Barren	0%	0%

- 4c. Based on the field investigations, broad generalizations about the vegetation species compositions were made for reaches of the river and named after the community which most closely corresponds to the reach. Table F.3 lists the phreatophyte species assumed for the communities in the river system.

TABLE F.3. GEOGRAPHIC AREAS AND ASSOCIATED PHREATOPHYTE COMMUNITIES

<u>ZONE</u>	<u>PHREATOPHYTE COMMUNITY</u>
Winslow	tamarisk
Holbrook	70% tamarisk/30% baccharis
St. Johns	tamarisk
Springerville	50% tamarisk/50% willow
Snowflake	cottonwood/willow
Show Low	cottonwood/willow
Sanders/Puerco River	tamarisk
Chevelon Ranger Station	alder/willow
Alpine	cottonwood/willow
Greer	40% cottonwood/willow/60% grasses

- 4d. From Figure 1 in Rantz (1968) estimates of the coefficient K can be made based solely on depth to water for each species in the basin. Table F.4 contains the K values used in the calculations.

TABLE F.4. COEFFICIENT K VALUES FOR SELECTED SPECIES AND  
AND DEPTH TO WATER

<u>SPECIES</u>	<u>DEPTH TO WATER</u>	<u>K</u>
Tamarisk	3 feet	1.60
Tamarisk	5 feet	1.35
Cottonwood/willow	2 feet	1.89
Cottonwood/willow	3 feet	1.50
Baccharis	3 feet	1.20
Baccharis	5 feet	0.80

Rantz used the same curve for both cottonwood and willow, therefore, in riparian communities comprised of primarily those two species, it was not necessary to determine the percentages in each. No curve existed for alder or grasses. Because alders are similar in structure to cottonwoods, the cottonwood/willow curve was utilized for alder communities. Water loss from grasses in the reach from Springerville to the headwaters (Greer zone) was assumed to be one acre foot per acre.

- For each riparian zone, a water use value was calculated based on the zone's climate and the depth to water along the river reach. The zone provided the species composition within the polygon and the climatic variable F. The depth to water combined with the species information determined K. Two examples follow that illustrate the determination of the base water use from a 100 percent vegetated channel. It is assumed that a completely vegetated channel has no bare soil, therefore, the bare soil evaporation component of ET would approach zero. All of the losses are assumed the result of transpiration by the vegetation.

EXAMPLE 1

POLYGON 79

ZONE 3

DEPTH TO WATER 3 FEET

100% Tamarisk

K = 1.60

F = 34.22

U = KF = (1.60)(34.22) = 55 inches/year = 4.6 feet/year

EXAMPLE 2

POLYGON 189

ZONE 2 DEPTH TO WATER 5 FEET  
 70% Tamarisk 30% Baccharis  
 $K = (1.35 * 0.7) + (0.8 * 0.3) = 1.18$   
 $F = 36.86$   
 $U = KF = (1.18)(36.86) = 43 \text{ inches/year} = 3.6 \text{ feet/year}$

6. Two major factors generally considered to affect evaporation from bare soil are the depth to groundwater and the nature of the soil from which evaporation is taking place. Weeks, et al. (1987) published a graph of annual rates of bare soil ET from various experiments. The graph illustrates the inverse relationship that existed between depth to groundwater and bare soil ET in all of the published reports. It does not, unfortunately, illustrate any obvious relationships between soil characteristics and bare soil ET. Using this graph as a guide, a conservative value for ET of 1.0 foot per year from bare soil has been chosen for reaches where the water level below the alluvium was assumed to be three feet. A value of 0.5 foot per year bare soil evaporation was chosen for the reach where the water level was assumed to be five feet.
7. For each vegetation class within each zone, the mean ground cover was multiplied by the water use amount. That value was added to the portion of the class not covered by vegetation times the annual evaporation value for bare soil. Examples 3 and 4 calculate the consumptive use for each of the four vegetation classes within the polygons in examples 1 and 2.

EXAMPLE 3

	TRANSPIRATION		EVAPORATION		ET (AF/AC/YR)
Dense	(4.6 * 0.90)	+	(1.0 * 0.10)	=	4.24
Moderate	(4.6 * 0.60)	+	(1.0 * 0.40)	=	3.16
Sparse	(4.6 * 0.30)	+	(1.0 * 0.70)	=	2.08
Bare Ground			(1.0 * 1.00)	=	1.0

## REFERENCES

- Akers, J.P., and J.W. Harshbarger, 1958. Groundwater in Black Mesa Basin and Adjacent Areas, *in* Anderson, R.Y. and J.W. Harshbarger, (eds), New Mexico Geological Society Ninth Field Conference, 1958, Guidebook of the Black Mesa Basin, Northeastern Arizona, p. 173-183.
- Arizona Department of Water Resources, 1989. Hydrology of the Little Colorado River System. Special Report to the Settlement Committee. In Re the General Adjudication of the Little Colorado River System and Source.
- Baker, A.A., C.H. Dane and J.B. Reeside, 1936. Correlation of the Jurassic Formations of Parts of Arizona, New Mexico, Colorado and Utah: U.S. Geological Survey Professional Paper 183, p. 1-66.
- Brown, J.G., and J.H. Eychaner, 1988. Simulation of Five Ground-water Withdrawal Projections for the Black Mesa Area, Navajo and Hopi Indian Reservations, Arizona: U.S. Geological Survey Water-Resources Investigations Report 88-4000, 51 p.
- Cooley, M.E., J. Akers, and P.R. Stevens, 1964. Selected Lithologic Logs, Drillers' Logs, and Stratigraphic Sections, Pt. 3 of Geohydrologic Data in the Navajo and Hopi Indian Reservations, Arizona, New Mexico and Utah: Arizona State Land Department Water Resources Report 12-C, 157 p.
- \_\_\_\_\_, 1966. Maps Showing Location of Wells, Springs, and Stratigraphic Sections, Pt. 4 of Geohydrologic Data in the Navajo and Hopi Indian Reservations, Arizona, New Mexico and Utah: Arizona State Land Department Water Resources Report 12-D, 2 sheets.
- \_\_\_\_\_, J.W. Harshbarger, J.P. Akers, and W.F. Hardt. 1969. Regional Hydrogeology of the Navajo and Hopi Indian Reservation, Arizona, New Mexico, and Utah: U.S. Geological Survey Professional Paper 521-A, 61 p.
- Davis, G.E., W.F. Hardt, L.K. Thompson, M.E. Cooley. 1963. Geohydrologic data in the Navajo and Hopi Indian Reservations, Arizona, New Mexico, and Utah: Part 1, Records of Groundwater Supplies: Arizona State Land Department Water-Resources Report 12-A.

## REFERENCES (continued)

- Drever, J.I., 1988, *The Geochemistry of Natural Waters*. 2nd ed., 437 p., Prentice Hall, Inc.
- Dulaney, A.R., 1989, *The Geochemistry of the "N" Aquifer System, Navajo and Hopi Indian Reservations, Northeastern Arizona*: M.S. Thesis, Northern Arizona University, 201 p.
- \_\_\_\_\_, 1991, *Water Chemistry of the Navajo/Lukachukai Aquifer System, Black Mesa Basin and Vicinity, Arizona*: Abstract from Arizona Hydrological Society, Fourth Annual Symposium Program.
- Eychaner, J.H., 1981. *Geohydrology and effects of water use in the Black Mesa area, Navajo and Hopi Indian Reservations, Arizona*: U.S. Geological Survey Open File Report 81-911, 46p.
- \_\_\_\_\_, 1983. *Geohydrology and Effects of Water Use in the Black Mesa Area, Navajo and Hopi Indian Reservations, Arizona*: U.S. Geological Survey Water-Supply Paper 2201, 26p.
- Haynes, D.D. and R.J. Hackman, 1978. *Geology, Structure, and Uranium Deposits of the Marble Canyon 1° x 2° Quadrangle, Arizona*: U.S. Geological Survey Miscellaneous Investigations Series Map I-1003, 2 sheets.
- Harshbarger, J.W., C.A. Repenning, and J.H. Irwin. 1957. *Stratigraphy of the Uppermost Triassic and the Jurassic rocks of the Navajo Country*: U.S. Geological Survey Professional Paper 291, 74 p.
- Hart, R.J. and J.P. Sottolare, 1988. *Progress report on ground-water, surface-water, and quality-of-water monitoring program, Black Mesa Area, northeastern Arizona, 1987-1988*: U.S. Geological Survey Open-File Report 88-467, 27 p.
- Hem, J.D., 1985. *Study and Interpretation of Chemical Characteristics of Natural Water* (3rd ed.): U.S. Geological Survey Water-Supply Paper 2254, 263 p.

## REFERENCES (continued)

- Hill, G.W. and Sottolare, J.P., 1987. Progress report on ground-water, surface-water, and quality-of-water monitoring program, Black Mesa Area, northeastern Arizona, 1987: U.S. Geological Survey Open-File Report 87-458, 18 p.
- Holser, W.T. and I.R. Kaplan, 1966. Isotope geochemistry of sedimentary sulfates: *Chem. Geol.* 1, p. 93-135.
- Hydro Geo Chem, Inc., 1990. Water Sampling and Flow Measurement Procedures for the Investigation of Surface/Subsurface Flow Components for Selected Black Mesa Drainages, Little Colorado River Basin, Arizona; submitted to the U.S. Justice Department. 28 p.
- International Atomic Energy Agency (IAEA), 1981. Stable Isotope Hydrology, Deuterium and Oxygen-18 in the Water Cycle: Monograph, Technical Report Series No. 210.
- James, H.C., 1974. Pages from Hopi History. The University of Arizona Press, 258 p.
- Levings, G.W. and C.D. Farrar. 1977. Maps showing Groundwater Conditions in the Southern part of the Black Mesa Area, Navajo, Apache, and Coconino Counties, Arizona. U.S. Geological Survey Water Resources Investigations 77-41.
- Kiersch, G.A., 1955a. Metalliferous Minerals and Mineral Fuels - Geology, Evaluation, and Uses, Vol. I Mineral Resources, Navajo and Hopi Indian Reservations: University of Arizona Press, 75 p.
- \_\_\_\_\_ 1955b. Nonmetallic Minerals - Geology, Evaluation, and Uses, Vol. II Mineral Resources, Navajo and Hopi Indian Reservations: University of Arizona Press, 105 p.
- \_\_\_\_\_ 1955c. Construction Materials - Geology, Evaluation, and Uses, Vol. III Mineral Resources, Navajo and Hopi Indian Reservations: University of Arizona Press, 81 p.

## REFERENCES (continued)

- Kister, L.R., and J.L. Hatchett, 1963. Selected Chemical Analyses of the Ground Water, Pt. 2 of Geohydrologic Data in the Navajo and Hopi Indian Reservations, Arizona, New Mexico and Utah: Arizona State Land Department Water Resources Report 12-B, 58 p.
- Levings, G.W. and C.D. Farrar. 1977. Maps showing groundwater conditions in the Monument Valley and northern part of the Black Mesa areas, Navajo, Apache, and Coconino Counties, Arizona: U.S. Geological Survey Water Resources Investigations 77-44.
- Luttrell, P.R., 1978. Basin Analysis of the Kayenta Formation (Lower Jurassic), Central Portion Colorado Plateau: M.S. Thesis, Northern Arizona University, 212 p.
- McGavock, E.H., R.J. Edmonds, E.L. Gillespie, and P.C. Halpenny. 1966. Geohydrologic Data in the Navajo and Hopi Indian Reservations, Arizona, New Mexico, and Utah - Part 1A, Supplemental Records of Groundwater Supplies: Arizona State Land Department Water-Resources Report 12-E, 55p.
- \_\_\_\_\_, and G.W. Levings. 1973. Groundwater in the Navajo Sandstone in the Black Mesa, Arizona: Guidebook of Monument Valley and Vicinity, Arizona and Utah, New Mexico Geological Society, 24th Annual Field Conference Guidebook.
- Office of Surface Mining and Reclamation and Enforcement (OSMRE), 1989. Cumulative Hydrologic Impact Assessment of the Peabody Coal Company Black Mesa/Kayenta Mine: Reclamation and Enforcement, Western Field Operations, Denver, Colorado.
- O'Sullivan, R.B., C.A. Repenning, E.C. Beaumont, and H.G. Page. 1972. Stratigraphy of the Cretaceous rocks and the Tertiary Ojo Alamo Sandstone, Navajo and Hopi Indian Reservations, Arizona, New Mexico, and Utah: U.S. Geological Survey Professional Paper 521-E, 65p.
- Page, H.G. and C.A. Repenning. 1958. Late Cretaceous Stratigraphy of Black Mesa, Navajo, and Hopi Indian Reservations, Arizona, in R.Y. Anderson and J.W. Harshbarger (eds), Guidebook of the Black Mesa Basin, Northeastern Arizona, New Mexico Geological Society Ninth Field Conference, p. 115-122.

## REFERENCES (continued)

- Parkhurst, D.L., D.C. Thorstenson, and L.N. Plummer, 1980: PHREEQE - A Computer Program for Geochemical Calculations. U.S. Geological Survey Water Resources Investigations 80-96, 145p.
- Rantz, S.E., 1968. A suggested method for estimating evapotranspiration by native phreatophytes: U.S. Geological Survey Professional Paper 600-D., p. D10-D12.
- Sargent, C.G., 1984. Intertonguing Kayenta and Navajo Sandstone (Lower Jurassic?) on Northeastern Arizona: M.S. Thesis, Northern Arizona University, 129 p.
- Stetson Engineering, Inc., 1962. Feasibility of Obtaining a Groundwater Supply from Black Mesa, Arizona (prepared for Peabody Coal Company). 28 p.
- Stumm, W. and J.M. Morgan, 1970. Aquatic Chemistry, An Introduction Emphasizing Chemical Equilibria in Natural Waters. Wiley-Interscience. 583 p.
- U.S. Department of Energy, 1989. Remedial Action Plan Site Design for Stabilization of the Inactive Uranium Mill Tailings Site, Tuba City, Arizona: Albuquerque, U.S. Department of Energy, UMTRA Project Office.